Circadian rhythms in glucocorticoid signalling and pulmonary inflammation

A thesis submitted to the University of Manchester for the degree of Doctor of Philosophy in the Faculty of Life Sciences

2015

Louise M. Ince

List of Contents

List of Figures **9**

List of Tables **11**

List of Common Abbreviations **12**

Abstract **13**

Declaration **14**

Copyright Statement **14**

Acknowledgements **15**

Chapter 1: Introduction ***16***

1.1 Inflammation and disease **17**

1.2 The circadian clock **18**

1.2.1 Entrainment of the circadian pacemaker to external stimuli 20

1.2.1.1 Photic entrainment 20

1.2.1.2 Non-photic entrainment 21

1.2.2 Pace of the molecular oscillator 22

1.2.3 Outputs of the circadian oscillator system 22

1.2.4 The circadian hierarchy 22

1.2.4.1 Synchronisation of peripheral oscillators 23

1.3 Circadian rhythms in inflammation **25**

1.3.1 Clinical evidence of rhythmic inflammation 25

1.3.2 Circadian disruption and inflammation 26

1.3.3 Clocks in immune cells 28

1.3.4 Timed inflammatory challenges 29

1.4 Glucocorticoids **30**

1.4.1 The glucocorticoid receptor and inflammation 32

1.4.2 Rhythmic glucocorticoid production 39

1.4.2.1 Extra-adrenal glucocorticoid synthesis 43

1.4.3 Glucocorticoid metabolism 44

1.4.4 Glucocorticoids and rhythmic inflammation 45

1.5 Pulmonary inflammation **46**

1.5.1 Lung structure and physiology 47
1.5.1.1 Conducting zone 48
1.5.1.2 Respiratory zone 48
1.5.1.2.1 Type I pneumocytes 48
1.5.1.2.2 Type II pneumocytes 49
1.5.1.2.3 Bronchiolar epithelial cells 51
1.5.1.2.4 Alveolar macrophages 51
1.5.2 Circadian rhythms in the lung 52

1.6 Model systems 52
1.6.1 Inflammatory models 53
1.6.2 Manipulation of glucocorticoid rhythms 54
1.6.2.1 Surgical 54
1.6.2.2 Pharmacological 55
1.6.3 Genetic 56
1.6.3.1 Cre-loxP recombination 56
1.6.3.1.1 GR floxed mice 59
1.6.3.1.2 Lung-specific Cre drivers 60

1.7 Hypotheses, aims and objectives 61

Chapter 2: Methods 67

2.1 Animal husbandry 68
2.1.1 Genotyping 68

2.2 Surgical techniques 69
2.2.1 Adrenalectomy 69
2.2.2 Subcutaneous corticosterone pellet implant 70

2.3 *In vivo* experimental procedures and sample collection 71
2.3.1 Wheel-running 71
2.3.2 Blood sample collection via tail tipping 71
2.3.3 Intraperitoneal lipopolysaccharide challenge 71
2.3.4 Aerosolised lipopolysaccharide challenge 72
2.3.4.1 Bronchoalveolar lavage 72
2.3.4.2 Cell counting 73
2.3.4.3 Cytospin 73
2.3.4.4 Flow cytometry 74

2.3.4.5 Tissue for protein or RNA extraction 76
2.3.4.6 Blood for serum 76
2.3.4 Timed injections of corticosterone 77
2.3.4.1 Pilot (dose-response) 77
2.3.4.2 Phase reversal experiment 77
2.3.4.2.1 Circadian series 79
2.3.4.2.2 Blood for serum 79
2.3.4.2.3 Tissue for protein or RNA extraction 79
2.4 *Ex vivo* experimental procedures 79
2.4.1 Photomultiplier tube experiments 79
2.4.1.1 Synchronisation experiments 81
2.4.1.2 Rhythm analysis 81
2.4.2 Processing of tissue for immunohistochemistry 81
2.4.3 Immunohistochemistry 82
2.4.4 Processing of tissue for in situ hybridisation 83
2.4.5 *In situ* hybridisation 84
2.4.5.1 Preparation of radiolabelled probes 84
2.4.5.2 Hybridisation 86
2.4.5.3 Imaging and analysis 87
2.4.6 RNA extraction 88
2.4.7 Reverse transcription 88
2.4.8 qPCR 88
2.4.9 ELISAs 89
2.4.9.1 Corticosterone 89
2.4.9.2 Interleukin-6/CXCL5 89
2.4.10 Bioplex 91
2.4.11 Protein extraction 94
2.4.12 Protein quantification 95
2.4.13 Western Blot 95
2.5 Statistics 97
Chapter 3: Impact of adrenalectomy upon rhythmic pulmonary inflammation 98
3.1 Introduction 99
3.2 Hypothesis tested and experimental approaches 100

3.3 Results 102

3.3.1 Adrenalectomy abolishes diurnal variation in serum corticosterone concentration 102

3.3.2 Adrenalectomy does not affect the behavioural output from central pacemaker 103

3.3.3 Adrenalectomy does not affect the phase of the local pulmonary oscillator 103

3.3.4 Adrenalectomy causes a loss of circadian gating of the neutrophilic response to aerosolised LPS 106

3.3.5 Adrenalectomy causes an increase in the inflammatory response to systemic LPS 108

3.4 Discussion 109

3.4.1 Circulating glucocorticoids and behavioural rhythms 109

3.4.2 Adrenalectomy and the pulmonary oscillator 110

3.4.3 Adrenalectomy and rhythmic inflammation 111

3.4.3.1 Aerosolised LPS _____ 111

3.4.3.2 Systemic LPS _____ 112

3.5 Conclusions 113

Chapter 4: The effect of timed corticosterone administration on the relative phasing of circadian clock gene expression in the lung 114

4.1 Introduction 115

4.2 Hypothesis tested and experimental approaches 117

4.2.1 Establishment of an appropriate dose of exogenously administered corticosterone to mimic endogenous peak concentration 118

4.2.2 Phase reversal 119

4.3 Results 121

4.3.1 Exogenous administration of corticosterone via intraperitoneal injection causes a dose-dependent increase in serum corticosterone concentration 121

4.3.2 Timed exogenous administration of corticosterone to adrenalectomised mice alters circadian circulating corticosterone profiles 123

4.3.3 Timed exogenous administration of corticosterone to adrenalectomised mice fails to reverse clock gene rhythms in the lung 126

4.3.3.1 *Period2* _____ 126

4.3.3.2 *Bmal1* 128

4.4 Discussion **130**

4.4.1 Pilot study 130

4.4.2 Circadian series 131

4.4.2.1 Corticosterone 131

4.4.2.2 Clock gene expression 132

4.5 Conclusions **134**

Chapter 5: Effects of consistent circulating corticosterone concentration upon rhythmic pulmonary inflammation ***135***

5.1 Introduction **136**

5.2 Hypothesis tested and experimental approaches **138**

5.2.1 Establishment of subcutaneous implant dose 139

5.2.2 Timed inflammatory challenge 140

5.3 Results **142**

5.3.1 Consistent circulating concentrations of corticosterone can be obtained via subcutaneous implant of sustained release pellet 142

5.3.2 Increased corticosterone at CT0 within physiological range does not suppress inflammatory response to aerosolised lipopolysaccharide 143

5.3.3 Corticosterone clamp does not affect the circadian-gated response to aerosolised LPS 144

5.4 Discussion **147**

5.4.1 Corticosterone clamp effects on circulating corticosterone concentration 147

5.4.2 Corticosterone clamp effects on rhythmic pulmonary inflammation 148

5.4.3 Note 150

5.5 Conclusions **151**

Chapter 6: Targeted disruption of glucocorticoid receptor signalling in bronchiolar epithelial cells ***152***

6.1 Introduction **153**

6.2 Hypothesis tested and experimental approaches **156**

6.3 Results **160**

6.3.1 *GR*$^{flox/flox}$*Ccsp*^{icre}/PER2::Luc (*Ccsp-GR*$^{-/-}$) mice show disrupted glucocorticoid receptor expression in the bronchial epithelium 160
6.3.2 Lung slices from *Ccsp-GR*$^{-/-}$ mice retain circadian rhythms of bioluminescence in culture and retain the ability to be resynchronised by dexamethasone administration 162
6.3.3 *Ccsp-GR*$^{-/-}$ mice exhibit a loss of circadian gating in their response to aerosolised LPS challenge, yet remain sensitive to dexamethasone-mediated suppression of inflammation 164

6.4 Discussion 172
6.4.1 Generation of *Ccsp-GR*$^{-/-}$ mouse line 172
6.4.2 Rhythmic bioluminescence in *Ccsp-GR*$^{-/-}$ mice 174
6.4.3 Pulmonary inflammatory phenotype of *Ccsp-GR*$^{-/-}$ mice 178

6.5 Conclusions 181

Chapter 7: Discussion 182

7.1 Summary of key findings 183

7.2 Discussion 184
7.2.1 Circadian rhythms in response to immune challenge 185
7.2.2 Mechanisms linking molecular clock elements to immunity 187
7.2.2.1 BMAL1/CLOCK 188
7.2.2.2 CRYs 190
7.2.2.3 REV-ERBs/RORs 191
7.2.3 Circadian rhythms in immune cell trafficking 194
7.2.4 The role of glucocorticoids and the glucocorticoid receptor in inflammation 195
7.2.4.1 The role of glucocorticoids and the glucocorticoid receptor in regulating rhythmic responses to inflammatory challenge 196
7.2.4.1.1 Caveats of work presented 205
7.2.5 Future work 207
7.2.5.1 Non-glucocorticoid regulation of rhythmic pulmonary neutrophilia 207
7.2.5.2 Glucocorticoid signalling in additional cell types 209
7.2.5.3 Macrophage-epithelium cross-talk 210
7.2.5.4 Circadian remodelling of chromatin architecture 211
7.2.6 Conclusions 212

Appendices ***213***

Appendix 1 - Genotyping reactions, primer sequences and gel recipe **214**

GR flox 214

Ccsp^{icre} 215

Per2-Luc 216

Agarose gels 217

Appendix 2 - Recording media recipe **218**

Appendix 3 – *In situ* hybridisation buffer recipes **219**

Hybridisation buffer 219

TEN Buffer 219

Appendix 4 - qPCR sequences and conditions **220**

TaqMan primers 220

SYBR primers 220

Cycling conditions 221

Reaction recipes 221

Appendix 5 - Sample ELISA standard curves **222**

Appendix 6 – Corticosterone ELISAs post-adrenalectomy **224**

Chapter 3 224

Chapter 4 225

Appendix 7 – Additional corticosterone clamp data **226**

Appendix 8 – *Ccsp^{icre}* Western Blot **228**

References ***229***

Word count: 61,836

List of Figures

Figure 1.1: The mammalian molecular clock 19
Figure 1.2: Influence of photic signals upon central pacemaker phase 21
Figure 1.3: Signalling pathway of lipopolysaccharide-induced cytokine production 27
Figure 1.4: Steroid biosynthesis in the adrenal cortex 31
Figure 1.5: Glucocorticoid receptor signalling 33
Figure 1.6: Chromatin remodelling..... 37
Figure 1.7: Factors regulating rhythmic glucocorticoid production. 42
Figure 1.8: Lung structure and distal cell types 50
Figure 1.9: Cre-loxP recombination..... 58
Figure 1.10: Overview of model and focal points of project 62
Figure 2.1: Experimental procedure for phase-reversal experiment..... 78
Figure 3.1: Circulating serum corticosterone concentrations across a circadian period 102
Figure 3.2: Wheel-running activity periods of intact and adrenalectomised mice .. 104
Figure 3.3: Clock gene expression in lungs from saline-treated intact and adrenalectomised animals 105
Figure 3.4: Response of intact and ADX mice to aerosolised lipopolysaccharide .. 107
Figure 3.5: Interleukin-6 production in response to timed systemic lipopolysaccharide challenge in intact and adrenalectomised mice..... 108
Figure 4.1: Experimental procedure for dose-response experiment 119
Figure 4.2: Experimental procedure for phase-reversal experiment..... 120
Figure 4.3: Serum corticosterone concentration before and after intraperitoneal corticosterone injection 122
Figure 4.4: Serum corticosterone concentration before and after intraperitoneal corticosterone injection in adrenalectomised animals..... 123
Figure 4.5: Serum corticosterone concentration across a circadian cycle 125
Figure 4.6: *Period2* expression in lung tissue across a circadian cycle 127
Figure 4.7: *Bmal1* expression in lung tissue across a circadian cycle 129
Figure 5.1: Experimental protocol for corticosterone clamp studies 141
Figure 5.2: Circulating serum corticosterone concentrations across a circadian period 142
Figure 5.3: Inflammatory response to aerosolised LPS at CT0 with various doses of corticosterone implant..... 143

Figure 5.4: Circulating serum corticosterone concentrations prior to experiment... 144
Figure 5.5: Response of intact and corticosterone-clamped mice to aerosolised lipopolysaccharide... 146
Figure 6.1: Targeting strategy and generation of *Ccsp-GR*$^{-/-}$ mice... 157
Figure 6.2: Testing for GR loss in bronchiolar epithelial cells of *Ccsp-GR*$^{-/-}$ mice. 161
Figure 6.3: Oscillations of PER2::Luc-driven bioluminescence in organotypic lung slices... 163
Figure 6.4: Pulmonary inflammatory response to lipopolysaccharide challenge at CT12... 165
Figure 6.5: Pulmonary inflammatory response to lipopolysaccharide challenge at CT0... 166
Figure 6.7: Model hypotheses for synchronising effects of dexamethasone in the lung ... 175
Figure 7.1: The mammalian molecular clock ... 188
Figure 7.2: Graphical representation of hypotheses tested and additional areas of interest... 199
Figure A7.1: Response of intact and corticosterone-clamped mice to aerosolised lipopolysaccharide... 226
Figure A7.2: Circulating serum corticosterone concentrations after experiment 227

List of Tables

Table 2.1: Antibody dilutions and fluorophores used for flow cytometry..... 76
Table 2.2: Dilution factors for samples used in IL-6 and CXCL5 ELISAs..... 90
Table 2.3: Standard values and bead regions for bioplex assay..... 93
Table 4.1: Group sizes for circadian series experiments..... 125
Table 6.1: Summary of bronchoalveolar lavage cytokine analysis via bioplex..... 170
Table 6.2: Comparison of lung slice rhythmicity and resetting capacity of dexamethasone treatment in different models..... 176

List of Common Abbreviations

ACTH	Adrenocorticotropic hormone
ADX	Adrenalectomised
BAL	Bronchoalveolar lavage
Bmal1/BMAL1	Brain and muscle aryl hydrocarbon receptor nuclear translocator (ARNT)-like 1 (*gene*/PROTEIN)
Ccsp/CCSP	Clara cell secretory protein (*gene*/PROTEIN)
Clock/CLOCK	Circadian Locomotor Output Cycles Kaput (*gene*/PROTEIN)
CORT	Corticosterone
Cre/Cre	Cre (causes recombination) recombinase (*gene*/Protein)
Cry/CRY	Cryptochrome (*gene*/PROTEIN)
CT	Circadian time (indicating constant conditions)
DD	Constant darkness
ELISA	Enzyme-linked immunosorbent assay
Flox	Flanked by *loxP* sites
GR	Glucocorticoid receptor
GRE	GR response element
HPA (axis)	Hypothalamic-pituitary-adrenal (axis)
iCre	Improved Cre
Il6/IL-6	Interleukin 6 (*gene*/PROTEIN)
i.p.	Intraperitoneal
LD	Light-dark cycle
LoxP	Locus of X-over P1
LPS	Lipopolysaccharide
Luc/LUC	Luciferase (*gene*/PROTEIN)
LysM/LysM	Lysozyme M (*gene*/PROTEIN)
Per/PER	Period (*gene*/PROTEIN)
Rora/RORα	Retinoic acid-related orphan nuclear receptor alpha (*gene*/PROTEIN)
SCN	Suprachiasmatic nucleus
Star/StAR	Steroidogenic acute regulatory (*gene*/PROTEIN)
TLR	Toll-like receptor
ZT	Zeitgeber time (indicating the presence of an external timing cue)

Abstract

The University of Manchester

Submitted by Louise Ince for the degree of Doctor of Philosophy and entitled: **Circadian rhythms in glucocorticoid signalling and pulmonary inflammation**, 2015.

The circadian clock drives ~24hr rhythms in a variety of processes, from gene expression through to behaviour, facilitating anticipation of daily changes in the external environment and temporal separation of internal processes. This pacemaker is a critical regulator of immune function and many inflammatory diseases show time-of-day variation in symptom severity. Disruption of the pacemaker by manipulation of the daily cycle of light and dark exposure (experimental 'jet lag') is known to exacerbate inflammatory responses to innate immune challenge, and recent evidence has highlighted immuno-modulatory roles for components of the molecular oscillator in peripheral tissues. The adrenal-derived glucocorticoid hormones are potent anti-inflammatory molecules and are capable of modulating circadian oscillations in peripheral tissues. This, along with their rhythmic secretion profile, makes them key candidates as mediators of circadian regulation of inflammatory signalling.

Utilising adrenalectomy, timed glucocorticoid administration, hormone clamp and genetic targeting of the glucocorticoid receptor in mice, I present evidence for an interaction between glucocorticoid signalling and the circadian pacemaker in regulating the pulmonary inflammatory response to lipopolysaccharide (LPS) challenge. The neutrophilic response to aerosolised LPS exhibits a clear time-of-day effect *in vivo*, which is lost after disruption of endogenous glucocorticoid production via adrenalectomy. However, replacement of a rhythmic circulating glucocorticoid concentration with a flat daily average using a subcutaneous hormone clamp does not disrupt the inflammatory rhythm. Finally, a novel mouse strain was produced with disrupted expression of the glucocorticoid receptor (GR) in bronchial epithelial cells (*Ccsp-GR*$^{-/-}$). These cells are critical regulators of circadian rhythmicity in the lung and drive rhythmic neutrophil influx in response to LPS stimulation through production of the chemokine CXCL5. Loss of GR in the bronchial epithelium was associated with a loss of rhythmic neutrophil influx after challenge, but anti-inflammatory sensitivity to the synthetic glucocorticoid dexamethasone remained.

Collectively, these data show that appropriate temporal modulation of pulmonary inflammation requires functional glucocorticoid signalling, although the ligand itself does not need to oscillate. The retention of anti-inflammatory dexamethasone sensitivity suggests a role for cross-talk between the bronchial epithelium and additional cell populations, consistent with recent evidence for immuno-suppressive macrophage-epithelium communication in the lung. These are the first studies to dissect the mechanistic links between clocks, glucocorticoids and immunological responses in a target tissue.

Declaration

No portion of the work referred to in this thesis has been submitted in support of an application for another degree or qualification of this or any other university or other institute of learning.

Copyright Statement

Acknowledgements

I would like to thank my supervisory team of Prof. Andrew Loudon, Prof. David Ray, Dr. Julie Gibbs and Prof. Kathryn Else for their excellent guidance and support throughout this project. Julie, in particular, has been a mentor not only in terms of the scientific direction of the project and practical lab skills but also with respect to career progression and has been an inspirational figure for this young scientist.

Members of the Loudon and Ray lab groups have been fantastic to work with, and I would especially like to acknowledge the technical and emotional support provided by Nicola Begley, Dr. Shona Wood and Marie Pariollaud. Dr. Ben Saer and Dr. Zhenguang Zhang have both contributed their skills to the work contained in this thesis, for which I am very grateful, and the lab has been a fantastic place to develop skills and ideas over the last three years.

Dr. Laura Matthews has also been a great support throughout this project, not only for her immunofluorescent wizardry but also for providing friendly advice when needed and her persistent enthusiasm for introducing new ideas and techniques to the group.

I would also like to thank my family for getting me to this point. From a young age, I was encouraged to question how things worked and fit together, and I think the simultaneous reinforcement of my creative and methodical sides has led to me pursuing a career in academic science. My parents have invested a lot of time (and money!) in getting me this far, and I will forever be grateful for their support.

Finally, to my husband, Chris, who will be very glad that I might finally graduate (again!) and enter the real world of work. His support over the last three years has been invaluable, particularly with respect to providing food and copious amounts of tea during the writing process, and I could not have asked for a better partner.

Chapter 1: Introduction

1.1 Inflammation and disease

The mammalian immune system is highly effective at protecting the organism from a variety of pathogens, including viruses, bacteria, and parasites. Triggered by the presence of such pathogens or by damaged host cells, inflammation is a key component of this defence. Under normal circumstances this forms a protective mechanism, however, when inappropriate or prolonged inflammation occurs extensive tissue damage and remodelling can occur, resulting in chronic pain and swelling in the affected areas along with altered tissue function (Barton 2008).

Aberrant inflammation is a common feature of many disease states, including asthma, arthritis, and chronic obstructive pulmonary disease (Barnes 2000; Cutolo & Masi 2005). Persistent inflammation results in elevated levels of diffusible factors such as cytokines, which often act systemically via the bloodstream. Chronic inflammation in one area can therefore predispose an organism to developing further inflammatory pathology by creating a state of 'systemic inflammation'. Although not classically considered to be inflammatory conditions, obesity and metabolic syndrome are correlated with chronic, low-grade systemic inflammation (Gregor & Hotamisligil 2011). By understanding the factors which predispose towards a pathological response, the impact of inflammatory diseases can be lessened; risk factors can be identified and novel anti-inflammatory treatments developed.

One such detrimental factor is that of circadian disruption. The body's internal clock, which runs at a pace of ~24hrs (*circa* – about, *dies* – a day), creates an internal representation of external time, serving to synchronise bodily functions to appropriate times of day. For example, by restricting behaviour to times when an animal is less likely to be seen by predators or separating biologically incompatible processes (Panda & Hogenesch 2004). The possession of a circadian clock can confer a survival advantage (Pittendrigh & Minis 1972; Woelfle et al. 2004) and it is therefore not surprising to find that species from bacteria to mammals are capable of generating circadian rhythms (Dunlap 1999). This clock has wide-ranging effects upon physiology – generating rhythms in locomotor activity, hormone secretion and even cognitive function (Panda & Hogenesch 2004). It has been proposed that this circadian rhythm influences the immune system to prime it to respond more strongly at times when the organism is most likely to encounter a pathogen, and to inhibit the

response to conserve energy at other times of day (Gibbs et al. 2012). The clock can become disrupted, however, as a result of aging or environmental disturbances such as jet lag or prolonged shift work. When the clock is disrupted experimentally, the immune system appears to become disinhibited and the inflammatory response is exacerbated (Castanon-Cervantes et al. 2010). This makes the circadian clock and its regulation of the immune system an exciting new target for immuno-modulatory therapies.

1.2 The circadian clock

The mammalian molecular clock comprises two interlocked transcription-translation feedback loops (figure 1.1). The loops converge upon BMAL1 (brain and muscle aryl hydrocarbon receptor nuclear translocator-like 1, also known as ARNTL or MOP3) and CLOCK (circadian locomotor output cycles kaput), two basic-helix-loop-helix transcription factors which bind to E-boxes in gene promoter regions (Ko & Takahashi 2006). In the negative feedback loop of the clock, the BMAL1-CLOCK dimer promotes transcription of *Period* (*Per)* and *Cryptochrome* (*Cry)* genes; the protein products of which form heterodimers. The PER-CRY dimer then translocates back to the nucleus and binds to BMAL1-CLOCK, repressing its activity and thus repressing *Per* and *Cry* transcription. As transcription decreases, PER and CRY levels fall and the repression of BMAL1-CLOCK activity is lifted, and so the cycle begins again.

The second loop is formed as the BMAL1-CLOCK dimer promotes transcription of two nuclear hormone receptors: RORα (retinoic acid-related orphan nuclear receptor α) and REV-ERBα. Both RORα and REV-ERBα bind to ROREs (ROR response elements), which lie in the promoter regions of a variety of genes, including *Bmal1*. The binding of RORα promotes transcription, whereas REV-ERBα acts as a repressor, and the rhythmic alternation of activity of these two competing nuclear hormone receptors generates a fluctuation in the levels of BMAL1 (Ko & Takahashi 2006).

These two loops integrate to produce rhythmic oscillations of proteins with a period of approximately 24hrs. This molecular rhythm occurs in the majority of mammalian cell types and tissues, including the lungs, liver and heart, and is reflected by

rhythmic firing rates of neurons in the suprachiasmatic nucleus (SCN), where the master clock is located (Piggins & Guilding 2011). In the absence of stimuli the clock will 'free run' at the endogenous period (τ) of the molecular oscillations, but under normal circumstances the clock is entrained to external cues and maintains a rhythm synchronous with the most salient feature of the external environment.

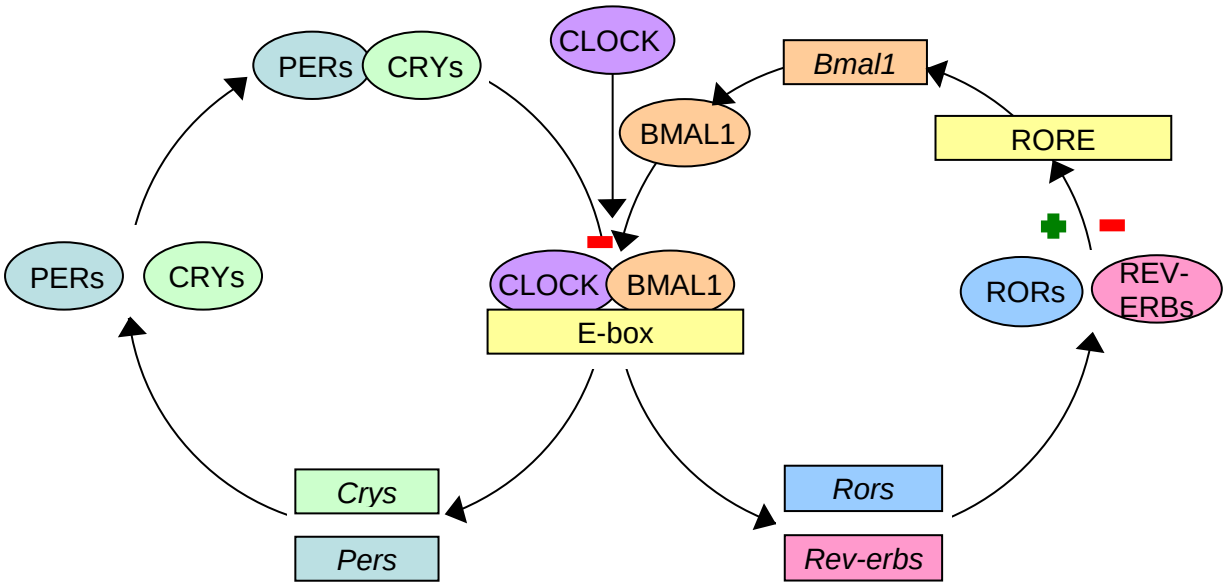

Figure 1.1: The mammalian molecular clock

Interlocked transcription-translation feedback loops, which converge upon the BMAL1-CLOCK dimer, make up the molecular clock in mammalian cells. The BMAL1-CLOCK dimer binds to E-boxes in gene promoters, positively regulating the transcription of genes such as *Crys*, *Pers*, *Rorα* and *Rev-erbα*. PER and CRY proteins heterodimerise and inhibit the activity of BMAL1-CLOCK, forming a negative feedback loop. RORα and REV-ERBα proteins influence transcription through ROR response elements (ROREs) in the promoter regions of genes, including *Bmal1*, to promote or inhibit transcription respectively.

BMAL1 – brain and muscle arnt-like 1; CLOCK – circadian locomotor output cycles kaput; CRY – cryptochrome; PER – period; ROR – retinoic acid-related orphan nuclear receptor; RORE – ROR response element; + – promotes transcription; - – inhibits transcription.

1.2.1 Entrainment of the circadian pacemaker to external stimuli

1.2.1.1 Photic entrainment

The mammalian clock is entrained to (i.e. synchronised with) an external cycle by zeitgebers ('time givers'), the most prominent of which is light. Light enters the eyes and stimulates photoreceptors in the retina. In the presence of light, these cells depolarise (Berson et al. 2002) and signal via the retinohypothalamic tract (RHT) to the SCN by releasing the neuropeptides PACAP (pituitary adenylate cyclase-activating polypeptide) and glutamate (Reppert & Weaver 2002; Hattar et al. 2002). These excitatory signals drive an influx of calcium which results in a signalling cascade of kinase activation and phosphorylation of the cAMP response element binding protein (CREB). Phosphorylated CREB can then bind the cAMP response element (CRE) in the promoter of the *Period 1* gene, promoting transcription (Albrecht et al. 1997; Kuhlman et al. 2003; Maywood et al. 2002). *Per1* induction is followed by suppressed K^+ currents and increased firing frequency in the core of the SCN, which in turn co-ordinates a shift in the rhythmic firing of the nuclei as a whole (Kuhlman et al. 2003).

The sensitivity and response of the SCN to this photic input varies according to the phase of the clock (Rusak & Groos 1982) – light delivered at the start of the dark phase will cause a phase delay (effectively lengthening the day and keeping the clock in that phase for longer), whereas light delivered at the end of the dark phase will cause an advance (shortening the night by providing a ‘morning’ signal, advancing the phase of the clock prematurely to a daytime profile). The differential response of the clock to stimuli delivered at different times of the cycle can be plot as a phase response curve (figure 1.2). The differential result from the same stimulus is driven by the profiles of signalling molecules activated and genes induced at each time. For example, for a phase delay (pulse at the start of the night), both *Per1* and *Per2* are induced, whereas phase advance was associated with induction of *Per1* but not *Per2* (Hirota & Fukada 2004).

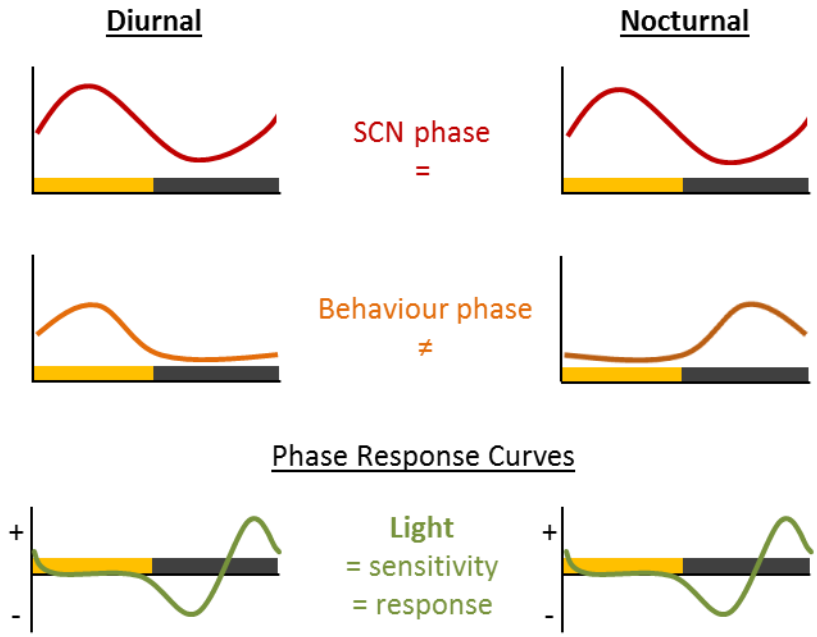

Figure 1.2: Influence of photic signals upon central pacemaker phase

Whilst diurnal and nocturnal animals have different behavioural phases (orange), the state of the central pacemaker remains the same in both (SCN phase, red). Various photic and non-photic stimuli can either advance (+) or delay (-) the central clock when administered at different times in the cycle, often summarised as phase response curves (green). Both nocturnal and diurnal animals show the same window of sensitivity to photic signals (largely during the anticipated dark phase) and an equal pattern of response.

1.2.1.2 Non-photic entrainment

Additional modulation of the firing rate of SCN neurons can be achieved via non-photic pathways. Innervation from the intergeniculate leaflet (IGL) of the thalamus (neuropeptide Y/GABAergic) and median raphe (serotonergic) are inhibitory and suppress *Per* expression in the SCN (Piggins & Guilding 2011; Maywood et al. 2002), whilst the hormone melatonin can activate receptors in the SCN directly to phase shift firing rhythms (Dubocovich et al. 2005).

In addition to the neurotransmitters and neuropeptides, behavioural rhythms can also be affected by metabolic status and animals can entrain to restricted food access. Interestingly, this type of entrainment does not affect clock gene expression in the SCN (Damiola et al. 2000). This has prompted investigations into the existence of a separate oscillator, termed the food-entrainable oscillator (FEO), which may coexist

with the SCN and drive the circadian rhythm should the light → SCN system cease to function or should restricted food access become the most important factor to time (Blum et al. 2012).

1.2.2 Pace of the molecular oscillator

Post-translational modifications play a key role in determining the pace of the molecular clock. A simple transcription-translation feedback loop could complete a cycle in a few hours; a fraction of the time taken by the circadian clock (Kwon et al. 2011; Kalsbeek et al. 2012). Other factors must therefore influence the system to lengthen the period to 24hrs. To date, proteins mediating acetylation, phosphorylation, SUMOylation, and ubiquitination have all been found to interact with the clock to regulate period (Kwon et al. 2011; Lee et al. 2001). Of these proteins, the casein kinase enzymes CK1ε and CK1δ are particularly important in the regulation of clock speed, phosphorylating PER proteins and promoting degradation. The tau mutation of CK1ε ($Ck1\varepsilon^{Tau}$), which causes a gain-of-function, accelerates the clock speed in mice and hamsters, reducing the free-running period to around 20 hours. In accordance with this, pharmacological inhibition of CK1δ lengthens the period by approximately 8 hours, and is accompanied by an increase in PER stability (Meng et al. 2010).

1.2.3 Outputs of the circadian oscillator system

The circadian clock has multiple outputs, ranging from promoting and inhibiting gene expression to driving behavioural rhythms and hormone secretion (Panda & Hogenesch 2004). The most obvious rhythmic output is that of the sleep-wake cycle, but it is interesting to note that the phase of the SCN is comparable in diurnal and nocturnal animals, yet their activity patterns clearly differ. Thus, interpretation of SCN-derived signals also plays a key role in determining the end output of the clock (Dibner et al. 2010).

1.2.4 The circadian hierarchy

The mammalian clock is organised in a hierarchical manner, with the SCN as the master pacemaker. The molecular clockwork resides in many tissues, but, unlike the SCN, these peripheral clocks cannot maintain synchronised oscillations for more than a few days without a synchronising agent. Early work showed that when the

SCN is lesioned, animals are rendered arrhythmic as the peripheral clocks lose their endogenous co-ordinating signals (Moore & Eichler 1972). Rhythmicity of behaviour can be restored with the transplant of a new SCN, but this is not necessarily reflected in other outputs, such as the endocrine rhythms of glucocorticoid and melatonin production (Meyer-Bernstein et al. 1999). The precise mechanism by which peripheral clocks and rhythms are synchronised with the SCN is still debated, but there is strong evidence for both humoral and neural input (Stratmann & Schibler 2006; Dibner et al. 2010).

1.2.4.1 Synchronisation of peripheral oscillators

The SCN has direct neural connections with a range of brain areas, including the subparaventricular zone, the paraventricular nucleus and the arcuate nucleus. Neural connections are key mediators in synchronising neuroendocrine rhythms, as SCN grafts do not restore these rhythms once they have been abolished. However, circadian rhythms of behaviour do not require this neural connection and diffusible factors were able to promote rhythmicity following an SCN graft in arrhythmic cryptochrome deficient mice (Sujino et al. 2003). Circadian rhythms in the liver and kidney can also be re-instated in SCN-lesioned mice via non-neuronal signals, indicating that humoral factors must also be able to synchronise some peripheral clocks (Guo et al. 2006).

Metabolism of glucose, fatty acids and cholesterol are regulated by the circadian clock, and restricted access to food can reset peripheral clocks, possibly by altering the redox state of the cell (Stratmann & Schibler 2006). Circulating hormones also play a role in peripheral clock synchronisation, with the glucocorticoid dexamethasone able to synchronise *Per1* expression in peripheral cells via activation of the glucocorticoid receptor (GR), although the SCN itself remains insensitive to this signal as no detectable GR expression is present in this region (Balsalobre et al. 2000). Glucocorticoid rhythms can also affect the speed with which peripheral clocks entrain to a new temporal schedule, whether that schedule is a light:dark cycle or restricted food access (Le Minh et al. 2002; Kiessling et al. 2010). Peripheral clocks remain sensitive to this hormone throughout the circadian cycle, and so glucocorticoid signalling appears to be a key mechanism by which the central clock can influence peripheral rhythms (Balsalobre et al. 2000).

The relative contributions of neural and humoral signalling mechanisms were investigated by Mahoney et al. (2010), who induced split rhythms in golden hamsters and measured clock gene expression in peripheral tissues. In hamsters, exposure to continuous light (LL) leads to a dissociation between the clockwork in the left and right suprachiasmatic nuclei. This causes the different sides of the brain to be tuned to different times, which could be reflected in the clock gene expression in the contralateral component of bilateral organs. If the neural signal was the predominant synchroniser, then splitting should also induce dissociation between the phases of the peripheral clocks as neural signals should innervate the contralateral component only. As humoral signals pass through the blood, which does not discriminate between left and right sides of the body, if this is the main way in which peripheral clocks are entrained then splitting should affect both components equally.

Significant asymmetry in *Per1* expression was observed in the SCN of the split hamsters, confirming that the procedure had successfully induced a split molecular rhythm in the master clock. Asymmetry was also observed in some peripheral organs, although the extent of this was tissue-specific and suggests that the degree of neural control varies between organs (Mahoney et al. 2010).

No consensus has yet been reached upon how peripheral clocks are entrained by the master pacemaker. The general mechanism of humoral vs. neural signalling appears to vary from tissue to tissue and, given how detrimental asynchrony can be to the body (Castanon-Cervantes et al. 2010; Bechtold et al. 2010), there may well be multiple methods employed to ensure synchrony is achieved. In this project, the role of glucocorticoid receptor signalling will be investigated as this pathway is also known to influence inflammatory pathology and may mediate some of its anti-inflammatory effects through the clock (Tronche et al. 1998). It is worth bearing in mind, however, that these receptors are unlikely to be the sole pathways by which peripheral clock synchrony can be influenced in any one tissue.

1.3 Circadian rhythms in inflammation

Rhythmic outputs of the circadian system have already been well-characterised in behaviour, hormone concentrations and metabolism (Panda & Hogenesch 2004), and there is mounting evidence linking circadian disruption with immune dysfunction (Castanon-Cervantes et al. 2010; Nakamura et al. 2011; Gibbs et al. 2012).

1.3.1 Clinical evidence of rhythmic inflammation

Inflammatory symptoms in conditions such as asthma and rheumatoid arthritis commonly fluctuate over a 24hr period. This rhythm is not simply a reflection of our sleep-wake cycles, however, and is instead linked to an underlying endogenous rhythm driven by the circadian clock (Spengler & Shea 2000; Cutolo & Straub 2008; Burioka et al. 2010). In healthy people, serum concentrations of pro-inflammatory factors such as interleukin-6 (IL-6) vary throughout the day. Peak concentration is reached at approximately 6AM, early in the active phase, but this rapidly drops over the next 3 hours. In rheumatoid arthritis, however, not only are the concentrations of IL-6 higher, but the circadian pattern is altered and the early-morning surge takes longer to dissipate. This is manifest as an increase in joint pain and stiffness during these hours (Cutolo & Straub 2008). Similarly, lung function varies across the day, even in non-asthmatics (Spengler & Shea 2000), but additional factors further reduce this at a time when lung function is at its lowest, exacerbating symptoms (Burioka et al. 2010).

In response to the increasing awareness of symptom variability across a day, more investment has been made in designing drugs and treatment regimen to deliver active components at the time they are most required. This approach, termed ‘chronotherapy’, serves to optimise treatment efficiency – reducing the concentration of drug required and thereby reducing the risk and/or severity of side effects (Burioka et al. 2010). Circadian regulation of drug efficacy has already been shown for traditional inflammatory disorders and treatments, such as use of glucocorticoid agonists in treating asthma and rheumatoid arthritis (Beam et al. 1992; Buttgereit et al. 2010), and also for chemotherapy agents such as gemcitabine (Iwata et al. 2011). Treatment at the right time resulted in decreased discomfort from adverse effects and/or increased relief from symptoms, increasing the therapeutic index of the drug.

This not only serves to better treat the diseases in question but also increases the likelihood of patient adherence to treatment schemes (Kaur et al. 2013).

1.3.2 Circadian disruption and inflammation

In addition to the evidence from patients in the clinic, experimental data has shown that environmental disruption of the circadian clock can exacerbate inflammation (Castanon-Cervantes et al. 2010). Using a protocol which mimics chronic jet lag, Castanon-Cervantes et al. subjected mice to multiple 6hr advances of the external light-dark cycle - replicating flights eastwards across 6 times zones each time (the equivalent of a trip from New Orleans to London) - over a period of four weeks. After being allowed to adjust to the final light-dark cycle for one week, shifted and un-shifted mice were challenged with a high dose of lipopolysaccharide (LPS); a component of the outer membrane of gram-negative bacteria and a ligand of the innate immune receptor toll-like receptor 4 (TLR4). Upon binding to TLR4, LPS triggers the production and secretion of pro- inflammatory cytokines, including IL-6, from innate immune cells such as the macrophage (figure 1.3).

Although mice successfully re-entrained to the new light-dark cycle after the repeated shifts, survival rates after injection of 12.5mg/kg LPS (intraperitoneal, i.p.) were drastically reduced for mice shifted 4 times over the 4-week period in comparison to un-shifted mice. The risk of death for mice shifted 4 times was '5.7x higher than [un-shifted] controls' (Castanon-Cervantes et al. 2010), illustrating a clear negative consequence of chronic circadian disruption.

Further investigation by the group showed that in mice shifted 4 times, significantly higher concentrations of the macrophage-derived pro-inflammatory cytokines IL-6, interleukin-18 (IL-18), macrophage inflammatory protein-2 (MIP-2) and leukaemia inhibitory factor (LIF) were found in serum samples taken 24hrs after challenge, even with a lower LPS dose of 5mg/kg. This elevated production was not simply caused by larger numbers of macrophages in the peritoneal cavity, and was instead due to a heightened response of the cells in the 4x-shifted mice, indicating that the chronic jet lag protocol made the macrophages more sensitive to the LPS challenge. Whilst very few people are likely to be subjected to jet lag in this way, these results

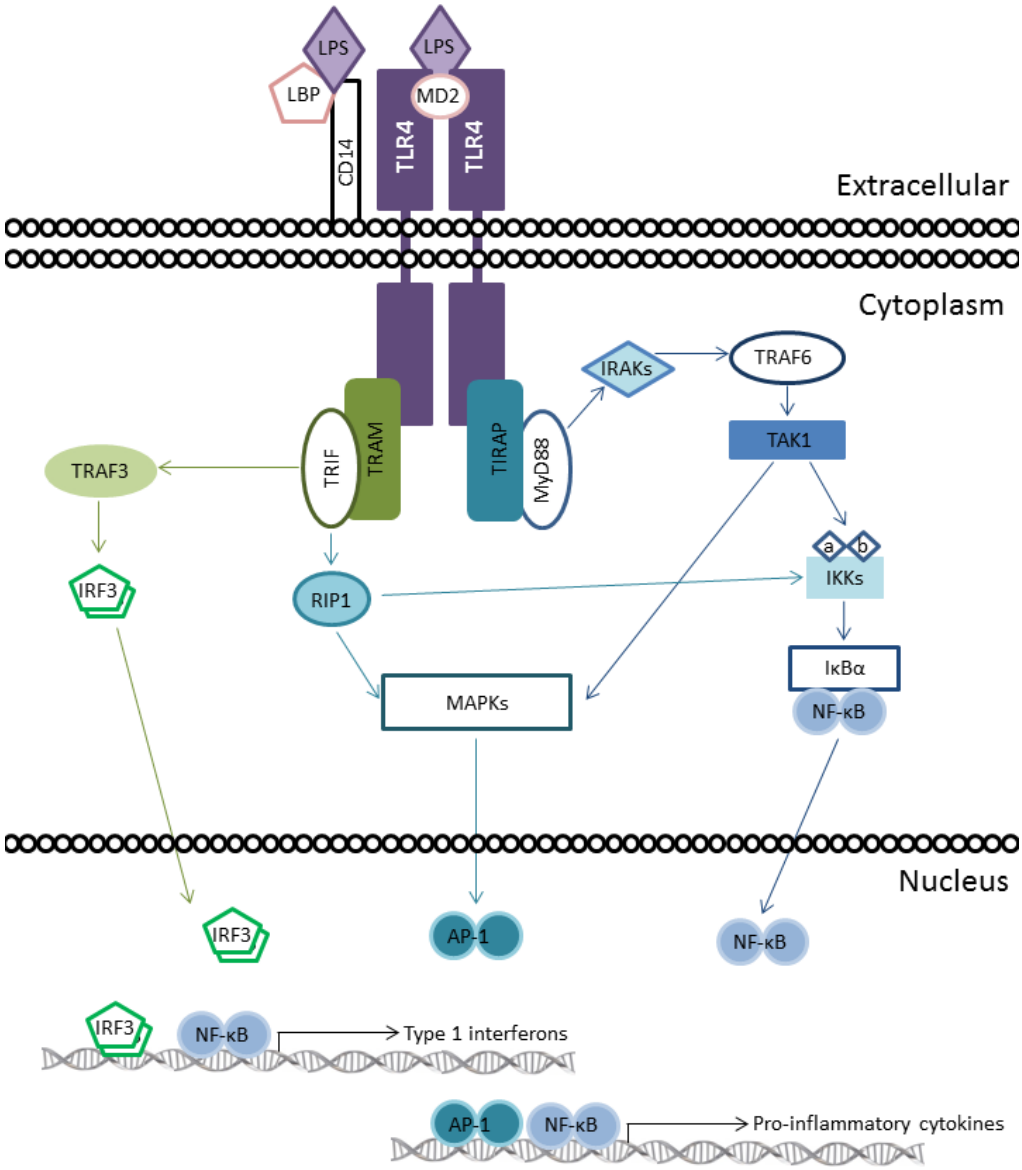

Figure 1.3: Signalling pathway of lipopolysaccharide-induced cytokine production

Lipopolysaccharide (LPS) binds to LBP, which enables interaction with CD14 and the TLR4/MD2 complex on the surface of cells. This triggers receptor dimerization and activation of intracellular signalling pathways. The TIRAP/MyD88 pathway (dark blue arrows) causes release of NF-κB from its regulatory molecules and activates AP-1 via MAPKs. The TRAM/TRIF pathway (green & teal arrows) can also activate AP-1 and NF-κB, via RIP1, along with IRF3. Activation of TLR4 therefore leads to induction of pro-inflammatory cytokines and type 1 interferons.

AP-1 – activator protein 1, CD14 – cluster of differentiation 14, IκBα - NF-κB inhibitor α, IKKs – IκB kinases, IRAKs – interleukin-1 receptor-associated kinases, IRF3 – interferon regulatory factor 3, LBP – LPS binding protein, LPS – lipopolysaccharide, MAPKs – mitogen-activated protein kinases, MD2 – lymphocyte antigen 96, MyD88 – myeloid differentiation primary response gene 88, NF-κB – nuclear factor-κB, RIP1 – receptor-interacting protein 1, TAK1 – transforming growth factor-β-activated kinase 1, TIR – toll-interleukin-1 receptor, TIRAP – TIR domain-containing adaptor protein, TLR4 – toll-like receptor 4, TRAF6 – tumour necrosis factor receptor-associated factor 6, TRAM – TRIF-related adaptor molecule, TRIF – TIR domain-containing adaptor inducting interferon β. Adapted from Lu et al. 2008.

have wider implications given the discrepancy between the phase of our internal circadian oscillations and work schedules in situations such as shift work. This experiment showed a clear link between circadian disruption via manipulation of the external environment and aberrant inflammation.

1.3.3 Clocks in immune cells

The severe disruption caused by jet lag paradigms are thought to not only be due to a general desynchrony with the external light:dark cycle, which has shifted unexpectedly, but also internal desynchrony between peripheral oscillators. Almost all cell types possess a molecular clock, and some tissues may switch to a new time zone more quickly than others, leading to processes being misaligned for multiple days until all tissues are re-entrained to the new schedule.

Many of the immune cells have already been investigated and show functional molecular clocks and circadian rhythms (Keller et al. 2009; Fortier et al. 2011; Nakamura et al. 2014; Fonken et al. 2015). In addition, the numbers of circulating haematopoietic stem cells and mature leukocytes are also rhythmic, peaking during the rest phase. Release of immune cells from the bone marrow is under circadian control, regulated by adrenergic signalling through the sympathetic nervous system (Scheiermann et al. 2012).

Recruitment of immune cells to tissues is also under circadian control, but is generally in anti-phase to the peak circulating numbers, occurring during the active phase. The rhythmic migration to tissue is also regulated by adrenergic signalling, in conjunction with tissue-specific rhythmic expression of adhesion molecules which facilitate transmigration (Scheiermann et al. 2012). It is therefore not surprising that immunological responses may vary according to time of day, and that clock disruption may uncouple this normally tight regulation to have detrimental effects. An additional aspect of chronotherapy could therefore also involve a subset of drugs designed to target clock disruption or clock proteins to ameliorate inflammatory symptoms (Antoch et al. 2005).

1.3.4 Timed inflammatory challenges

A further line of evidence for the role of circadian rhythms in regulating inflammation comes from studies using timed challenges to target the immune system. Circadian rhythms in sensitivity to immune challenge have been known for some time (Halberg et al. 1960), but the mechanistic links between the phase of the circadian cycle and severity of inflammatory response are just beginning to be uncovered. A recent paper from our lab has shown that a subset of cytokines are differentially induced after an intraperitoneal LPS challenge at different times of day (Gibbs et al. 2012). Using a non-lethal dose of LPS, 1mg/kg, mice were injected at either CT0 or CT12 (the start of the resting phase or active phase, respectively) and serum samples taken 4hrs later. In response to the LPS challenge, serum concentrations of the pro-inflammatory cytokines IL-6, interleukin-12 (IL-12), chemokine ligand 5 (CCL5 also known as 'regulated on activation, normal T cell expressed and secreted' or RANTES) and chemokine C-X-C motif ligand 1 (CXCL1) were significantly higher after challenge at CT12 compared to challenge at CT0. This circadian variation (or temporal 'gating') was lost when the core clock gene *Bmal1* was selectively disrupted in macrophages or upon global loss of the clock gene *Rev-erbα*. Interestingly, the loss of gating did not reduce serum concentration of IL-6 to average levels at both time points – rather, the response observed after CT0 challenge was elevated and comparable with the response at CT12, indicating that the clock appears to have a suppressive effect on this type of inflammatory response.

In addition to the macrophage-mediated innate immune response, probed using LPS challenge, investigations into circadian regulation of inflammation have also targeted the Immunoglobulin E (IgE)-mediated allergic response (Nakamura et al. 2011). In this study, mice were sensitised subcutaneously with IgE and then challenged intravenously 24hrs later with a cross-linking agent to promote an allergic reaction in the sensitised area. The intravenous injection vehicle included a dye, which was used to visualise vascular permeability (a measure of the inflammatory response) 30 minutes later. These challenges were performed at one of four time points – ZT4 (early-mid rest/light phase), ZT10 (late rest/light phase), ZT16 (early-mid active/dark phase) and ZT22 (late active/dark phase) – and in wild-type mice a significantly lower degree of vascular permeability was observed

in response to challenge at ZT16 than at any other time, indicating a lower inflammatory response. However, this time-of-challenge effect was lost in *Per2*$^{m/m}$ mice, which have a loss-of-function mutation in the clock gene *Per2*. Nakamura et al. proceeded to hypothesise that this disrupted rhythm was linked to the disrupted corticosterone rhythms in these mice, and implicated glucocorticoids in mediating the rhythmic inflammatory response in wild-type animals.

1.4 Glucocorticoids

Glucocorticoids are a family of steroid hormones produced in the adrenal glands. The glands themselves are segregated into four distinct zones (figure 1.4A) – the inner medulla and three layers which comprise the outer cortex: the zona reticularis (ZR, closest to the medulla), the zona fasciculata (ZF, central) and the zona glomerulosa (ZG, furthest from the medulla). Cells in each cortical layer preferentially express different enzymes, resulting in a distinct pattern of hormone biosynthesis where each layer produces a subset of hormones. For example, adrenal androgens are produced in the ZR, whereas mineralocorticoids are produced in the ZG. Glucocorticoids, such as cortisol or corticosterone, are produced in the ZF (McKay & Cidlowski 2003).

The steroidogenic pathway by which glucocorticoids are produced begins with the transfer of cholesterol to mitochondria by the steroidogenic acute regulatory protein (StAR) (figure 1.4B). This is the rate-limiting step of the entire reaction (Stocco & Clark 1996). Once inside a mitochondrion, cholesterol is transformed into pregnenolone by cholesterol side-chain cleavage enzyme (encoded by the *CYP11A1* gene). Pregnenolone is then metabolised into corticosterone, the major acting glucocorticoid in rodents, in three stages, with progesterone and deoxycorticosterone formed in the intermediate steps. The major human glucocorticoid, cortisol, is formed in a similar series of reactions, mediated by the same enzymes. Conversion into the cortisol pathway can occur at either the pregnenolone or progesterone stages by the 17α-hydroxylase enzyme (encoded by the *CYP17A1* gene). This enzyme converts pregnenolone into 17α-hydroxypregnenolone and progesterone into 17α-hydroxyprogesterone. 17α-hydroxypregnenolone can also be converted into 17α-hydroxyprogesterone, which is then metabolised into 11-deoxycortisol and finally into cortisol.

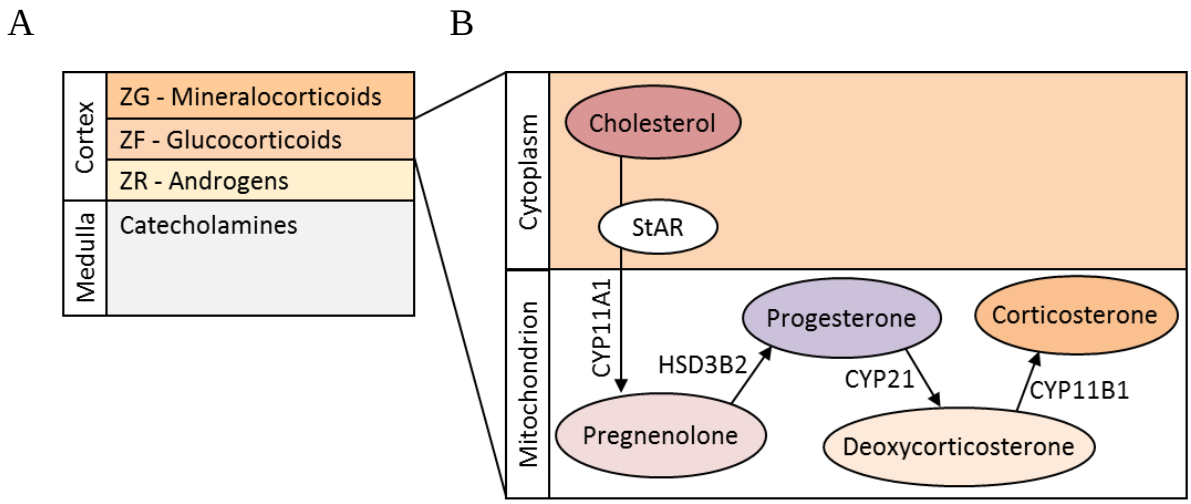

Figure 1.4: Steroid biosynthesis in the adrenal cortex
A) The adrenal cortex is split into three distinct layers, each producing a subset of steroid hormones. Mineralocorticoids are produced in the zona glomerulosa (ZG), glucocorticoids are produced in the zona fasciculata (ZF) and adrenal androgens are produced in the zona reticularis (ZR). B) Steroidogenic acute regulatory protein (StAR) mediates the transfer of cholesterol from the cytoplasm to the mitochondria, enabling steroidogenesis to occur. The pathway shown is that of corticosterone.
CYP11A1 - cholesterol side chain cleavage monooxygenase; CYP11B1 - 11β-hydroxylase; CYP21 - 21-hydroxylase; HSD3B2 - 3β-hydroxysteroid dehydrogenase, StAR – steroidogenic acute regulatory protein, ZF – zona fasciculata, ZG – zona glomerulosa, ZR – zona reticularis.

1.4.1 The glucocorticoid receptor and inflammation

Glucocorticoids have long been recognised as potent anti-inflammatory agents. Activation of the glucocorticoid receptor (GR) promotes processes which increase the available energy supply, such as feeding, gluconeogenesis and lipolysis. Competing energy-consuming functions, including immune and reproductive systems, are simultaneously inhibited. This signalling is important for homeostatic maintenance and cell proliferation/differentiation, but the ability to quickly elevate energy production is also key to the stress response (Tronche et al. 1998).

Like all nuclear hormone receptors, GR possesses an N-terminal regulatory domain (which enables the recruitment of cofactors), a DNA-binding domain, hinge region, ligand-binding domain and C-terminal domain. Both the DNA-binding domain and ligand-binding domain contain nuclear localisation signals which facilitate migration to the nucleus upon ligand binding. Three main variants are known in humans; GRα, GRβ and GRγ. GRα and GRβ are generated by alternative splicing of exon 9 and differ in their C-terminal domains (Kadmiel & Cidlowski 2013). GRγ is a result of an insertion of an arginine at position 453, which resides in the DNA binding domain (Rivers et al. 1999).

The dominant form of GR is GRα, which itself exists in multiple isoforms due to altered translation initiation sites within exon 2 (Kadmiel & Cidlowski 2013). GRβ, with its altered C-terminal, can act as a dominant-negative GRα inhibitor by antagonizing GRα-mediated transcriptional repression (Taniguchi et al. 2010). The balance of these two isoforms is critical for appropriate glucocorticoid sensitivity, with recent evidence showing that alterations in the ratio of GRα:GRβ is associated with methotrexate-induced glucocorticoid sensitisation and mood disorders (Gross & Cidlowski 2008). GRγ forms approximately 5-6% of total GR and may simply be a reflection of ‘leaky’ splicing but may also have a dominant-negative function with respect to gene repression by GRα activation (Stevens et al. 2004; Taniguchi et al. 2010). The pathophysiological relevance of each glucocorticoid receptor variant requires further investigation, but is beyond the scope of this project. Instead, the focus will be on the dominant GRα isoform, with considerations for how GRβ and GRγ may also be affected or may influence results.

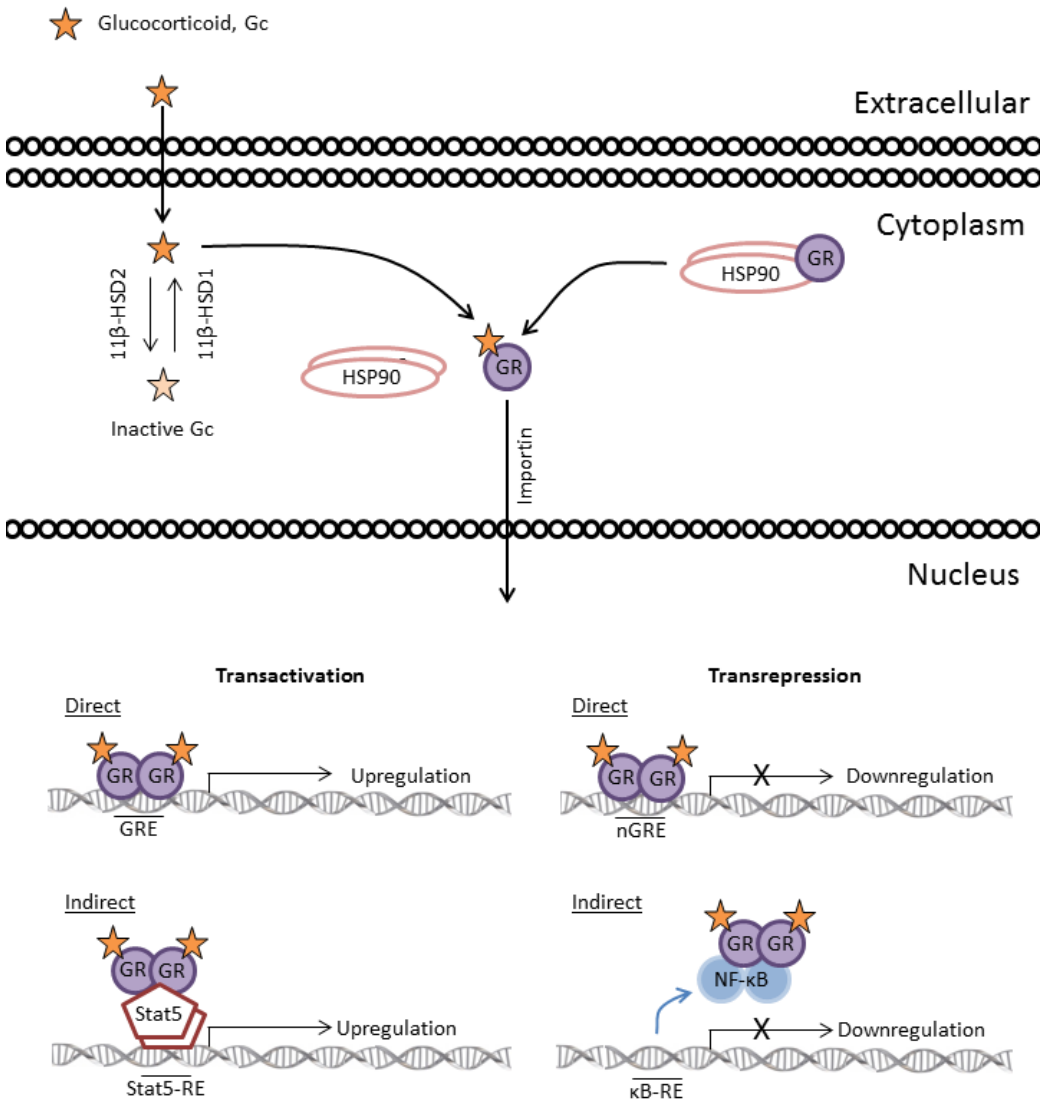

Figure 1.5: Glucocorticoid receptor signalling

Glucocorticoids (Gcs) are lipophilic, and can pass through the cell membrane. Once inside the cytoplasm, Gcs may be inactivated by the enzyme 11β-HSD2. Conversely, inactive Gcs can be activated by the 11β-HSD1 enzyme. This pairing of reactions allows cells to fine tune the effects of Gc exposure. Active Gcs bind to the glucocorticoid receptor (GR), releasing it from its chaperone complex which includes a heat shock protein 90 (HSP90) dimer. The Gc-GR complex is then transported into the nucleus via importin and can exert multiple effects upon transcription. Both direct and indirect transactivation result in upregulation of affected genes; direct transactivation requires GR to bind as a homodimer to GR response elements (GREs) in the genome, whereas indirect transactivation is mediated by binding of the GR dimer to additional transcription factors bound at their own response elements (e.g. Stat5). Similarly, direct and indirect transrepression can occur; direct transrepression requires binding of GR to negative GREs, whilst indirect transrepression sees GR dimers binding to other transcription factors and preventing them from binding to their response elements.

11β-HSD1 - 11β-hydroxysteroid dehydrogenase 1, 11β-HSD2 - 11β-hydroxysteroid dehydrogenase 2, AP-1 – activator protein 1,GR – glucocorticoid receptor, GRE – GR response element, HSP90 – heat shock protein 90, κB-RE – NFκB response element, NF-κB – nuclear factor-κB, , nGRE – negative GRE, Stat5 – signal transducer and activator of transcription 5, Stat5-RE – Stat5 response element.

At the molecular level, GRα has both direct and indirect effects on gene expression (figure 1.5). Upon activation via ligand-binding, the GR is released from a chaperone complex and can translocate from the cytoplasm to the nucleus of the cell. The active GR can then dimerize and bind to positive glucocorticoid response elements (GREs) or to negative glucocorticoid response elements (nGREs) in the promoter regions of genes to directly promote (via GRE binding) or inhibit (via nGRE binding) gene expression. Indirect effects on gene expression are exerted via binding to other transcription factors, such as nuclear factor κB (NF-κB), activator protein 1 (AP-1) or signal transducer and activator of transcription 5 (Stat5), or by competing for common co-factors (Tronche et al. 1998). The anti-inflammatory effects of GR signalling are generally achieved through indirect transrepression (Gross & Cidlowski 2008).

Post-translational modifications and the recruitment of cofactors are highly important in mediating the effects of GR activation. Repressive cofactors such as NCoR1 (nuclear co-repressor 1) and SMRT (silencing mediator for retinoid or thyroid-hormone receptors) can recruit histone deacetylases (HDACs) which can modulate chromatin structure and down-regulate gene expression (Chen & Evans 1995). Co-activator complexes which include histone acetyltransferases such as GRIP1 or methyltransferases such as Merm1 can lead to positive chromatin remodelling, enabling access for transcription machinery (Jangani et al. 2014).

Whilst chromatin was previously thought of as merely a way of packaging DNA, it is becoming more and more evident that the organisation of DNA wrapped around histones (forming nucleosomes) allows tight regulation of access to DNA in a cell-specific and time-specific manner. How tightly the DNA is wound, and the extent of DNA-histone interactions can regulate how easily transcription factors can access their binding sites and exert their effects. Multiple mechanisms exist for modulating the DNA-histone binding affinity (Voss & Hager 2014), including replacement of classical histones with less stable variant histones, sliding of histones along DNA to expose regions of ‘open’ chromatin, co-ordinated binding of multiple transcription factors and binding of ‘pioneer’ factors which can mimic nucleosome components and open up new sites for other transcription factors to bind (figure 1.6).

The ability of transcription factors to manipulate chromatin accessibility is of particular relevance to this project, as both GR and circadian clock proteins are known to alter chromatin accessibility. GR associates with remodelling complexes and manipulates the chromatin architecture in a process known as 'assisted loading' (figure 1.6E). In this situation, the transcription factor (GR) recruits a remodelling complex via protein-protein interactions which can alter the strength of DNA-histone binding (i.e. how tightly the DNA is wound) through a combination of acetylation and/or methylation of the DNA or histones. This facilitates further binding by opening up additional transcription factor response elements (Miranda et al. 2013).

In contrast, chromatin modification by the molecular clockwork appears to be through the action of the CLOCK-BMAL1 heterodimer as a pioneer factor (figure 1.6F). In this model, rhythmic binding of CLOCK-BMAL1 promotes rhythmic alterations in chromatin structure, including nucleosome removal and incorporation of the variant histone H2A.Z, particularly in the gene bodies and enhancer sites (Menet et al. 2014). Once these chromatin regions are 'open' transcription factors, such as GR, can bind to their response elements, and so a time-of-day effect in the ability of these transcription factors to exert their effects is generated.

Functional readouts of altered chromatin accessibility can be obtained by utilising chromatin immunoprecipitation (ChIP) to target specific markers of activation or direct chromatin assays such as FAIRE-seq, ATAC-seq or DNase-seq to detect 'open' regions (Tsompana & Buck 2014). In the case of GR, it has been shown that treatment of NIH3T3 and N2A cell lines with dexamethasone increases histone 3 lysine 4 tri-methylation (H3K4Me3) and histone 3 lysines 9/14 acetylation (H3K9/14Ac) at the transcription start sites and GREs in the known Gc up-regulated genes *Sgk1* (serum and glucocorticoid regulated kinase 1) and *Per1*. These chromatin modification markers were associated with an increase in mRNA for these genes, showing a direct correlation between the 'active' markers, RNA polymerase recruitment and gene expression (Xydous et al. 2014).

Similar advances have been made in profiling the temporal dynamics of chromatin accessibility, with a recent study utilising ChIP in mouse liver across a circadian cycle to assess histone modifications and RNA polymerase recruitment. In this paper, ChIP-seq revealed time-of-day variation in RNA polymerase II occupancy along with robust rhythms of the poised enhancer markers H3K4Me3 and H3K9Ac and the active enhancer marker histone 3 lysine 27 acetylation (H3K27Ac) at transcription start sites (Koike et al. 2012).

In addition to a potential role for the circadian clock in regulating chromatin accessibility and therefore access to GR binding sites, direct interactions between the molecular clock and the glucocorticoid receptor are also critical for some GR functions. The core clock proteins cryptochrome 1 (CRY1) and cryptochrome 2 (CRY2) have recently been shown to regulate transcriptional effects of GR activation (Lamia et al. 2011). In *Cry1*$^{-/-}$;*Cry2*$^{-/-}$ (double knockout) mice, the loss of CRYs dramatically alters the range of genes up- and down-regulated by dexamethasone treatment. CRY deficiency increases the number of up-regulated genes and decreases the number of repressed genes, shifting the polarity of GR signalling towards gene activation. This has strong implications for the metabolic side effects of Gc therapy, which are largely driven by GR up-regulation of gluconeogenic genes. Accordingly, *Cry1*$^{-/-}$;*Cry2*$^{-/-}$ mice exhibited impaired glucose tolerance and constitutively high serum corticosterone, both markers of metabolic syndrome (Lamia et al. 2011).

However, the disruption of GR signalling in the *Cry* double knockouts appeared to exclude the suppressive effects of GR upon the pro-inflammatory NF-κB network. Whilst *Cry1*$^{-/-}$;*Cry2*$^{-/-}$ bone marrow-derived macrophages showed higher basal expression of some pro-inflammatory cytokines (interleukin-6, monocyte chemoattractant protein 1 and inducible nitric oxide synthase), these cytokines were comparably suppressed by dexamethasone in *Cry1*$^{-/-}$;*Cry2*$^{-/-}$ cells and wild type littermate controls. Expression of tumour necrosis factor α (*Tnfα*) and chemokine (C-C motif) ligand 4 (*Ccl4*) showed no difference between genotype in either basal, LPS-stimulated or dexamethasone-treated conditions (Lamia et al. 2011).

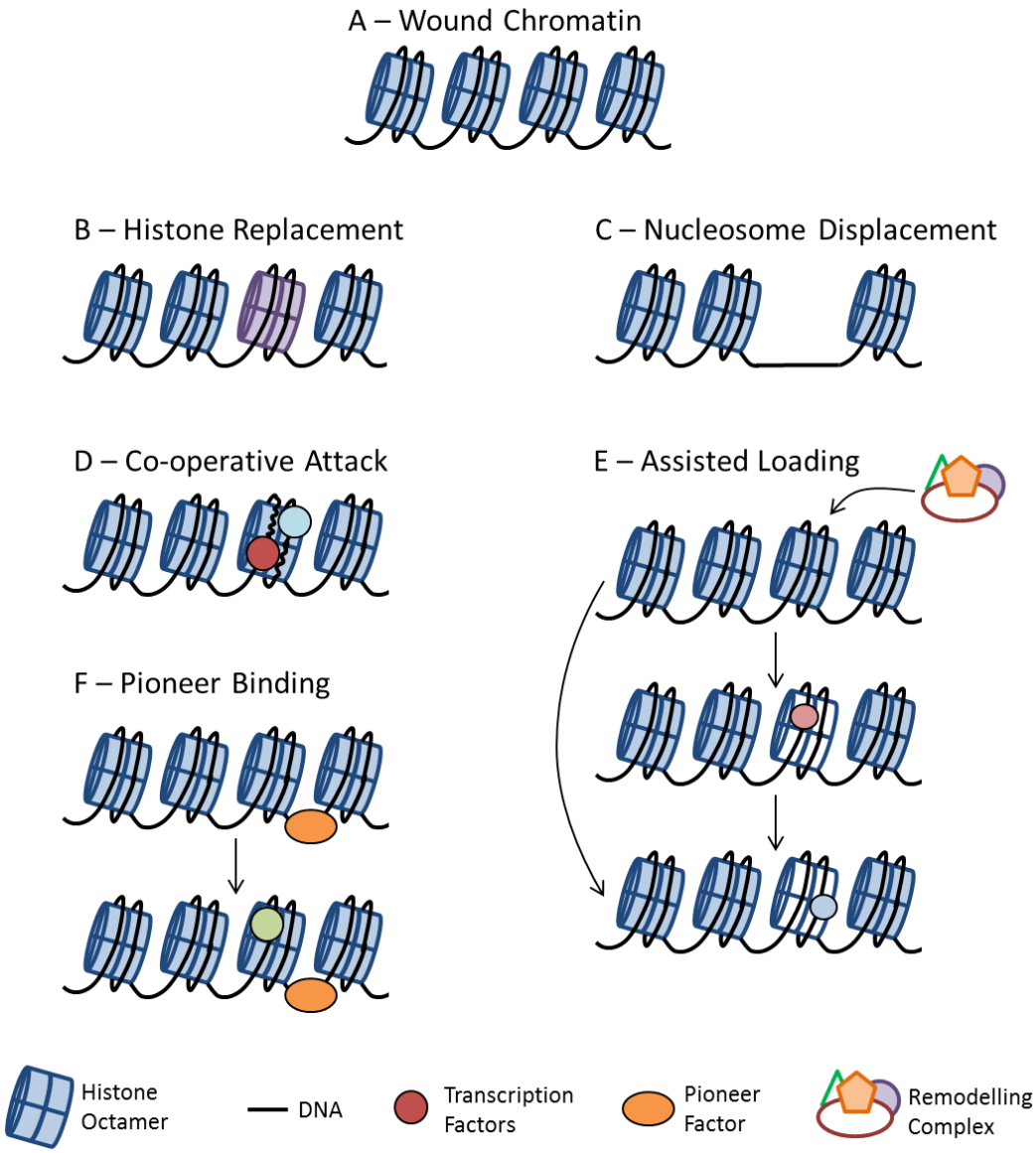

Figure 1.6: Chromatin remodelling

A) Chromatin is held in a wound state as nucleosomes; DNA wrapped around histone octamers. Connections between the DNA and histones regulate how accessible sequences are for transcription machinery. Accessibility can be altered in numerous ways, illustrated in B-F. B) Histone replacement – the histone octamer usually consists of the core histones H2A, H2B, H3 and H4 (two of each). However, histone H2A can be replaced by the variant histones H2AZ or H2AX, and H3 can be replaced by H3.3. Alteration of the histone make-up of the nucleosome results in altered DNA-histone interactions, which affects nucleosome stability. C) Nucleosome displacement – sliding or displacement of entire nucleosomes will leave sections of DNA accessible for transcription factor binding. D) Co-operative attack – co-ordinated action of two transcription factors may overcome the energy required to re-organise chromatin. E) Assisted loading – remodelling complexes may be recruited by transcription factors, creating transient local modifications which open windows for transcription factor binding (sequentially or individually). F) Pioneer binding – some proteins ('pioneers') may interact with closed chromatin, effectively opening a region of chromatin which facilitates binding of other transcription factors.

Figure and legend adapted from Voss & Hagar (2014).

Isolating the beneficial anti-inflammatory effects from the adverse metabolic effects of GR activation is an area of active research, which aims to generate dissociated GR agonists (DIGRAs, also known as selective GR agonists or SEGRAs), and this novel finding provides one mechanism by which similar results may be obtained. By using CRY stabilisers or treating patients when CRY is at its peak, it may be possible to reduce some of the metabolic side-effects of Gc therapy whilst maintaining anti-inflammatory efficacy (Lamia et al. 2011).

GR activity can also be modulated by post-translational modifications. The GR possesses multiple sites for post-translational modifications, including 8 serine residues that have been shown to undergo phosphorylation, 2 lysines which can be acetylated, and additional lysine residues which facilitate ubiquitination and SUMOylation (Kadmiel & Cidlowski 2013). Manipulation of these sites can lead to altered recruitment of HDACs, impaired nuclear translocation, and/or destabilisation of the GR protein, and are strongly implicated in glucocorticoid-resistant inflammation (Wallace & Cidlowski 2001; Mercado et al. 2012). GR signalling therefore has diverse transcriptional effects which depend upon available co-factors, post-translation modifications of the GR itself and accessibility of DNA binding sites, which may themselves be regulated by the circadian clock and local cellular environment.

In addition to genomic effects, more rapid non-genomic effects of GR signalling have also been reported. These effects are thought to be mediated by cytoplasmic or membrane-bound GR interaction with MAPK (mitogen activated protein kinase) pathways (Ayroldi et al. 2012). MAPKs control many physiological functions, including inflammatory signalling (figure 1.3), and are organised as phosphorylation cascades, where activation of one protein allows it to activate the next molecule in the pathway. Dysregulation of MAPK pathways is associated with various inflammatory disorders, including rheumatoid arthritis, asthma and psoriasis. The precise mechanisms of GR-MAPK interaction is still unclear, but it is known that due to the direct protein-protein interaction, some of these inhibitory functions are possible even when the DNA binding and dimerization abilities of GR are disrupted (Ayroldi et al. 2012).

Glucocorticoids are therefore potent suppressors of inflammation, albeit with additional metabolic effects through transcription activation, and it is not surprising that they are widely prescribed anti-inflammatory agents (Busillo & Cidlowski 2013). They are also key candidates for mediating rhythms in inflammatory responses due to their interactions with the molecular clock, ability to synchronise peripheral oscillators and their rhythmic endogenous secretion.

1.4.2 Rhythmic glucocorticoid production

The secretion of cortisol/corticosterone occurs in both a circadian and ultradian (shorter than a day) manner (Shiotsuka & Jovonovich 1974). The ultradian rhythm generates discrete pulses of release, which generates a circadian variation in circulating hormone concentration, with more sparse, smaller spikes of corticosterone concentration during the circadian trough and more frequent, larger ones during the peak in Lewis rats and a similar pattern observed in humans (Windle et al. 1998; Lightman et al. 2008). Peak concentrations occur at the start of the active phase; during the light phase (around CT/ZT0) for diurnal mammals, including humans, and during the dark phase (around CT/ZT12) for nocturnal mammals, such as rodents. These pulses are controlled by both humoral and neural inputs, via the hypothalamic-pituitary-adrenal (HPA) axis and the autonomic nervous system respectively. Stimulation of the HPA axis by stress results in the release of corticotropin releasing hormone (CRH) from paraventricular neurons in the hypothalamus. This hormone stimulates the pituitary gland, prompting the release of adrenocorticotropic hormone (ACTH). ACTH then acts upon the adrenal cortex to stimulate the production and release of glucocorticoids, which in turn inhibit the hypothalamus and pituitary, forming a negative feedback loop (Tronche et al. 1998).

Neural connections exist between the SCN and paraventricular nucleus, via the dorsomedial hypothalamus, indicating that the central pacemaker can modify firing rates of these hypothalamic neurons and influence adrenal outputs via the HPA axis (Dickmeis 2009). However, rhythmic activity of the HPA axis is not reflected in rhythmic levels of ACTH, suggesting that additional signals contribute to the production of the glucocorticoid rhythm (Kalsbeek et al. 2012).

Indirect neural connections from the SCN, via the periventricular nuclei, through the spinal cord and splanchnic nerve also link the central pacemaker and adrenal gland (Buijs et al. 1999). This autonomic innervation plays a key role in regulating adrenal sensitivity to ACTH and provides a second mechanism by which the SCN influences glucocorticoid production (Dickmeis 2009; Kalsbeek et al. 2012). By utilising this combination of methods, the SCN can tightly align the rate of glucocorticoid secretion with the external environment.

The adrenal can also be influenced by light exposure at both the level of clock gene expression (*Per2* in the adrenal is induced by light) and hormone production. The induction of corticosterone secretion by light is independent of ACTH and the stress axis, and occurs even during the subjective day, when the SCN molecular clock is insensitive to light pulses (Kiessling et al. 2014). The ability for light to entrain the adrenal directly, potentially circumventing the SCN altogether, illustrates the importance of this endocrine organ in orchestrating synchrony with the outside environment.

Genetic manipulations of SCN coupling and the molecular clockwork have also shed light upon the regulation of glucocorticoid synthesis. The neuropeptide VIP (vasoactive intestinal polypeptide) and its receptor, VPAC2, are essential for appropriate circadian function of the SCN, synchronising the clock neurons and maintaining coherent oscillations in action potential firing. In VPAC2 deficient mice, the SCN lacks synchrony and animals are rendered behaviourally arrhythmic in constant darkness (Maywood et al. 2006). In-keeping with a role for SCN regulation of corticosterone production, serum corticosterone concentrations in these animals were also arrhythmic in constant conditions and showed an unexpected phase advance even when housed in a light:dark cycle. The alterations in corticosterone were also present in adrenal clock gene expression (*Per1, Bmal1*) and expression of steroidogenic enzymes (Fahrenkrug et al. 2012). A loss of diurnal rhythmicity was also seen when faecal and plasma corticosterone concentration was measured in global *Bmal1*-deficient mice (Leliavski et al. 2014).

In addition, the adrenal glands themselves possess a semi-autonomous oscillator which influences the glucocorticoid rhythm by regulating its responsiveness to HPA and splanchnic input (Chung et al. 2011a; Leliavski et al. 2015). The CLOCK-BMAL1 heterodimer has been shown to bind to an E-box in the *StAR* promoter, directly influencing Gc production at the rate-limiting step (Son et al. 2008). Genetic manipulation of the adrenal clock using an anti-sense *Bmal1* construct driven by the adrenal-expressed MC2R promoter showed the importance of the adrenal intrinsic oscillator, as rhythms of StAR protein expression, corticosterone secretion and behaviour were severely dampened in constant darkness, but not in a light:dark cycle. These results show a role for the endogenous oscillator in generating a robust rhythm in Gc secretion under constant conditions, which can be masked or driven by light when in light:dark cycles (Son et al. 2008).

Thus, circadian regulation mediated by SCN control of both the HPA axis and autonomic innervation, plus the intrinsic adrenal oscillator and the potential for extra-SCN entrainment to light:dark cycles contribute to the generation of a robust circadian rhythm in glucocorticoid secretion (Dickmeis 2009). The convergence of these inputs upon the adrenal gland, illustrated in figure 1.7, suggests it is an important node in the circadian hierarchy and highlights glucocorticoids as key factors in relaying circadian signals to peripheral tissues.

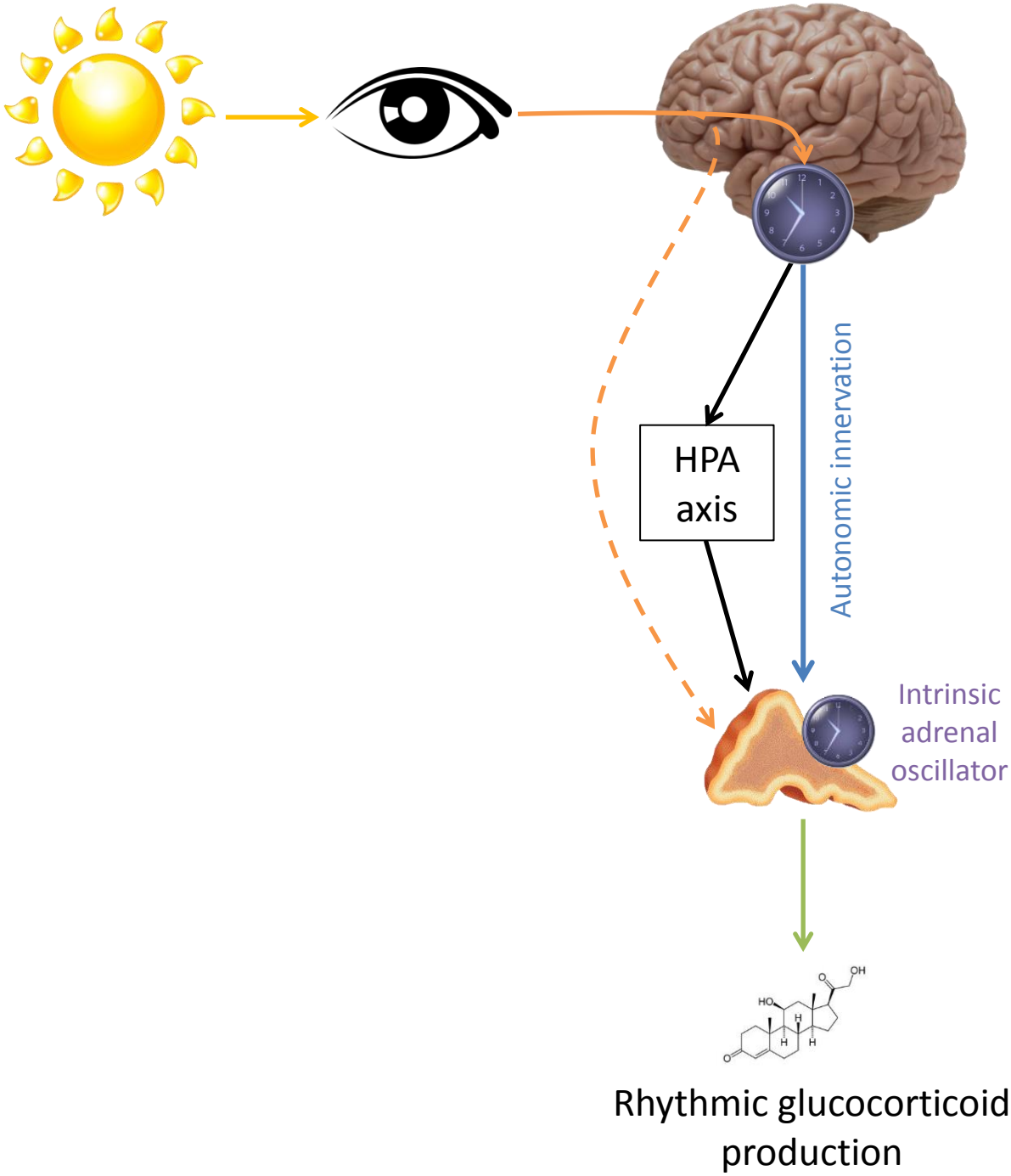

Figure 1.7: Factors regulating rhythmic glucocorticoid production.

Multiple regulatory inputs converge upon the adrenal glands to drive rhythmic production of glucocorticoid hormones. Light enters the eye, which signals through the retinohypothalamic tract to entrain the central clock in the brain, which in turn can influence the adrenal glands via HPA (hypothalamus-pituitary-adrenal) axis activity (black arrows) or autonomic innervation (blue arrow). Light is also proposed to indirectly influence the adrenal in a mechanism which may bypass the pacemaker altogether (dashed orange arrow) and the adrenals themselves possess an intrinsic oscillator (purple). Multiple inputs and redundancy implicates the adrenals as a critical node in the circadian hierarchy.

1.4.2.1 Extra-adrenal glucocorticoid synthesis

Whilst the majority of circulating glucocorticoids are produced by the adrenal glands, there is mounting evidence for extra-adrenal synthesis in tissues such as the lung, gut and skin, particularly in response to inflammatory challenge (Taves et al. 2011).

In the gut, for example, steroidogenic enzymes such as StAR, CYP11A1 and 3β-HSD (figure 1.4) have been detected in mouse gut epithelium, which can produce Gcs *de novo* (Cima et al. 2004). Similarly, CYP11A1 and CYP11B2 are present in human colon biopsies and human colonic tissue can produce cortisol when cultured (Sidler et al. 2011). Interestingly, this pathway is insensitive to ACTH stimulation but can be directly stimulated by TNFα, which may form a negative feedback loop in the regulation of gut immune homeostasis, which is dysregulated in colitis and inflammatory bowel disease (Kostadinova et al. 2014).

In other tissues, such as the lung and liver, synthesis of Gcs is dependent upon circulating factors, as local Gc production is abolished after adrenalectomy. This implicates the local conversion of inactive circulating hormones to active hormones via the 11β-HSD1 enzyme as the major regulator of pulmonary Gc synthesis. The lung can produce relatively large amounts of Gcs in response to LPS administration, but not after an allergic-type challenge with ovalbumin, demonstrating selectivity in which inflammatory pathways may stimulate Gc production (Hostettler et al. 2012). It remains unclear why the lung utilises the 11β-HSD1 pathway to locally activate circulating hormones despite simultaneously expressing the steroidogenic enzymes required to produce Gcs *de novo*.

The regulation of glucocorticoid production in extra-adrenal tissues is diverse, and there is little information regarding a diurnal pattern in extra-adrenal synthesis. Whilst adrenalectomy effectively abolishes circulating glucocorticoids in some animals (such as the rat), in others (including mice) it remains detectable in serum at a low, constant concentration (Dalm et al. 2008). Previously attributed to accessory adrenal cortical nodes (Hummel 1958), this may also reflect extra-adrenal production from additional tissues. Whilst the lack of fluctuation in

circulating concentration may appear to imply a constant rate of extra-adrenal production, it is also possible that different tissues are operating at different times, which would also give rise to a dampened circulating rhythm. Further investigations into circadian regulation of extra-adrenal glucocorticoid synthesis are required to more fully understand the local dynamics of Gc production in these tissues.

1.4.3 Glucocorticoid metabolism

Glucocorticoids are predominantly bound to corticosteroid binding globulin (CBG) in the bloodstream, which keeps the hormone inactive until contact is made with CBG receptors or cleavage enzymes. This allows delivery of free corticosteroids to specific tissues, whilst limiting the exposure of other organs to free steroids which can easily diffuse across cell membranes (Gross & Cidlowski 2008).

Intracellular ligand availability is also tightly regulated, with cells utilising the redox capacities of the 11β-hydroxysteroid dehydrogenase (11β-HSD) enzymes (figure 1.5). Active glucocorticoids are oxidised to form inactive glucocorticoids via 11β-HSD2, whilst 11β-HSD1 can reduce inactive steroids into active forms again. This regulation is particularly important in the kidney, where the mineralocorticoid receptor (MR) is highly expressed and important for regulation of blood pressure and salt concentration. Here, conversion of cortisol into inactive cortisone prevents binding to the MR and disruption of this pathway (Gross & Cidlowski 2008).

Ultimately, glucocorticoids are metabolised in the liver and secreted into the small intestine through the bile duct. In rats, approximately 80% of corticosterone metabolites are excreted in faeces, with the remaining 20% through urine (Bamberg et al. 2001). The excretion patterns of glucocorticoid metabolites closely match the circadian pattern of circulating concentrations seen in serum or plasma, with a phase delay of 6-9 hours (Cavigelli et al. 2005).

1.4.4 Glucocorticoids and rhythmic inflammation

The work of Nakamura et al. (2011) addressed the possibility that rhythmic corticosterone signalling may play a role in regulating rhythmic inflammation after observing that the loss of temporal gating of an allergic reaction in *Per2*$^{m/m}$ mice (described in section 1.3.4) was also associated with a disrupted corticosterone rhythm. Adrenalectomy was used to determine whether the loss of rhythmic signals from the adrenals, including corticosterone, were responsible for the time-of-day effects observed in wild-type animals. Inflammation was attenuated in response to challenge at ZT16 compared to ZT4 in sham-operated animals, as had been seen in wild-type mice, but this effect was lost in adrenalectomised animals – clearly implicating adrenal-derived factors in regulating the rhythmic inflammatory response to allergic challenge. It remains to be seen whether the same is true for the innate immune response to lipopolysaccharide (LPS).

An interesting paradox seen in the timed systemic LPS challenge, targeting the innate immune system, is that elevated cytokine production occurs in response to challenge at the start of the active phase – the time at which the circulating corticosterone concentration is high (Gibbs et al. 2012). The allergic response, on the other hand, fits well with the concept of glucocorticoids as anti-inflammatory agents, as the severity of response was lowest at ZT16, when the serum corticosterone concentration was high. This may be an indication that glucocorticoids may not have the same influence over the circadian gating of inflammation elicited by systemic LPS challenge. However, a more tissue-specific model utilising aerosolised LPS to target the lung shows an inverted relationship between time-of-challenge and inflammation severity compared to the systemic model (Gibbs et al. 2014). The lung model therefore fits with a hypothesis of enhanced glucocorticoid-mediated inhibition of inflammation at certain times of day (as is seen in the allergic challenge). It would be valuable to use both of these LPS challenge models to investigate the role that rhythmic glucocorticoid signalling may play in mediating rhythmic patterns in innate inflammation.

1.5 Pulmonary inflammation

Lung inflammation ranges from the acute virus/fungus/bacteria-induced responses to chronic responses involving tissue remodelling and alterations of immune homeostasis, such as asthma and chronic obstructive pulmonary disease (COPD). Chronic inflammatory lung conditions are rising in prevalence, with COPD now affecting approximately 5% of the US population. COPD is one of the top 6 causes of death in the USA and on the increase, and prevalence of asthma is also rising (American Thoracic Society - http://www.thoracic.org/).

There is a close link between acute inflammatory challenges, such as rhinovirus and influenza which are themselves major causes of morbidity, and development of chronic pathology. A feedback loop is also formed in which chronic pulmonary inflammation then increases both susceptibility to acute infections and severity of symptoms (Hallstrand et al. 2014). The propagation of this vicious cycle is due to the constant exposure of the lung to the external environment and the subsequent need to down-regulate inflammation to a greater extent than in other tissues.

Lung immune homeostasis involves complex interactions between cell types to maintain a high threshold for determining an inhaled particle as a threat. In order to prevent excessive inflammatory responses, the immune cells are held in a suppressed state by the lung tissue. The cluster of differentiation 200 protein (CD200, also known as OX-2 membrane glycoprotein) is a key mediator of this signal. CD200 is expressed by the lung epithelium and binds to its receptor, CD200R, on inflammatory cells to trigger a suppressive signal. After acute infection, CD200R expression is increased, suppressing the pulmonary immune cells to enable tissue repair. Unfortunately, this hyper-suppressive state allows subsequent infections to go un-checked and bacteria or viruses to replicate. This mechanism is thought to be behind the high occurrence of pneumonia after influenza infection (Snelgrove et al. 2011).

Turnover of immune cells in the airways is slow, and the alteration of response threshold may persist and contribute to long-term remodelling of the homeostatic signals keeping pulmonary inflammation at bay. In asthma, for example, the altered inflammatory set-point leads to increased expression of interleukin-13 and

reduced interferon responses, leading to an inability to protect against inhaled agents (Hallstrand et al. 2014).

The most common treatment for chronic pulmonary inflammation is inhaled glucocorticoids (Gcs). The lungs are easily targeted by aerosolised drugs, which allows the active compounds to be delivered locally and reduces systemic side effects. Glucocorticoid therapy is usually very successful at modulating symptoms in asthma as it can both suppress the overactive MAPK pathways and suppress production of inflammatory cytokines. However, a subset of asthmatic patients exist which do not response to Gcs, and Gc therapy is less effective in patients with COPD (Barnes & Adcock 2003; Barnes et al. 2004). This difference may be due to the main granulocyte mediators in these diseases (eosinophils for asthma, neutrophils for COPD) or simply reflect the extent and duration of tissue remodelling which has occurred, as more progressed diseases are more likely to exhibit a Gc-resistant component of airway obstruction (Buist 2003).

As each of these diseases differ in their primary immune effector cells but are ultimately initiated by a combination of innate immune cells and the lungs themselves, the focus of pulmonary immune mediators is now shifting away from classic immune cells and towards regulation by the airway epithelium (Snelgrove et al. 2011; Hallstrand et al. 2014). The cross-talk between airway tissue and resident immune cells is likely to be very important in regulating time-of-day sensitivity to inflammatory stimuli.

1.5.1 Lung structure and physiology

The lungs are essentially a branched structure, stemming from the nose & mouth, which converge on the trachea. The trachea splits into two bronchi, which feed into the left and right lungs. The bronchi then split into bronchioles and finally alveoli (figure 1.8). This branching serves to increase the surface area for the lungs' main function - gas exchange. In fact, in a healthy adult human, the surface area of the lungs is equivalent to the size of a tennis court (American Lung Association, www.lung.org/your-lungs/how-lungs-work). The role of the lungs is to supply O_2 to the bloodstream and remove waste CO_2. Therefore, the lungs are in constant contact with the outside world. They are an excellent model with

which to study the role of rhythmic glucocorticoids in inflammation as not only are lung diseases highly prevalent with a variable response to Gcs, the lungs themselves can be targeted directly via inhalation of compounds, limiting the exposure of other organs which could confound results. The lungs themselves are made up of multiple cell types, with varying contributions to circadian timing and inflammation.

1.5.1.1 Conducting zone

The conducting zone consists of the trachea, bronchi and proximal bronchioles. No gas exchange occurs here; the main function is to conduct air down to the alveoli and provide an early defence against infection. As such, the major cell types in the conducting zone are chondrocytes (cartilage, to maintain an open structure), secretory glands and goblet cells (which secrete mucus to catch dust, bacteria and other invading material) and ciliated epithelial cells which conduct the mucus upwards and out of the airway. Capillaries and smooth muscle cells are also found around the conducting zone of the lungs (Tomashefski Jr. & Farver 2008).

1.5.1.2 Respiratory zone

As the airways progress to the more distal regions, cartilage is no longer present and alveoli begin to branch from distal bronchioles. Smooth muscle is still present and there is a rich blood supply via capillaries to maximise gas exchange. The major cell types here are the following:

1.5.1.2.1 Type I pneumocytes

The type I alveolar cells (type I pneumocytes) cover the vast majority (~97%) of alveolar surface area. These large, thin cells facilitate gas exchange at the blood:air interface (Tomashefski Jr. & Farver 2008). In contrast to type II pneumocytes and bronchiolar epithelial cells (described below), staining for the core clock proteins PER2 and CLOCK was not readily visible in type I pneumocytes, and they are not implicated in driving circadian rhythms in the lung (Gibbs et al. 2009).

Robust inflammatory responses have been observed in cultured rat primary type I pneumocytes stimulated with lipopolysaccharide (Wong et al. 2012; Wong & Johnson 2013). These papers challenged the view that type I cells contribute little to the alveolar immune response. The type I cells express toll-like receptor 4 (TLR4) and can respond to LPS by producing tumour necrosis factor α (TNFα), interleukin- 6 (IL-6), interleukin-1β (IL-1β) (Wong et al. 2012). In fact, isolated type I pneumocytes expressed each of these inflammatory molecules to a greater extent than isolated type II cells. Co-culture of either cell type with alveolar macrophages enhanced cytokine production in a dose-dependent manner, highlighting the role of the alveolar environment and cell-cell communication in generating an acute inflammatory response (Wong & Johnson 2013).

1.5.1.2.2 Type II pneumocytes

Type II pneumocytes cover the remaining surface area of the alveoli (~3%) and are primarily secretory cells with progenitor capacity (Bhaskaran et al. 2007). The type II cells synthesise and secrete surfactant proteins (SP-A, B, C and D), which are required for clearance of fluid from lungs at birth as the foetus transitions from an amniotic environment to a gaseous environment (Rooney et al. 1994). Underdevelopment of the type II cells/surfactant system is a major cause of infant respiratory distress syndrome in premature or underdeveloped babies, and Gc treatment of mothers is recommended to stimulate lung development and surfactant production in at-risk pregnancies (Roberts & Dalziel 2006). In adulthood, surfactant proteins continue to provide protection from airway collapse by decreasing the surface tension of the alveolar environment, allowing the lungs to inflate more easily. The surfactant proteins have also been shown to play a role in lung host defence (Wright 2004).

As well as producing the multi-functional surfactant proteins, the type II alveolar cells can also act as progenitors for type I cells in response to tissue damage (Bhaskaran et al. 2007). Whilst the type II cells have been shown to express CLOCK and PER2, subsequent experiments showed that lung slices were unable to maintain oscillations without the presence of bronchiolar epithelial cells (Gibbs et al. 2009). This suggests that the type II alveolar cells are not master regulators

of circadian rhythms in the lung, but they may still play a role in the rhythmic inflammatory response.

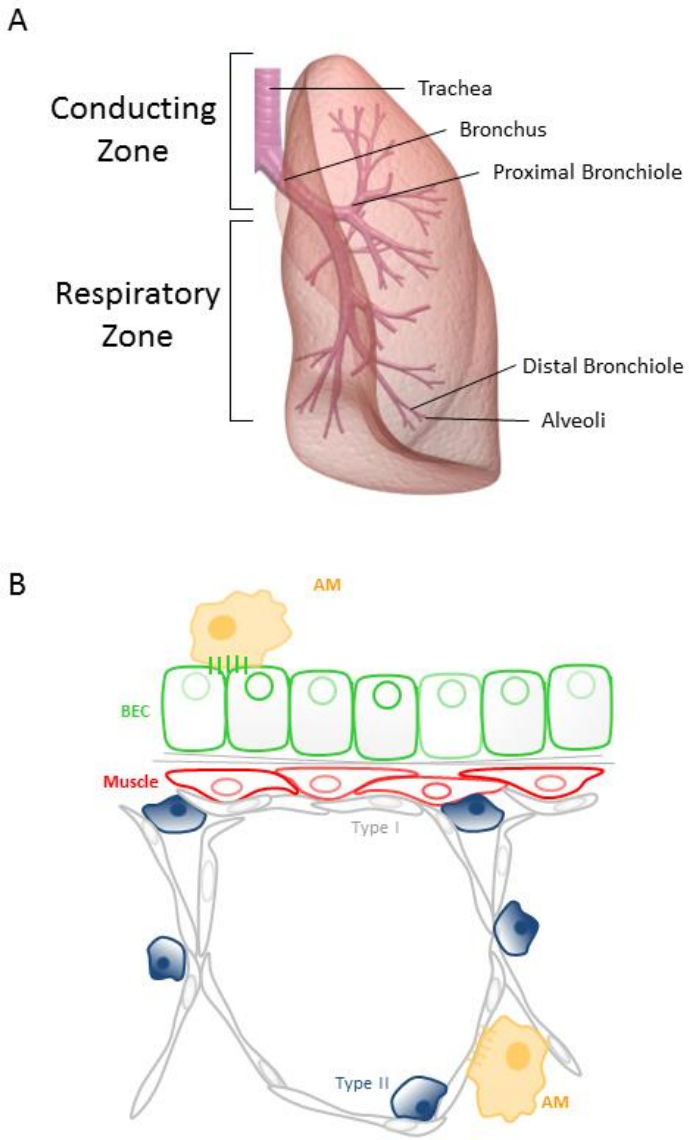

Figure 1.8: Lung structure and distal cell types

A) The progressive branching structure of the lung; from the upper conducting zone down to the more distal airways where gas exchange occurs (respiratory zone). B) Major cell types present in the distal bronchioles and alveoli are airway smooth muscle (red), type I and type II pneumocytes (grey and blue, respectively), bronchiolar epithelial cells (BEC, green) and alveolar macrophages (AM, yellow).

1.5.1.2.3 Bronchiolar epithelial cells

Previously known as Clara cells or club cells, the bronchiolar epithelial cells are non-ciliated secretory cells (Tomashefski Jr. & Farver 2008). A small subset has been identified as candidate progenitor cells and may assist type II pneumocytes in repairing the airways after insult (Wang et al. 2012). Their primary function is secretion of surfactant, lysozymes and CCSP (club cell secretory protein – also known as uteroglobin or secretoglobin family 1A member 1). CCSP is almost exclusively expressed by bronchiolar epithelial cells, although recent evidence has shown expression in a small portion of bone marrow cells (Bustos et al. 2013). The precise role of CCSP is still unclear, but it is thought to be beneficial in fighting infection and promoting tissue repair (Wong et al. 2009).

The CCSP +ve cells have widely been shown to have immuno-modulatory functions, either through secretion of surfactants and CCSP or through cytoplasmic cytochrome P-450 activity, which breaks down engulfed airborne toxins (Van Winkle et al. 1999). Along with their immuno-modulatory functions, the bronchiolar epithelial cells co-express GR, CLOCK and PER2, and are major regulators of the clock in the lung (Gibbs et al. 2009; Gibbs et al. 2014). These cells are likely to be key regulators of rhythmic pulmonary inflammation (Gibbs et al. 2014).

1.5.1.2.4 Alveolar macrophages

The lungs' resident immune cells are the alveolar macrophages (AMs), which protect against inhaled pathogens. They express toll-like receptors (TLRs) on their surface and secrete pro-inflammatory cytokines in response to TLR activation. Contrary to previous expectations of a 'patrolling' role of the AMs, it has recently been shown that some of these cells are sessile and rely on the flow of liquid in alveoli to wash pathogens towards them, rather than migrating towards bacteria (Westphalen et al. 2014). These cells also serve an immunosuppressive function by communicating with the lung epithelium; an effect which is dependent upon synchronous spikes of Ca^{2+} influx in the AMs and gap junction connections with the alveolar epithelium. Connexin 43 deletion in AMs prevented synchronous Ca^{2+} spikes and increased secretion of the pro-inflammatory cytokines MIP-1α (macrophage inhibitory protein 1 alpha), CXCL1 and CXCL5. Whilst MIP-1α is

predominantly produced by the AMs themselves, CXCL1 and CXCL5 are thought to be of epithelial origin, indicating a bi-directional signalling between the two cells types to suppress inflammation (Westphalen et al. 2014). It is highly likely that cross-talk between these two cells will influence circadian regulation of the pulmonary inflammatory response.

1.5.2 Circadian rhythms in the lung

The lungs exhibit robust oscillations of clock gene expression and rhythmic bioluminescence can be seen in organotypic slices from Per2::luciferase clock gene reporter mice (Yoo et al. 2004; Gibbs et al. 2009; Gibbs et al. 2014). These rhythms are dependent upon the presence of the bronchiolar epithelial cells, as selective depletion of this cell type via naphthalene exposure results in severely dampened bioluminescence rhythms (Gibbs et al. 2009). In-keeping with a functional role of a clock in this tissue, normal lung function exhibits a circadian rhythm, with a trough in expiratory volume during the rest phase (Spengler & Shea 2000). Some respiratory diseases, such as asthma and COPD (Durrington et al. 2014) exhibit circadian rhythms in severity, and the lung shows a time-of-day variation in response to oxidative injury and bacterial challenge (Pekovic-Vaughan et al. 2014; Gibbs et al. 2014). It has also been shown that cigarette smoke can modulate the expression of clock genes in the lungs whilst simultaneously increasing pulmonary inflammation (Hwang et al. 2014), implicating the need for a functional clock to modulate the inflammatory response. There is therefore strong evidence for circadian modulation of the pulmonary immune response, but little work has been performed to address the role that rhythmic endocrine signalling may play in mediating the circadian pattern of inflammation in the lung.

1.6 Model systems

When modelling something as complex as the immune and endocrine systems, it is currently impossible to recapitulate all aspects of an organism's response *in vitro*. It is therefore inevitable that *in vivo* investigations will be required in some circumstances. Bearing in mind the 3Rs (replacement, reduction and refinement), it is imperative to choose a suitable model, both in terms of experimental design and the organism itself.

The best experimental animal for this research is the mouse. Alongside *Drosophila melanogaster*, the mouse has proven to be a valuable model organism in the field of chronobiology. *Mus musculus* shares our molecular clockwork (Dunlap 1999) and is also a powerful tool for modelling human immune function and diseases (Mestas & Hughes 2004; Rosenthal & Brown 2007). Whilst its small size can be a problem in some cases, such as in serial sampling of blood, this is outweighed by the sheer variety of genetic models available and their ability to closely model a range of human disorders.

1.6.1 Inflammatory models

The overall aim of this investigation is to measure the impact of altered glucocorticoid signalling and peripheral clock entrainment upon innate inflammation. To elicit an immune response, an established protocol of lipopolysaccharide (LPS) administration will be used to enable comparison with published work (Castanon-Cervantes et al. 2010; Gibbs et al. 2012; Gibbs et al. 2014).

Lipopolysaccharide is a component of the outer membrane of Gram-negative bacteria and causes an inflammatory response capable of interfering with the circadian clock (Marpegán et al. 2005). Castanon-Cervantes et al. (2010) used intraperitoneal administration to elicit a systemic response in mice which had been subjected to multiple phase shifts to assess the impact of simulated jet lag and circadian disruption upon acute inflammation. Serum cytokine concentrations were quantified by multiplex and enzyme-linked immunosorbent assay (ELISA) and core body temperature was measured to assess the severity of the immune response. Similar measurements were made by Gibbs et al. (2012) following administration of ligands targeting REV-ERBα. In order to selectively target the lung, LPS is administered as an aerosol which can be inhaled. Following challenge, lungs are then lavaged and the obtained fluid can be analysed for cytokine concentrations and immune cell content (Gibbs et al. 2014). This protocol will be used to model the pathology of lung inflammation and is a useful comparison to the systemic response.

1.6.2 Manipulation of glucocorticoid rhythms

1.6.2.1 Surgical

Surgical methods have previously been employed in order to disrupt the glucocorticoid rhythm in rodents, both in relation to circadian timing and immune function (Nakamura et al. 2011; Conway-Campbell et al. 2010). Adrenalectomy removes the glands altogether, including regions which serve other functions, and so special care must be taken when using such animals. For example, due to the loss of aldosterone production, animals must receive additional salt (0.8-1% in drinking water) in order to maintain electrolyte homeostasis and increase survival (Richter 1936). Once endogenous glucocorticoid production has been abolished by adrenalectomy, it can be re-established by the introduction of a new organ (transplant) or by exogenous administration (e.g. injection, drinking water, or subcutaneous pellet).

Transplantation has been utilised in chronobiology by Kiessling et al. (2010), who transplanted adrenal glands from *Per2;Cry1* double-mutant mice into adrenalectomised wild-type (WT) animals to create otherwise-WT mice with clock-deficient adrenal glands. An 8 week recovery time was reported, in order to allow complete re-innervation of the tissues, and WT to WT transplants were also performed to control for the effects of the procedure itself. In this example, behavioural and hormone rhythms re-entrained more quickly in mice with clockless adrenals after a 6 hour phase advance. The shift in the corticosterone secretion rhythm preceded that of activity, indicating that hormonal signalling can act as a modulator of behavioural rhythmicity and further illustrating that adrenal Gcs can act as a buffer between the central pacemaker and peripheral clock rhythms.

Exogenous administration of glucocorticoids can also be used to impose an otherwise abnormal rhythm of circulating hormone upon an organism. There are a variety of methods available, including food/water supplementation, injection, and continuous-release implants. Supplementing food or water is the least invasive of these options, as normal food/water can be replaced with supplemented food/water at specific times to create a set rhythm (Dalm et al. 2008). However, dosage can be difficult to control as the quantity consumed may vary, and mice

may need to be housed individually for dosing to be accurately calculated. Implants will release an accurate dose but require an initial surgical procedure to install the pellet subcutaneously.

Finally, exogenous administration via injection can provide a set dose at specific times. Dosing can therefore be calculated beforehand, but the injections themselves and handling involved make it more disruptive to the natural behaviour of the animal than simple food or water replacement. Due to the short half-life of circulating corticosterone, it is also likely that multiple administrations will be required because sparse injections do not reliably mimic a natural rhythm (Lightman et al. 2008). The experimental set-up designed by Lightman et al. would be ideal for automated dosing and blood sampling, but has not yet been implemented with mice.

1.6.2.2 Pharmacological

Pharmacological methods can also be used to manipulate the glucocorticoid rhythm, as an alternative to surgical abolition and re-establishment. Kiessling et al. (2010) stated that pharmacological inhibition of glucocorticoid synthesis via the 11β-hydroxylase inhibitor metyrapone (MET) 'seems more practical' than the surgical methods described above. Metyrapone blocks cortisol/corticosterone synthesis by inhibiting the enzyme required for the final stage of the reaction: 11-deoxycortisol → cortisol and deoxycorticosterone → corticosterone respectively (Schteingart 2009; Chung et al. 2011b). This allows steroidogenesis to occur normally until this point, minimising the impact upon other systems by enabling mineralocorticoid and adrenal androgen production to continue. Blocking these reactions may still affect the other steroidogenic reactions, however, as this manipulation effectively increases the reagents/precursors available because they are not being converted into cortisol or corticosterone. This method is still more specific to the glucocorticoid system than adrenalectomy though, and the animals would not require saline supplements. Doses of metyrapone can be controlled and the applied in the same way as the corticosterone replacement methods described above.

In addition to blocking synthesis of glucocorticoids, the signalling rhythm can also be disrupted by antagonism of receptors. The synthetic steroid mifepristone acts as an anti-glucocorticoid, binding to the GR (Schteingart 2009). It is therefore possible to allow the adrenal glands themselves to function normally but block the effects of the glucocorticoids produced. However, mifepristone is also a progesterone antagonist, so its effects are not restricted to the glucocorticoid system. Off-target effects must therefore be taken into consideration when using non-GR-specific drugs such as mifepristone, and more targeted methods such as metyrapone administration or genetic manipulations are more appropriate for this particular project.

1.6.3 Genetic

Genetic manipulation has revealed much of what we currently know about the circadian molecular clockwork. One of the most important advances in chronobiology is the addition of the luciferase enzyme sequence (*Luc*) following the *Per2* sequence. The combination of these sequences, known as *Per2::Luc* or $Per2^{Luc}$, enables the oscillations of *Per2* transcription to be visualised in real-time (Yoo et al. 2004). When cells from *Per2::Luc* organisms are cultured in a medium containing luciferin, the luciferase enzyme catalyses a reaction which produces light. This light can be measured by photomultiplier tubes and rhythmic peaks and troughs in luminance can be observed. This construct therefore allows the rhythm of tissues to be determined without destroying the sample, enabling long-term measurements to be made and allowing the effects of pharmacological manipulation to be seen *ex vivo*.

Alongside this whole-organism manipulation, knockouts can be generated in discrete subsets of cells by utilising the Cre-loxP system. This model has already been used successfully in many fields, including neuroscience and immunology, to create conditional knockouts in tissues of interest (Gavériaux-Ruff & Kieffer 2007; Gibbs et al. 2012; Gibbs et al. 2014).

1.6.3.1 Cre-loxP recombination

Cre-loxP recombination allows genes to be targeted in specific cells or at specific stages of development. This combats a major problem with systemic genetic

manipulation, that of embryonic lethality, by allowing genes to be expressed normally until a specified stage or in a specified tissue. The regional specificity of the system also enables the function of genes in select tissues to be evaluated, circumventing potential masking effects of whole-organism genetic manipulation (Gavériaux-Ruff & Kieffer 2007). This is particularly useful in this project as whole body knockout of the glucocorticoid receptor is lethal (Tronche et al. 1998).

The Cre-loxP system utilises the viral enzyme Cre (causes recombination), which catalyses recombination of DNA between two loxP (locus of X-over P1) sites. The loxP sites themselves comprise two palindromic 13 base-pair sequences and an asymmetric 8 base-pair sequence in the centre which confers directionality. The result of the Cre-mediated recombination is dependent upon the relative orientations of the two loxP sites (Branda & Dymecki 2004).

Excision of DNA can be achieved if the loxP sites are arranged on the same chromosome arm and in the same orientation (figure 1.9A). Here, the section flanked by loxP sites ('floxed') forms a cyclical product and is degraded. This process can also occur in the opposite direction; a cyclical loxP-containing fragment can be integrated into a gene with a single loxP site, although this is much less common due to degradation of the cyclical fragments. Inversion of DNA is possible when two loxP sites on the same chromosome face each other (figure 1.9B), whilst translocation can occur if loxP sites are situated on different chromosomes (figure 1.9C). By integrating loxP sites into specific regions of a gene, mutations causing dominant negatives, null proteins or even gain-of-function can be created (Kos 2004).

Temporal or regional specificity is gained by controlling where Cre is expressed. This is achieved by inserting the Cre sequence after a gene known to be expressed only at the desired time or in the region of interest – a 'driver' gene. Thus, whenever the driver is transcribed, Cre will also be produced and able to cause recombination of any floxed sequences present.

Generating the conditional knockouts therefore requires the breeding of animals containing a floxed gene of interest with those expressing Cre attached to an appropriate driver. The efficiency of the system is variable, depending both upon the gene of interest and the driver chosen, but it has already been used successfully in experiments directly related to circadian control of lung inflammation, with macrophage/neutrophil-specific (*LysM)* (Clausen et al. 1999) and bronchiolar epithelial cell-specific (*Ccsp)* (Bertin et al. 2005) drivers shown to work well with the clock gene *Bmal1* (Gibbs et al. 2012; Gibbs et al. 2014) to specifically disrupt the molecular clockwork in these cells. More recently, adrenal-specific (driven by *0.5Akr1b7*) Cre expression has also been achieved (Lambert-Langlais et al. 2009).

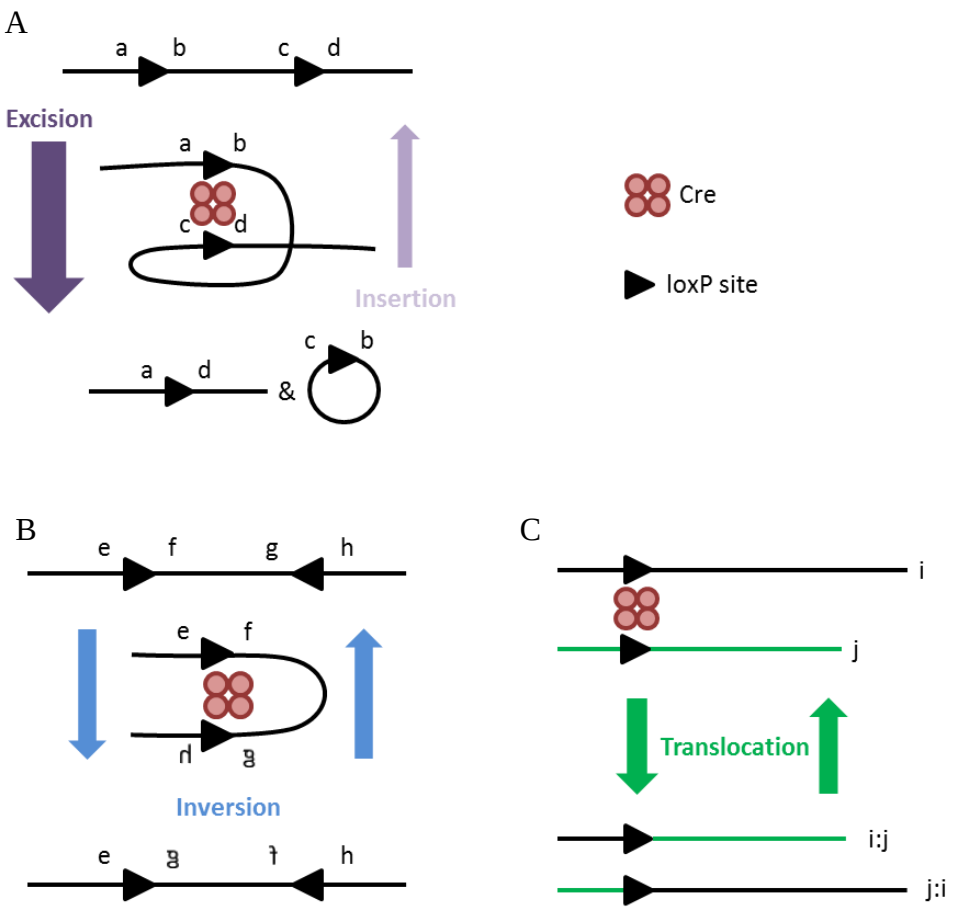

Figure 1.9: Cre-loxP recombination

In the presence of Cre: A) Excision and insertion occurs between two loxP sites (black arrows) in the same orientation. B) Inversion occurs between inverted loxP sites. C) Translocation occurs between loxP sites on non-homologous chromosomes. Letters a-d and e-h represent orientation of DNA strands, letters i and j represent chromosomes themselves. Coloured arrows indicate direction and relative frequency of reaction.

Legend and image adapted from Branda and Dymecki (2004).

1.6.3.1.1 GR floxed mice

Of particular relevance to this project is the *GR*^{flox} (*Nr3c1*^{tm2Gsc}) mouse line, developed by Günther Schütz and colleagues (Tronche et al. 1999). This strain, which was backcrossed onto a C57BL/6 background, contains an insertion of two loxP sites which flank exon 3 of the glucocorticoid receptor gene (*Nr3c1*). Exon 3 encodes a region involved in DNA binding, and homozygous whole-body deletion results in perinatal death, likely due to acute respiratory distress caused by underdeveloped lungs and fluid retention in the alveolar space (Cole et al. 1995).

Other inducible mutations of GR exist, including a *GR*^{Hypo} mutant in which exon 2 of the gene is targeted for deletion (Cole et al. 1995) and the *GR*^{Dim} mutant where the loxP sites flank exon 4 (Tronche et al. 1998). However, both of these strains retain some residual GR function after Cre-mediated recombination. In the case of the *GR*^{Hypo} mutation, a small proportion of whole-body targeted mice survived to adulthood, indicating some residual functioning GR (Cole et al. 1995). Indeed, the exon 2-KO mice retain a truncated form of GR which is able to bind the synthetic ligand dexamethasone (Cole et al. 2001). Further analysis revealed comparable expression levels of exons 3-9 in wild type and exon 2-KO mice, with almost no expression of exons 1 & 2 in the *GR*^{Hypo} mice.

In *GR*^{Dim} mice, a point mutation (A458T) is induced in exon 4. This amino acid change from alanine to threonine prevents dimerization of the receptor with various results regarding GR function. Initial reports indicated a loss of DNA binding to glucocorticoid response elements (GREs) and GRE-dependent transactivation with retention of other GR-mediated functions which do not require direct binding to GREs (Tronche et al. 1998). However, later experiments have revealed residual genomic effects as the *GR*^{Dim} receptors can still form multimers without a functional dimerization domain (Adams et al. 2003). Working with either of these strains would therefore provide confounded results that would be difficult to interpret. Whilst at a later stage they could certainly be useful to separate out different functions of the GR in the proposed model, a more complete knockout would be preferable. As global knockout of exon 3 most closely mimicked that of global whole-gene GR knockout, and these mice have since been termed *GR*^{Null} after recombination, this strain would be the most

appropriate to use to investigate loss of GR signalling in the lung (Tronche et al. 1998).

1.6.3.1.2 Lung-specific Cre drivers

Lung development is highly dependent upon glucocorticoid receptor function and knockout of GR in the lung can have lethal effects, so the choice of Cre driver must be carefully considered. The perinatal death observed in global GR knockouts can be recapitulated with certain lung-specific drivers, such as surfactant protein C (SP-C). The combination of an SP-C inducible Cre mouse (*SPC/rtTA, tet-O-Cre*), in which Cre expression is induced by doxycycline administration, and a floxed GR (in this case, exons 1c and 2) mouse resulted in a novel strain which would lose GR expression in SP-C-expressing cells after administration of doxycycline (Manwani et al. 2010). Termed *GRepi*$^{-}$ mice due to the specificity of SP-C expression in the lung epithelium, mice treated from embryonic days 6.5 (before onset of lung formation) to 18.5 displayed neonatal mortality and abnormal lung development in 50% of cases. Loss of GR in SP-C expressing cells resulted in increased lung cellularity with reduced airspace. Reduced differentiation of epithelial cells was also observed, as measured by reduced surfactant protein production and reduced mRNA expression of the apical epithelial Na^{+} channel (ENaC) which regulates the removal of fluid and Na^{+} from the lungs. The authors also report reduced mRNA expression of type 1 epithelial cell markers *T1α* and *Aqp5*, along with the bronchiolar epithelial marker *Ccsp* (Manwani et al. 2010).

The cellular focus of this project has already been identified as the bronchiolar epithelial cell, for which a specific Cre line (*Ccsp*^{icre}) already exists. This mouse strain has already been successfully crossed with a *Bmal1* floxed line to knock out the molecular clock in bronchiolar epithelial cells (Gibbs et al. 2014), but it remains to be seen whether loss of GR in these cells will result in a viable mouse or perinatal lethality. It has been established that there is an overlap in CCSP and SPC expression (1.1% of terminal bronchiole cells were found to co-express CCSP and pro-SPC), and that CCSP +ve cells can demonstrate stem cell features such as self-renewal and expression of stem cell markers *in vitro* (Wang et al. 2012).

It is therefore possible that the phenotype observed in the SPC-driven knockout will be reproduced in the CCSP-driven knockout, and that loss of GR in potential stem cells will have detrimental consequences. However, we have already highlighted the CCSP +ve bronchiolar cells as key mediators of both circadian rhythms in the lung and the pulmonary inflammatory response (Gibbs et al. 2009; Gibbs et al. 2014), so if the *Ccsp-GR*$^{-/-}$ mice are viable, they should provide extremely useful information when challenged with aerosolised lipopolysaccharide at different time points, and may also shed light on the cell types mediating suppression of pulmonary inflammation via glucocorticoid treatment.

By utilising the targeted disruption of glucocorticoid signalling via deletion of the receptor in a candidate effector cell, combined with disruption glucocorticoid ligand production and manipulation of rhythms in circulating concentrations, it will be possible to elucidate which factors of rhythmic Gc-GR signalling are necessary to drive the circadian variation in the pulmonary innate inflammatory response.

1.7 Hypotheses, aims and objectives

Previous research has revealed a clear effect of the circadian clock upon the response to immune challenge (Castanon-Cervantes et al. 2010; Nakamura et al. 2011; Gibbs et al. 2012). There is strong evidence to support a role for glucocorticoid receptor signalling in mediating, at least in part, the synchronisation between peripheral and central clocks, but the contribution of such signalling to circadian regulation of inflammation remains unclear. Therefore, elucidating the role of glucocorticoid signalling in mediating the influence of the circadian clock upon innate inflammation is the focus of this thesis, which is divided into four main hypotheses and chapters (figure 1.10).

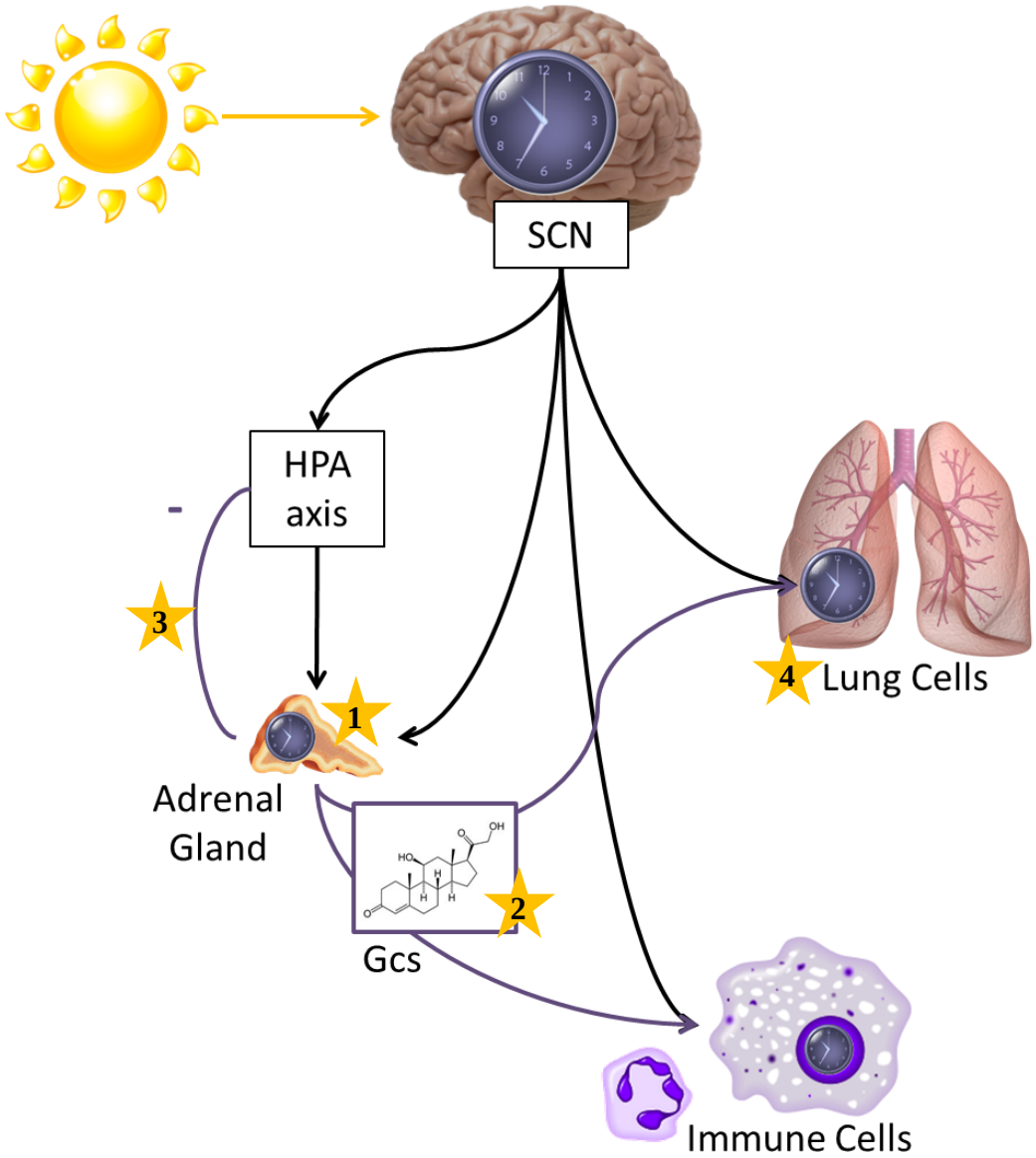

Figure 1.10: Overview of model and focal points of project

The circadian clock is arranged in a hierarchical format, with a master pacemaker in the suprachiasmatic nucleus (SCN) of the brain. This clock is entrained by light and communicates to clocks in peripheral tissues to synchronise oscillations across the body via a combination of neural and humoural signals (black arrows). The glucocorticoid hormones (Gcs) are a prime example of humoural synchronising agents. The master pacemaker can regulate the rhythmic production of these hormones by the adrenal gland at multiple levels. The Gcs provide a negative feedback to the HPA axis, but also provide an additional entrainment signal to other peripheral tissues (purple arrows). Stars indicate hypotheses tested within this project: 1) Chapter 3 - Impact of adrenalectomy upon rhythmic pulmonary inflammation, 2) Chapter 4 – Effect of timed corticosterone administration on relative phasing of clock gene expression in the lung, 3) Chapter 5 – Effects of consistent circulating corticosterone concentration upon rhythmic pulmonary inflammation, 4) Chapter 6 – Targeted disruption of glucocorticoid receptor signalling in bronchiolar epithelial cells.

Hypothesis 1: Rhythmic adrenal glucocorticoid signals drive the circadian regulation of inflammatory response in the lung.

Aim: Disrupt endogenous glucocorticoid signalling via adrenalectomy, and establish the impact upon time-of-day variation in innate inflammation.

Objectives:

- Characterise the daily profile of circulating glucocorticoid concentrations in intact and adrenalectomised animals.

- Determine whether loss of rhythmic circulating glucocorticoids via adrenalectomy disrupts clock-driven behavioural rhythms (via wheel running) and/or clock gene rhythms in target tissue (via qPCR).

- Challenge intact and adrenalectomised animals with lipopolysaccharide at different times in the circadian cycle and measure the resulting inflammatory response via quantification of cell infiltration and measurement of cytokine concentrations.

- Compare the influence of adrenalectomy upon the inflammatory response to systemic endotoxin challenge (intraperitoneal injection) and pulmonary challenge (aerosolised lipopolysaccharide).

Chapter 3 – Impact of adrenalectomy upon rhythmic pulmonary inflammation

Hypothesis 2: Reversal of the phase of glucocorticoid rhythm will reverse the phase of pulmonary clock gene expression and the phase of peak inflammatory response.

Aim: Impose a reversed rhythm of circulating glucocorticoid concentrations via adrenalectomy and exogenous administration of corticosterone. Measure effects upon clock gene expression in the lung and circadian variation in inflammatory response to aerosolised lipopolysaccharide.

Objectives:

- Determine an appropriate dose of corticosterone to deliver via injection to mimic endogenous peak concentrations.

- Administer previously determined dose over several days to adrenalectomised animals in anti-phase to usual peak concentrations and assess phasing of lung clock via qPCR to establish phase reversal.

- Repeat exogenous anti-phase glucocorticoid administration protocol and challenge with aerosolised lipopolysaccharide at multiple time points. Determine whether the rhythmic inflammatory response profile has also inverted via quantifying cell infiltration and cytokine production.

Chapter 4 – The effect of timed corticosterone administration on the relative phasing of circadian clock gene expression in the lung

Hypothesis 3: Rhythmic glucocorticoids are required for normal circadian regulation of the pulmonary inflammatory response.

Aim: Replace the rhythmic endogenous glucocorticoid profile with constant circulating concentrations and establish the impact upon time-of-day variation in innate pulmonary inflammation.

Objectives:

- Determine an appropriate dose of sustained release corticosterone implant (subcutaneous) to deliver a constant circulating concentration within the physiological range. Characterise the daily profile of circulating glucocorticoid concentrations in intact and implanted animals.

- Challenge intact and implanted animals with aerosolised lipopolysaccharide at multiple time points and measure the inflammatory response via quantification of cell infiltration and measurement of cytokine concentrations.

Chapter 5 – Effects of consistent circulating corticosterone concentration upon rhythmic pulmonary inflammation

Hypothesis 4: Glucocorticoids exert their effects on the rhythmic pulmonary inflammatory response via the glucocorticoid receptor (GR) in bronchiolar epithelial cells.

Aim: Disrupt expression of the glucocorticoid receptor from bronchiolar epithelial cells and assess impact upon lung rhythmicity and circadian regulation of the inflammatory response to aerosolised LPS.

Objectives:

- Generate a mouse strain which lacks GR in bronchiolar epithelial cells by breeding $GR^{flox/flox}$ mice with $Ccsp^{icre}$ mice, maintain on a Per2::Luc background to facilitate bioluminescence monitoring.

- Assess lung rhythmicity and the ability to be synchronised by glucocorticoids by monitoring organotypic lung slices from $Ccsp\text{-}GR^{-/-}$ mice and wild type littermates under photomultiplier tubes (PMTs), and measuring their synchronising response to the synthetic glucocorticoid dexamethasone.

- Challenge $Ccsp\text{-}GR^{-/-}$ mice and wild type littermates with aerosolised LPS at different time points and measure any differences in the magnitude and rhythm of inflammatory response (cell infiltration and cytokine production).

- Assess differences between genotypes in the immunosuppressive effects of dexamethasone administration before LPS treatment at different time points.

Chapter 6 – Targeted disruption of glucocorticoid receptor signalling in bronchiolar epithelial cells

Chapter 2: Methods

2.1 Animal husbandry

All work within this project was carried out under Home Office licence, in accordance with the Animals (Scientific Procedures) Act of 1986. Male C57BL/6J mice aged 8wks were purchased from Harlan Laboratories or Charles River Laboratories, both UK. Mice bred in-house were used at approximately the same age for comparison. *Nr3c1*^{tm2Gsc} (hereafter known as *GR*^{flox}) transgenic mice were purchased from the European Mutant Mouse Archive (EMMA) as frozen embryos and re-derived by Harlan Laboratories, UK. The *GR*$^{flox/flox}$*Ccsp*$^{icre/+}$/PER2::Luc (subsequently called *Ccsp-GR*$^{-/-}$) strain was bred on site using the *GR*^{flox} line and an already established *Ccsp*$^{icre/+}$/PER2::Luc strain. All animals were housed in a 12hr light – 12hr dark (12:12 LD) lighting schedule with food and water available *ad libitum*, unless otherwise stated.

2.1.1 Genotyping

Mice from transgenic lines (*Ccsp-GR*$^{-/-}$ and *GR*$^{flox/flox}$ littermates on PER2::Luc background) were ear punched for identification and the ear clips used for DNA extraction and genotyping. Tissue samples were stored at -20°C prior to DNA extraction using a QiaAmp kit (Qiagen).

DNA extraction began with incubation of tissue samples in 50µl animal tissue lysis (ATL) buffer and 10µl proteinase K (both part of kit) at 56°C for 1hr. Samples were vortexed after 30minutes to ensure thorough mixing and digestion. Following incubation, 4µl RNase A (20mg/ml, Roche) was added, the solutions were mixed by vortexing and incubated at room temperature for 2 minutes. 100µl buffer AL (part of kit) was added and the mixture incubated at 70°C for 10 minutes. To precipitate DNA, 100µl 100% ethanol was added and solutions vortexed for 15 seconds. The resulting mixture was added to a spin column (part of kit), which was centrifuged at 6,000g for 1 minute. The filtrate was discarded and 250µl of wash buffer AW1 (part of kit) added. The columns were spun again at 6,000g for 1 minute. The filtrate was discarded again, and 250µl of wash buffer AW2 (part of kit) added. Columns were then spun for 3 minutes at 16,000g to thoroughly wash the membrane. The top of the spin column was removed from the outer filtrate tube and placed into a clean 1.5ml Eppendorf tube and 100µl nuclease-free water added to the membrane. Tubes were left to sit at room

temperature for 1 minute to allow the water to soak the entire membrane and then spun at 6,000g for 1 minute to elute the DNA. DNA samples collected were stored at -20°C prior to use in genotyping PCR reactions.

Genotyping of the GR^{flox} allele was undertaken using a previously published triplex reaction to simultaneously detect the presence of a wild type (225 base pairs), flox (275bp), and/or null (390bp) fragment (Tronche et al. 1999).

Assessment of $Ccsp^{icre}$ status was performed using primers directed at the iCre sequence, resulting in a binary outcome of Cre^{+ve} (500bp) or Cre^{-ve} (no amplification). Animals were always bred as heterozygotes to wild-types, so no animals were produced that were homozygous for the $Ccsp^{icre}$ allele.

Genotyping for PER2::Luc was performed as a triplex reaction using primers targeting the normal and modified *Per2* gene, such that wild type (230bp) and $Luciferase^{+ve}$ (650bp) alleles could both be detected. Heterozygotes yielded both products.

All PCR products were run on a 2% agarose-TBE gel containing ethidium bromide to visualise DNA bands. Electrophoresis was performed in TBE buffer at 80V for 1 hour. Easyladder 1 and Hyperladder 4 (both Bioline) were used as appropriate to allow determination of fragment sizes. All primer sequences, reaction mixes and cycling conditions are given in appendix 1.

2.2 Surgical techniques

2.2.1 Adrenalectomy

Adrenalectomies were performed in-house on 8 week old mice via a dorsal approach under isoflurane anaesthesia. Oxygen flow rate was set at 0.5l/min with an isoflurane concentration of 5% for induction and 2-3% for maintenance. Mice were weighed, the skin on the back was shaved and disinfected with iodine, and an incision (~1cm) was made parallel but to the right of the spine. A small opening was made in the muscle below this incision, through which the right adrenal was located and removed via blunt dissection. Following suturing of the

muscle and skin, this procedure was repeated for the left side. Vetergesic (buprenorphine, 0.05mg/kg i.p.) was given peri-operatively, with a second dose the following morning, and animals were monitored and weighed for at least one week before any additional procedures were performed. All adrenalectomised mice were given 1% saline as drinking water in order to maintain salt balance.

Confirmation of successful adrenalectomy was performed by collecting serum samples via tail tipping (procedure detailed below) and performing an ELISA for corticosterone (see below). A small number of intact animals also underwent the tail bleed procedure in each experiment to act as controls.

2.2.2 Subcutaneous corticosterone pellet implant

Surgery was performed in-house under isoflurane anaesthesia. Oxygen flow rate was set at 0.5l/min with an isoflurane concentration of 5% for induction and 2-3% for maintenance. Mice were weighed and the skin at the nape of the neck was shaved and disinfected with iodine. A small incision (~1cm) was made in the skin, and forceps inserted between the skin and muscle to make a pocket. One pellet (21-day release corticosterone pellet, Innovative Research of America) was inserted into the pocket and the skin incision sutured closed. Vetergesic (buprenorphine, 0.05mg/kg i.p.) was given peri-operatively and animals were monitored for at least one week before any additional procedures were performed. No alteration of dietary constituents was necessary.

For the pilot dose-response experiment, 3 concentrations of corticosterone pellet were used: 2.5mg (n=6), 5mg (n=6) and 7.5mg (n=6), along with a placebo pellet (n=7). Naïve animals were used as control group (n=5) and did not undergo anaesthesia or any surgical procedures. To assess circulating concentrations of corticosterone in serum, blood samples were obtained via tail tipping (procedure detailed below) at ZT0, ZT4, ZT8, ZT12, ZT16 and ZT20 to obtain a profile across a day, and samples were assayed using a corticosterone ELISA (Enzo Life Sciences, protocol below).

Based on the data from the pilot study, a 2.5mg pellet was chosen for use in subsequent experiments.

2.3 *In vivo* experimental procedures and sample collection

2.3.1 Wheel-running

Animals were individually housed with free access to food, water, and a running wheel. All cages were contained in a light-tight cabinet, with lighting schedules set at 12:12 LD for 9-15 days followed by constant darkness (DD) for a further 11-12 days. Data was recorded and analysed using ClockLab software (Actimetrics).

2.3.2 Blood sample collection via tail tipping

Animals were restrained by hand for the procedure, with their heads covered to minimise stress. A small section (<1mm) of tail tip was severed using a sterile blade. The tail was squeezed to release a small volume of blood (<20µl) into a 0.5ml Eppendorf tube. The wound was elevated and pressed with absorbent tissue to facilitate clotting, and the animal quickly returned to their home cage. The blood sample was left to clot at room temperature for 2-3 minutes, then transferred to ice and spun at 10,000g for 10 minutes at 4°C. The supernatant was stored at -80°C prior to analysis using the low volume protocol for corticosterone ELISA (detailed below).

2.3.3 Intraperitoneal lipopolysaccharide challenge

Animals were maintained in 12:12 LD for at least 7 days prior to lipopolysaccharide (LPS) injection. Wheel-running activity was used to assess re-entrainment of the adrenalectomised mice to the LD cycle. For 24 hours prior to the experiment, the lighting schedule was switched to DD, to control for potential masking effects of the light:dark cycle upon the endogenous rhythm. The use of only 24 hours constant darkness rather than allowing animals to free-run completely allows any subsequent manipulations to be performed at the same time for all animals, preventing the need for calculation of individual circadian times (CTs) via behavioural monitoring (Aschoff 1965). All work from this point until decapitation was performed in darkness (using infrared viewing equipment).

At CT0 and CT12, 250µl of 0.1mg/ml LPS (isolated from E.Coli 0127:B8, L4516, Sigma) in saline vehicle was injected into the peritoneal cavity of 3-4 mice per

genotype. 4h later (either CT4 or CT16), the mice were sacrificed via cervical dislocation, decapitated, and blood collected for cytokine analysis. Samples were allowed to clot at room temperature for 2-3 minutes, before being transferred to ice. The samples were then spun at 10,000g for 10 minutes at 4°C and the supernatant stored as aliquots at -80°C.

2.3.4 Aerosolised lipopolysaccharide challenge

As for intraperitoneal LPS challenge, animals were maintained in 12:12 LD for at least 7 days before lipopolysaccharide (LPS) exposure. For 24 hours prior to the experiment, the lighting schedule was switched to DD, to control for potential masking effects of the light:dark cycle upon the endogenous rhythm. All procedures between this point and dissection occurred in constant darkness, with infrared goggles used to view animals and perform the experimental procedures. At the indicated time points (specified in each chapter), mice were transferred in constant darkness to a Perspex exposure chamber and their tails marked with ink to indicate home cage. The lid was then sealed and the chamber transferred to a biological safety cabinet with a flow rate of 0.579m/s.

Approximately 7ml of 2mg/ml lipopolysaccharide (isolated from *E.Coli* 0127:B8, L3129, Sigma) in 0.9% saline vehicle, or vehicle alone, was added to a jet nebuliser and inserted into the exposure chamber. The nebuliser was switched on for 20 minutes, after which the lid of the chamber was removed to quickly vent remaining vapours. Once the vapours had cleared, the lid was then re-sealed and the exposure chamber was removed from the biological safety cabinet. Mice were transferred back to their home cages, using the markings for identification, which remained in constant darkness. 5 hours following challenge, mice were sacrificed via intraperitoneal injection of 200 µl pentobarbitone (Pentoject). After visible breathing had ceased, mice were then transferred to light to facilitate dissection.

2.3.4.1 Bronchoalveolar lavage

The chest cavity was opened and a hole made in the trachea using microdissecting scissors. A cannula was made from a 23G needle (BD Microlance 3, Becton Dickinson) inserted into plastic tubing (Fine bore, 0.58mm internal diameter, 0.96 external diameter, Smiths), which was then inserted into the trachea. 1ml of

chilled bronchoalveolar lavage (BAL) fluid, consisting of 3.72g/l EDTA and 0.1% w/v BSA in dH_2O, was instilled into the lungs using a 1ml syringe. The fluid was then withdrawn using the same syringe, and exudate transferred to 1.5ml Eppendorf tube. Samples were stored on ice before further processing.

BAL samples were quantified in 0.05ml increments and then spun for 7 minutes at 200g to pellet cells and debris. The supernatant was transferred to a fresh 1.5ml tube and stored at -80°C for cytokine analysis. Cell pellets were resuspended in 0.5ml fresh BAL fluid and used for cell counting and cytospin production.

2.3.4.2 Cell counting

For cell counting, 5µl of the resuspended cell pellet was added to 10ml CASYton fluid (Roche), an isotonic, isosmotic dilution fluid for use with CASY cell counter (CASY 1 TT, Schärfe). This mixture was inverted to mix, and then run through the CASY counter with settings as follows: dilution 1:2000, capillary 150µm, runs 2. Gating was set to 6.00µm minimum and 40µm maximum to exclude debris. The number of cells counted was automatically expressed as cells/ml on the CASY counter, so adjustment was made by dividing by 2 to take into account the resuspension volume of 0.5ml. This gave a value for the total number of cells obtained per animal. To enable comparison between groups, this cell count was normalised to cells/ml by dividing the raw cell count by the volume of BAL extracted for each animal.

2.3.4.3 Cytospin

For generation of cytospins, 200µl of the resuspended cell pellet was applied into the funnel of a Cytospin 3 (Shandon). Slides were spun at 500rpm (approximately 28g) for 5 minutes and allowed to dry flat overnight before staining.

Cytospins were stained using Leishman's Eosin Methylene Blue Solution (Merck, 1053870500) to enable visual discrimination between macrophages and neutrophils. Slides were incubated in neat solution for 3 minutes, followed by a dilute solution (15% neat Leishman's stain, 10% buffer solution - 1 buffer tablet pH 7.2 Merck 1094680100 in 1l dH_2O to make stock buffer solution, 75% dH_2O) for 6 minutes. Slides were then washed in a series of 3 baths of buffer solution, 1

minute in each. Finally, slides were dehydrated and cleared with 4 dips in 95% ethanol, 4 dips in 100% ethanol and 2 dips in xylene, then left to dry for 5-10 minutes. Coverslips were applied using DePeX mountant and slides left to dry overnight before imaging.

Imaging was performed on a Leica bright field microscope (DM2000), using a Leica DFC295 camera and Leica Application Suite (LAS) 3.2.0 software. White balance was set to auto and images were taken at 20x magnification, ensuring images saved were representative of the slide as a whole by avoiding the edges of the impact area. Three images per slide were taken, and a differential count performed using ImageJ software (http://rsbweb.nih.gov/ij/download.html) and the cell counter plugin (http://rsbweb.nih.gov/ij/plugins/cell-counter.html). Cells were classified as either 'macrophage', due to the dark blue nucleus and pale blue cytoplasm; 'neutrophil', due to the purple hue and occasionally-visible multi-lobed structure; or 'other', which appeared larger than debris or dye smears but were not readily identifiable as macrophages or neutrophils.

Differential counts were expressed as a proportion of total cells counted in each image, and these values were averaged across the three images. These proportionate results were then multiplied by the cell count obtained from the CASY cell counter to give a differential cell count per ml of returned BAL.

2.3.4.4 Flow cytometry

Staining

In the final aerosolised LPS experiment, differential cell count was determined using flow cytometry. In this case, BAL fluid was processed as above but resuspended in 0.2ml fresh BAL fluid. Calculations for cell counting using the CASYcounter were adjusted accordingly. The remaining 195µl cell suspension was transferred to a 96-well U bottom plate on ice, one sample per well. 10µl/sample was removed and pooled in an additional well to use as a live/dead control sample. This sample was split in half, with half incubated in a 1.5ml Eppendorf tube at 95°C for 1 minute and then returned to the well. All samples were made up to 200µl with PBS and spun at 3,000g for 2 minutes in an Eppendorf 5804R plate spinner. Supernatant was disposed of and 50µl/well

live/dead stain added (Invitrogen, L10119 diluted 1:1000 in PBS). The plate was incubated at 4°C for 20 minutes and covered with tin foil to protect from light. Following incubation, the plate was spun at 3,000g for 2 minutes and supernatant disposed of. The pellet was resuspended in 200µl PBA (PBS with 1%BSA and 0.1% sodium azide), spun again and supernatant disposed of.

A blocking step was performed using 30µl/well anti-CD16 antibody (eBioscience, 14-0161) diluted 1:100 in PBA. The plate was incubated at 4°C for 20 minutes and protected from light. Following incubation, 100µl PBA was added to each well, the plate spun at 3,000g for 2 minutes and supernatant disposed of. The pellet was resuspended in 200µl PBA, spun again and supernatant disposed of.

An antibody cocktail was then used to simultaneously stain for multiple markers (see table 2.1 for fluorochromes and dilutions). 30µl antibody cocktail was added to each well and the plate incubated at 4°C for 20 minutes in darkness. Following incubation, 100µl PBA was added to each well, the plate spun at 3,000g for 2 minutes and supernatant disposed of. The pellet was resuspended in 200µl PBA, spun again and supernatant disposed of.

Cells were resuspended in 50µl/well PBA and 50µl/well fix solution (3.6% formaldehyde in PBA) added. The plate was incubated at room temperature for 20 minutes in darkness and then spun at 3,000g for 2 minutes. Supernatant was disposed of and the pellet resuspended in 200µl PBA. The plate was spun again, supernatant disposed of and cells resuspended in 100µl PBA.

Stained cells were stored overnight at 4°C and protected from light until run on flow cytometer.

Antibody	Fluorophore	Dilution	Supplier (ID)
CD11b	PerCP-Cy5.5	1:100	eBioscience (M1/70)
CD11c	APC	1:200	eBioscience (N418)
F4/80	PE-Cy7	1:200	eBioscience (BM8)
Ly-6G (Gr-1)	AlexaFluor-488	1:100	eBioscience (RB6-8C5)
MHCII	PE	1:100	eBioscience (M5/114.15.2)

Table 2.1: Antibody dilutions and fluorophores used for flow cytometry
These antibodies were used simultaneously as a cocktail, diluted in PBA (PBS with 1%BSA and 0.1% sodium azide), in order to identify different cell populations. In separate earlier steps, live/dead stain (Invitrogen, L10119) was used at 1:1000 in PBS and anti-CD16 antibody (eBioscience, 14-0161) used at 1:100 in PBA.

Analysis of cell populations

Due to the minimal contribution to the thesis and timing of experiments, analysis of cell populations was performed by Dr. Zhenguang Zhang. A BD Biosciences LSR II flow cytometer was used to process suspensions, along with FACSDiva software to collect data and FlowJo software to analyse cell populations.

Appropriate gating of positive and negative populations was set up using compensations beads (OneComp eBeads, eBioscience) for each fluorophore to correct for spill-over into other channels. Cell suspensions were analysed using a high flow rate and an automated stop at 30,000 counts. Neutrophils were counted as the proportion of cells which were Ly-6G positive.

2.3.4.5 Tissue for protein or RNA extraction

Tissue samples taken for RNA and protein extraction were snap frozen on dry ice and stored at -80°C.

2.3.4.6 Blood for serum

Blood samples from mice challenged with aerosolised LPS were taken from vessels in the neck or thigh, as decapitation and collection of trunk blood would sever the trachea and compromise the lavage process. Vessels were cut with scissors and blood collected with a sterile pastette. Samples were dispensed into

1.5ml Eppendorf tubes and allowed to clot at room temperature for 2-3 minutes before being transferred to ice. The samples were then spun at 10,000g for 10 minutes at 4°C and the supernatant stored as aliquots at -80°C.

2.3.4 Timed injections of corticosterone

2.3.4.1 Pilot (dose-response)

A pilot study to assess dosage was performed on intact animals. Blood sampling was performed via tail bleed at ZT12 in order to establish the endogenous peak level of corticosterone concentration. A second tail bleed was performed at ZT0 to generate a baseline low level prior to injection. Animals were then injected at ZT0.5 with corticosterone (Fluka, Sigma) diluted in corn oil (Fluka, Sigma) to a concentration of approximately 0mg/kg (vehicle only) 3mg/kg, 20mg/kg, 30mg/kg or 100mg/kg, into the peritoneal cavity (n=5/group). Injection volumes were 300µl. To assess corticosterone concentrations following injection, serial tail bleeds were performed 20mins (ZT0.83), 40mins (ZT1.17), 60mins (ZT1.5) and 120mins (ZT2.5) post-injection. A terminal blood sample was taken at ZT4 (210mins post-injection). These time points were chosen to reflect the expected half-life of corticosterone in blood (20 minutes), allowing a decay rate to be measured, and to terminate before the endogenous rise in corticosterone as these animals were adrenal-intact.

Pilot blood samples were run on a corticosterone ELISA (protocol below), and vehicle-only values were subtracted from test values in an attempt to account for the contribution of an intact stress-response to handling producing endogenous corticosterone. Peak values post-injection were compared with endogenous peak values (ZT12) and decay rates were both considered before deciding upon a dose of 10mg/kg to take forward into the main experiment.

2.3.4.2 Phase reversal experiment

Animals were divided into 4 groups – adrenalectomy only (ADX), adrenalectomy with anti-phase corticosterone (ZT0.5 CORT), adrenalectomy with in-phase corticosterone (ZT11.5 CORT) and intact (n=24/group). Adrenalectomy was performed for each of the first three groups as previously described and animals were allowed to recover for 1 week before corticosterone treatment commenced.

At the indicated times, the ZT0.5 CORT group and ZT11.5 CORT group received daily administration of approximately 10mg/kg corticosterone in corn oil via intraperitoneal injection (figure 2.1). Injection volume was refined to 100µl. To confirm previous results measuring decay rates in intact animals, 5 ZT0.5-injected animals were sampled via tail bleed at 20mins (ZT0.83), 40mins (ZT1.17), 60mins (ZT1.5) 120mins (ZT2.5) and 210mins (ZT4) post-injection, matching pilot time points.

Injections persisted for 7 days in a 12 hours light – 12 hours dark lighting schedule, and for a further 24 hours of constant darkness (when injections were delivered in darkness). Injections were maintained during the circadian series sampling procedure (described below).

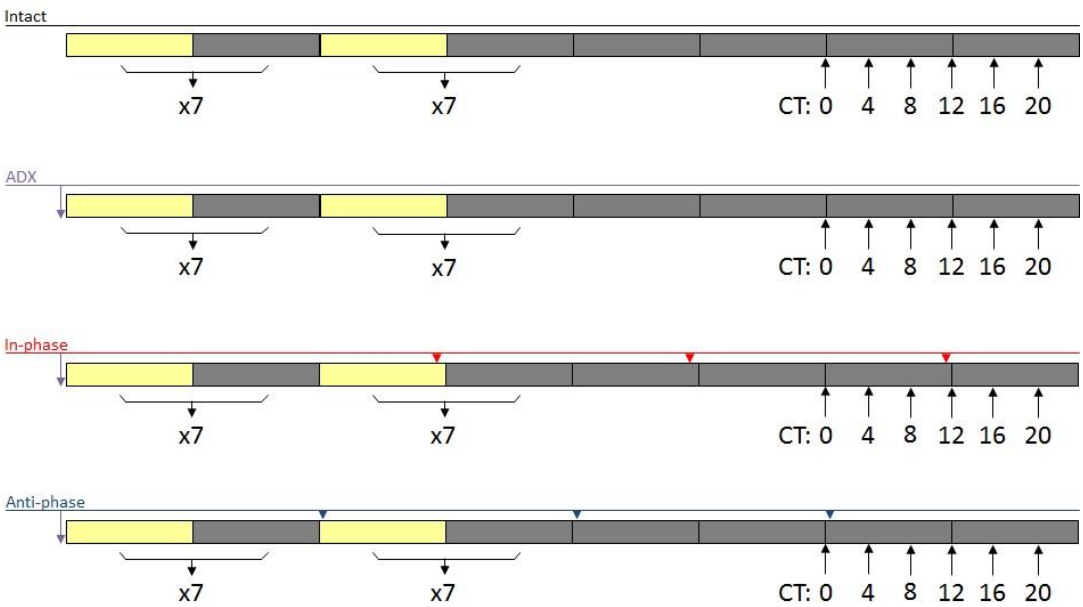

Figure 2.1: Experimental procedure for phase-reversal experiment

Animals were divided into 4 groups – intact, adrenalectomised (ADX), in-phase (ZT11.5 CORT) and anti-phase (ZT0.5 CORT). ADX, in-phase and anti-phase animals were all adrenalectomised (purple arrows). 1 week following adrenalectomy, injections of corticosterone began for the in-phase and anti-phase groups at the specified times (ZT11.5, red arrows, or ZT0.5, blue arrows, respectively). Injections continued daily for 7 days and into the sampling period. All four groups were transferred to constant darkness (DD) for 24 hours prior to the sampling period, and then 4 animals per group culled at each of the sampling time points (black arrows).

2.3.4.2.1 Circadian series

Animals were housed in constant darkness for 24hrs prior to sample collection, in order to avoid confounding effects of the external light-dark cycle and test for a true circadian rhythm which persists in constant conditions. At 6 time points across the day (CT0, 4, 8, 12, 16 and 20), animals were sacrificed by cervical dislocation, followed by decapitation in darkness.

2.3.4.2.2 Blood for serum

Blood samples were taken from trunk blood, and allowed to clot at room temperature for 2-3 minutes before being transferred to ice. The samples were then spun at 10,000g for 10 minutes at 4°C and the supernatant stored as aliquots at -80°C. For non-terminal circadian series, blood was collected via tail tipping (see procedure above).

2.3.4.2.3 Tissue for protein or RNA extraction

Tissue samples taken for RNA and protein extraction were snap frozen on dry ice and stored at -80°C.

2.4 *Ex vivo* experimental procedures

2.4.1 Photomultiplier tube experiments

Mice were sacrificed using an intraperitoneal injection of 200µl pentobarbitone (Pentoject). The chest cavity was opened and a hole made in the trachea using microdissecting scissors. A cannula was made from a 23G needle (BD Microlance 3, Becton Dickinson) inserted into plastic tubing (Fine bore, 0.58mm internal diameter, 0.96 external diameter, Smiths), which was then inserted into the trachea. 1ml of warmed (35°C) 2% agarose (type IXA, Sigma, UK) in Hanks' Balanced Salt Solution (HBSS, H6648, Sigma) was infused through the cannula to inflate the lung. The trachea was then clamped below the insertion point with tissue clamps and the cannula removed. Following this, the mouse was placed face down onto ice for 15 minutes to allow the agarose to set.

Once the agarose had set, lungs and heart were dissected out *en bloc* and placed in ice cold HBSS to rinse. Lung lobes were separated prior to slicing, so that individual lung lobes could be used.

One by one, lung lobes were attached to the chuck of a vibratome (Campden Instruments Integraslice 7550MM) using superglue (Permabond 102 industrial cyanoacrylate adhesive). Once the glue had set (<30s), the chuck was immersed into the vibratome tank, which contained HBSS. An integrated liquid cooling system was used to maintain a tank/HBSS temperature of 4°C. 275µm sections were cut using a stainless steel blade (Campden Instruments) at 80Hz, 0.2mm/s. Sections were transferred to 1ml warmed (37°C) DMEM media without foetal bovine serum (FBS) but with added Penicillin/Streptomycin (P0781, Sigma – 1% v/v) and L-glutamine (G7513, Sigma – 1% v/v); one slice per well of a 24-well cell culture plate (Corning). Plated tissue slices were incubated at 37°C, 5% CO_2 for 30 minutes. Media was then replaced with fresh DMEM (+Penicillin/Streptomycin and L-glutamine) and plates returned to the incubator for a further 30 minutes. This process was repeated for a total of 4 media changes to wash away the melted agarose. After the 4th media change, tissue slices were left in the incubator overnight to ensure the tissue was infection-free prior to rhythm measurement.

After the overnight incubation, tissue slices were placed onto organotypic cell culture membranes (Millicell low profile 0.4µm insert, Millipore) inside 35mm cell culture dishes (Corning), 1 slice per dish. 1ml recording medium was added to each (recipe in appendix 2).

Vacuum grease (Dow Corning) was applied to the rim of the 35mm dish base, and a 50mm diameter glass coverslip (VWR) applied. Slight pressure was used to seal the coverslip to the dish, and the dish was then transferred to a 37°C incubator housing the photomultiplier tubes (PMTs - Hamamatsu, Japan). Each tissue slice was enclosed in an individual monitor, and multiple monitors were housed in each incubator. The PMTs were set to record in 60s bins, counting number of photons detected in this time. Recordings continued for 1-3 weeks without media changes, precise times are detailed within the individual results.

2.4.1.1 Synchronisation experiments

To assess the ability of lung slices to be resynchronised, bioluminescence rhythms were monitored until they had dampened (approximately 10 days) and then stimulated with dexamethasone or media alone. Dexamethasone was administered as 1µl of a 200µM concentration in recording media, to give a final concentration of 200nM once added to the 35mm dish. As a control, 1µl recording medium was added to at least one tissue slice per genotype per experiment. Recordings were maintained for a further 5-7 days to determine whether re-synchronisation had occurred.

2.4.1.2 Rhythm analysis

Bioluminescence data was recorded as photon counts per minute and normalised using a 24hr moving average to produce oscillations about a mesor of 0counts/min. Normalised data was then entered into cosinor rhythm analysis software (Refinetti 1992) to assess period and amplitude.

2.4.2 Processing of tissue for immunohistochemistry

Mice were sacrificed using an intraperitoneal injection of 200 µl pentobarbitone (Pentoject). The chest cavity was opened and a hole made in the trachea using microdissecting scissors. A cannula was made from a 23G needle (BD Microlance 3, Becton Dickinson) inserted into plastic tubing (Fine bore, 0.58mm internal diameter, 0.96 external diameter, Smiths), which was then inserted into the trachea. Lungs were inflated with 1ml ice cold 4% paraformaldehyde (PFA) infused via the cannula. The trachea was then clamped below the insertion point with tissue clamps and the cannula removed. The lungs and heart were removed *en bloc*, and transferred to a 50ml Falcon tube containing 35ml ice cold 4% paraformaldehyde (PFA) for fixation. Tissue was stored in 4% PFA overnight at 4°C on a rocker.

Following fixation overnight, the tissue was transferred to 70% ethanol to avoid over-fixation and dissected into individual lung lobes. The large left lobe was used for histological analysis. Tissue processing was performed overnight in a Microm Spin Tissue Processor, moving through a series of incubations in 70%

IMS (7 hours), 90% IMS (45 mins), 95% IMS (45 mins), 100% IMS (45 mins x 3), xylene (30 mins x 3) and finally molten paraffin wax (1 hour x 2).

A final incubation of 1hr was performed in molten wax in a vacuum oven (65°C, 23inHg or -0.8bar) to facilitate evaporation and improve infiltration. Following this, lung samples were embedded in paraffin wax blocks and left to set.

Tissue sections were cut to a thickness of 5µm using a Leica 2255 microtome, mounted onto glass slides (X-tra Adhesive, Leica Biosystems) and allowed to dry for a minimum of 48 hours.

2.4.3 Immunohistochemistry

Slides first underwent rehydration via incubation in xylene (5 mins), xylene (5 mins), 100% ethanol (2 mins) and 90% ethanol (2 mins). Slides were rinsed in dH_2O followed by 20 minute incubation in 250ml PBS with 750µl 30% hydrogen peroxide on a rocker at room temperature. 3x 5 minute washes in PBS were performed to remove traces of H_2O_2.

Antigen retrieval was achieved by boiling in 1x sodium citrate buffer (diluted down from 10x stock solution of 30g sodium citrate in 1l dH_2O, pH6.0) for 20 minutes, followed by a 20 minute cooling period in the same buffer. Slides were then washed in 0.05% Tween-20 in PBS, 3x 5 minute washes. A blocking step was performed by incubating slides overnight in TNB buffer (TSA kit, Perkin Elmer) at 4°C in a humidified container.

TNB buffer was removed the following morning, and primary antibody (rabbit anti-GR M-20, Santa Cruz) was added at 1:100 in TNB buffer. Slides were incubated at room temperature for 1 hour in a humidified container.

Slides were then washed in 0.05% Tween-20 in PBS - 3x 5 minutes - and secondary antibody (biotinylated goat anti-rabbit) applied at a concentration of 1:500 in TNB buffer. Slides were incubated for 1 hour at room temperature in a humidified container and then washed 3 times in 0.05% Tween-20 in PBS for 5 minutes each.

Streptavidin-HRP was added at a concentration of 1:200 in PBS and slides incubated at room temperature for 30 minutes in a humidified container. Following this, 3x 5 minute 0.05% Tween-20 in PBS washes were performed.

Tyramide substrate was added (TSA kit with TMR, Perkin Elmer) as a 1:50 dilution in the diluent provided. Slides were incubated at room temperature for 10 minutes in a humidified container, followed by a further 3x 5 minute 0.05% Tween-20 in PBS washes.

Slides were mounted using an aqueous mounting medium containing a DAPI nuclear stain (Vector Laboratories). One drop was added per slide, a glass coverslip applied and sealed on all sides using nail polish. Slides were left to dry at room temperature in the dark for 24 hours prior to imaging.

2.4.4 Processing of tissue for in situ hybridisation

Mice were sacrificed using an intraperitoneal injection of 200 µl pentobarbitone (Pentoject). The chest cavity was opened and a hole made in the trachea using microdissecting scissors. A cannula was made from a 23G needle (BD Microlance 3, Becton Dickinson) inserted into plastic tubing (Fine bore, 0.58mm internal diameter, 0.96 external diameter, Smiths), which was then inserted into the trachea. The right bronchus was clamped using a tissue clamp and right lung lobes removed and snap frozen on dry ice for protein and RNA analysis. The left lung lobe was inflated with 500µl 50% OCT tissue freezing medium (Leica Biosystems) in PBS infused via the cannula. The trachea was then clamped below the insertion point with a tissue clamp and the cannula removed. The left lung lobe was removed and transferred to a piece of autoclaved tin foil on dry ice. Tissue clamps were then removed and the lung lobe left to solidify. Once frozen solid, the lung lobe was wrapped in the autoclaved tin foil, labelled, and stored at -80ºC prior to slide preparation.

Frozen lungs were sectioned using a Leica CM3050 cryostat with object temperature set to -21ºC and chamber temperature set to -23ºC. Cryostat blade, brushes and chuck were treated with RNase Zap (RNase decontamination

solution, Life Technologies) and the chamber itself cleaned with 70% ethanol to minimise contamination. Tissue sections were left in the chamber to acclimatise for at least 1 hour before sectioning commenced, then mounted onto the chuck using OCT tissue freezing medium. 12µm coronal sections were cut through each tissue sample and transferred to polysine slides (VWR International), 5 sections per slide. Slides were left to dry at room temperature for 5-10 minutes, then transferred to dry ice and frozen at -80ºC for storage.

2.4.5 *In situ* hybridisation

In situ hybridisation (ISH) was used to assess expression of GR (*Nr3c1*) mRNA in lung slices taken from $GR^{flox/flox}$ and $Ccsp\text{-}GR^{-/-}$ animals. Due to the precise nature of this protocol, the use of radioactive isotopes, and the minimal contribution to the overall thesis, this work was performed by another lab member, Dr. Ben Saer, who is already proficient at this technique.

Frozen slides (4/genotype) were fixed in 4% PFA for 15 minutes. Following fixation, slides were washed twice in PBS (5 minute incubation for each). A solution of triethanolamine (TEA, Sigma-Aldrich) and acetic anhydride (AA, Sigma-Aldrich) was prepared fresh using 3ml TEA, 520µl AA and 200ml 0.9% NaCl (Promega Ltd). This solution was used to acetylate the sections, which prevents non-specific binding and reduces background signal. Slides were incubated in the TEA/AA solution for 10 minutes at room temperature with gentle agitation from a magnetic stirrer, then washed in 0.1M PBS for 5 minutes. Dehydration was achieved using a series of ethanol incubations of increasing concentration (70% for 5 minutes, 80% for 5 minutes, 90% for 5 minutes, 95% for 10 minutes, 100% for 10 minutes). Slides were then placed in chloroform for 5 minutes and then left to air dry in a fume hood.

2.4.5.1 Preparation of radiolabelled probes

The prGR9 plasmid was a generous gift from Prof. Karen Chapman (Edinburgh University), which expresses the complementary sections to exons 5-9 of rat GR but has been shown to work for mouse tissue (Michailidou et al. 2008). The plasmid was linearised using restriction enzymes (Roche Diagnostics) to generate a template for sense (using *Eco*RI) and antisense (using *Ava*I) transcripts. 20µg of

plasmid was added to 10µl 10x reaction buffer (Roche Diagnostics) and 10µl restriction enzyme (10U/µl). This mixture was brought to a final volume of 100µl using nuclease-free water (Life Technologies). Samples were mixed by vortexing and incubated at 37ºC for 4 hours. 5µl of each reaction mix was then run on an agarose gel to check for efficient linearization. These samples were run on a 1% agarose in TBE gel, along with an un-linearised plasmid control.

For each linearization reaction, a phenol chloroform extraction was then used on the remainder of the linearization mix to isolate the DNA. For this, 400µl phenol:chloroform:iso-amyl alcohol 25:24:1 pH8.0 (Sigma-Aldrich) and 300µl nuclease-free water were added to the remaining linearised product. This mixture was vortexed and then centrifuged at 13,000g for 5 minutes. The upper (aqueous) phase was transferred to a fresh Eppendorf tube along with 350µl of chloroform (Sigma-Aldrich) and centrifuged at 13,000g for 5 minutes; the lower phases were disposed of. The upper (aqueous) phase was transferred to a fresh Eppendorf tube along with 1/10 volume of 3M sodium acetate (Sigma-Aldrich) and 1µl 20mg/ml glycogen (Roche Diagnostics). The mixture was vortexed and 2x volume of ice cold 100% ethanol added. The resulting mixture was left to precipitate at -80ºC for 1 hour. Following precipitation, samples were centrifuged at 13,000g for 45 minutes at 4ºC to pellet the DNA. The supernatant was removed and the pellet washed with 100µl 70% ethanol before a final centrifugation at 13,000g for 5 minutes. The supernatant was removed and the pellet left to air dry at room temperature. The pellet was then resuspended in 15µl nuclease-free water and DNA yield quantified using a NanoDrop 1000 (Thermo Scientific).

Prior to radiolabelling, cold transcription was performed for both sense and anti-sense probes to ensure a transcriptional product could be obtained from the reaction. 1µg linearised template was added to 2µl DTT, 4µl 5x transcription buffer, 1µl each of rATP, rCTP, rGTP and rUTP (all 10mM) and 1µl RNase inhibitor (all Promega). For the sense construct, 2.5µl SP6 RNA polymerase (Promega) was added. For the anti-sense construct, 1.5µl T7 RNA polymerase (Promega) was added. Each mixture was made up to 20µl with nuclease-free water and then incubated at 37ºC for 45 minutes. Following incubation, 3µl RQ1 DNase (Promega) was added in order to degrade the DNA template. The mixture

was incubated at 37ºC for a further 10 minutes to facilitate this reaction. To assess successful transcription, solutions were run on a 1% agarose-TBE gel.

Synthesis of radioactive probes followed the same process as cold transcription, except the rUTP was replaced with uridine 5'-triphosphate α-^{33}P (Perkin Elmer) and samples were not run through an agarose gel. Radiolabelled probes were purified prior to use by running through illustra ProbeQuant G-50 micro columns (GE Healthcare Ltd.) to remove unincorporated nucleotides. The gel matrix was prepared by vortexing followed by centrifugation at 735g for 1 minute as per manufacturer's instructions and then placed into microcentrifuge tubes. Sample volumes were made up to 50µl with DEPC-treated water and then added to the columns (one column per sample). Samples were spun at 735g for 2 minutes. 50µl deiodinised formamide 99.5% (Sigma-Aldrich) was added to each elute and tubes incubated at 65ºC for 5 minutes followed by 2 minutes incubation on ice. To assess radioactivity counts, 1µl sample was added to 4ml scintillation fluid (National Diagnostics) and measured using a Tri-Carb 2100CA Liquid Scintillation Analyser (Perkin Elmer). This ensured the amount of radiolabelled probe was consistent across all slides. For each probe, a measure of 15 x 10^5 counts per minute was added per 100µl hybridisation buffer (see appendix 3 for recipe and preparation).

2.4.5.2 Hybridisation

100µl hybridisation buffer/probe solution (pre-heated to 60ºC) was added to each slide and a hybrid-slip (Sigma-Aldrich) added over the top. Hybridisation was performed overnight at 60ºC in a humidified chamber.

The following morning, hybrid-slips were removed and slides washed in 2x SSC buffer (Promega) with 50% formamide at room temperature for 10 minutes, followed by 2 x 30 minute incubations at 60ºC in 2x SSC-50% formamide buffer pre-heated to 60ºC. The slides were then incubated in RNase A (20µg/ml in TEN buffer, recipe in appendix 3) at 37ºC for 30 minutes to degrade unbound probes. This was followed by 2 further incubations in 2x SSC-50% formamide buffer pre-heated to 60ºC, for 15 minutes each, and then a 30 minute incubation in 0.5x SSC pre-heated to 60ºC, all performed at 60ºC. Slides were then passed through 5

minute incubations in increasing ethanol concentrations (70%, 95% and 100%) at room temperature.

2.4.5.3 Imaging and analysis

Slides were taped, tissue side up, to the inside of a development cassette. Inside a dark room, a sheet of Kodak BioMax MR film (Sigma-Aldrich) was applied over the top of the slides to enable imaging. The development cassette was then sealed shut with autoclave tape and left at -80ºC for 2 weeks. After this exposure period, the cassette was brought back to room temperature and opened inside a dark room. The film was processed using a JP-33 Film Processor (JPI Healthcare).

The developed film was scanned with a CoolSNAP-Pro camera (Photometrics) with light box illumination (Jencons Scientific). Signal intensity was determined by measuring the optical density of regions of interest in Image Pro Plus 6.0 software (Media Cybernetics). Relative optical density was calculated for bronchioles for each animal (n=4/genotype) using the following formula:

$$ROD = (-Log_{10}(ROI/LB)) - (-Log_{10}(C/LB))$$

Where:
ROD = relative optical density
ROI = region of interest
LB = light box
C = control region

Optical densities for both film and light box are consistent for all samples, and a control region was selected for each section. 2-3 bronchioles on each lung section were analysed (yielding 52-59 measures) per animal. Relative optical densities of each were averaged per animal, to give 4/genotype, and values are expressed as proportions of the wild-type mean.

2.4.6 RNA extraction

RNA extraction from tissue was performed using Trizol reagent (Invitrogen) and mechanical homogenisation at a speed of 6.0m/s, 3x 40s cycles (Lysing matrix D tube and FastPrep machine, MP Bio). Following homogenisation, chloroform was added and the mixture centrifuged at 12,000g for 15 minutes at 4°C. The aqueous phase was removed, added to isopropanol and incubated on ice for 10 minutes before being centrifuged at 12,000g for 10 minutes at 4°C. The pelleted RNA was washed with 75% ethanol, vortexed and spun at 12,000g for 5 minutes at 4°C. The supernatant was removed and the pellet left to air dry for 10 minutes before being resuspended in 200µl RNase-free water and stored at -80°C.

2.4.7 Reverse transcription

RNA samples were analysed using a NanoDrop 1000 (Thermo Scientific) to determine RNA concentration and quality. 250-500ng RNA was treated with DNase and incubated at 37°C for 30 minutes. At this point, DNase stop was added and the mixture incubated at 65°C for 10 minutes and then cooled on ice. The resulting mixture was then used for reverse transcription into cDNA, using a high capacity RNA-to-cDNA kit (Applied Biosystems). cDNA samples were stored at -20°C prior to use in quantitative PCR (qPCR).

2.4.8 qPCR

cDNA was analysed via quantitative PCR, using either TaqMan probes and primers with a StepOne Plus machine (ABI) for 96-well plates (chapter 3) or SYBR green primers and an ABI Prism 7700 machine for 384-well plates (chapter 4). Cycling conditions are given in appendix 4, along with primer sequences and master mix recipes.

SYBR green primers for mouse *18S*, *β-actin*, *Bmal1* and *Per2* were designed in-house or are sequences taken from Reddy et al. (2007) and were produced by MWG Operon, as were TaqMan *β-actin*, *Bmal1*, *Per1* and *Per2* primers. TaqMan *Rev-erbα* primer/probe mixture is commercially available from Applied Biosystems (Mm00520708_m1). All non-proprietary primer and probe sequences are given in appendix 4.

Gene expression levels were normalised to the housekeeping gene, *18S* or *β-actin*, and relative quantification levels (using the $2^{-\Delta\Delta Ct}$ method) are presented. Normalisation protocols and reference samples are detailed in each chapter.

2.4.9 ELISAs

2.4.9.1 Corticosterone

ELISAs for corticosterone were performed using corticosterone EIA kits from Enzo Life Sciences, according to the manufacturer's instructions for low volume samples. Briefly, 5µl sample was mixed with an equal volume of the supplied steroid displacement reagent (diluted 1:100 in PBS), vortexed, and incubated at room temperature for 5 minutes. 190µl of supplied elution buffer was then added to the mixture, giving a final sample dilution of 1:40. 100µl of the diluted samples were added to the plate and standard protocol then followed. Plates were read at 405nm on a Biotek plate reader, and standard curves generated for each plate. Corticosterone concentrations were calculated from a linear trend line fit to a semi-log standard plot using Microsoft Excel. An example standard curve is included in appendix 5.

2.4.9.2 Interleukin-6/CXCL5

The IL-6 and CXCL5 ELISAs were performed using R&D systems quantikine kits. The protocol is the same for each cytokine, but concentrations of antibodies and dilution factors vary. Where this is the case, the two values are given in brackets. 96-well high-binding, flat-bottomed, clear polystyrene ELISA plates (R&D systems) were first coated with the supplied capture antibody diluted in PBS (IL-6 2.0µg/ml; CXCL5 4.0µg/ml); 50µl capture antibody solution was added to each well. Plates were tapped to ensure even coverage of all wells and incubated overnight at room temperature. All incubations were performed with a plate sealer applied.

The following morning, plates were washed three times with 0.05% Tween-20 in PBS. For each wash, wash buffer wash dispensed into wells using a Vaccu-Pette/96 (Sigma), plates were tapped to agitate the liquid and then inverted over the sink to dispose of the used buffer. After the final wash, plates were inverted

and blotted against absorbent paper towels. A blocking buffer of 0.5% BSA in PBS (made fresh on the day) was then added to each well - 150µl/well. Plates were incubated with this blocking buffer for 1hr at room temperature.

The wash step was repeated (3x washes in 0.05% Tween-20 in PBS), and samples and standards were added to the plate. A 7-point standard curve of 2-fold serial dilutions was used, with a high standard of 1,000pg/ml along with a 'blank' consisting of diluent only (both assays). Samples were diluted in either bronchoalveolar lavage fluid (for BAL samples) or the blocking buffer (0.5% BSA in PBS, for blood samples) and 50µl of standard/sample was added to each well. Dilution factors are detailed in table 2.2.

Treatment group	Dilution Factor	
	IL-6 assay	CXCL5 assay
Intraperitoneal saline	4	-
Intraperitoneal LPS (intact)	4	-
Intraperitoneal LPS (ADX)	40	-
Aerosolised saline	4	2.5
Aerosolised LPS (all groups)	4	10

Table 2.2: Dilution factors for samples used in IL-6 and CXCL5 ELISAs
In order to keep test concentrations within the measurable range of the enzyme-linked immunosorbent assay (ELISA), samples had to be diluted to varying degrees. The exacerbated inflammatory response seen in the adrenalectomised (ADX) intraperitoneal lipopolysaccharide (LPS) group, for example, meant a higher dilution factor had to be used to stay within range of the interleukin-6 assay.

Standards were assayed in duplicate, whereas samples were assayed individually to preserve the sample. Plates were incubated with samples and standards for 2 hours at room temperature before being washed a further three times as before. Detection antibody was made up to working concentration (400ng/ml IL-6; 50ng/ml CXCL5) in the blocking buffer (0.5% BSA in PBS) and 50µl added to each well. Plates were then incubated for another 2 hours at room temperature.

Plates were washed again (3x washes in 0.05% Tween-20 in PBS), and 50µl Streptavidin-HRP (R&D systems), 1:200 in blocking buffer, was added to each well. Plates were covered and incubated away from direct sunlight for 20 minutes at room temperature, followed by an additional 3 washes. A substrate solution was made from a 1:1 mixture of Colour Reagent A (H_2O_2) and Colour Reagent B (Tetramethylbenzidine), both from R&D systems (DY999). 50µl substrate mixture was added to each well and plates were incubated for 20 minutes at room temperature away from direct sunlight. Without washing plates, 50µl stop solution (2N H_2SO_4) was added to each well to stop the reaction, and plates were tapped to ensure an even mixing and colour formation.

Plates were read at 450nm on a Biotek plate reader, using the 0µg/ml standard as a blank. Sample concentrations were calculated using log-log standard plots with linear trend lines fitted in Microsoft Excel. An example standard curve for each cytokine is included in appendix 5.

2.4.10 Bioplex

The bioplex assay is analogous to an ELISA but measures multiple analytes simultaneously by using colour-coded microparticles for each analytes. When the plate is read, one laser detects the type of analyte being measured (colour of particle, pre-determined by kit) and another measures the concentration of that analyte (streptavidin-PE-derived signal generated during assay). The kit used in this work was a magnetic luminex screening assay from R&D systems, which was read on a Bio-Rad Bio-Plex 200 system with Bio-Rad software. All bronchoalveolar lavage fluid samples were run neat and standard ranges are given in table 2.3. All buffers and reagents were provided as part of the R&D Systems assay kit.

Standards were prepared from three stock vials provided (A, B and C). Each vial was reconstituted with calibrator diluent RD6-52 as per instructions. Each vial was allowed to sit for 15 minutes with gentle agitation prior to making dilutions. A high standard cocktail was then made from 100µl each of A, B and C, along with 700µl calibrator diluent RD6-52 to make 1ml total volume. This served as standard 1. Serial 3-fold dilutions were then performed from 100µl previous

standard + 200µl calibrator diluent RD6-52. At each step, standards were mixed thoroughly before proceeding with the next dilution. 6 standards were made in total.

Next, the microparticles were resuspended by a brief centrifugation (to spin down liquid from inside the cap) and a gentle vortex. For a full 96-well plate, 500µl microparticle cocktail was mixed with 5ml assay diluent RD1W in the opaque mixing bottle provided. 50µl of the diluted microparticle solution was added to each well of the 96-well plate provided. Standards and samples were then added to the appropriate wells, 50µl/well, along with 2 wells containing 50µl calibrator diluent RD6-52 to serve as a blank control. Standards and blank were run in duplicate and samples were run individually. The plate was then sealed using the foil plate sealer provided and incubated for 2hrs at room temperature on an orbital shaker set at 800rpm.

Wash buffer was prepared by mixing 20ml wash buffer concentrate with 480ml dH_2O to make 500ml wash buffer. The plate was washed using a magnetic micro-plate washer (Bio-Rad), which was attached to the underside of the plate while the plate was inverted to remove liquid. The magnet was removed before wash buffer added (100µl/well), to allow resuspension of the microparticles and a more thorough wash. The magnet was then reapplied and the plate inverted to remove wash buffer. This process was repeated twice for a total of three washes. With the magnet still in place, the plate was gently blotted against absorbent paper to remove as much liquid as possible before proceeding with the assay.

Biotin antibody was then prepared by a brief centrifugation and a gentle vortex. 500µl antibody cocktail was mixed with 5ml assay diluent RD1W in the second opaque mixing bottle provided. 50µl of the diluted biotin antibody solution was added to each well and the plate was sealed with a fresh foil plate sealer. The plate was placed back on the orbital shaker at 800rpm for a further 1hr at room temperature.

Analyte	Low standard	High standard	Bead region
CRG-2 (CXCL10)	177	42,900	37
CXCL5	58.1	14,130	66
Eotaxin (CCL11)	11	2,670	74
G-CSF (CSF3)	46.5	11,300	39
GM-CSF (CSF2)	18.9	4,600	12
IFNγ	25.9	6,300	33
IL-1α	53.5	13,000	47
IL-1β	345	83,800	19
IL-2	10.3	2,510	22
IL-5	11.1	2,700	26
IL-6	65.8	16,000	27
IL-10	27.2	6,600	28
IL-12 p70	58	14,100	15
IL-13	135	32,910	29
IL-17	164	39,900	30
KC (CXCL1)	51.4	12,500	13
MCP-1 (CCL2)	337	81,800	18
M-CSF (CSF1)	9.88	2,400	45
MIP-1α (CCL3)	11.1	2,700	46
MIP-1β (CCL4)	138	33,500	51
MIP-2 (CXCL2)	5.76	1,400	20
RANTES (CCL5)	78.6	19,100	38
TNFα	2.26	550	14

Table 2.3: Standard values and bead regions for bioplex assay

Standards were provided pre-mixed as part of the magnetic luminex screening assay (R&D systems). A standard curve was generated from serial 3-fold dilutions to give the high and low standard concentrations detailed. 'Bead regions' denote the unique colour attributed to each analyte and serve as a way of identifying which protein is being measured.

The wash was repeated as before, for a further three applications and removals of wash buffer. Again, the plate was gently blotted against absorbent paper to remove residual liquid. Streptavidin-PE was prepared by brief centrifugation and a gentle vortex, and diluted to working concentration by adding 220µl concentrate to 5.35ml wash buffer. 50µl working streptavidin-PE was added to each well and the plate was sealed with a fresh foil plate sealer. The plate was placed back on the orbital shaker at 800rpm for 30 minutes at room temperature. During this time, the Bio-Rad Bio-Plex 200 machine was prepared as the lasers can take up to 30 minutes to warm up and the machine must always be calibrated before use. These processes were performed according to the on-screen instructions provided by the machine.

A final wash step (3x washes) was performed and microparticles resuspended with 100µl wash buffer per well. The plate was incubated for 2 minutes on the orbital shaker (800rpm) to ensure a thorough mixing and resuspension. The plate was then read on a Bio-Rad Bio-Plex 200 machine with the following settings (specified by the R&D Systems kit):

Microparticle regions:	See table 2.3
Events/bead:	50
Flow rate:	60µl/minute (fast)
Sample size:	50µl
Doublet discriminator gates:	8,000 and 16,500
Collect:	Median fluorescence intensity (MFI)

Concentrations of samples were calculated automatically by the software using blank-subtracted median fluorescence intensity values and a 5-parameter logistic (5-PL) curve for each analyte.

2.4.11 Protein extraction

Extraction of protein from snap-frozen tissue was performed using T-PER (Thermo Scientific), a proprietary detergent. T-PER was mixed with protease inhibitors (Complete mini protease inhibitor tablets, Roche, 1 tablet/10ml), and phosphatase inhibitors (cocktail 2 and cocktail 3, Sigma, 100µl each/10ml) to

make an extraction buffer. For lung, one whole lung lobe was added to 1ml ice cold buffer in a Lysing Matrix D tube (MP Biomedicals). Tissue was homogenised using an MP Biomedicals FastPrep machine at a speed of 6.0m/s for 40s. After homogenisation, the sample was spun at 10,000g for 1 minute at 4°C. The supernatant was transferred to a 1.5ml Eppendorf tube and stored at -80°C until required for analysis.

2.4.12 Protein quantification

Protein concentrations were quantified using bicinchoninic acid (BCA) assay. Standards were prepared as separate dilutions from a stock standard of 1mg/ml BSA in T-PER, to give a 6-point curve consisting of 0, 100, 200, 400, 800 and 1,000µg/ml concentrations; 200µl of each. 1ml colourless bicinchoninic acid solution and 120µl blue copper II sulphate pentahydrate (4%) solution per sample (plus 6 standards) was mixed as a master mix and vortexed until the solution was a uniform light green colour. Samples were prepared as two dilutions – 1:25 and 1:50. 1ml of the green BCA working reagent was added to 50µl of each standard/sample and vortexed gently. Mixtures were incubated at 37°C for 30mins.

Following incubation, 200µl of each solution was transferred to a Falcon 96-well plate. Standards were assayed in triplicate and samples in duplicate. Absorbance was measured at 540nm on a Biotek plate reader, using the 0µg/ml standard as a blank. Protein concentrations were calculated using a log-log standard curve with linear trend line fitted and multiplied by dilution factor as appropriate.

2.4.13 Western Blot

Protein concentration was quantified by bicinchoninic acid (BCA) assay (assay). 40µg protein was added to an Eppendorf tube and made up to 19.5µl in the T-PER protein extraction buffer (Thermo Scientific). 7.5µl NuPAGE 4x LDS sample buffer (Life Technologies) was added, along with 3µl 1M DTT (Life Technologies) to make a total volume of 30µl. The mixture was then incubated at 70°C for 10 minutes to denature the protein. Samples were loaded into a 4-15% Mini-PROTEAN TGX precast gel (Bio-Rad), 15µl/well. An additional lane

contained 10µl Precision Plus Protein Kaleidoscope Standard (Bio-Rad) protein ladder to enable estimation of protein size (10-250kDa).

Proteins were separated by SDS polyacrylamide gel electrophoresis (SDS-PAGE), using 1xTris/Glycine/SDS running buffer (Bio-Rad) and 150V for 1hr then transferred to a Protran nitrocellulose membrane (Whatman, 0.2 µm pore size) at room temperature for 1hr at 30V using a methanol-based transfer buffer. After transfer, the membrane was stained with Ponceau S to check for efficient protein transfer and cut into three sections, corresponding to the regions that GR, β-actin and CCSP should reside in, using the protein ladder and Ponceau stain as guidance. One cut was made between the 50kDa and 75kDa bands, the other between to 20kDa and 25kDa bands. The three sections were then rinsed with TBST - Tris-HCl pH 7.6 buffered saline (TBS) solution with 0.1% Tween-20 (Sigma) and kept in separate dishes for the rest of the staining protocol. Each membrane was blocked with 3% skim milk powder in TBST for 1 hour at room temperature without agitation.

Antibodies were diluted into the 3% skim milk in TBST solution and applied to the corresponding section of membrane. The top section, 75kDa upwards, was incubated with rabbit polyclonal anti-GR (M-20) antibody (Santa Cruz); the middle section, 25kDa-50kDa, was incubated with rabbit polyclonal anti-β-actin (AbCam); the lower section, 20kDa and below, was incubated with rabbit polyclonal anti-CCSP (Merck Millipore). All primary antibodies were used at a concentration of 1:1000 and membranes were incubated overnight at 4°C with gentle agitation.

Membranes were washed 3 × 20 min with TBST with agitation to remove unbound antibody. Secondary HRP-linked antibody (goat anti-rabbit) was added diluted 1:5000 in 3% milk in TBST and membranes incubated at room temperature for 1hr with agitation. A further 3 x 20 minute washes in TBST were performed to remove unbound secondary antibody and the membranes transferred to a clean weigh boat.

Imaging was performed using chemiluminescence – a 1:1 mixture of luminol and hydrogen peroxide (both Life Technologies) was washed over the membranes for 5 minutes. Membranes were then transferred to an imaging cassette and processed in a dark room using Kodak BioMax XAR Film (Sigma-Aldrich) and JP-33 Film Processor (JPI Healthcare). GR and β-actin images are the result of a 3 minute exposure, whereas CCSP was exposed for 30s.

2.5 Statistics

Data was analysed using SPSS 22 (IBM) and Prism 6 (GraphPad), and graphs plotted with Microsoft Excel. Data is presented as mean +/- standard error of the mean (SEM), and a significance value of $p<0.05$ was used as standard. Where multiple comparisons were made, the p value was lowered according to the Bonferroni correction protocol (adjusted p value = original p value divided by number of tests performed). In some experiments, outliers were removed using the Median Absolute Deviation. Briefly, the median value is determined for each sample, and deviations of all samples from the median are calculated. The median of those deviations is then used as a measure of whether an individual data point can be considered an outlier. If a data point fell outside of the median +/- 2x median of deviations, then it was excluded. This measure is very similar to the common mean +/- 2 x standard deviation protocol, but is less affected by outliers themselves and is therefore a more reliable test (Leys et al. 2013). Where outliers were removed, this is made explicit in text and figure legends and the logic behind the exclusion will be stated in the corresponding sections.

Chapter 3: Impact of adrenalectomy upon rhythmic pulmonary inflammation

3.1 Introduction

Corticosterone is known to play a role in regulating rhythmic inflammation. Nakamura et al. (2011) observed a loss of temporal gating of an allergic skin reaction in *Per2*$^{m/m}$ mice, which have a loss-of-function mutation leading to a loss of rhythmicity when in constant darkness (Zheng et al. 1999). In their model, mice were sensitised with a subcutaneous injection of anti–TNP IgE which induces a local anaphylactic reaction. 24 hours later, mice were challenged with DNP-BSA mixed with Evans blue dye to allow visualisation of the extent of leakage from the vasculature, a measure of vascular permeability. Images of the skin were taken 30 minutes later and analysed via densitometry. In wild type animals, a significant decrease in permeability ('blueness') was seen after challenge at ZT16 compared to ZT4, 10 or 22. No time-of-challenge effect was seen in the *Per2*$^{m/m}$ mice.

The loss of inflammatory rhythm in the *Per2* mutants was also associated with a dampened rhythm and elevated concentration of circulating corticosterone, even in a light:dark cycle. Adrenalectomy was used to determine whether the loss of rhythmic signals from the adrenals, including corticosterone, were responsible for the time-of-day effects observed in wild-type animals. Vascular permeability was attenuated in response to challenge at ZT16 compared to ZT4 in sham-operated animals, as had been seen in wild-type mice, but this effect was lost in adrenalectomised animals – clearly implicating adrenal-derived factors in regulating the rhythmic inflammatory response to allergic challenge. Whether the same is true for the innate immune response is tested in this chapter.

3.2 Hypothesis tested and experimental approaches

Hypothesis 1: Rhythmic adrenal glucocorticoid signals drive the circadian regulation of inflammatory response in the lung.

Aim: Disrupt endogenous glucocorticoid signalling via adrenalectomy, and establish the impact upon time-of-day variation in innate inflammation.

Objectives:

- Characterise the daily profile of circulating glucocorticoid concentrations in intact and adrenalectomised (ADX) animals.

Mice were adrenalectomised and blood samples collected via tail bleed at multiple time points across one day. Sample timings were zeitgeber time (ZT) 0 (lights on), ZT4, ZT8, ZT12 (lights off), ZT16 and ZT20. Serum was analysed via ELISA to determine corticosterone concentration.

- Determine whether loss of rhythmic circulating glucocorticoids via adrenalectomy disrupts clock-driven behavioural rhythms (via wheel running) and/or clock gene rhythms in target tissue (via qPCR).

ADX and intact control animals were individually housed with running wheels and wheel-running activity monitored in 12:12 light:dark (12:12 LD) and constant darkness (DD) as a proxy measure of central pacemaker rhythmicity. Clock gene rhythms in target tissue was analysed in saline-challenged animals from later experiments. Tissue was snap frozen at time of collection (CT5, 5 hours after lights would normally come on, or CT17, 5 hours after lights would normally go off) and RNA extracted. For these samples, 250ng RNA was reverse transcribed to cDNA and relative quantification of *Bmal1*, *Per1*, *Per2* and *Rev-erbα* clock genes was performed via qPCR. These genes were chosen to represent each arm of the clock (+ve loop, -ve loop and auxiliary loop), along with an acutely-sensitive Gc target (*Per1*) which may be expected to change. All cycle threshold values were made relative to *β-actin*, which was used as a housekeeping gene, and

these values were then normalised to a reference intact sample at CT5 using the $2^{-\Delta\Delta Ct}$ method.

- Challenge intact and ADX animals with lipopolysaccharide (LPS) at different times in the circadian cycle and measure the resulting inflammatory response via quantification of cell infiltration and measurement of cytokine concentrations.

ADX and intact control mice were group-housed in 12:12 LD for one week, followed by 24hrs DD. Animals were then challenged with aerosolised LPS or saline vehicle at either CT0 (time lights would normally come on) or CT12 (time lights would normally go off). Infra-red goggles were used to allow treatments to be performed in darkness. Animals were culled 5 hours later and inflammatory cell influx and chemoattractant concentration in bronchoalveolar lavage fluid was measured.

- Compare the influence of adrenalectomy upon the inflammatory response to systemic endotoxin challenge (intraperitoneal lipopolysaccharide injection) and pulmonary challenge (aerosolised lipopolysaccharide).

ADX and intact control mice were group-housed in 12:12 LD for one week, followed by 24hrs DD. Animals were then challenged with intraperitoneal injection of LPS or saline vehicle at either CT0 or CT12. Infra-red goggles were used to allow treatments to be performed in darkness. Animals were culled 4 hours later and pro-inflammatory cytokine concentration in serum was measured. The slightly earlier time point was chosen to reflect the difference in response latencies of the two challenges – systemic IL-6 tends to peak earlier than pulmonary CXCL5.

3.3 Results

In order to assess successful adrenalectomy, corticosterone was measured in serum samples collected 1 week after surgery. Blood samples were taken via tail tipping from each adrenalectomised mouse, along with intact controls at a time when circulating glucocorticoids (Gcs) should be elevated (dark phase, ZT14). Figures for each of these tests are in appendix 6. This confirmed effective adrenalectomy and safe inclusion in subsequent experiments and analyses. Animals showing circulating concentrations above 25ng/ml were treated with caution, and were stratified across experimental groups to minimise the impact of potentially incomplete adrenalectomy whilst avoiding wastage of animals.

3.3.1 Adrenalectomy abolishes diurnal variation in serum corticosterone concentration

Profiling of corticosterone concentration in serum across a 20-hr period showed a significant effect of time in intact animals (repeated measures ANOVA with Greenhouse-Geisser correction for lack of sphericity, $F_{(2.567,\ 10.267)} = 7.428$, $p<0.05$). With the same test applied to samples from adrenalectomised animals, no significant effect of time was observed ($F_{(1.734,\ 12.139)} = 1.924$, $p=0.190$). Data is presented in figure 3.1.

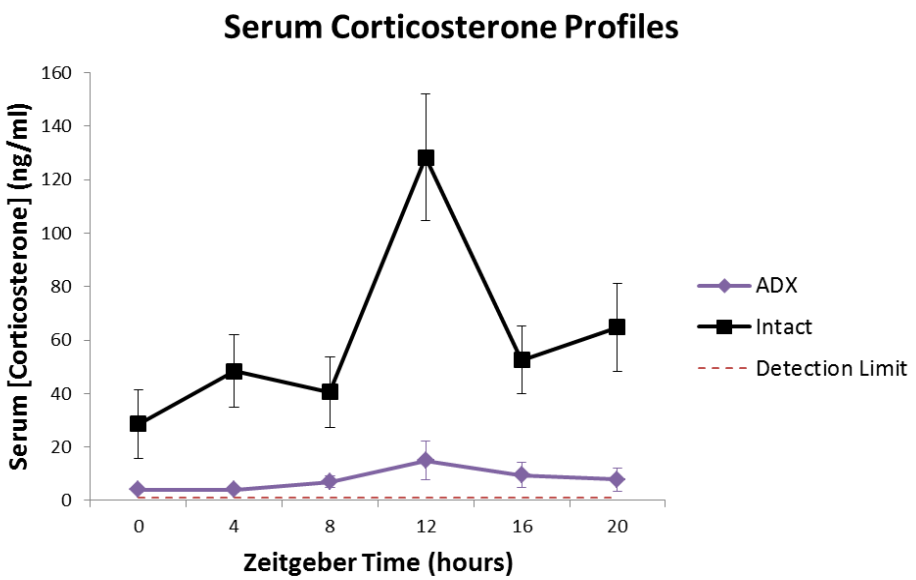

Figure 3.1: Circulating serum corticosterone concentrations across a diurnal period
Serial samples of tail blood from intact (n=5) and adrenalectomised (n=8) mice across one day.

3.3.2 Adrenalectomy does not affect the behavioural output from central pacemaker

To measure the effect of adrenalectomy on the central circadian rhythm, wheel-running behavioural analysis was performed as a proxy to illustrate rhythmicity of the SCN. Wheel revolutions were counted and analysed using ClockLab software (Actimetrics) and representative actograms plotted from this data are shown in figure 3.2A. Analysis of period (figure 3.2B) showed no effect of light schedule (mixed ANOVA with Greenhouse-Geisser correction for lack of sphericity – $F_{(1,8)}=3.951$, $p=0.082$) and no significant effect of adrenalectomy (mixed ANOVA with Greenhouse-Geisser correction for lack of sphericity – $F_{(1,8)}=0.022$, $p=0.886$). No clear qualitative difference between the activity rhythms of intact and adrenalectomised animals was observed.

3.3.3 Adrenalectomy does not affect the phase of the local pulmonary oscillator

Quantitative PCR was performed on lung samples from mice exposed to aerosolised saline (see below) in order to assess the effect of adrenalectomy on the local pulmonary oscillator phase. Analysis of relative expression (RQ) of each gene by two unpaired t-tests showed a significant effect of time upon the expression of *Bmal1*, *Per2* and *Rev-erbα* in intact animals ($p<0.025$ for each gene), with increased *Bmal1* and *Rev-erbα* mRNA at CT5 compared to CT17 and *Per2* oscillating in anti-phase, as expected (figure 3.3). In adrenalectomised animals, the same pattern was observed although neither *Bmal1* transcript nor *Per2* were not significantly different ($p=0.1$ and $p=0.04$ respectively). *Rev-erbα*, however, showed a significant time of collection effect ($p<0.025$). *Per1* showed no time-of-day variation in either group – $p=0.99$ for intact animals and $p=0.74$ for adrenalectomised animals.

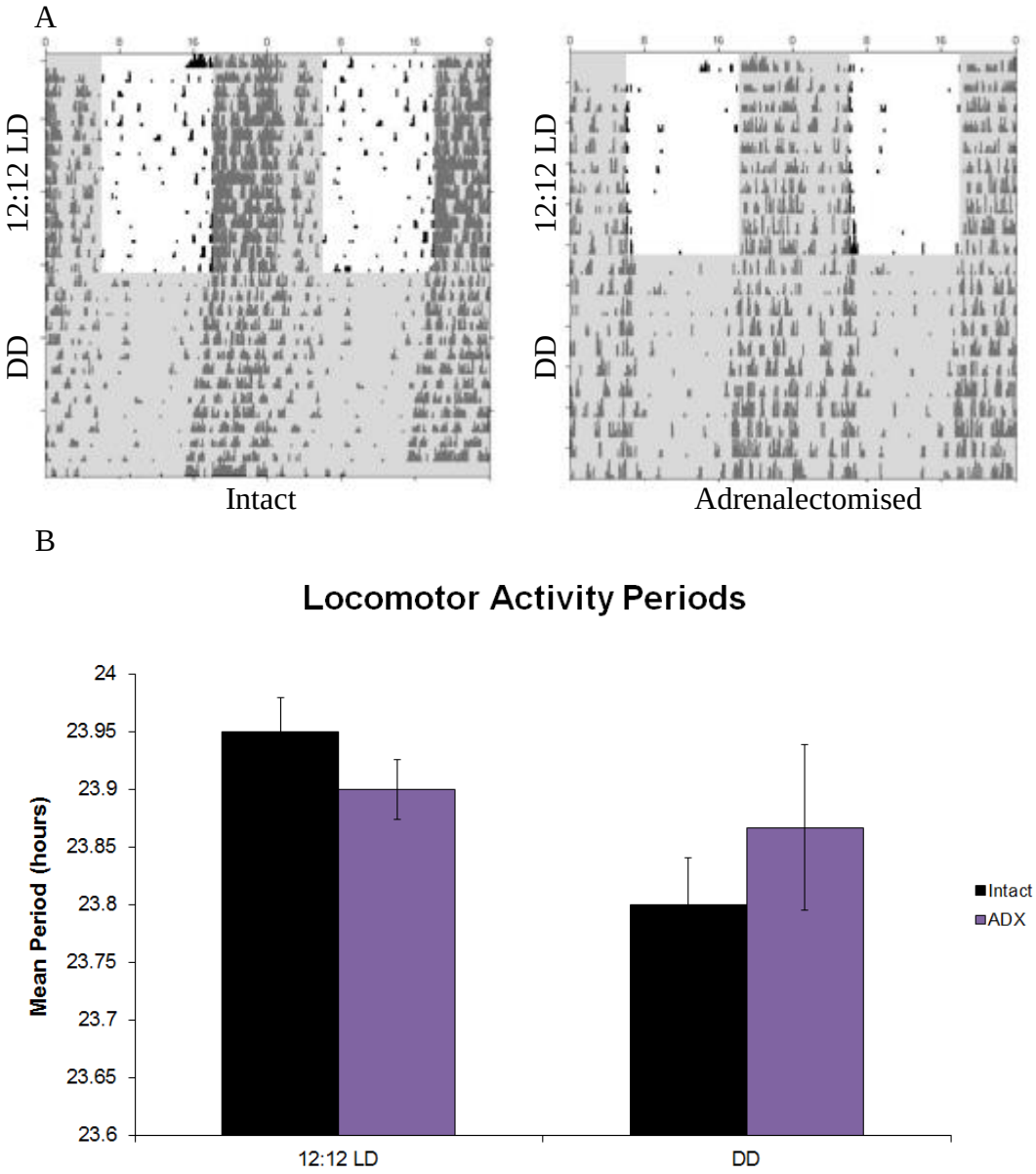

Figure 3.2: Wheel-running activity periods of intact and adrenalectomised mice

Mice were individually housed with free access to a running wheel. Cages were kept in a light-tight cabinet set to a 12hr-light/12hr-dark (12:12 LD) lighting schedule for 9-15 days, followed by constant darkness (DD) for a further 11-12 days. A) Daily wheel-running activity, measured by wheel revolutions, is double-plotted along the x-axis such that each line shows 48hrs of data – the latter 24hrs of which is the first 24hrs of the next line. Grey shading denotes lights off. Plots are representative of 4-6/group, with intact on the left, adrenalectomised on the right. B) Activity periods, defined by the length of a cycle of activity and inactivity, were calculated using ClockLab software (Actimetrics) and average period per condition is shown (intact n=4/condition, ADX n=6/condition).

ADX – adrenalectomised; 12:12 LD – 12 hours light:12 hours dark lighting schedule; DD – constant darkness.

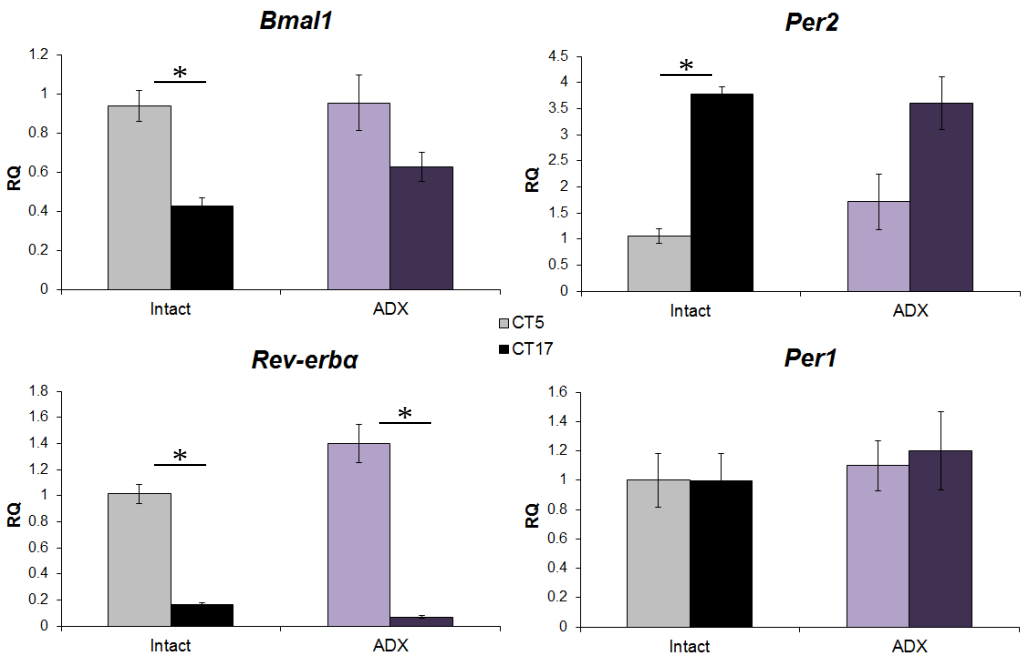

Figure 3.3: Clock gene expression in lungs from saline-treated intact and adrenalectomised animals

Lungs collected from aerosolised saline-treated animals were analysed for clock gene expression. Legend indicates time of collection. Results of unpaired t-tests show expression of *Bmal1* was increased at CT5 compared to CT17 in intact animals, but the difference was not significant in ADX animals; *Rev-erbα* transcript was elevated at CT5 in both groups; expression of *Per2* was in anti-phase to both *Bmal1* and *Rev-erbα* (high at CT17, low at CT5) in both groups although did not reach significance in ADX animals; no time-of-day effect was seen in *Per1* for either group. P values were adjusted to 0.025 to account for two comparisons per gene.

ADX – adrenalectomised; Bmal1 – brain and muscle arnt-like 1; CT – circadian time; CT5 - 5 hours after lights would usually come on, CT17 – 5 hours after lights would usually turn off; Per (1 and 2) – period (1 and 2); RQ – relative quantity. denotes significance at p<0.05.*

3.3.4 Adrenalectomy causes a loss of circadian gating of the neutrophilic response to aerosolised LPS

Assessment of the impact of adrenalectomy upon the rhythmic inflammatory response to aerosolised lipopolysaccharide (LPS) was performed by challenging mice at either CT0 (when lights would normally come on) or CT12 (when lights would normally turn off). Bronchoalveolar lavage and lung tissue samples were collected 5 hours later. Total cell counts in bronchoalveolar lavage fluid were elevated after challenge with lipopolysaccharide compared to treatment with saline vehicle; unpaired t-test, $t_{(57.834)}= -7.07$, $p<0.05$ (figure 3.4A). Comparison of time-of-challenge effects by independent samples two-tailed t-test (with correction for two comparisons) shows an effect of time that borders significance in intact animals ($t_{(23)}=2.387$, $p=0.026$), but not for those adrenalectomised ($t_{(24)}=0.420$, $p=0.678$).

As expected, further investigation into the cell types underlying this elevation in total cell infiltrate revealed that the invading cells were predominantly neutrophils (figure 3.4B). Combination of total cell count and differential proportions obtained by manually counting cytospins allowed comparison of neutrophil number according to time of LPS challenge (figure 3.4C). Analysis by independent samples two-tailed t-test (with correction for two comparisons) shows a significant effect of time upon neutrophil number in intact animals ($t_{(22)}=2.545$, $p=0.018$), but not in adrenalectomised animals ($t_{(23)}=0.482$, $p=0.634$).

Measurement of a key candidate chemokine, CXCL5, by ELISA showed a trend for a time-of-day variation in intact animals (figure 3.4D), although this did not reach significance (unpaired t-test, $t_{(10)}=2.018$, $p=0.071$). No significant differences were seen in adrenalectomised animals ($t_{(10)}=0.036$, $p=0.972$).

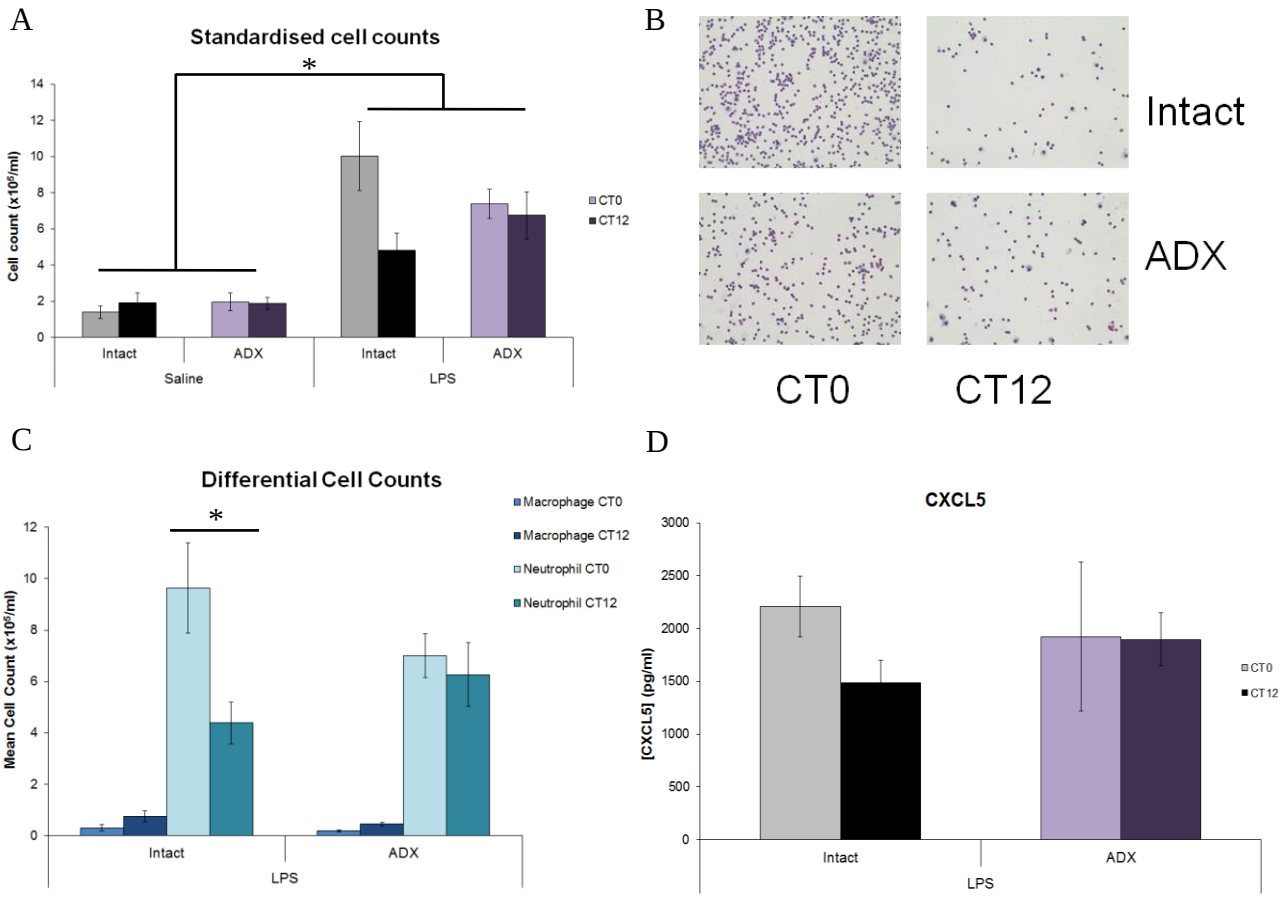

Figure 3.4: Response of intact and ADX mice to aerosolised lipopolysaccharide

Mice were exposed to 2mg/ml lipopolysaccharide (LPS) in saline or saline alone for 20mins at the indicated time points and culled 5hrs later. A) Total cell counts measured in bronchoalveolar lavage (BAL) fluid after saline or LPS challenge. B) Representative cytospins from BAL fluid following LPS challenge. C) Differential cell counts calculated from cytospin proportions and total cell counts from LPS-challenged animals. D) Concentration of the neutrophil chemoattractant CXCL5 in BAL fluid following LPS challenge. For all panels, n=3-6/group for saline, n=12-13/group for LPS.

3.3.5 Adrenalectomy causes an increase in the inflammatory response to systemic LPS

In a separate approach, intraperitoneal LPS was utilised to address the role of rhythmic glucocorticoid signals in modulating systemic inflammatory responses. The pro-inflammatory cytokine interleukin-6 (IL-6) was used as a marker as it is known to be highly responsive to this challenge. Mice were challenged with intraperitoneal injection of 1mg/kg LPS at either CT0 or CT12. Animals were culled 4 hours later and trunk blood collected for analysis. Serum IL-6 concentration fell below the limits of detection for the majority of samples from vehicle-treated animals, so statistical tests were only performed on those which received LPS (figure 3.5).

Analysis by two-way ANOVA shows a significant effect of surgery ($F_{(1,18)}$=201.924, $p<0.05$) but no significant effect of time of challenge ($F_{(1,18)}$=0.198, $p=0.661$). No significant interaction was observed ($F_{(1,18)}$=0.130, $p=0.723$).

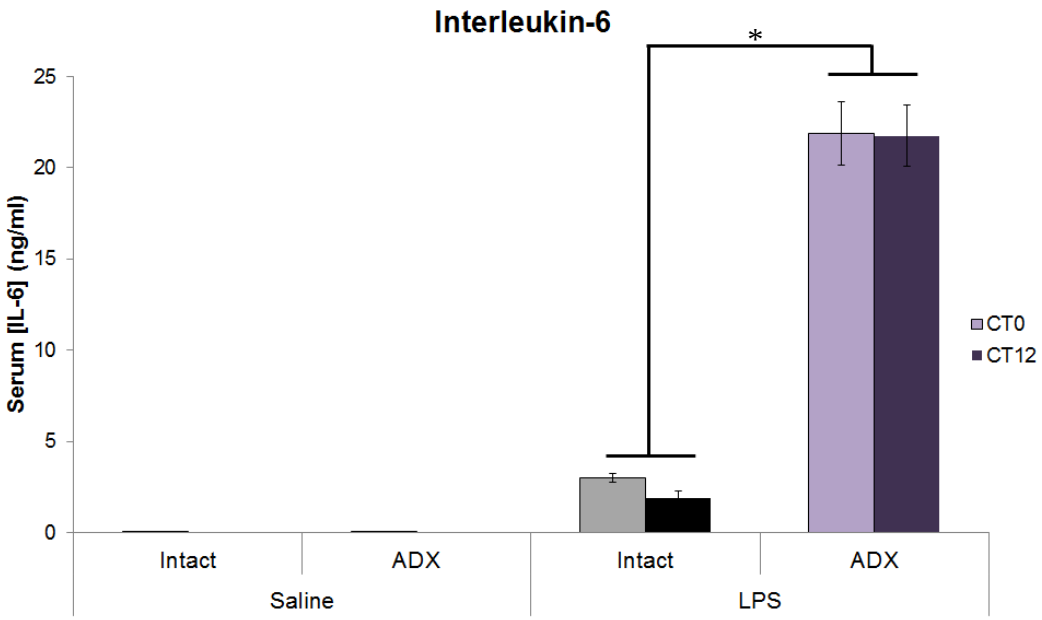

Figure 3.5: Interleukin-6 production in response to timed systemic lipopolysaccharide challenge in intact and adrenalectomised mice

Mice were challenged via intraperitoneal injection of lipopolysaccharide at either CT0 or CT12. Terminal blood samples were taken 4 hours after challenge and serum concentration of interleukin-6 (IL-6) quantified via ELISA as a measure of inflammation. A significant effect of surgery was observed in LPS-treated animals; two-way ANOVA ($F_{(1,18)}$=201.924, $p<0.05$), n=4-6/group.

3.4 Discussion

The aim of this chapter was to assess the impact of abolition of the rhythmic glucocorticoid (Gc) signal upon circadian regulation of innate pulmonary inflammation. This was tested by employing adrenalectomy to remove the major endogenous source of circulating Gcs, and testing various parameters.

3.4.1 Circulating glucocorticoids and behavioural rhythms

Glucocorticoid concentrations in serum have long been recognised to be rhythmic, both in humans (cortisol) and in rodents (corticosterone) (Kalsbeek et al. 2012). The first data presented in this chapter clearly shows an increase in corticosterone in intact animals during the dark phase, which is expected in nocturnal mammals. In adrenalectomised animals this rhythmic increase is lost and only very low concentrations of corticosterone are detected.

As the adrenal glands are the major source of circulating corticosterone, it is expected that adrenalectomy affects the corticosterone concentration in serum. Corticosterone does not disappear entirely from the circulation in adrenalectomised mice, however, and basal levels of 5-25ng/ml have been reported - thought to be produced by small groups of adrenal cells remaining in the body (Dalm et al. 2008). It is possible that the corticosterone detected in the ADX samples in this study was from such cells, which could provide a basal concentration which is then built upon by the adrenal glands.

Tissues such as the lung and intestines have also been shown to produce corticosterone locally (Taves et al. 2011), but in the case of the lung, this was found to be adrenal-dependent and caused by local conversion of inactive compounds into the active hormone (Hostettler et al. 2012). This could prove to be an interesting line of investigation, as local production in the lung may influence the response to pulmonary LPS challenge, and may also be rhythmic. A first step in this direction would be to test for rhythmic mRNA or protein expression of key conversion enzymes in a circadian series of lung samples, followed by further investigation into the cell types responsible for this production. If it is found to be bronchial epithelial cells, which are key players in

the circadian pulmonary response, then this would help to establish a link between the circadian clock, rhythmic inflammation and local corticosterone production in the lung. It may therefore be impossible to abolish glucocorticoid production in the mouse entirely by surgical means.

In order to assess the impact of a disrupted glucocorticoid rhythm upon rhythmic inflammation, it is important to avoid any central circadian disruptions which may confound results obtained. Wheel-running behavioural analysis was therefore performed as a proxy to illustrate rhythmicity of the central pacemaker in the SCN. Both 12:12LD and DD conditions were used to test entrainment to a light-dark cycle and the endogenous rhythm of intact and ADX C57BL/6J mice. Both qualitative inspections of the wheel-running plots and quantitative analysis of activity periods indicate that adrenalectomy does not affect the rhythmicity of wheel-running activity and therefore has not affected central circadian rhythms in the SCN. This is consistent with previous literature investigating the effects of ADX upon wheel-running activity in rats (Moberg & Clark 1976), where no significant alterations in rhythmicity were observed although a general decrease in locomotor activity was reported in ADX rats.

The lack of an effect upon the central clock is also anticipated from previous reports using dexamethasone to synchronise peripheral tissues (Balsalobre et al. 2000). Whilst Gcs act as strong entrainment stimulus for peripheral clocks, the SCN appears insensitive to such signals. In situ hybridisation targeting the glucocorticoid receptor (GR) in the SCN shows a distinct lack of mRNA expression, and although it is possible for Gc-sensitive neurons to signal to SCN neurons, the current consensus is that Gcs do not affect the rhythmicity of the central clock (Balsalobre et al. 2000).

3.4.2 Adrenalectomy and the pulmonary oscillator

Expression patterns of *Bmal1*, *Per1*, *Per2* and *Rev-erbα* are as expected from the literature (Sujino et al. 2012; Hwang et al. 2014). Whilst the time-of-day differences in relative mRNA quantity do not reach significance for *Bmal1* or *Per2* in adrenalectomised animals, the values are within the same range as intact animals and the lack of significance appears to be due to larger variability rather

than an underlying change in rhythm. The fact that a high amplitude oscillation remains in *Rev-erbα* transcript is indicative of an intact molecular oscillator in the lungs of adrenalectomised animals. One gene rhythm which was expected to change with surgery was *Per1*, which has previously been shown to dampen in the liver and kidney of rats following adrenalectomy (Sujino et al. 2012). However, no time-of-day difference was observed in intact animals either. This may be due to the time of collection - *Per1* peaks slightly before *Per2*, and CT5 and CT17 lie on the rising and falling phase of transcription (respectively). It would therefore be impossible to tell whether a *Per1* expression rhythm is present or is flat about the mesor, as both scenarios would yield approximately equal transcript levels at these time points. In general, however, the pulmonary oscillator phase appears unaltered by adrenalectomy.

3.4.3 Adrenalectomy and rhythmic inflammation

Adrenalectomy has previously been shown to abolish the rhythmic variation in the inflammatory response to a cutaneous allergic challenge (Nakamura et al. 2011). This paper showed that the loss of circadian inflammatory response in $Per2^{m/m}$ mutant mice was associated with a loss of rhythmic concentrations of circulating corticosterone. However, no other work has been undertaken targeting the innate immune system. The data presented here therefore constitute novel findings, and it appears that the rhythmic inflammatory response to pulmonary or systemic LPS challenge are both modulated by glucocorticoid signalling, but not in the same manner.

3.4.3.1 Aerosolised LPS

Exposure of animals to aerosolised lipopolysaccharide results in cell infiltration into the lung (figure 3.4A). In intact animals, the extent of this invasion is dependent upon the timing of the challenge, with elevated cell influx after challenge at CT0 than at CT12. These data have been reproduced in wild-type control littermates of genetically modified animals (Gibbs et al. 2014), and is a consistent pattern throughout this thesis. The pattern fits well with the circulating Gc rhythm, which is low at CT0 when the cell influx is greatest, and high at CT12 when cell influx is lower.

Combination of the total cell counts (figure 3.4A) and cytospin data (figure 3.4B) resulted in a differential cell count (figure 3.4C) which illustrates that the major contribution to this time-of-day effect is neutrophil recruitment. The neutrophil chemoattractant CXCL5 was identified as a key candidate driving this neutrophil influx (Gibbs et al. 2014), and the profile of CXCL5 concentration in the BAL from the animals challenged in this chapter is consistent with the neutrophil counts, although it does not reach significance in intact animals (figure 3.4D).

In ADX animals, however, the time-of-day effect upon cell count in lavage fluid is abolished. This indicates that the rhythmicity of adrenal-derived factors is important for generating the circadian variation in the innate pulmonary inflammatory response. Although the adrenals produce multiple humoral signals, such as catecholamines and sex steroids, the adrenal-derived glucocorticoids are strong candidates to mediate these effects through CXCL5. Transcription of *Cxcl5* is repressed by glucocorticoids and GR binding to the *Cxcl5* promoter is rhythmic in intact animals, with increased binding at CT12 compared to CT0 (Gibbs et al. 2014). It is interesting to note that the system is not entirely de-repressed with the loss of Gcs, as CXCL5 production and neutrophilia remain within the range of intact animals. This would imply that additional factors are also present to generate a tonic suppressive signal, and that the circulating Gcs are underlying only the rhythmic component of the response. What this suppressive signal is and which cell types are generating it remain to be determined.

3.4.3.2 Systemic LPS

The systemic inflammatory challenge data show no significant time-of-day variation in IL-6 production in intact animals. This is inconsistent with earlier findings (Gibbs et al. 2012), which showed an increase in IL-6 production after challenge at CT12 versus CT0.

The elevated response of ADX animals to LPS at both time points highlights the actions of adrenal-derived factors as systemic anti-inflammatory agents, although it cannot be concluded that this is due to glucocorticoids as the adrenals produce a variety of other factors which may influence physiology. This provides an

interesting contrast to the results of the aerosolised LPS challenge, where the rhythmic variation is lost, but inflammation is not exacerbated.

The difference between the effects of Gc loss are reflective of the differences between the two models. In the aerosolised model, it is hypothesised that the major cell type regulating the inflammatory response is the bronchial epithelial cell, which secretes the neutrophil chemoattractant CXCL5. In the systemic model, however, interleukin-6 is the more dominant cytokine and is produced by macrophages and circulating monocytes. It may be the case, then, that circulating glucocorticoids are more important to suppress systemic inflammation driven by circulating immune cells, but less so for tissue-specific responses driven by the local resident cells where Gcs have more of a modulatory role in driving a rhythmic repression.

3.5 Conclusions

In summary, this chapter presents confirmation that adrenalectomy abolishes the diurnal rhythm of circulating glucocorticoid concentration in mice, without affecting behavioural rhythms or the phase of the lung oscillator. Novel data addressing the impact of adrenalectomy upon circadian gating of two types of innate inflammatory challenge show that adrenalectomy abolishes the circadian gating of neutrophil influx after pulmonary challenge and is associated with increased production of the pro-inflammatory cytokine interleukin-6 after systemic challenge. It is therefore apparent that adrenal-derived factors are important mediators of the circadian gating of the innate inflammatory response in these models, although more targeted methods will need to be used to directly tie this to glucocorticoid signalling as the adrenal glands produce a wide array of humoral signalling molecules.

Chapter 4: The effect of timed corticosterone administration on the relative phasing of circadian clock gene expression in the lung

4.1 Introduction

The endogenous circulating glucocorticoid rhythm has both circadian and ultradian rhythms. Corticosterone (in rodents) and cortisol (in humans) are secreted into the circulation in a pulsatile manner, with spikes approximately every hour and an overall peak at the start of the organism's active phase (Lightman et al. 2008). For humans, this is early in the day (~ZT0), whereas for nocturnal rodents, this is the start of the night (~ZT12). As a true circadian rhythm, these profiles also persist under constant conditions such as constant darkness.

Glucocorticoids (Gcs) are able to entrain peripheral oscillators by binding to glucocorticoid response elements (GREs) in the *Per1* and *Per2* genes and modulating clock phase (Balsalobre et al. 2000). In vivo, the rhythmic glucocorticoid signal is accompanied by many other potential entrainment and synchronising signals, including temperature, metabolic signals from feeding, and neural signals from adrenergic innervation. In order to uncouple the contribution of the glucocorticoid signal from these additional factors, Sujino et al. (2012) delivered corticosterone to rats in the opposite pattern to the endogenous rhythm, essentially uncoupling the glucocorticoid rhythm from the other entraining signals.

In their experiment, adrenalectomised rats were given daily injections of corticosterone (27mg/kg) at ZT0.5 – the opposite time to the endogenous peak at ~ZT12. As the behaviour and feeding patterns remained the same, the glucocorticoid rhythm was therefore in anti-phase to metabolic and neural signals and clock gene rhythms in various tissues could be measured to assess which of these signals individual tissues had entrained to. Initial analysis of clock gene expression in liver and kidneys of control and adrenalectomised (ADX) rats showed no difference in rhythmic expression of *Bmal1*, *Per2* or *Cry1* between treatments, but *Per1* oscillation was abolished and low constant expression was reported in ADX rats.

Following these acute experimental studies, the group then tested whether repeated daily treatment with corticosterone injection for a period of seven days

could entrain clock gene expression to an exogenous glucocorticoid rhythm. A series of 27mg/kg doses of corticosterone delivered at ZT0.5 was sufficient to shift the phase of *Per2*, *Cry1* and *Bmal1* expression in the lung and kidney to match the phase of glucocorticoid signal. Clock gene expression in the liver was unaffected. This suggests that the liver is more robustly entrained by feeding or other zeitgebers, whereas the lung and kidney are more receptive to the glucocorticoid signal with a shift in phase to match the timing of corticosterone delivery.

If the rodent lung is preferentially entrained by Gcs in this manner (Sujino et al. 2012), it may be possible to selectively reverse this tissue without affecting the phase of oscillations in circulating immune factors or other immune tissues. If the circadian component of the pulmonary inflammatory response is predominantly governed by the clock gene oscillations in the lung, as appears to be the case based on lung-specific clock knockout models (Gibbs et al. 2014), then reversing the phase of these oscillations should also reverse the phase of the rhythmic neutrophil recruitment in response to lipopolysaccharide (LPS). The aim of this chapter is therefore to replicate the findings of Sujino et al. (2012) in mice – assessing the ability of the lung to entrain to anti-phase delivery of corticosterone – and then apply a timed LPS exposure protocol to mice with altered clock gene oscillations in the lung to determine whether the rhythmic neutrophilia also changes phase.

4.2 Hypothesis tested and experimental approaches

Hypothesis 2: Reversal of the phase of glucocorticoid rhythm will reverse the phase of pulmonary clock gene expression and the phase of peak inflammatory response.

Aim: Impose a reversed rhythm of circulating glucocorticoid concentrations via adrenalectomy and exogenous administration of corticosterone. Measure effects upon clock gene expression in the lung and circadian variation in inflammatory response to aerosolised lipopolysaccharide.

Objectives:

- Determine an appropriate dose of corticosterone to deliver via injection to mimic endogenous peak concentrations.

- Administer previously determined dose over several days to adrenalectomised animals in anti-phase to usual peak concentrations and assess phasing of lung clock via qPCR to establish phase reversal.

- Repeat exogenous anti-phase glucocorticoid administration protocol and challenge with aerosolised lipopolysaccharide at multiple time points. Determine whether the rhythmic inflammatory response profile has also inverted by quantifying cell infiltration and cytokine production.

4.2.1 Establishment of an appropriate dose of exogenously administered corticosterone to mimic endogenous peak concentration

Pilot experiments were undertaken to establish a dose to take forward into the larger study, using intact C57BL6/J male mice to limit the severity of the procedure. Adrenalectomy was not deemed necessary as the time of administration was ZT0.5, when endogenous production is low. Vehicle-treated animals were used to quantify stress-induced corticosterone production caused by the injection procedure. By using intact animals, this also enabled the measurement of each animal's endogenous peak circulating corticosterone concentration, providing internal controls in a repeated measures design.

First, blood samples were taken via tail bleed at ZT12 to provide a measure of the endogenous circulating corticosterone concentration at its anticipated peak (figure 4.1). The next sample was collected at ZT0 as a baseline 'low' value. Intraperitoneal injections of 3mg/kg, 10mg/kg, 30mg/kg or 100mg/kg corticosterone dissolved in corn oil or an equivalent volume of corn oil alone were given at ZT0.5 (n=4/group), based on the design of Sujino et al. (2012). Corn oil was used a vehicle as corticosterone is insoluble in water.

Following injection, the next three blood samples were taken via tail bleed every twenty minutes, which is the approximate half-life of corticosterone in blood (Sainio et al. 1988). These samples were therefore taken at ZT0.83 (injection + 20 minutes), ZT1.17 (injection + 40 minutes) and ZT1.5 (injection + 60 minutes). A final tail bleed was performed at ZT2.5 (2hrs post-injection) and terminal samples collected at ZT4 in order to establish whether circulating concentrations had returned to pre-treatment baselines. All samples were processed for serum and analysed for corticosterone concentration via ELISA. Due to the short timeframes involved with the blood sampling, the pilot experiment was performed over multiple days, with doses stratified across days.

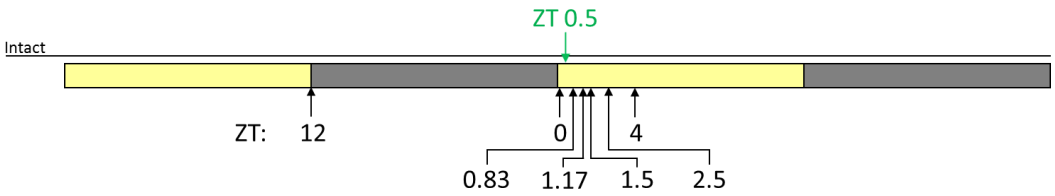

Figure 4.1: Experimental procedure for dose-response experiment

Intact animals were used for a pilot experiment to determine an appropriate dose of corticosterone to administer in the main experiment. Blood samples (black arrows) were taken by tail tipping at ZT12 and ZT0. Mice were weighed, doses calculated and intraperitoneal injections were administered at ZT0.5 (green arrow). Either 0mg/kg (vehicle control), 3mg/kg, 10mg/kg, 30mg/kg or 100mg/kg corticosterone in corn oil was given to each mouse (n=4/group). Blood samples were taken at ZT0.83, ZT1.17, ZT1.5 and ZT2.5. Mice were culled via cervical dislocation at ZT4 and terminal samples of trunk blood collected.

4.2.2 Phase reversal

For the main experiment, animals were divided into 4 groups – adrenalectomy only (ADX), adrenalectomy with delivery of corticosterone at ZT0.5 (ZT0.5 CORT, approximating a corticosterone rhythm in anti-phase to the endogenous oscillation), adrenalectomy with delivery corticosterone at ZT11.5 (ZT11.5 CORT, approximating a corticosterone rhythm in-phase with the endogenous oscillation) and intact (n=24/group). Adrenalectomised animals were allowed to recover for 1 week before additional treatments (figure 4.2).

At the indicated times, the ZT0.5 CORT group and ZT11.5 CORT group were injected (intraperitoneal) with 10mg/kg corticosterone in corn oil. To confirm previous results measuring the half-life of exogenous corticosterone in intact animals, 5 ZT0.5-injected animals were sampled via tail bleed at 20mins (ZT0.83), 40mins (ZT1.17), 60mins (ZT1.5) 120mins (ZT2.5) and 210mins (ZT4) post-injection, matching pilot time points.

Injections persisted for 7 days in a 12 hours light – 12 hours dark lighting schedule, and for a further 24 hours of constant darkness (when injections were delivered in darkness). Terminal sampling took place across a circadian cycle, with 4 mice/group sacrificed at each time point (CT0, 4, 8, 12, 16 and 20). Injections persisted throughout the sampling period. This sampling procedure differs slightly from that of Sujino et al. (2012), but it was deemed necessary in

order to be transferable to the aerosolised LPS challenge procedure which would be implemented if the phase of clock gene oscillations could be altered. This protocol allows the measurement of rhythms without the masking effect of the light:dark cycle whilst maximising the chance of influencing clock gene expression by maintaining corticosterone injections. However, this is not a true 'circadian' series, as the injection of corticosterone itself acts as a zeitgeber, giving entrainment signals to peripheral tissues. The time points are still designated as CTs for the purpose of this chapter, to indicate that the sampling took place in constant darkness, but it should be noted that they are not strictly 'circadian times'.

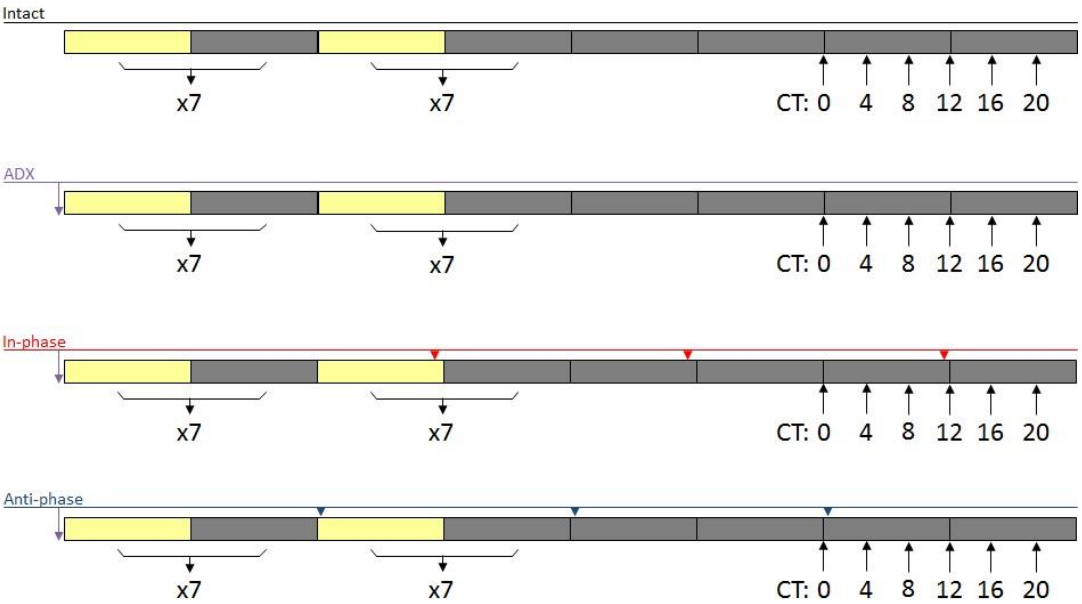

Figure 4.2: Experimental procedure for phase-reversal experiment

4 groups of animals were used – intact, adrenalectomised (ADX), 'in-phase' (ZT11.5 CORT) and 'anti-phase' (ZT0.5 CORT). ADX, in-phase and anti-phase animals were all adrenalectomised (purple arrows). 1 week following adrenalectomy, injections of corticosterone began for the anti-phase and in-phase groups at the specified times (ZT0.5 – blue arrows - or ZT11.5 – red arrows - respectively). Injections continued daily for 7 days and into the sampling period. All four groups were transferred to constant darkness (DD) for 24 hours prior to the sampling period, and then 4 animals per group culled at each of the sampling time points (black arrows).

4.3 Results

4.3.1 Exogenous administration of corticosterone via intraperitoneal injection causes a dose-dependent increase in serum corticosterone concentration

Intraperitoneal injection of corticosterone elicited a transient increase in serum corticosterone concentrations in intact animals (figure 4.3A) relative to both vehicle-injected controls and those observed in the circadian series in chapter 3. One-way ANOVA showed a significant difference between corticosterone concentrations 20 minutes post-injection (figure 4.3B); $F_{(4,19)}=23.723$, $p<0.05$. Levene's test for homogeneity of variances was significant ($p<0.05$), so post hoc tests were performed using the Games-Howell correction which does not assume equal variances. Individual comparisons showed 10mg/kg, 30mg/kg and 100mg/kg to be significantly higher than vehicle alone. In addition, 3mg/kg was significantly lower than 30mg/kg and 100mg/kg but did not differ from 0mg/kg or 10mg/kg. 10mg/kg, 30mg/kg and 100mg/kg did not vary significantly from each other.

Vehicle delivery alone (0mg/kg) caused an increase in corticosterone above the endogenous figures expected (chapter 3) due to activation of the HPA axis in these intact animals. To account for the activation of the stress axis in this experiment, vehicle only values were subtracted from the corticosterone-injected values to yield data attributable to the corticosterone-induced rise in circulating corticosterone, rather than that induced by the procedure itself (figure 4.3C). This is only an approximation of the relative contributions of procedure and dose in increasing serum corticosterone, but more accurately models expected doses in adrenalectomised animals (which lack an intact stress response).

The dose-dependent increase in peak serum corticosterone concentration was accompanied by longer signal duration (broader peak). Accounting for vehicle-induced increases, for both the 3mg/kg and 10mg/kg dose, corticosterone concentrations had returned to baseline within the 4hr sampling period. However, 3.5 hours after injection, circulating corticosterone concentration in animals given 30mg/kg were 1.5-fold higher than samples taken at ZT0 and those injected with

100mg/kg corticosterone were still 7-fold higher than in samples taken at ZT0. Based on these findings, it was determined that 10mg/kg would be the most appropriate dose to take forward, providing a higher peak concentration than strictly necessary but providing a longer duration of corticosterone in the circulation which more closely mimics the endogenous night-time profile.

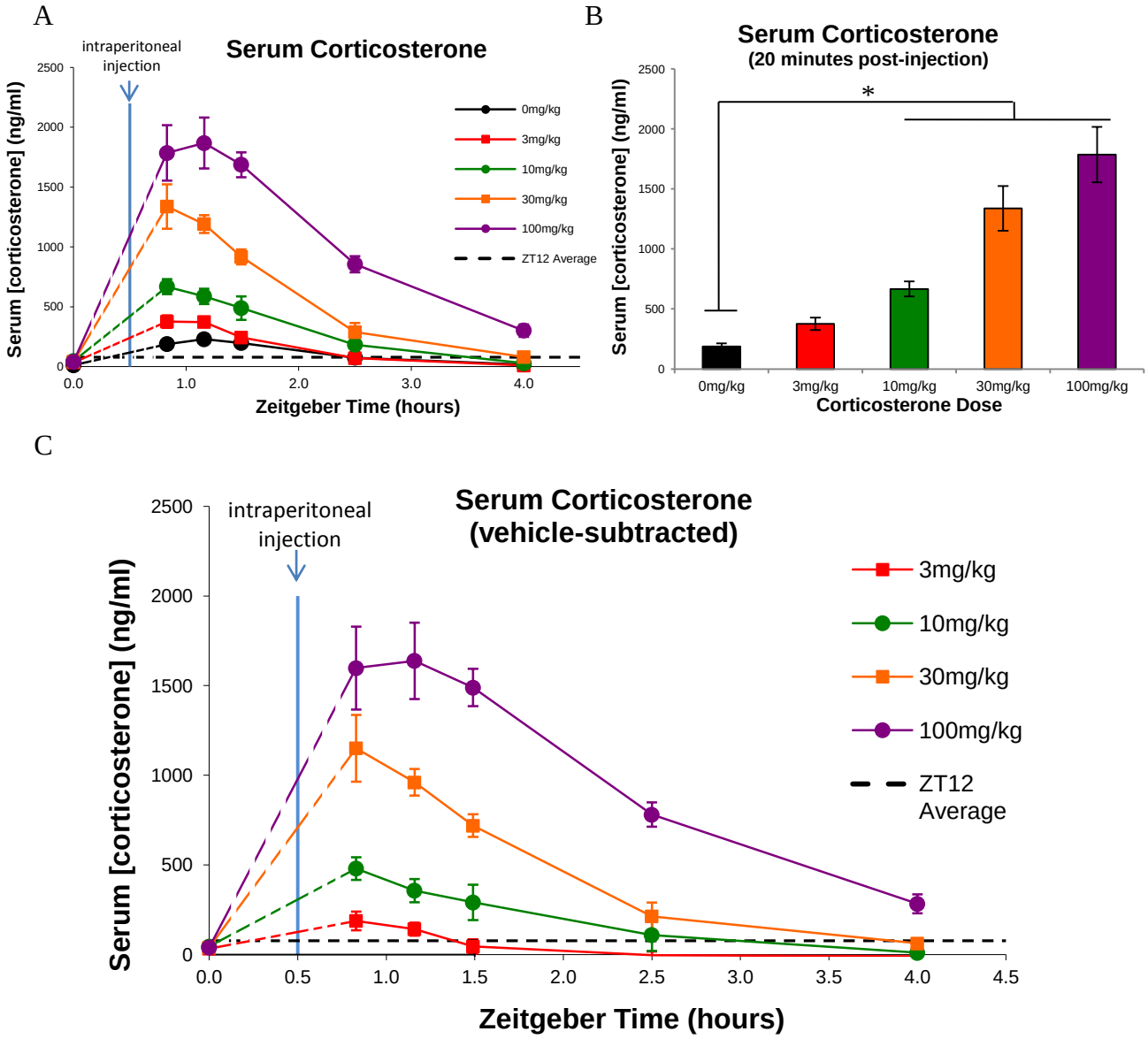

Figure 4.3: Serum corticosterone concentration before and after intraperitoneal corticosterone injection

A) Serial samples of tail blood from intact mice injected at ZT0.5 with corticosterone in corn oil vehicle or vehicle alone. B) Comparison of corticosterone concentration 20 minutes post-injection across each dose. * denotes significant difference, $p<0.05$, one-way ANOVA with Games-Howell correction for post hoc comparisons. C) Approximation of corticosterone-induced increase in serum corticosterone by subtraction of vehicle-induced values. For each chart, n=4/group. Dashed horizontal line on A and C denotes average circulating concentration of all animals at ZT12 prior to experiment. Dashed coloured lines shows extrapolated plot between ZT0 and 20 minutes post-injection values.

4.3.2 Timed exogenous administration of corticosterone to adrenalectomised mice alters circadian circulating corticosterone profiles

Confirmation of successful adrenalectomy was performed via blood sampling 1 week post-surgery. Samples were collected at ZT12 and corticosterone concentration measured via ELISA. Animals from the ADX, ZT0.5 CORT and ZT11.5 CORT groups with concentrations higher than 25ng/ml were treated with caution for further analyses, and suspect data points were cross-referenced back to corticosterone data to check for possible incomplete adrenalectomy and exclusion from analysis. Samples higher than 50ng/ml were excluded outright. Data from these assays are shown in appendix 6.

One subgroup of adrenalectomised animals underwent the same sample collection protocol as in the pilot study, to check the protocol was having the desired effects. Data from this group is presented in figure 4.4 and values were comparable with the values expected from vehicle-subtracted 10mg/kg group (green line) in figure 4.3C.

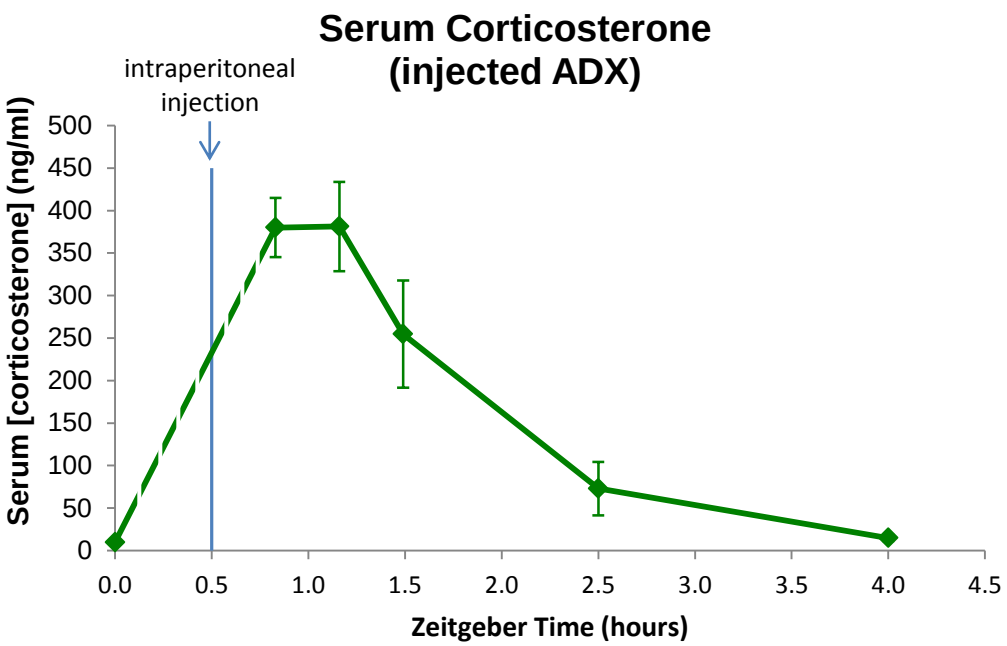

Figure 4.4: Serum corticosterone concentration before and after intraperitoneal corticosterone injection in adrenalectomised animals

Serial samples of tail blood from adrenalectomised (ADX) mice injected at ZT0.5 with 10mg/kg corticosterone in corn oil vehicle. N=3-5/time point. Dashed line indicates extrapolated plot between ZT0 and 20 minutes post-injection values.

For the circadian series, trunk blood collected at each time point was assessed for corticosterone concentration via ELISA. Data from the intact control group did not show the rhythm anticipated from previous data (figure 4.5A, compare with figure 3.1). Analysis using one-way ANOVA shows no significant effect of time; $F_{(5,23)}=0.286$, $p=0.915$.

As expected, circulating concentrations in the adrenalectomised group showed a low, flat profile (figure 4.5B). One ADX sample (collected at CT12) was removed from analysis due to high corticosterone detected in the post-adrenalectomy assessment (>50ng/ml). This animal was deemed incompletely adrenalectomised. One ADX sample at CT20 fell below the detection limit of the ELISA, so for statistical tests this value was made to equal the detection limit (1.08ng/ml), rather than excluding the data point. One-way ANOVA indicated no significant rhythm; $F_{(5,22)}=1.666$, $p=0.197$.

Administration of exogenous corticosterone at ZT11.5 replicated the anticipated endogenous rhythm, with a peak at CT12 (figure 4.5C). Multiple samples were excluded from this groups due to incomplete adrenalectomy (ZT12 values >50ng/ml). These samples were – 2xCT0, 3xCT8, 1xCT16, 1xCT20. In addition, 1xCT4 and 1xCT8 animal died during the treatment protocol. One-way ANOVA on the remaining samples showed a significant effect of time; $F_{(4,14)}=62.785$, $p<0.05$. Post hoc tests using the Bonferroni correction confirm that CT12 is significantly higher than all other time points ($p<0.05$).

Injections of corticosterone at ZT0.5 resulted in a dampened oscillation (figure 4.5D). Multiple samples were excluded from this group due to incomplete adrenalectomy (>50ng/ml). These samples were – 1xCT0, 2xCT16, 1xCT20. In addition, 1xCT8 and 1xCT16 animal died during the treatment protocol. One-way ANOVA showed no significant effect of time; $F_{(5,18)}=2.720$, $p<0.068$.

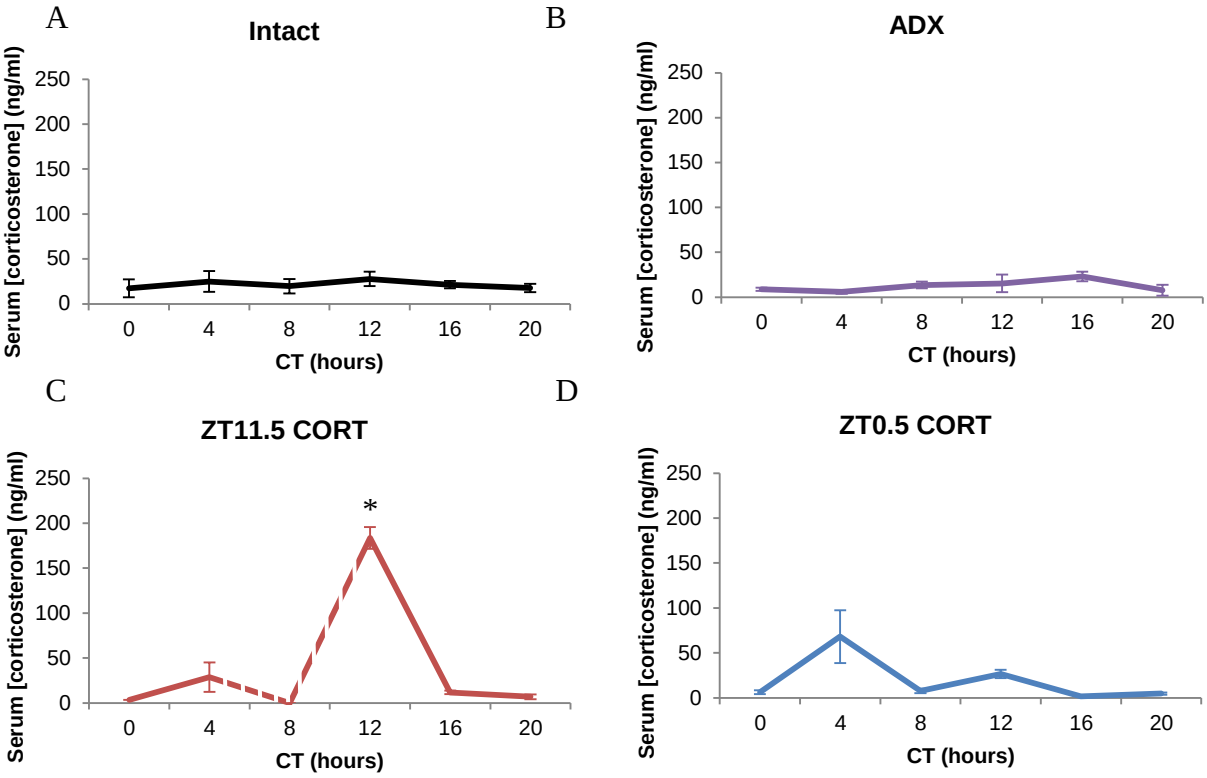

Figure 4.5: Serum corticosterone concentration across a circadian cycle

Circadian series of circulating corticosterone concentration collected from A) intact animals, B) adrenalectomised animals, C) animals injected with 10mg/kg corticosterone at ZT11.5 (in-phase CORT), D) animals injected with 10mg/kg corticosterone at ZT0.5 (anti-phase CORT). See table 4.1 for group sizes. All graphs plot on same axis scale for comparison. Dashed line between CT4 and CT12 in panel C denotes extrapolated pattern, no data exists for CT8.

*ADX – adrenalectomised; CORT – corticosterone; CT – circadian time. * denotes significant difference vs. all other time points at the 0.05 level (one-way ANOVA with Bonferroni correction).*

n	CT0	CT4	CT8	CT12	CT16	CT20
Corticosterone	4, 4, 2, 3	4, 4, 3, 4	4, 4, 0, 3	4, 3, 4, 4	4, 4, 3, 1	4, 4, 3, 3
Period2	3, 3, 2, 2	3, 3, 3, 3	4, 3, 0, 3	3, 3, 3, 3	3, 3, 3, 1	3, 4, 3, 3
Bmal1	3, 3, 2, 3	4, 3, 3, 3	4, 3, 0, 2	3, 2, 3, 3	3, 3, 2, 1	3, 4, 2, 3

Table 4.1: Group sizes for circadian series experiments

Various animals were excluded from analysis due to incomplete adrenalectomy, death, or determination as an outlier using the median absolute deviation protocol. Sample sizes for each group in each test are given in the table. Colours denote treatment group and correspond to colour code in figures 4.5-4.7: black – intact, purple – adrenalectomised, red – in-phase corticosterone (ZT11.5 injection), blue – anti-phase corticosterone (ZT0.5 injection).

CT – circadian time (of collection); ZT – zeitgeber time.

4.3.3 Timed exogenous administration of corticosterone to adrenalectomised mice fails to reverse clock gene rhythms in the lung

Lung samples collected from the same animals were processed for RNA and 250ng reverse transcribed to cDNA. Quantification of transcript was performed by quantitative PCR using the $2^{-\Delta\Delta Ct}$ method, normalised to quantity of *β-actin* detected. *Per2*, *Bmal1* and *β-actin* were measured in each sample in order to assess the state of both the positive and negative arms of the core transcription-translation feedback loop. Some samples were excluded due to incomplete adrenalectomy (see above), and, due to high variability within groups, the median absolute deviation method was used for each group at each time point to assess outliers.

4.3.3.1 *Period2*

Intact animals showed a strong rhythm in relative abundance of *Per2*, peaking at CT12 (figure 4.6A). One sample was excluded from each of the following groups after being identified as an outlier: CT0, CT4, CT12, CT16 and CT20. Analysis using one-way ANOVA shows a significant effect of time; $F_{(5,18)}=19.968$, $p<0.05$. Levene's test for homogeneity of variances was significant, so post hoc tests were performed using the Games-Howell correction, which does not assume equal variances. Post hoc tests show CT0<CT16, and CT4<CT8 and CT16.

Adrenalectomised animals showed a similar profile (figure 4.6B). One ADX sample (collected at CT12) was removed from analysis due to high corticosterone in the previous test (>50ng/ml). This animal was deemed incompletely adrenalectomised. Inspection of data from qPCR led to a further four data points being excluded as outliers – 1xCT0, 1xCT4 1xCT8, and 1xCT16. Analysis using one-way ANOVA shows a significant effect of time; $F_{(5,18)}=5.388$, $p<0.05$. Levene's test for homogeneity of variances was significant, so post hoc tests were performed using the Games-Howell correction, which does not assume equal variances. Despite an overall effect of time, comparison of individual groups did not show any significant differences.

Administration of exogenous corticosterone at ZT11.5 replicated the intact rhythm, with a peak at CT12 (figure 4.6C). Multiple samples were excluded from

this groups due to incomplete adrenalectomy (ZT12 values >50ng/ml). These samples were – 2xCT0, 3xCT8, 1xCT16, 1xCT20. In addition, 1xCT4 and 1xCT8 animal died during the treatment protocol and 1xCT12 sample was detected as an outlier. One-way ANOVA on the remaining samples showed no significant effect of time; $F_{(4,13)}=3.532$, $p=0.054$.

Injections of corticosterone at ZT0.5 resulted in a dampened profile (figure 4.6D). Multiple samples were excluded from this group due to incomplete adrenalectomy (>50ng/ml). These samples were – 1xCT0, 2xCT16, 1xCT20. In addition, 1xCT8 and 1xCT16 animal died during the treatment protocol. Outliers identified were: 1xCT0, 1xCT4 and 1xCT12. One-way ANOVA showed no significant effect of time; $F_{(5,14)}=2.180$, $p=0.146$.

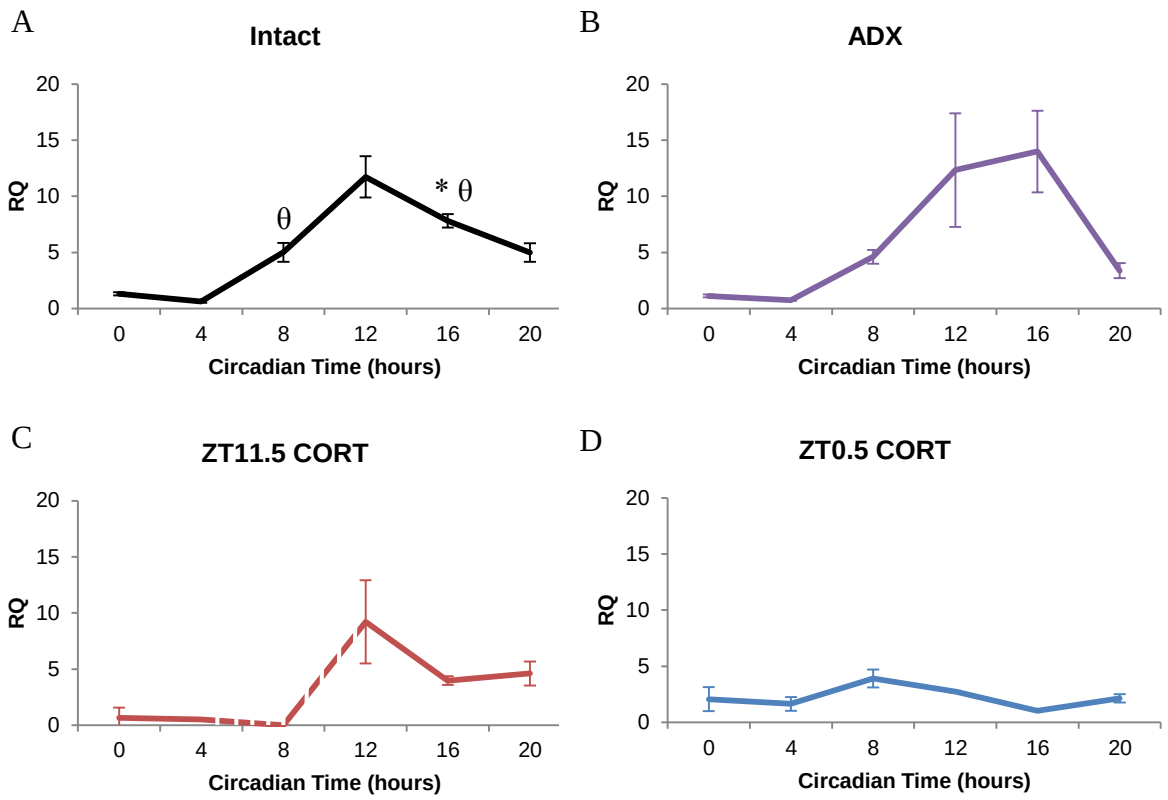

Figure 4.6: *Period2* expression in lung tissue across a circadian cycle

Circadian series of *Per2* expression in lungs from A) intact animals, B) adrenalectomised animals, C) animals injected with 10mg/kg corticosterone at ZT11.5 (in-phase CORT), D) animals injected with 10mg/kg corticosterone at ZT0.5 (anti-phase CORT). See table 4.1 for group sizes. All graphs plot on same axis scale for comparison. Dashed line between CT4 and CT12 in panel C denotes extrapolated pattern, no data exists for CT8.

*ADX – adrenalectomised; CORT – corticosterone; Per2 – Period2. * denotes significant difference vs. CT0 and θ denotes significant difference vs. CT4 at the 0.05 level (one-way ANOVA with Bonferroni correction).*

4.3.3.2 *Bmal1*

Intact animals also showed a strong rhythm in relative abundance of *Bmal1*, peaking at CT0 (figure 4.7A). One sample was excluded from each of the following groups after being identified as an outlier: CT0, CT12, CT16 and CT20. Analysis using one-way ANOVA shows a significant effect of time; $F_{(5,19)}=15.285$, $p<0.05$. Levene's test for homogeneity of variances was significant, so post hoc tests were performed using the Games-Howell correction, which does not assume equal variances. Post hoc tests show CT20>CT8 and CT12.

Again, adrenalectomised animals showed a similar profile to intact animals (figure 4.7B). One ADX sample (collected at CT12) was removed from analysis due to high corticosterone in the previous test (>50ng/ml). This animal was deemed incompletely adrenalectomised. Inspection of data from qPCR led to a further four data points being excluded as outliers – 1xCT4 1xCT8, 1xCT12 and 1xCT16. In addition, 1xCT0 sample was excluded due to a failure of amplification in the qPCR reaction. Analysis using one-way ANOVA shows a significant effect of time; $F_{(5,17)}=9.220$, $p<0.05$. Levene's test for homogeneity of variances was significant, so post hoc tests were performed using the Games-Howell correction, which does not assume equal variances. Post hoc tests show CT4>CT8 and CT12, and that CT12<CT16 and CT20.

Administration of exogenous corticosterone at ZT11.5 replicated the intact rhythm, with a nadir at CT12 (figure 4.7C). Multiple samples were excluded from this groups due to incomplete adrenalectomy (ZT12 values >50ng/ml). These samples were – 2xCT0, 3xCT8, 1xCT16, 1xCT20. In addition, 1xCT4 and 1xCT8 animal died during the treatment protocol and 1xCT12, 1xCT16 and 1xCT20 samples were detected as outliers. One-way ANOVA on the remaining samples showed a significant effect of time; $F_{(4,11)}=21.937$, $p<0.05$. Levene's test for homogeneity of variances was not significant, so post hoc tests were performed using the Bonferroni correction. Post hoc tests show CT12<CT0, CT4 and CT20 and that CT16<CT0 and CT4.

Injections of corticosterone at ZT0.5 resulted in an altered profile around CT20 (figure 4.6D). Multiple samples were excluded from this group due to incomplete adrenalectomy (>50ng/ml). These samples were – 1xCT0, 2xCT16, 1xCT20. In addition, 1xCT8 and 1xCT16 animal died during the treatment protocol. Outliers identified were: 1xCT4, 1xCT8 and 1xCT12. One-way ANOVA showed no significant effect of time; $F_{(5,14)}=3.194$, $p=0.062$.

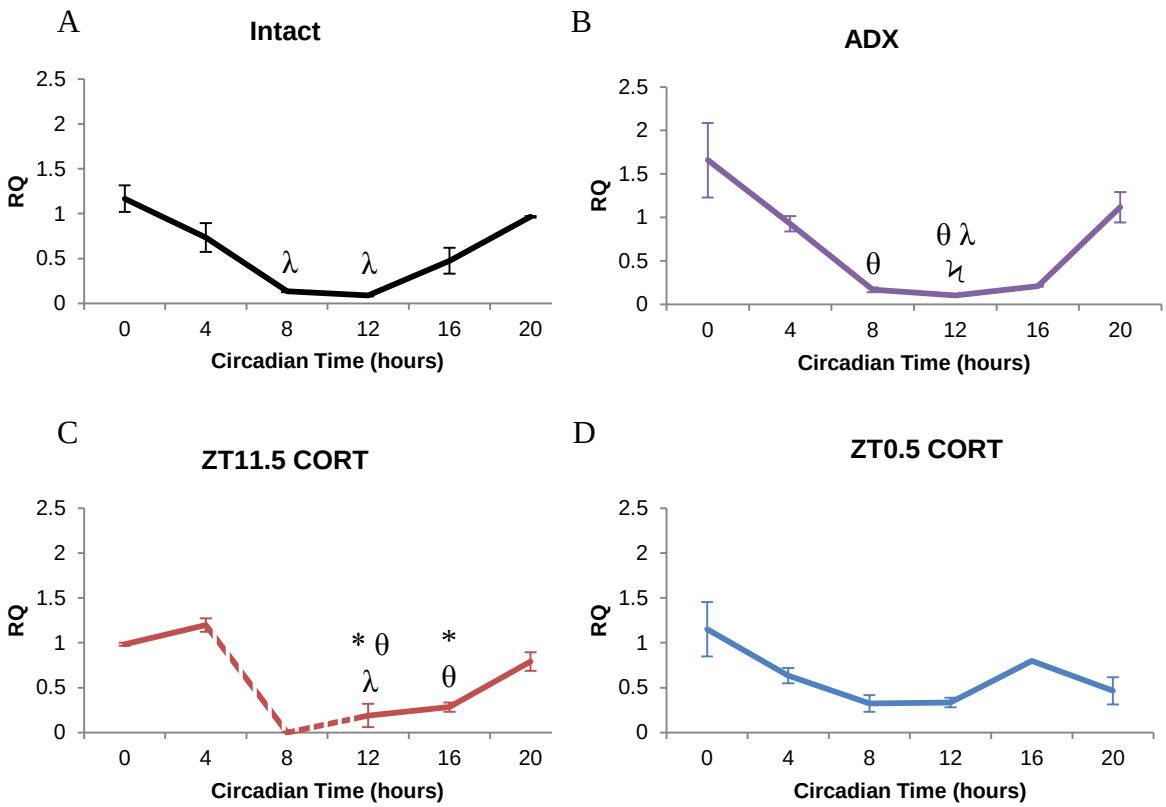

Figure 4.7: *Bmal1* expression in lung tissue across a circadian cycle

Circadian series of *Bmal1* expression in lungs from A) intact animals, B) adrenalectomised animals, C) animals injected with 10mg/kg corticosterone at ZT11.5 (in-phase CORT), D) animals injected with 10mg/kg corticosterone at ZT0.5 (anti-phase CORT). See table 4.1 for group sizes. All graphs plot on same axis scale for comparison. Dashed line between CT4 and CT12 in panel C denotes extrapolated pattern, no data exists for CT8.

*ADX – adrenalectomised; Bmal1 – brain and muscle arnt-like 1; CORT – corticosterone. * denotes significant difference vs. CT0; θ denotes significant difference vs. CT4; ϰ denotes significant difference vs. CT16; λ denotes significant difference vs. CT20 at the 0.05 level (one-way ANOVA with Bonferroni correction).*

4.4 Discussion

4.4.1 Pilot study

Exogenous administration of corticosterone into intact animals via intraperitoneal injection resulted in an increase in circulating corticosterone (figure 4.3A); higher doses (10, 30 and 100mg/kg) produced significantly higher concentrations than vehicle alone (figure 4.3B). As the pilot investigations were performed in intact animals, the procedure itself is likely to have activated the HPA axis through the stress caused by restraint and injection. This stress response will trigger an increase in endogenous production of glucocorticoids and is the probable cause of the elevated circulating concentration in the vehicle-only group. In order to account for the HPA axis activation and more closely model the responses of adrenalectomised animals, the vehicle-only average at each time point was subtracted from each of the other groups (figure 4.3C).

From the vehicle-subtracted data (figure 4.3C), both 3mg/kg and 10mg/kg show moderate increases in circulating corticosterone concentration. 30mg/kg and 100mg/kg were excluded as they were deemed to be outside the physiological range of concentrations that an animal would ordinarily encounter (Malisch et al. 2007; Lolait et al. 2007). Whilst these concentrations may be more likely to produce effects, the aim of the experiment was to mimic an endogenous rhythm, not use supraphysiological concentrations as a proof of principle. Of the lower doses, the 10mg/kg dose was chosen to take forward into the main experiment, rather than the 3mg/kg dose, due to the longer duration of signal. In order to try to replicate an endogenous pattern it was important to avoid a sharp spike and try to replicate more of an oscillation, with a broader peak. This was more apparent in the 10mg/kg group, which took longer to return to baseline concentrations than in the 3mg/kg group. For practical reasons also, the higher dose was deemed more likely to produce an effect than the lower dose, whilst still being within the physiological (albeit stressed) range of the animals. Measurements of the same parameters in adrenalectomised mice showed similar results – an elevation 20 minutes after injection followed by a broad profile, returning to baseline by ZT4 (figure 4.4).

4.4.2 Circadian series

4.4.2.1 Corticosterone

Analysis of corticosterone rhythms was performed via ELISA. Unexpectedly, samples from intact animals did not exhibit the time-of-day variation previously seen (figure 4.5A, compared to figure 3.1). This does not appear to have been an assay failure, as no sample fell below the detection limit and the majority of samples from all groups were run on the same plate. A second assay was performed for these animals, to test whether an error had occurred in the ELISA process, but results remained the same.

As anticipated, samples from adrenalectomised animals showed no effect of time and remained low throughout the day (figure 4.5B). Injection of 10mg/kg corticosterone at ZT11.5 elicited a rhythm which peaked at CT12, as expected. The peak of this profile is 184ng/ml; below that anticipated from pilot data (figure 4.4 – peak concentration approximately 380ng/ml). This difference may be due to inter-assay variability, as the CT0 value for this experiment is also lower than in figure 4.4, so the whole profile may be shifted down the y axis in this case. Importantly, the profile strongly resembles an endogenous pattern and concentrations do not exceed pilot data and reach a supraphysiological level.

Injection of the same dose of corticosterone (10mg/kg) at ZT0.5 failed to yield a significant time-of-day variation in circulating concentration (figure 4.5D). This is to be expected, however, as previous data (figure 4.4) showed that circulating concentration had returned to baseline by ZT4 (equivalent to CT4 in this study). These time points were chosen to enable direct comparison of clock gene expression with published work (Sujino et al. 2012), but unfortunately lead to a situation where the change in corticosterone profile is difficult to detect in the ZT0.5-injected group. As the CT0 time point is before the injection, and the CT4 time point is 3.5 hours after injection, it is unlikely that this pattern of sample collection would pick up the surge of corticosterone. In contrast, the CT12 time point falls only 30 minutes after injection in the ZT11.5 group and so a clear response can be observed (figure 4.5C). The slight elevation in concentration at ZT4, although not enough to cause a significant time-of-day effect across the

treatment group, may still be indicative of the falling phase of corticosterone concentration after injection.

4.4.2.2 Clock gene expression

Quantitative PCR (qPCR) was used to measure relative quantity of mRNA for two clock genes – *Per2* and *Bmal1*. These clock genes oscillate in anti-phase and represent the negative (*Per2*) and positive (*Bmal1*) arms of the core transcription-translation feedback loop.

In intact animals, both *Per2* and *Bmal1* were found to oscillate (figures 4.6A and 4.7A respectively). These rhythms were anti-phasic, with *Per2* peaking at CT12 and *Bmal1* peaking at CT0/CT20. *Per2* showed a much higher amplitude oscillation, with peak values 12x higher than nadir compared to only a 5-fold change in *Bmal1*.

Both genes were also rhythmically expressed in anti-phase in adrenalectomised animals (figures 4.6B and 4.7B). Amplitudes were comparable with intact animals, although *Per2* expression remained high at CT16 instead of dropping down sharply (figure 4.6B compared to 4.6A).

Animals injected with corticosterone at ZT11.5 (in-phase, mimicking endogenous pattern) showed a trend for an oscillation in *Per2* which matched intact and adrenalectomised profiles (figure 4.6C) but this did not reach significance ($p=0.054$). The *Bmal1* oscillation was significantly rhythmic. Although the graph is skewed by the loss of the CT8 group making the data point equate to zero (3 incomplete adrenalectomies, 1 death), the statistics are unaffected and this observation is therefore still robust despite the loss of one time point.

Animals injected at ZT0.5, however, showed no rhythm in either *Per2* or *Bmal1* (figure 4.6D and 4.7D respectively), although *Bmal1* does show a trend for an intact rhythm ($p=0.062$).

The data from intact and ADX control groups are as expected from the literature (Sujino et al. 2012). In their experiments into restricted feeding and timed

glucocorticoid delivery in rats, Sujino et al. (2012) found no effect of adrenalectomy upon *Per2* or *Bmal1* rhythms in the liver or kidney. Similarly, in chapter 3, adrenalectomised mice still show a trend for rhythmic clock gene expression in the lung (albeit with samples at CT5 and CT17, rather than CT0 and CT12 – figure 3.3).

Limited work has been performed regarding the effects of anti-phase delivery of corticosterone *in vivo* upon pulmonary oscillator phase. Sujino et al. (2012) used a dose of 27mg/kg in rats to elicit a phase reversal of *Per2*, *Bmal1* and *Cry1* in the kidney and lung. In this model, the liver was unaffected by the anti-phase delivery of glucocorticoids and maintained oscillation patterns in-keeping with the feeding and locomotor activity rhythms. Whilst the data presented in this chapter fails to show a reversal of the clock gene expression rhythm in the ZT0.5-injected group, a dampening of both *Per2* and *Bmal1* rhythms did occur, indicating additional effects beyond that of the adrenalectomy (as ADX animals were still rhythmic).

However, it is difficult to draw robust conclusions from this data due to the small samples sizes in the tests performed. Due to the difficulties in performing the experiment on a large scale and the relatively low variability usually observed in these measures, a group size of 4/time point was originally decided upon and was enough to yield significant variation in the intact and adrenalectomised groups. Various factors reduced group size, including death of animals during protocol and incomplete adrenalectomy. The duration of the protocol and requirement for all treatments to be performed concurrently made it very difficult to adapt the groups to accommodate these losses during the experiment. The corticosterone-injected groups were disproportionately affected by these factors, reducing the group size down to 1 or even 0 in some cases (table 4.1).

The low group sizes for corticosterone-injected animals reduce the power of statistical tests and therefore the ability to pick up differences between time points. This may be the reason for the non-significant trends in ZT11.5-injected *Per2* (figure 4.6C) and ZT0.5-injected *Bmal1* (figure 4.7D). It is therefore difficult to conclude from this data whether the pulmonary oscillator has truly been affected by phase-reversal of circulating corticosterone concentration.

4.5 Conclusions

The data presented in this chapter are insufficient to say whether reversal of corticosterone rhythm by timed daily injections can reverse the local oscillator in the lung, although the *Per2* expression rhythm does appear to be suppressed. It was therefore not taken forward into an inflammatory challenge model as originally intended. Supporting data show that exogenous administration of glucocorticoids (Gcs) to adrenalectomised animals can yield physiological circulating concentrations with a decay rate comparable to an intact profile, but the implementation of this protocol did not appear to reverse the phase of *Per2* or *Bmal1* oscillation in the lung. This protocol was therefore set aside in favour of alternative methods of manipulating the circulating corticosterone rhythm (chapter 5) and Gc-GR signalling in the lung (chapter 6).

Chapter 5: Effects of consistent circulating corticosterone concentration upon rhythmic pulmonary inflammation

5.1 Introduction

Having established that reducing circulating corticosterone to a low, constant concentration via adrenalectomy abolishes the rhythmic variation in pulmonary neutrophilia in response to aerosolised lipopolysaccharide (LPS) (chapter 3), the question remained whether circulating concentrations needed to be rhythmic or merely above a threshold concentration for the rhythmicity observed in intact animals to occur. In order to address this question, a corticosterone clamp model was used to fix circulating corticosterone at a desired concentration throughout the day, removing the endogenous rhythm but maintaining the same average concentration over a 24hr period.

The principle behind the clamp utilises the endogenous negative feedback loop which governs glucocorticoid production to suppress endogenous production. In a naïve animal, corticosterone will feed back at multiple levels of the HPA axis to inhibit further production, creating a negative feedback loop. By applying a constant exogenous supply of corticosterone the HPA axis is continuously inhibited and so endogenous glucocorticoid production is suppressed.

Multiple methods of corticosterone delivery are available, including repeated injections, subcutaneous pellets, mini-osmotic pumps and inclusion in food or in drinking water, each with benefits and drawbacks (Dalm et al. 2008; Herrmann et al. 2009). Although the most straightforward and stress-free approach would be to include corticosterone in the food or drinking water, mice exhibit strong rhythms in their consumption of chow and water, with increased consumption during the dark (active) phase and less during the light phase. Administering corticosterone via this method may therefore still generate rhythmic variations in concentration due to rhythmic changes in corticosterone consumption. More invasive methods of administration have the advantage of being independent of the animals' rhythms in behaviour, but are more stressful to the animal. Given the importance of generating a flat circulating signal for this experiment, these methods are preferable and were investigated further.

Having employed intraperitoneal injections to administer corticosterone in the previous chapter and monitoring the circulating corticosterone concentrations afterwards, it was clear that this method would not be the most effective way of generating a constant circulating concentration and would instead generate a surge shortly after injection which gradually decayed (chapter 4). Repeated injections would have to be given, increasing discomfort for the animal and resulting in a complex and time-consuming protocol which would generate oscillating concentrations with an ultradian rhythm. Each of the remaining options (mini-osmotic pump and sustained release pellet) required surgery to implant initially but minimal maintenance afterwards and minimal disruption to the animals once recovered from the anaesthesia. These methods were also more likely to deliver continuous infusion/secretion of corticosterone.

The two surgical methods were compared by Herrmann et al. (2009), who determined that the subcutaneous pellet was the better delivery method for obtaining consistent circulating concentrations of corticosterone. For this reason, the subcutaneous pellet was chosen as the method of exogenous corticosterone delivery for this chapter.

5.2 Hypothesis tested and experimental approaches

Hypothesis 3: Rhythmic glucocorticoids are required for normal circadian regulation of the pulmonary inflammatory response.

Aim: Replace the rhythmic endogenous glucocorticoid profile with constant circulating concentrations and establish the impact upon time-of-day variation in innate pulmonary inflammation.

Objectives:

- Determine an appropriate dose of sustained release corticosterone implant (subcutaneous) to deliver a constant circulating concentration within the physiological range.

Mice were implanted with sustained release corticosterone pellet (2.5mg, 5mg or 7.5mg) or placebo control pellet. One week later, blood samples were collected across a day and corticosterone concentration measured via ELISA.

- Challenge intact and implanted animals with aerosolised lipopolysaccharide at multiple time points and measure the inflammatory response via quantification of cell infiltration and measurement of cytokine concentrations.

Mice were implanted with sustained release corticosterone pellet (2.5mg) and exposed to aerosolised LPS at CT0, CT6, CT12 or CT18; inflammatory cell influx and chemoattractant concentration in bronchoalveolar lavage fluid were measured as inflammatory markers.

5.2.1 Establishment of subcutaneous implant dose

Three doses of corticosterone pellet were chosen in order to determine an appropriate dose to generate circulating corticosterone concentrations which were fixed at approximately the average daily concentration of naïve mice. Based on previous literature (Pruett & Padgett 2004; Hodes et al. 2012) and extrapolating to the circadian series collected in chapter 3, it was expected that a dose of 2-5mg would fulfil this criteria.

In the experiments performed by Pruett and Padgett (2004), circulating corticosterone concentrations in naïve female B6C3F1 (a cross between C57BL/6 and C3H) mice were compared to mice of the same strain which had been adrenalectomised and implanted with corticosterone pellets. The optimum dose to mimic and endogenous concentration of approximately 180ng/ml was determined as between 1.5 and 2.5mg. This circulating concentration is higher than our anticipated peak concentration, but there are strain and sex differences to take into account. Female mice tend to have higher and more variable circulating corticosterone concentrations than male mice, and this also varies between strains (Malisch et al. 2007). This may explain why there are differences in corticosterone concentration between their naïve B6C3F1 female mice and the naïve male C57BL/6 mice presented in this thesis (chapter 3). Relating this to the dose of corticosterone pellet required also requires extra considerations, as male mice tend to be larger and this is also affected by strain. For example, based on example growth curves from Harlan Laboratories (www.harlan.com), at 8 weeks of age, female B6C3F1 mice weigh approximately 20g, male B6C3F1 weigh 25g, female C57BL6/J weigh 18g and male C57BL6/J weigh 24.5g. Therefore, male C57BL6/J mice may require a higher dose of pellet than female B6C3F1 mice to achieve a similar concentration of circulating factors as they are physically larger and will have a higher blood volume.

This is exemplified in the experiments performed by Hodes et al., where a dose of 5mg was used in adult male C57BL/6 mice (without adrenalectomy) to effectively replicate endogenous circulating concentrations. Doses of 10mg (2 x 5mg pellets) or 20mg (4 x 5mg pellets) increased the circulating corticosterone concentration. This data was presented as a fold-change and without details of sampling time, so

it is difficult to tie this to an approximate concentration, but it is clear that there is variability between strains, sexes and studies. Therefore, doses of 2.5mg and 5mg were chosen as good candidates to mimic endogenous concentrations in intact male C57BL/6 mice, along with a 7.5mg dose to potentially clamp animals at the peak daily concentration.

Mice were implanted with either a 2.5mg (n=6), 5mg (n=6) or 7.5mg (n=6) corticosterone pellet, a placebo pellet (n=7), or did not undergo surgery to serve as naïve controls (n=5). All mice were group-housed in 12:12 light:dark cycles and monitored for 1 week following surgery to ensure full recovery before additional procedures were performed. Repeated tail bleeds were then performed every 4 hours for each animal, and blood processed for serum. Mice remained in LD during sampling to prevent sampling-induced phase shifts. Serum corticosterone was quantified via ELISA.

A preliminary experiment was then performed on this group of mice to test their inflammatory response to LPS at CT0; the point at which their circulating corticosterone is most different. Mice were transferred to constant darkness for 24hrs prior to challenge and then exposed to 2mg/ml aerosolised LPS in saline vehicle for 20 minutes at the start of subjective day, CT0. Bronchoalveolar lavage (BAL) samples were collected 5 hours later and analysed for cell numbers and CXCL5 production. This set of experiments in depicted in figure 5.1A.

5.2.2 Timed inflammatory challenge

Following establishment of a suitable dose of corticosterone pellet, a subsequent cohort were implanted with a 2.5mg pellet and then exposed to aerosolised lipopolysaccharide (LPS). Groups were pre-assigned to time points and blood samples collected 1 week after surgery and 4 days before challenge to assess corticosterone concentrations (figure 5.1B).

This cohort of animals were then subject to the aerosolised LPS exposure protocol utilised in chapter 1 – a period of 24hrs in constant darkness to avoid any masking effects of a light-dark cycle, followed by exposure to 2mg/ml LPS in 0.9% saline vehicle for 20 minutes. LPS exposure took place at either CT0 (start of subjective

day), CT 6 (middle of subjective day), CT12 (start of subjective night) or CT18 (middle of subjective night) and mice remained in constant darkness throughout. Samples were collected 5 hours later and analysed for inflammatory markers.

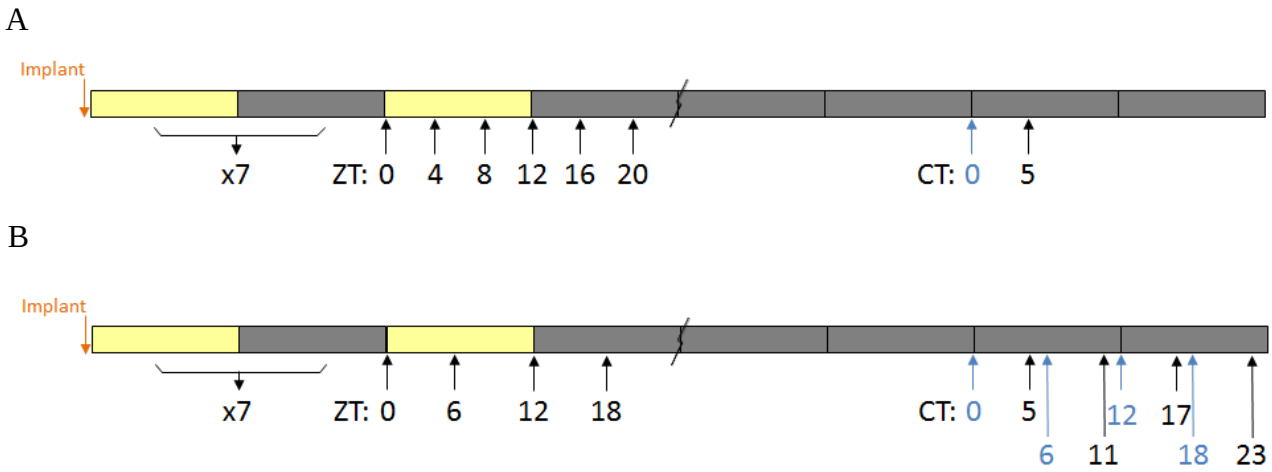

Figure 5.1: Experimental protocol for corticosterone clamp studies

A) Preliminary study to determine a suitable dose consisted of implant, 1week recovery and serial tail bleeds to test circulating corticosterone. After 6 days of recovery from sampling, animals were transferred to constant darkness for 24hrs and then exposed to aerosolised LPS at CT0 with terminal bronchoalveolar lavage samples collected at CT5. B) The timed LPS exposure experiment utilised 1 dose of implant (2.5mg) and intact controls, 1week of recovery, followed by single sampling at a time corresponding to subsequent aerosolised LPS exposure (0, 6, 12 or 18). After 4 days of recovery from sampling, mice were transferred to constant darkness for 24hrs and then exposed to aerosolised LPS at the designated time points. Orange arrows – implant, black arrows – sampling, blue arrows – LPS exposure, lightning bolt – interrupted axis.

5.3 Results

5.3.1 Consistent circulating concentrations of corticosterone can be obtained via subcutaneous implant of sustained release pellet

Corticosterone concentrations in both naïve and vehicle (placebo pellet) control groups peak at the start of the dark phase - ZT12 (figure 5.2). In contrast, each of the corticosterone pellet groups showed flattened rhythms; 2.5mg at approximately 75ng/ml, 5mg at approximately 90ng/ml and 7.5mg at approximately 100ng/ml.

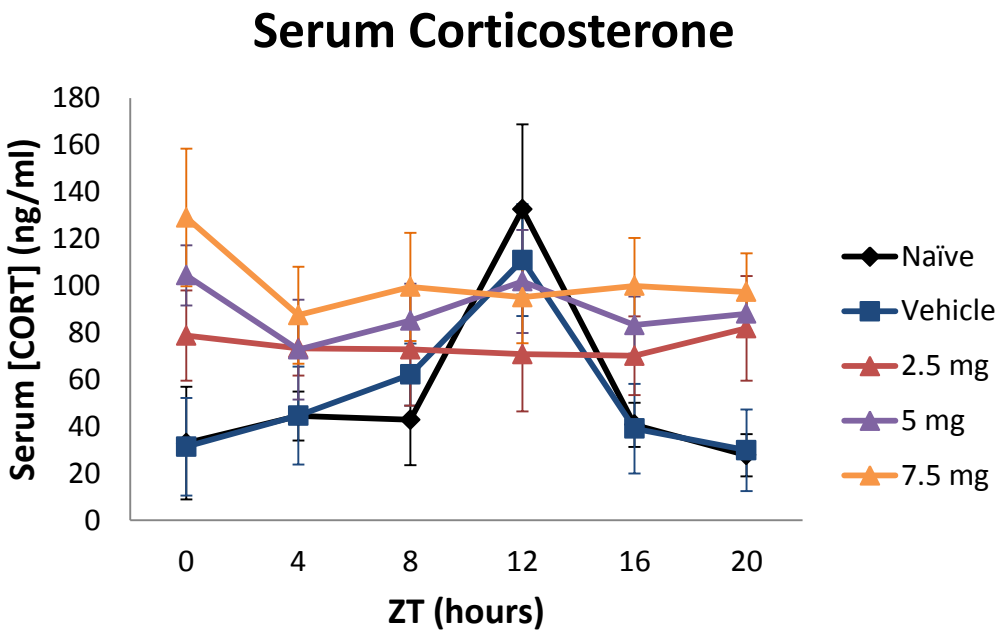

Figure 5.2: Circulating serum corticosterone concentrations across a circadian period
Serial samples of tail blood from naive (n=5), vehicle-implanted (n=7) and corticosterone-implanted (n=6/dose) mice across one day.

Statistical analysis of each group was performed using repeated measures ANOVA with prior assessment of sphericity using Mauchly's test (SPSS). A significant violation of sphericity was found for all groups, and so Greenhouse-Geisser correction was used to adjust degrees of freedom and p values accordingly. Significant rhythmicity was found in the vehicle control group ($F_{(1.384,8.303)}=6.073$, $p<0.05$) but not in any other treatment group. In the naive control group, $F_{(1.728,6.910)}=4.293$, $p=0.065$. In each of the pellet groups, corticosterone concentration did not vary over time: 2.5mg $F_{(1.320,5.280)}=0.309$, $p=0.662$; 5mg $F_{(1.702,5.107)}=0.745$, $p=0.499$; 7.5mg $F_{(2.422,9.687)}=2.326$, $p=0.145$.

5.3.2 Increased corticosterone at CT0 within physiological range does not suppress inflammatory response to aerosolised lipopolysaccharide

Despite varying concentrations of circulating corticosterone (figure 5.2), exposure to 2mg/ml aerosolised LPS at CT0 elicited no differences in total cell counts or CXCL5 production between groups (figure 5.3). One way ANOVA of cell counts showed $F_{(4,28)}=0.821$, $p=0.525$, and the same analysis of CXCL5 concentration showed $F_{(4,28)}=0.147$, $p=0.963$.

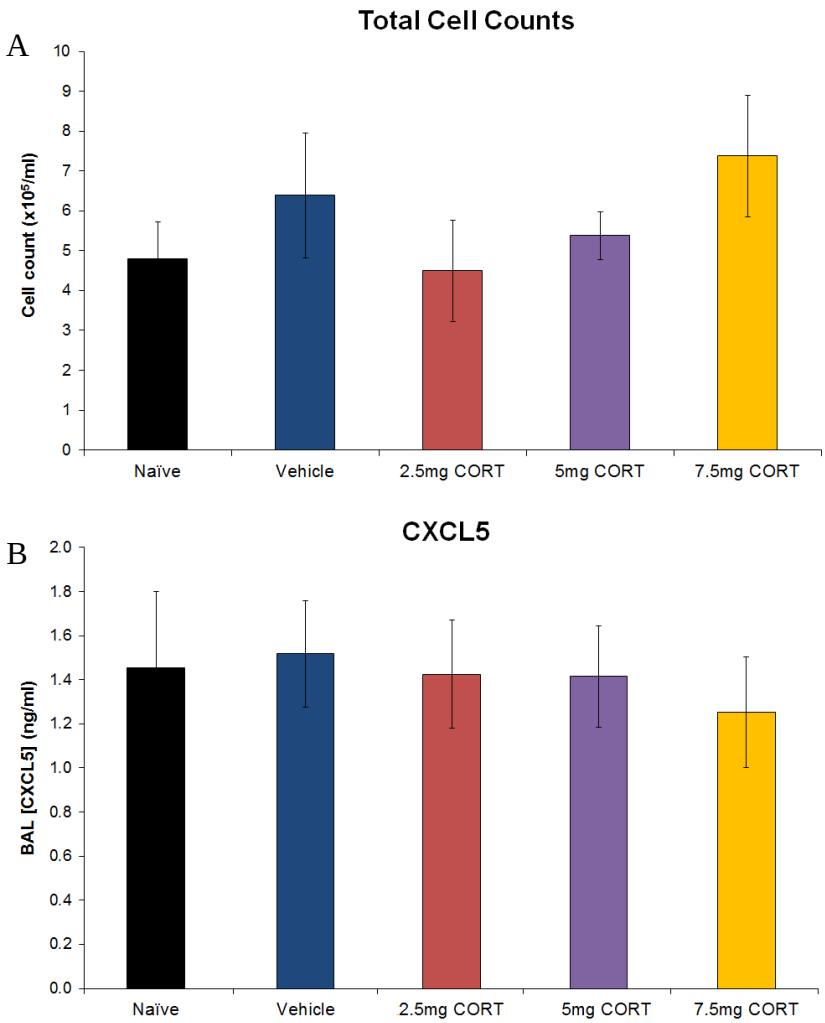

Figure 5.3: Inflammatory response to aerosolised LPS at CT0 with various doses of corticosterone implant

Mice were exposed to 2mg/ml lipopolysaccharide (LPS) in saline for 20mins at CT0 and culled 5hrs later. A) Total cell counts measured in bronchoalveolar lavage (BAL) fluid. B) Concentration of the neutrophil chemoattractant CXCL5 in BAL fluid. For both panels, naive (n=5), vehicle-implanted (n=7) and corticosterone-implanted (n=6/dose).

5.3.3 Corticosterone clamp does not affect the circadian-gated response to aerosolised LPS

Intact (non-implanted) controls showed considerable variability at CT0, and so the median absolute deviation method was used to test for outliers. Two data points with high measured concentrations were excluded using this method, which brought the mean concentration for this group down to the level shown in figure 5.4. A time-of-day variation was seen in circulating corticosterone in the intact animals (one-way ANOVA, $F_{(3,21)}=3.388$, $p<0.05$) with a significant increase at CT12 relative to CT0 and CT18 (post hoc tests using Bonferroni correction, $p<0.05$ for each). Animals implanted with the sustained release pellets had consistent concentrations across all time points (one-way ANOVA, $F_{(3,23)}=0.933$, $p=0.443$), indicating effective suppression of the HPA axis.

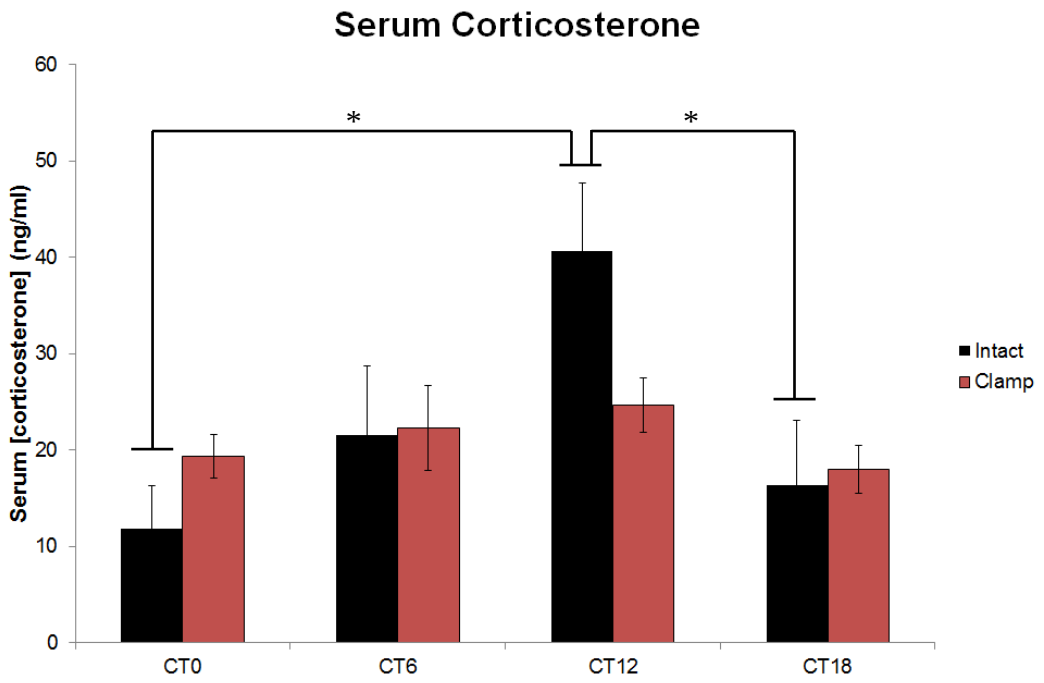

Figure 5.4: Circulating serum corticosterone concentrations prior to experiment
Corticosterone concentration in serum samples from tail blood taken at indicated time points. All groups are independent, n=6/condition except intact CT0 where two outliers were removed via the Median Absolute Deviation method. * denotes significance at $p<0.05$.

Following LPS challenge at CT0, CT6, CT12 or CT18, bronchoalveolar lavage samples were collected five hours later (CT5, CT11, CT17 or CT23) and used to assess pulmonary inflammation. Total cell counts were obtained and normalised to counts/ml lavage fluid (figure 5.5A). One-way ANOVA for each treatment showed a significant effect of time in both groups: intact $F_{(3,23)}=4.443$, $p<0.05$, clamp $F_{(3,23)}=6.214$, $p<0.05$. Post hoc analysis using the Bonferroni correction (equal variances) showed CT12<CT18 in intact animals, and analysis using the Games-Howell correction (unequal variances) showed CT12<CT6 in clamped animals. The CT0 vs. CT12 comparison was not significant for either group (intact $p=1$, clamp $p=0.079$).

Cytospins were produced from bronchoalveolar lavage fluid and used to make a differential cell count. Proportions of macrophages, neutrophils and 'other' were combined with the total cell count to give a measure of neutrophil number/ml (figure 5.5B). Again, one-way ANOVA was performed for each treatment group, but only the clamped animals showed a significant effect of time: intact $F_{(3,23)}=1.9$, $p=0.162$, clamp $F_{(3,21)}=10.805$, $p<0.05$. Post hoc analysis of clamped animals Games-Howell correction (unequal variances) showed that CT12<CT6. The CT0 vs. CT12 comparison was not significant ($p=0.06$).

Concentration of the neutrophil chemoattractant CXCL5 in the lavage fluid was analysed by ELISA. One-way ANOVA for each treatment showed a significant effect of time in both treatment groups: intact $F_{(3,22)}=3.759$, $p<0.05$, clamp $F_{(3,23)}=3.859$, $p=0.025$. Post hoc analysis using the Games-Howell correction (unequal variances) showed CT6<CT12 in intact animals, and analysis using the Bonferroni correction (equal variances) showed CT6<CT18 in clamped animals. The CT0 vs. CT12 comparison was not significant for either group (intact $p=0.230$, clamp $p=0.860$).

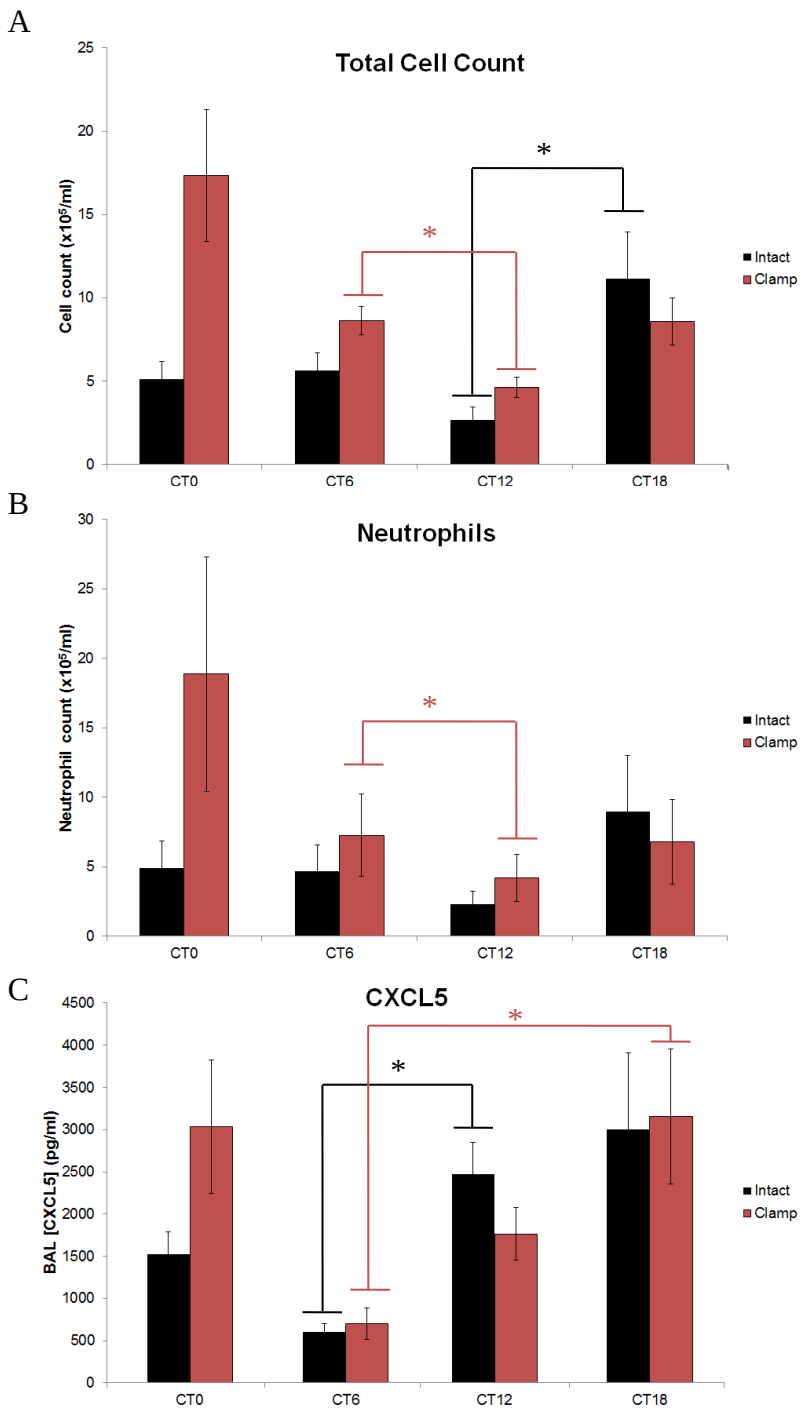

Figure 5.5: Response of intact and corticosterone-clamped mice to aerosolised lipopolysaccharide

Mice were exposed to 2mg/ml lipopolysaccharide (LPS) in saline for 20mins at the indicated time points and culled 5hrs later. A) Total cell counts measured in bronchoalveolar lavage (BAL) fluid after LPS challenge. B) Neutrophil counts calculated from cytospin proportions and total cell counts. C) Concentration of the neutrophil chemoattractant CXCL5 in BAL fluid. For all panels, n=6/group, * denotes significance at $p<0.05$.

BAL – bronchoalveolar lavage; CT – circadian time, time of challenge.

5.4 Discussion

5.4.1 Corticosterone clamp effects on circulating corticosterone concentration

Subcutaneous implant of sustained-release corticosterone pellets resulted in a consistent concentration of circulating hormone, as a proof-of-principle for subsequent experiments (figure 5.2). The doses chosen were all within the physiological range of naïve animals (30-140ng/ml) and increased pellet doses increased circulating hormone concentration accordingly, although this was not proportionate to dose.

A simple division of concentration detected by dose administered shows an efficacy of approximately 30ng/ml per mg for 2.5mg pellets, 18ng/ml per mg for 5mg pellets and 14ng/ml per mg for the 7.5mg pellet. This difference may reflect evidence of 'diminishing returns', where adding additional compound yields progressively less and less additional effect, or it may simply be a reflection that endogenous production is not completely suppressed by all doses and the circulating concentration is a combination of progressively less endogenous production and more exogenous administration, where the exogenous administration is still proportionate to dose. Once endogenous production is completely suppressed, the circulating concentrations should be proportionate to dose.

The fact that circulating corticosterone is not abolished by adrenalectomy must also be taken into account. Extra-adrenal (but endogenous) sources of corticosterone produce a low, consistent concentration (chapter 3), which may or may not also be suppressed by the pellet implants. Therefore, the concentrations observed in this chapter may be a combination of endogenous extra-adrenal corticosterone and exogenous corticosterone. Importantly though, these signals are not rhythmic.

These results indicate that the rhythmic component of endogenous corticosterone production was sufficiently repressed by all doses, as no oscillation in circulating concentrations were observed with any dose of pellet. The pellets have zero order

kinetics of compound release, meaning they will evenly release product over time, but this does not necessarily equate to an even circulating concentration as metabolism must also be taken into account. The pellets are merely a releasing agent and do not respond to changes in circulating concentrations (i.e. homeostatic release in response to low concentrations detected). These data therefore also show that corticosterone metabolism and clearance did not vary across the day as a consistent release rate yielded a consistent serum concentration.

5.4.2 Corticosterone clamp effects on rhythmic pulmonary inflammation

Despite changes in circulating corticosterone concentration, sustained release pellets had no effect on the pulmonary inflammatory response to aerosolised LPS in either an isolated CT0 time point or a circadian profile utilising 4 exposure times. This was unexpected given the results of chapter 3, where dampening of the rhythm to a low concentration via adrenalectomy abolished the time-of-day effect in neutrophil influx seen in intact animals.

Differences in corticosterone concentration were most pronounced at ZT0, where Gcs are low in control animals (figure 5.2). However, inflammatory challenge at the corresponding circadian time (CT0) showed no difference in inflammatory response for any dose of corticosterone pellet (figure 5.3). These results indicate that these doses of corticosterone are insufficient to provide an exogenous anti-inflammatory effect, despite being consistent with the peak concentration in intact controls (at ZT12), when inflammation is significantly lower.

The results of the corticosterone-clamped 4-time point exposure are consistent with those published for intact wild-type animals, with highest neutrophilia at CT0 (Gibbs et al. 2014). This effect was lacking in the wild-type mice in this experiment, which exhibited a blunted response to LPS at CT0. There are no obvious reasons for this to occur, as elevated neutrophilia at CT0 has been seen multiple times in the lab, and in my own earlier experiments, and the robust response to the LPS seen in clamped animals indicates that the exposure system was working as intended. Due to the abundance of other wild-type data showing

this trend, it was not deemed necessary to repeat this group. The lack of effect from the corticosterone clamp is not entirely unexpected, as although the very low corticosterone concentrations present in ADX animals was associated with a loss of rhythmic variation in inflammatory response, it may be that a threshold concentration required has been reached in clamped animals.

Mechanistically, this combination of results implies a signalling component downstream of the glucocorticoids themselves as the rhythmic lynchpin. If rhythmic repression exists without a rhythmic ligand, then attention must turn to aspects later in the signalling pathway and suggests that receptor activity is not just driven by availability of ligand.

It has already been shown that GR protein expression in the lung does not oscillate (Gibbs et al. 2009), so this result cannot be explained by fluctuating expression of the receptor. However, multiple regulatory mechanisms are involved in nuclear hormone signalling, including posttranslational modification of the receptor, availability of co-factors and access to DNA due to chromatin structure or occupancy by other transcription factor complexes. In order to elucidate the core driver behind rhythmic variation in the pulmonary inflammatory response, it will be necessary to investigate these possibilities.

Previous studies have shown that occupancy of GR at the promoter of *Cxcl5* is rhythmic in wild type animals but not in *Ccsp-Bmal1*$^{-/-}$ mice, which lack a functional clock in the bronchiolar epithelial cells. The regulation of GR binding by the cellular clock, despite normal rhythms in circulating ligand clearly illustrates that the cell-autonomous oscillatory mechanisms are more important than the systemic glucocorticoid signal in driving rhythmic inflammation, as long as enough ligand is present (Gibbs et al. 2014). In the case of the ADX animals, GR may well still be able to bind in a rhythmic manner due to an intact cellular clock but is unable to as there is limited activation by ligand binding.

It would therefore be of interest to investigate how the molecular clockwork can influence transcription factor binding. One strong possibility is the regulation of chromatin architecture by the clock. Members of the transcription-translation

feedback loop are already known to bind DNA, but recent evidence shows recruitment of additional proteins which can modify chromatin structure. CLOCK itself is a histone acetyltransferase (HAT), acetylating lysine residues within histones and promoting transcription (Doi et al. 2006), whilst PER proteins have been shown to complex with the histone methyltransferase HP1γ-Suv39h and/or the histone deacetylase HDAC1, transforming chromatin to a repressive state (Duong & Weitz 2014).

In accordance with this, the CLOCK:BMAL1 complex has been shown to remodel chromatin in a rhythmic manner, promoting nucleosome removal and opening chromatin at enhancer sites. This rhythmic opening was associated with the presence of the variant histone H2A.Z, which binds chromatin less tightly than it standard H2A counterpart. The rhythmic incorporation of H2A.Z was abolished in *Bmal1*$^{-/-}$ mice, thus, rhythmic CLOCK:BMAL1 binding promotes incorporation of a variant histone which increases chromatin accessibility (Menet et al. 2014). This circadian variation in accessibility would allow other transcription factors, such as GR, to bind more readily and may drive some of the rhythmic variations in their activity.

Next generation sequencing techniques could shed light on this hypothesis by assessing regions of open and closed chromatin at different times of day. By comparing *Bmal1*$^{-/-}$ tissue or cells with equivalents with a functional clock, either through DNase-seq (in which a DNA digest is performed to digest open chromatin and sequence the closed regions), ATAC-seq (where a transposase is used to amplify regions of open chromatin) or FAIRE-seq (where open chromatin is more readily fixed with formaldehyde and sequenced), it should be possible to determine whether a time-of-day remodelling of chromatin architecture occurs which is associated with the circadian clock (Tsompana & Buck 2014).

5.4.3 Note

Importantly, the corticosterone implant pellets are only guaranteed for a certain release time, after which the matrix will have decayed and the active compound is depleted. In an initial experiment, where time constraints meant the experiment was carried out later in the pellets' lifespan, the subtle reintroduction of rhythmic

corticosterone may be observed. The results for the inflammatory challenge and corticosterone profiles of these animals are given in appendix 7. Unsurprisingly, the data for the timed LPS challenges is consistent with the clamp animals shown here and previously published intact data, as they themselves do not differ. Care must be taken though, if utilising this method in other work, to ensure that the experiments take place well within the lifespan of the delivery system.

5.5 Conclusions

The work in this chapter implicates an interaction between glucocorticoids (Gcs) and target cell clocks in driving the rhythmic pulmonary response. Whilst the corticosterone clamp robustly generated a non-rhythmic daily profile of circulating Gcs, this had no effect upon the circadian gating of pulmonary inflammation. This novel data shows that rhythmicity of the Gc ligand is not necessary to generate time-of-day effects in pulmonary neutrophilia. Instead, attention should be turned towards the rhythmicity of GR binding to target genes and the potential for circadian regulation of binding site accessibility.

Chapter 6: Targeted disruption of glucocorticoid receptor signalling in bronchiolar epithelial cells

6.1 Introduction

Previous work has highlighted a role for the bronchiolar epithelial cells (also known as club cells or Clara cells) in driving circadian rhythmicity in the murine lung (Gibbs et al. 2009). Bioluminescence recordings of lung slices from *Period2-Luciferase* mice show rhythmic oscillations over 5 days in culture, as do isolated bronchiolar epithelial cells. However, after depletion of the bronchiolar cells via naphthalene exposure *in vivo*, lung slices taken from treated mice are arrhythmic when cultured. Naphthalene is metabolised by cytochrome P-450 monooxygenases, which are highly abundant in the bronchiolar epithelial cells, producing toxic metabolites which cause the cells to swell and exfoliate into the airway lumen (Van Winkle et al. 1999). The fact that selective loss of bronchiolar epithelial cells results in arrhythmic lung slices clearly shows that they are critical for maintaining rhythmicity in the murine lung, and they have since become key targets for investigations into rhythmic pulmonary physiology and pathology (Gibbs et al. 2014).

Bronchiolar epithelial cells are key mediators of inflammatory responses in the lung due to their secretion of surfactants and lysozymes, along with high cytochrome P-450 monooxygenase activity (Van Winkle et al. 1999). This makes complete ablation of the cell type an impractical way to test the effects of disrupted pulmonary rhythmicity upon rhythmic inflammatory responses as confounding effects may occur due to loss of the cell population. Rather, it is better to selectively disrupt circadian oscillations in the bronchiolar epithelial cells, so that some functionality may remain albeit potentially arrhythmic. This approach was utilised by Gibbs et al. (2014) by combining a *Bmal1*$^{flox/flox}$ mouse strain with the bronchiolar epithelial cell-specific Cre line *Ccsp*^{icre} to generate *Ccsp-Bmal1*$^{-/-}$ mice.

Selective loss of *Bmal1* in the bronchiolar epithelial cells (BECs) resulted in loss of rhythmic bioluminescence in these cells, although clock gene oscillations in whole lung remained consistent with wild-type (*Bmal1*$^{flox/flox}$, no Cre recombinase) littermates (Gibbs et al. 2014). Pulmonary responses to aerosolised lipopolysaccharide (LPS) were modulated by time-of-challenge in wild type

animals, but this effect was lost when the *Bmal1* signalling was disrupted in *Ccsp-Bmal1*$^{-/-}$ mice (Gibbs et al. 2014). Loss of circadian oscillations in the BECs was associated with enhanced recruitment of neutrophils to the lung at both time points (CT0 and CT12), which was associated with increased production of the neutrophil chemoattractant CXCL5. Despite enhanced neutrophilia, measurement of immune respiratory burst activity by myeloperoxidase (MPO) assay showed no difference between the two genotypes, suggesting the enhanced cell influx did not confer additional antibacterial benefit. This effect was seen in additional experiments utilising *Streptococcus pneumoniae* infection, where enhanced neutrophilia was again observed in *Ccsp-Bmal1*$^{-/-}$ animals but without changes in bacterial burden (Gibbs et al. 2014). These results illustrate the importance of an intact circadian clock in bronchiolar epithelial cells and implicate them as a lynchpin regarding circadian regulation of innate inflammation in the lung.

Gibbs et al. also addressed a potential mechanism whereby the circadian clock may regulate CXCL5 production and, therefore, time-of-day variation in neutrophil influx (Gibbs et al. 2014). The *Cxcl5* proximal promoter is known to contain glucocorticoid response elements (GREs), to which the glucocorticoid receptor (GR) can bind to repress transcription (John et al. 2008). Analysis of GR binding in lung tissue via chromatin immunoprecipitation (ChIP) revealed that at CT0, the time of increased neutrophil influx, GR binding to the *Cxcl5* promoter is significantly lower than at CT12, when GR binding is increased and the gene is suppressed. In contrast, the same analysis in *Ccsp-Bmal1*$^{-/-}$ lungs showed a drastically reduced association of GR with the *Cxcl5* sequence which showed no variation with time-of-day (Gibbs et al. 2014). This therefore raises the question of whether the interplay between the bronchiolar epithelial cell clock and GR signalling may be the underlying mechanism by which innate pulmonary inflammation is regulated by the circadian clock.

Whilst previous chapters have sought to address the contribution of rhythms in circulating ligand concentration (chapters 3-5), in order to investigate the specific role of rhythmic GR signalling in the bronchiolar epithelial cells a more targeted approach is required. Using the same cell-specific Cre line as Gibbs et al. (2014),

it should be possible to selectively disrupt GR in these cells when combined with a floxed GR mouse line.

Lung development is highly dependent upon glucocorticoid receptor function, however, and knockout of GR in cells expressing surfactant protein-C (SP-C) resulted in neonatal mortality and abnormal lung development (Manwani et al. 2010). An overlap between SP-C^+ cells and bronchiolar epithelial cells exists, as recent research has found a subset of pro-SP-C^+ $CCSP^+$ cells with stem cell capacities (Wang et al. 2012). There is therefore a possibility that a *Ccsp*-driven knockout may also result in perinatal death. If the mouse line is viable though, it is hypothesised that these animals will exhibit an altered response to timed lipopolysaccharide challenge and yield important information about the role of rhythmic glucocorticoid receptor signalling in the bronchiolar epithelium.

6.2 Hypothesis tested and experimental approaches

Hypothesis 4: Glucocorticoids exert their effects on the rhythmic pulmonary inflammatory response via the glucocorticoid receptor (GR) in bronchiolar epithelial cells.

Aim: Disrupt expression of the glucocorticoid receptor in bronchiolar epithelial cells and assess impact upon lung rhythmicity and circadian regulation of the inflammatory response to aerosolised LPS.

Objectives:

- Generate a mouse strain which lacks GR in bronchiolar epithelial cells and maintain on a Per2::Luc background to facilitate bioluminescence monitoring.

Nr3c1^{tm2Gsc} (known onwards as *GR*^{flox}) transgenic mice were purchased from the European Mutant Mouse Archive (EMMA) as frozen embryos and re-derived by Harlan Laboratories, UK, to produce two heterozygous breeding pairs. A homozygous *GR*$^{flox/flox}$ line was established on site and bred with *Bmal1*$^{flox/flox}$*Ccspicre*$^{/+}$/PER2::Luc mice already within the facility. Breeding pairs were set up as *Ccsp*$^{icre/+}$ (heterozygous for Cre sequence) crossed with *Ccsp*$^{+/+}$ (no Cre sequence, wild-type *Ccsp*) so that litters would be 50% Cre^{+} and 50% Cre^{-}, facilitating the use of 'wild-type' littermate controls (wild-type in this sense meaning no recombination of the GR gene, Cre^{-}). All animals were homozygous for *GR*^{flox} and for PER2::Luc (figure 6.1A). Assessment of successful recombination and loss of GR was performed by genotyping PCR (Tronche et al. 1999) (figure 6.1B and C), whole lung Western Blot, *in situ* hybridisation and immunofluorescence staining of lung slices.

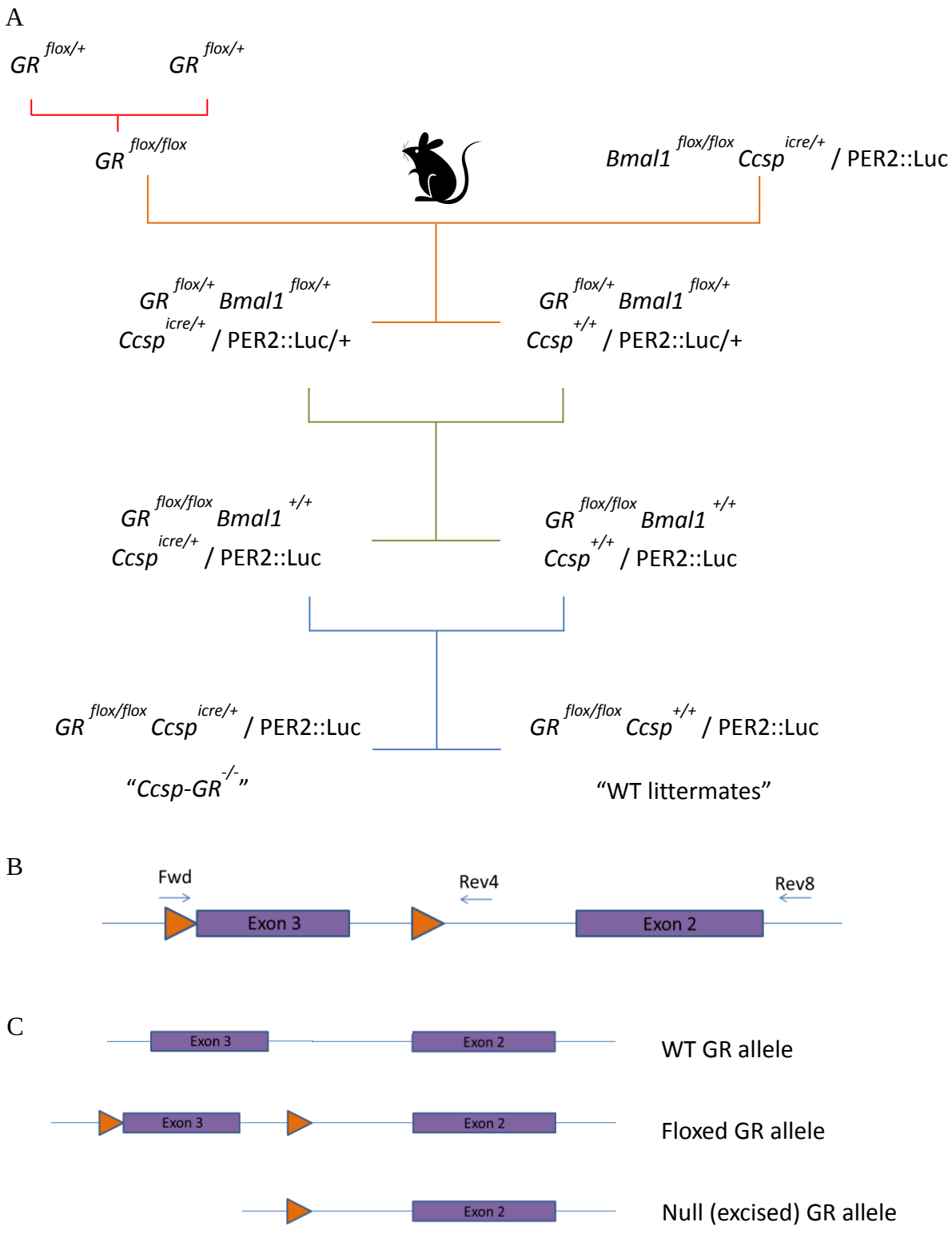

Figure 6.1: Targeting strategy and generation of *Ccsp-GR*$^{-/-}$ mice

A) Breeding strategy for generating *GR*$^{flox/flox}$*Ccsp*^{icre}/PER2::Luc (*Ccsp-GR*$^{-/-}$) colony. B) Location of loxP sites (orange triangles) and genotyping primers (blue arrows) in GR sequence, as determined by PCR and sequence analysis. C) In the presence of Cre, the genomic DNA between loxP sites will be excised and the sequence truncated.

- Assess lung rhythmicity and the ability to be synchronised by glucocorticoids by monitoring organotypic lung slices from *Ccsp-GR*$^{-/-}$ mice and wild type littermates under photomultiplier tubes (PMTs), and measuring their synchronising response to the synthetic glucocorticoid dexamethasone.

Organotypic lung slices (275µm) were obtained from female *Ccsp-GR*$^{-/-}$ and wild type (*GR*$^{flox/flox}$) littermate controls (all on PER2::Luc background) and bioluminescence monitored over time using photomultiplier tubes. All recordings took place at 37ºC in closed conditions (sealed dishes reliant on buffered medium to regulate CO_2 concentration). Photon counts were recorded over time and normalised to a 24hr moving average. Tissue slices were left undisturbed for several days to monitor endogenous oscillation.

After initial rhythms had dampened, a single administration of dexamethasone or media control was used to test resynchronisation capacity. Recordings were made for a further 5-7 days to assess resynchronisation and rhythmicity following this treatment. Normalised photon counts per slice were analysed by cosinor rhythm analysis software (Refinetti 1992) and means per genotype/treatment were compared by t-test.

- Challenge *Ccsp-GR*$^{-/-}$ mice and wild type littermates with aerosolised LPS at different time points and measure any differences in the magnitude and rhythm of inflammatory response (cell infiltration and cytokine production).

- Assess differences between genotypes in the immunosuppressive effects of dexamethasone administration before LPS treatment at different time points.

These two objectives were addressed in the same group of experiments. Male *Ccsp-GR*$^{-/-}$ and wild type (*GR*$^{flox/flox}$) littermate control mice (all on PER2::Luc background) were challenged with aerosolised LPS or saline vehicle at either CT0 or CT12. Those mice receiving aerosolised LPS were further split into two groups – one received an intraperitoneal injection of 1mg/kg dexamethasone (in saline vehicle) 1hr before LPS exposure, whilst the other received saline vehicle alone. As in previous experiments, mice were housed in constant darkness for 24hours prior to CT0 and remained in darkness throughout treatments.

Inflammatory cell influx and chemoattractant concentration in bronchoalveolar lavage fluid was measured 5 hours later. An initial experiment was performed at CT12, as this was the time at which the greatest difference was expected, followed by a second cohort challenged at CT0 once further litters had been weaned and genotyped. A third experiment utilising LPS-only challenge with dexamethasone or saline pre-treatment was performed at both CT0 and CT12 in one session.

6.3 Results

6.3.1 *GR$^{flox/flox}$Ccsp^{icre}*/PER2::Luc (*Ccsp-GR$^{-/-}$*) mice show disrupted glucocorticoid receptor expression in the bronchial epithelium

Assessment of successful knockout of GR in bronchiolar epithelial cells was performed using multiple approaches. First, the genotyping strategy used allows identification of floxed, wild-type and null (recombined, 'knockout') fragments (figure 6.2A). Null fragments were only observed in lung samples (not ear punches, which are routinely used for genotyping) of Cre^{+ve} animals.

Loss of GR at protein level was initially tested using Western Blot on whole lung tissue from *Ccsp-GR$^{-/-}$* and *GR$^{flox/flox}$* animals. However, no difference in GR abundance between the two genotypes was detected (figure 6.2B). Lower concentration of CCSP, known to be upregulated by GR (Berg et al. 2002), was detected in the *Ccsp-GR$^{-/-}$* but this was later found to be a result of the *Ccsp^{icre}* transgene as it was also observed in *Ccsp^{icre}* (no floxed genes) control mice (appendix 8).

Analysis of GR presence *in situ* was obtained via *in situ* hybridisation (performed by Dr. Ben Saer) and immunofluorescence (performed by Dr. Laura Matthews). Bronchioles from Ccsp-GR$^{-/-}$ animals showed significantly less GR mRNA expression relative to GR$^{flox/flox}$ counterparts (figure 6.2C and D); $t_{(6)}=4.898$, $p<0.01$. Immunofluorescence staining for GR (figure 6.2E, red) shows lower abundance of GR^{+} cells lining the bronchioles (white arrows) of *Ccsp-GR$^{-/-}$* mice compared to *GR$^{flox/flox}$* littermate controls, whilst blood vessels (left panel) and lung parenchyma (middle panel) do not differ.

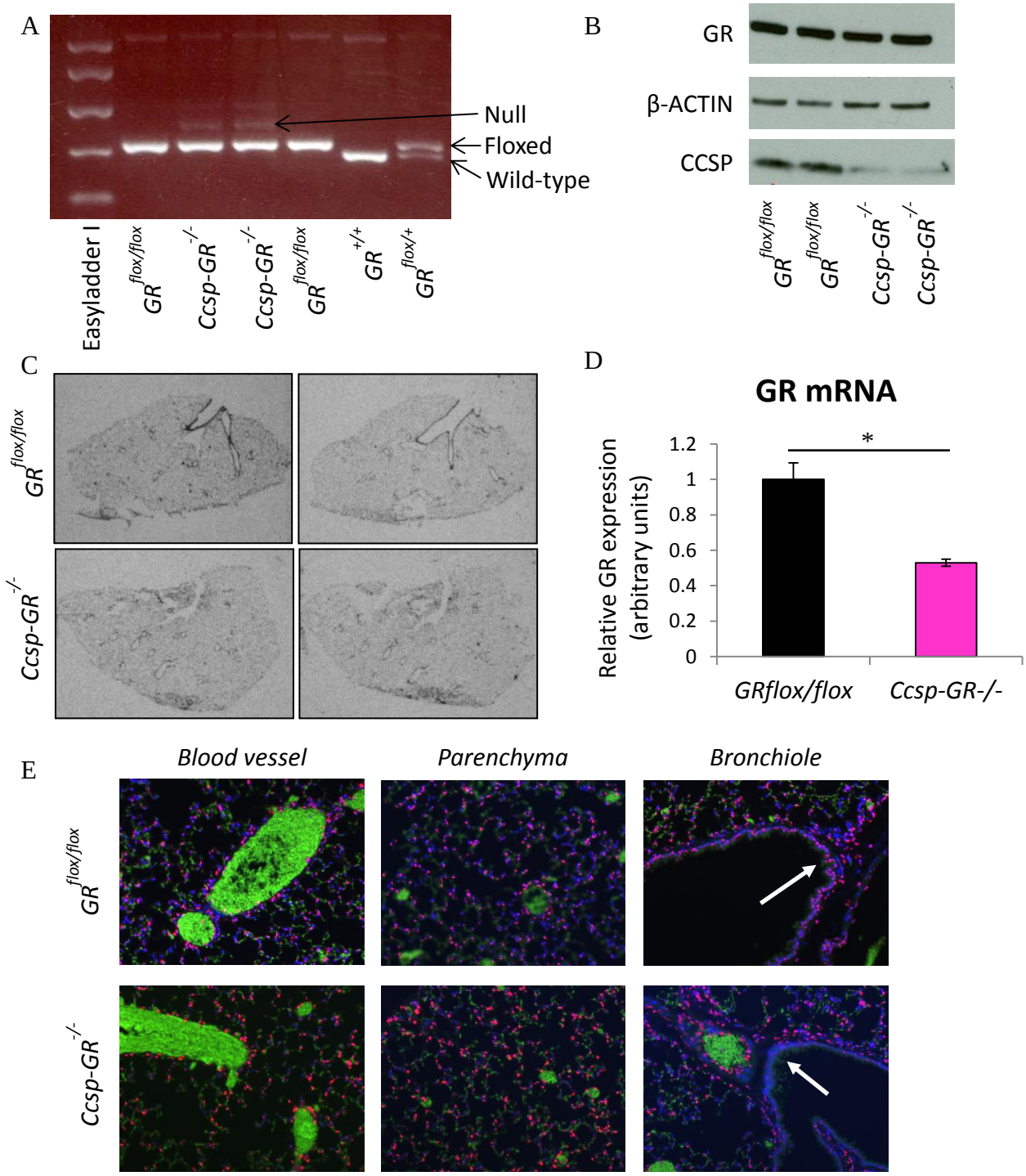

Figure 6.2: Testing for GR loss in bronchiolar epithelial cells of *Ccsp-GR*$^{-/-}$ mice

A) Example genotyping results from lungs of *Ccsp-GR*$^{-/-}$ mice and *GR*$^{flox/flox}$ littermates. *GR*$^{flox/+}$ and *GR*$^{+/+}$ samples included for comparison. B) Western blot analysis of whole lung from *Ccsp-GR*$^{-/-}$ and *GR*$^{flox/flox}$ animals. Proteins stained are GR (top, 90-95kDa), β-actin (middle, 42kDa) and CCSP (bottom, 10kDa). C) Example images of lung slices probed for GR mRNA via *in situ* hybridisation. D) Relative quantification of GR mRNA abundance from multiple lung slices measured via *in situ* hybridisation (n=4/genotype). E) Example images (20x magnification) of lung slices stained for GR (red) and cell nuclei (blue) via immunofluorescence. Green indicates background/autofluorescence. White arrows highlight bronchial epithelium. * *denotes significant difference at the 0.01 level.*

6.3.2 Lung slices from *Ccsp-GR*$^{-/-}$ mice retain circadian rhythms of bioluminescence in culture and retain the ability to be resynchronised by dexamethasone administration

Organotypic lung slices from *Ccsp-GR*$^{-/-}$ animals and *GR*$^{flox/flox}$ littermate controls both exhibited rhythmic oscillations of PER2::Luc-driven bioluminescence for several days (figure 6.3A). Cosinor analysis of data from hours 24-72 shows an average period of 24.5 hours for wild-type controls and 24.0 hours for *Ccsp-GR*$^{-/-}$ slices (figure 6.3B). Statistical analysis using independent samples t-test show no significant difference between means ($t_{(8)}$=1.339, p=0.217).

Application of dexamethasone successfully resynchronised both genotypes, restoring synchronous oscillations (figure 6.3C). Cosinor analysis of days 2 and 3 post-treatment shows an average period of 24.5 hours for dexamethasone-treated wild-type controls and 24.2 hours for dexamethasone-treated *Ccsp-GR*$^{-/-}$ slices (figure 6.3D). Media-treated controls still exhibited low amplitude oscillations after treatment, but with a lengthened period of 25.1 hours in *GR*$^{flox/flox}$ slices and 25.4 hours in *Ccsp-GR*$^{-/-}$ slices. Independent samples t-tests indicated no significant differences between the two treatments for *GR*$^{flox/flox}$ controls ($t_{(8)}$=1.239, p=0.250), but a significant lengthening of period with media treatment in the *Ccsp-GR*$^{-/-}$ slices ($t_{(8)}$=3.541, p<0.025 – corrected for multiple comparisons).

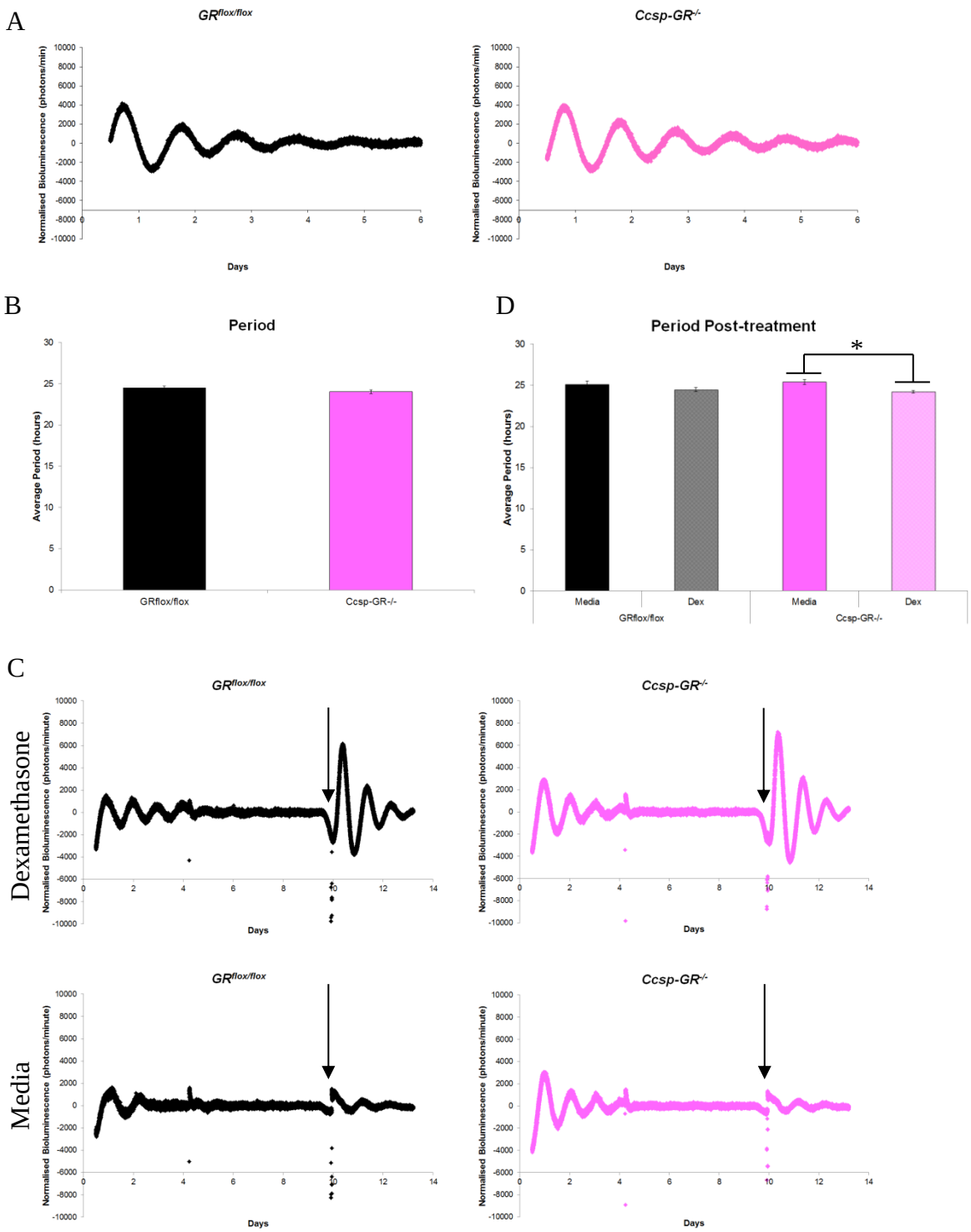

Figure 6.3: Oscillations of PER2::Luc-driven bioluminescence in organotypic lung slices A) Example bioluminescence recordings from *GR*$^{flox/flox}$ (black) and *Ccsp-GR*$^{-/-}$ (pink) lung slices. B) Average oscillation period of bioluminescence recording, determined by cosinor analysis of individual traces. C) Example bioluminescence recordings from *GR*$^{flox/flox}$ (black) and *Ccsp-GR*$^{-/-}$ (pink) lung slices before and after treatment with dexamethasone (top) or media alone (bottom). Time of treatment is indicated by black arrow. D) Average oscillation period of bioluminescence recording after treatment, determined by cosinor analysis of individual traces. *Photon counts per minute are normalised to a 24 hour moving average and traces are representative of 5 biological replicates. Dex – dexamethasone. * denotes significant difference at p<0.05.*

6.3.3 *Ccsp-GR*$^{-/-}$ mice exhibit a loss of circadian gating in their response to aerosolised LPS challenge, yet remain sensitive to dexamethasone-mediated suppression of inflammation

To examine the effects of the loss of GR in the bronchial epithelial cells upon pulmonary inflammation, *Ccsp-GR*$^{-/-}$ mice and *GR*$^{flox/flox}$ littermate controls were challenged using aerosolised lipopolysaccharide (LPS). The first experiment was performed at CT12, when glucocorticoids are at their endogenous peak and pulmonary inflammation at its nadir. Mice of each genotype were split into three groups. The 'saline' group received aerosolised saline for 20 minutes at CT12. The 'LPS' group received aerosolised LPS 2mg/ml in saline for 20 minutes at CT12, along with an intra-peritoneal injection of saline at CT11. The 'DEX + LPS' group received the same LPS challenge at CT12 but were pre-treated with intraperitoneal injection of 1mg/kg dexamethasone in saline at CT11. All mice were culled at CT17, lungs were lavaged and exudate analysed for cell counts and cytokine concentrations.

Total cell counts were analysed by two-way ANOVA after removal of one outlier in the *GR*$^{flox/flox}$ DEX+LPS group which exhibited a much greater cell count relative to the rest of that group. This animal was removed from all further analyses as it was suspected that the dexamethasone injection had not been successful. A significant effect of genotype was found ($F_{(1,27)}=9.021$, $p<0.01$), with *Ccsp-GR*$^{-/-}$ animals having a higher mean cell count, along with a significant effect of treatment ($F_{(2,27)}=3.809$, $p<0.05$). Means are plot in figure 6.4A. Post hoc tests with Bonferroni correction showed an elevated cell count in *Ccsp-GR*$^{-/-}$ mice for the LPS-only groups ($t_{(27)}=3.258$, $p<0.05$), but not the saline-treated or LPS + DEX groups.

Neutrophilia was only evident in LPS-treated animals, with macrophages underlying the elevated cell count in saline-treated *Ccsp-GR*$^{-/-}$ animals (data not shown). Comparison of neutrophil counts between LPS-treated groups (figure 6.4B) by two-way ANOVA showed a significant effect of genotype ($F_{(1,18)}=5.235$, $p<0.05$), and a borderline significant effect of treatment ($F_{(1,18)}=4.252$, $p=0.0539$). Based on total cell count data, it was predicted that the neutrophil count would be

elevated in the LPS-treated *Ccsp-GR*$^{-/-}$ animals but post hoc tests did not confirm this statistically ($t_{(18)}$=2.772, p=0.0755).

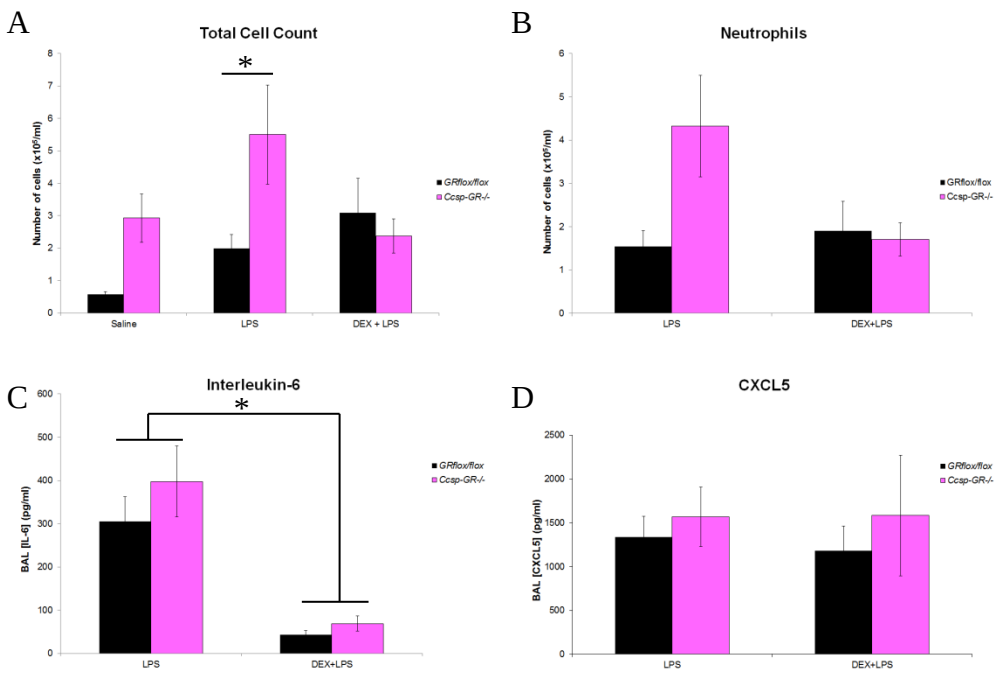

Figure 6.4: Pulmonary inflammatory response to lipopolysaccharide challenge at CT12
GR$^{flox/flox}$ (black) and *Ccsp-GR*$^{-/-}$ (pink) mice were challenged with aerosolised lipopolysaccharide (2mg/ml) in saline or saline vehicle alone for 20 minutes at circadian time 12. LPS-treated animals were pre-treated with intraperitoneal injection of saline vehicle ('LPS' group) or 1mg/kg dexamethasone in saline ('DEX+LPS' group) 1hr prior to LPS exposure. A) Total cell counts per ml bronchoalveolar lavage fluid. B) Neutrophil counts obtained from total cell counts and cytospin differential counts. C) Concentration of the pro-inflammatory cytokine interleukin-6 in bronchoalveolar lavage fluid. D) Concentration of the pro-inflammatory cytokine CXCL5 in bronchoalveolar lavage fluid.
*BAL – bronchoalveolar lavage; CT – circadian time; DEX – dexamethasone; IL-6 – interleukin-6; LPS – lipopolysaccharide. * denotes significant difference at p<0.05, n=5-6/group.*

Two candidate cytokines were analysed via ELISA: interleukin-6 (figure 6.4C) and CXCL5 (figure 6.4D). Interleukin-6 was strongly repressed by dexamethasone treatment in both genotypes (two-way ANOVA: treatment $F_{(1,19)}$=30.71, p<0.001, genotype $F_{(1,19)}$=1.208, p=0.2854). No significant differences were observed in CXCL5 (two-way ANOVA: treatment $F_{(1,19)}$= 0.1152, p=0.738, genotype $F_{(1,19)}$=0.8058, p=0.381).

A second experiment was performed focussing on the CT0 time point, following the same procedure. Pre-treated animals were injected at CT-1 (CT23 of the previous day) and aerosolised treatments took place at CT0. Tissue collection was performed at CT5.

Total cell counts were analysed by two-way ANOVA, which reported a significant effect of treatment ($F_{(2,34)}=3.973$, $p<0.05$), but no effect of genotype ($F_{(1,34)}=0.069$ $p=0.795$). Post hoc tests with Bonferroni correction showed no significant differences in any pairwise comparisons (figure 6.5A).

Neutrophilia in LPS-treated animals was also analysed by two-way ANOVA, which showed no significant effects of genotype, treatment, or interactions (figure 6.5B).

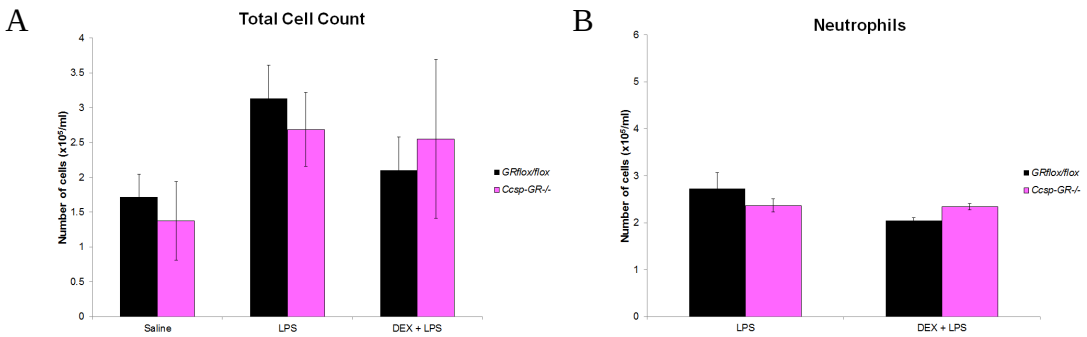

Figure 6.5: Pulmonary inflammatory response to lipopolysaccharide challenge at CT0
$GR^{flox/flox}$ (black) and *$Ccsp\text{-}GR^{-/-}$* (pink) mice were challenged with aerosolised lipopolysaccharide (2mg/ml) in saline or saline vehicle alone for 20 minutes at circadian time 0. LPS-treated animals were pre-treated with intraperitoneal injection of saline vehicle ('LPS' group) or 1mg/kg dexamethasone in saline ('DEX+LPS' group) 1hr prior to LPS exposure. A) Total cell counts per ml bronchoalveolar lavage fluid. B) Neutrophil counts obtained from total cell counts and cytospin differential counts.
CT – circadian time; DEX – dexamethasone; LPS – lipopolysaccharide.

Following assessments of responses at each time point individually, a third experiment was performed using only LPS and DEX + LPS groups at both time points. For this experiment, flow cytometry was used to label cells for quantification rather than cytospin and manual counting.

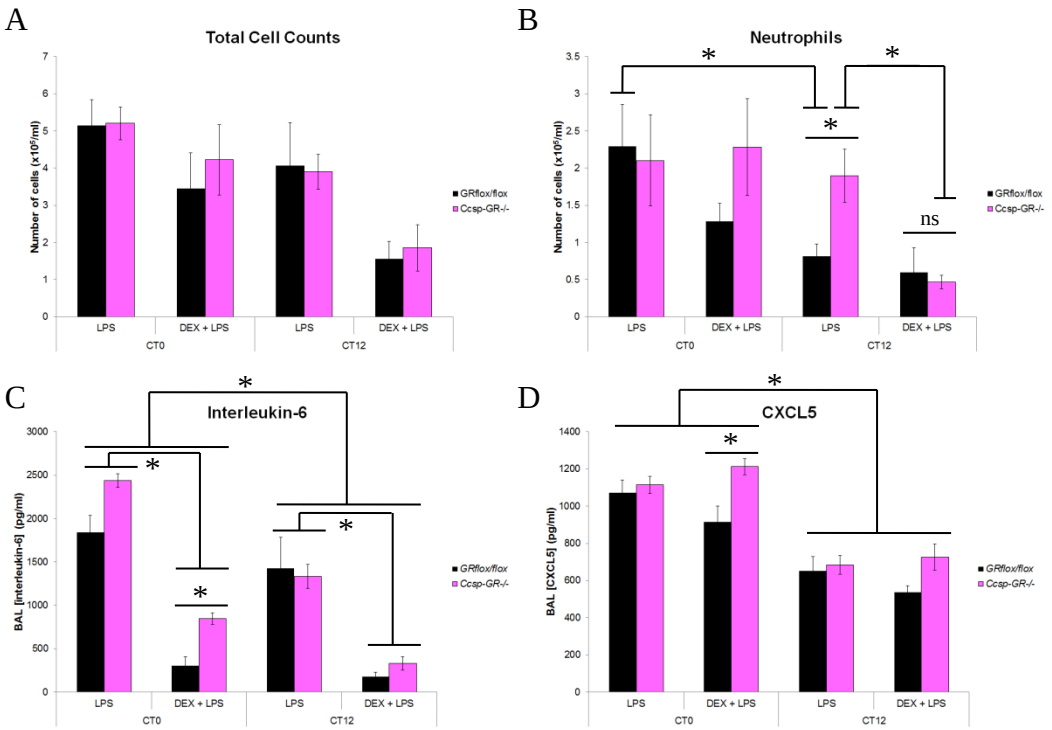

Figure 6.6: Pulmonary inflammatory response to lipopolysaccharide challenge at CT0 & CT12

GR$^{flox/flox}$ (black) and *Ccsp-GR$^{-/-}$* (pink) mice were challenged with aerosolised lipopolysaccharide (2mg/ml) in saline for 20 minutes at circadian time 0 or 12. Animals were pre-treated with intraperitoneal injection of saline vehicle ('LPS' group) or 1mg/kg dexamethasone in saline ('DEX+LPS' group) 1hr prior to LPS exposure. A) Total cell counts per ml bronchoalveolar lavage fluid. B) Neutrophil counts obtained from total cell counts and flow cytometry differential counts based on Ly6G expression. C) Concentration of the pro-inflammatory cytokine interleukin-6 in bronchoalveolar lavage fluid measured by bioplex. D) Concentration of the pro-inflammatory cytokine CXCL5 in bronchoalveolar lavage fluid measured by bioplex.

*BAL – bronchoalveolar lavage; CT – circadian time; DEX – dexamethasone; LPS – lipopolysaccharide. * denotes significant difference at p<0.05, n=4-7/group.*

Total cell counts 3-way ANOVA showed significant main effects of time ($F_{(1,40)}$=8.563, p<0.01, CT0 > CT12) and treatment ($F_{(1,40)}$=10.651, p<0.01, LPS > DEX + LPS) but no effect of genotype ($F_{(1,40)}$=0.041, p=0.842) or significant interactions. Pairwise comparisons yielded no significant differences at this level.

Analysis of neutrophil count via the same method indicated the same pattern - significant main effects of time ($F_{(1,40)}$=11.915, p<0.01, CT0 > CT12) and treatment ($F_{(1,40)}$=4.953, p<0.05, LPS > DEX + LPS) but no effect of genotype ($F_{(1,40)}$=1.887, p=0.177) or significant interactions. Post hoc tests of planned comparisons showed a significant time-of-challenge effect in LPS-treated wild types ($t_{(11)}$= 2.352, p<0.05), which showed enhanced neutrophilia at CT0. No such difference was found in *Ccsp-GR*$^{-/-}$ animals ($t_{(8)}$=0.3102, p=0.7643).

The altered phenotype appears to be caused by an increase in neutrophil count at CT12, as the *Ccsp-GR*$^{-/-}$ LPS group was significantly higher than *GR*$^{flox/flox}$ littermates at this time point (figure 6.6B): $t_{(10)}$=2.763, p<0.05. The enhanced neutrophilia was significantly reduced by dexamethasone pre-treatment, as the *Ccsp-GR*$^{-/-}$ CT12 DEX + LPS count was significantly lower than the equivalent LPS-only group ($t_{(10)}$=3.844, p<0.01) and no significant difference was observed between animals treated with DEX + LPS at CT12 (figure 6.6B). These results replicate the trend observed in the single time point experiment in figure 6.4B.

For this experiment, cytokine analysis was performed using bioplex to simultaneously measure the concentrations of 23 proteins in each sample. In comparison with previous experiments, IL-6 and CXCL5 data are shown in figures 6.6C and D (respectively). Each cytokine was analysed individually by 3-way ANOVA and results of main effects summarised in table 6.1.

CXCL5 was identified as a circadian chemokine, exhibiting a significant difference in concentration between time points (table 6.1, figure 6.6D). A significant effect of genotype was also observed, but CXCL5 was not found to be repressed by dexamethasone pre-treatment (table 6.1). Pairwise comparisons of CXCL5 concentrations using individual t-tests confirmed a significant effect of time for each comparison and no significant effects of treatment. Genotype differences were not significant except for the comparison between CT0 DEX + LPS groups ($t_{(10)}$=3.096, p<0.05), indicating a significantly higher concentration of CXCL5 in the *Ccsp-GR*$^{-/-}$ animals (figure 6.6D).

In comparison, interleukin-6 (IL-6) concentration varied significantly between times and treatments but no effect of genotype was observed (table 6.1). Post hoc comparisons using individual t-tests showed the effect of time was due to significant differences in the *Ccsp-GR*$^{-/-}$ groups ($t_{(8)}$=6.016, p<0.001 for LPS, $t_{(11)}$=4.890, p<0.001 for DEX + LPS) and no significant differences were found between *GR*$^{flox/flox}$ groups. Comparisons between genotypes showed the same pattern as those for CXCL5, with only the CT0 DEX + LPS groups showing a significant difference ($t_{(9)}$=8.660, p<0.001 – figure 6.6C).

Of the 23 cytokines tested in this experiment, 15 were detected (table 6.1). Those not detected were interferon-γ and interleukins 1β, 2, 5, 10, 12(p70), 13 and 17. Of those detected, 6 were circadian, 13 were suppressed by dexamethasone, and only 3 affected by genotype. CXCL5, G-CSF (CSF3), IL-6, KC (CXCL1) and MIP-2 (CXCL2) were all up-regulated at CT0, whereas interleukin-1α was elevated at CT12. Only CXCL5 and interleukin-1α did not show significant repression by dexamethasone. Both CXCL5 and GM-CSF (CSF2) were increased in *Ccsp-GR*$^{-/-}$ animals and MIP-1α (CCL3) was increased in wild-type controls (*GR*$^{flox/flox}$).

Cytokine	CT0 vs. CT12	LPS vs. DEX+LPS	*GR*$^{flox/flox}$ vs. *Ccsp-GR*$^{-/-}$
CRG-2 (CXCL10)	ns	*** (LPS)	ns
CXCL5	*** (CT0)	ns	** (*Ccsp-GR*$^{-/-}$)
Eotaxin (CCL11)	ns	*** (LPS)	ns
G-CSF (CSF3)	*** (CT0)	*** (LPS)	ns
GM-CSF (CSF2)	ns	*** (LPS)	** (*Ccsp-GR*$^{-/-}$)
IFNγ		not detected	
IL-1α	* (CT12)	ns	ns
IL-1β		not detected	
IL-2		not detected	
IL-5		not detected	
IL-6	** (CT0)	*** (LPS)	ns
IL-10		not detected	
IL-12 p70		not detected	
IL-13		not detected	
IL-17		not detected	
KC (CXCL1)	* (CT0)	** (LPS)	ns
MCP-1 (CCL2)	ns	*** (LPS)	ns
M-CSF (CSF1)	ns	*** (LPS)	ns
MIP-1α (CCL3)	ns	*** (LPS)	** (*GR*$^{flox/flox}$)
MIP-1β (CCL4)	ns	*** (LPS)	ns
MIP-2 (CXCL2)	* (CT0)	** (LPS)	ns
RANTES (CCL5)	ns	*** (LPS)	ns
TNFα	ns	*** (LPS)	ns

Table 6.1: Summary of bronchoalveolar lavage cytokine analysis via bioplex

Lavage fluid from *GR*$^{flox/flox}$ and *Ccsp-GR*$^{-/-}$ mice challenged with aerosolised lipopolysaccharide (2mg/ml) in saline for 20 minutes at circadian time 0 or 12 was analysed for 23 cytokines simultaneously via bioplex. Animals were pre-treated with intraperitoneal injection of saline vehicle ('LPS' group) or 1mg/kg dexamethasone in saline ('DEX+LPS' group) 1hr prior to LPS exposure and culled 5 hours following LPS challenge. Statistical analysis was performed by 3-way ANOVA for each cytokine individually. Where differences are significant, the group with highest concentration is given in brackets. Alternative names (standard nomenclature) are given next to the common name in column 1.

** p<0.05; ** p<0.01; ***p<0.001; ns – p>0.05. CCL – chemokine C-C motif ligand; CRG-2 – cytokine responsive gene 2; CSF – colony stimulating factor; CXCL – chemokine (C-X-C) motif ligand; G-CSF – granulocyte colony-stimulating factor; GM-CSF – granulocyte macrophage colony-stimulating factor; IFN – interferon; IL – interleukin; KC – keratinocyte chemoattractant; MCP-1 – macrophage chemotactic protein 1; M-CSF – macrophage colony-stimulating factor; MIP – macrophage inflammatory protein; RANTES – regulated on activation, normal T cell expressed; TNF – tumour necrosis factor.*

6.4 Discussion

6.4.1 Generation of *Ccsp-GR*$^{-/-}$ mouse line

Breeding of *GR*$^{flox/flox}$ mice with a bronchiolar epithelial cell-specific Cre line (*Ccsp*$^{icre/+}$) resulted in viable and fertile offspring. These mice, termed *Ccsp-GR*$^{-/-}$ if Cre^{+ve} and *GR*$^{flox/flox}$ if Cre^{-ve}, were bred with a PERIOD2::Luciferase background; enabling bioluminescence recording in the presence of luciferin. Initially, it was not certain whether the Cre^{+ve} animals would survive, given the importance of GR signalling in lung development and the neonatal mortality observed when GR is knocked out in other lung cell types (Manwani et al. 2010), but *Ccsp-GR*$^{-/-}$ mice were successfully created and survived into adulthood. Of course, this may simply be a result of unsuccessful knockout of the glucocorticoid receptor.

Analysis of GR knockout using genotyping PCR in the lung clearly shows the presence of a null (recombined) fragment in Cre^{+ve} animals (figure 6.2A), but this is not sufficient to show that GR mRNA and protein are no longer produced effectively. Western Blot results were inconclusive, as abundance of GR protein relative to β-actin did not vary between the two genotypes (figure 6.2B). However, CCSP^{+ve} (and therefore Cre^{+ve}) cells are a relatively small proportion of whole lung cells and the selective loss of GR only in this cell type may be masked by the high expression of GR throughout the rest of the lung. Quantification of CCSP protein abundance (relative to β-actin) shows a 50% decrease in protein in *Ccsp-GR*$^{-/-}$ compared with *GR*$^{flox/flox}$ littermate controls (figure 6.2B). *Ccsp* is known to be upregulated by GR activation, so this result is consistent with a loss of GR in *Ccsp*-expressing cells but may also be a result of haploinsufficiency caused by the presence of the *Ccsp*^{icre} transgene. *Ccsp*$^{icre/+}$ animals have one normal copy of the *Ccsp* gene and one which is modified to contain the Cre sequence. If this yields only one viable copy of the *Ccsp* gene, then a reduced quantity of protein product may result.

To examine the possibility of haploinsufficiency, a batch of *Ccsp*$^{icre/+}$ mice (with PER2::Luc background but no floxed genes) were also analysed using the same protein extraction, quantification and Western Blot protocol (appendix 8).

Ccsp$^{icre/+}$ mice were also found to have decreased abundance of CCSP protein when compared with wild-type littermate controls, indicating that the result observed in *Ccsp-GR*$^{-/-}$ lungs may be due to alterations in the *Ccsp* gene itself, and not related to the loss of GR. This raises important questions regarding the response of *Ccsp*$^{icre/+}$ mice to inflammatory challenge, as CCSP is an important regulator of pulmonary immune barrier function, but unpublished data from our lab (Zhang, Pariollaud) suggests that these mice do not display elevated neutrophilia in response to aerosolised lipopolysaccharide challenge, unlike *Ccsp-Bmal1*$^{-/-}$ (Gibbs et al. 2014). It would therefore be safe to use other *Ccsp*-targeted knockouts, such as the *Ccsp-GR*$^{-/-}$ line with the aerosolised LPS model without the disruption of the *Ccsp* gene being a confounding factor.

Further assessment of GR disruption in the bronchial epithelial cells utilised *in situ* hybridisation (to probe mRNA) and immunofluorescence (to detect protein). *In situ* data shows a significant reduction of GR mRNA in the bronchioles of *Ccsp-GR*$^{-/-}$ animals compared to *GR*$^{flox/flox}$ littermates, although the signal is not completely lost. It is not surprising to see some residual expression within this region, as the cell population is not homogenous and contains some CCSP^{-} cells. The CCSP^{-} cells will not express the Cre recombinase and should retain normal GR expression. The immunofluorescence staining (figure 6.2E) shows no variation in GR (red) in blood vessels or lung parenchyma, but there is a clear reduction in staining of the bronchiolar epithelium of *Ccsp-GR*$^{-/-}$ mice (bottom right). Again, some staining for GR is detectable in this region, reflective of the residual mRNA detected via *in situ* hybridisation.

It therefore appears that viable mice were produced with disrupted GR expression in the bronchial epithelium, indicating that GR in the bronchial epithelial cells is not critical for successful development and maturation of the murine pulmonary system.

6.4.2 Rhythmic bioluminescence in *Ccsp-GR*$^{-/-}$ mice

Depletion of bronchial epithelial cells (BECs) in the lung is known to render lung slices arrhythmic in culture (Gibbs et al. 2009). Targeted disruption of *Bmal1* in the BECs, however, does not affect whole slice rhythmicity but does abolish PERIOD2::Luciferase oscillations in the bronchial epithelium (Gibbs et al. 2014). From these experiments it therefore appears that the bronchial epithelial cells need to be present to maintain coherent oscillations in whole lung bioluminescence but they do not themselves require a functional clock. One possible explanation for this is that the BECs act as gatekeeper cells – interpreting timing signals and relaying them to other cell types which are able to oscillate (pneumocytes, for example). This function may not necessarily require an intact BEC clock but may instead require some (as yet unknown) unique property of this cell type to read the timing signal and disseminate it to the rest of the lung. How lung cells interact and communicate timing signals remains unknown and would certainly be an interesting area of research for the chronobiology field.

One candidate is the external glucocorticoid signal, already established as a rhythmic stimulus which is capable of modulating clock phase in peripheral tissues (Balsalobre et al. 2000). The glucocorticoid receptor, GR, is expressed by bronchial epithelial cells, which could interpret this external timing signal and relay it to the rest of the lung (figure 6.7A). This theory is hampered by the fact that GR is ubiquitously expressed in the lung, and so other cells will also be able to sense circulating glucocorticoids (although they may not have the capacity to convert it to a synchronising signal). However, the theory is easily tested either in *Ccsp-GR*$^{-/-}$ lungs or in lung slices from naphthalene-treated (BEC-depleted) animals. Although Gibbs et al. (2009) stop short of overtly testing the BEC-depleted slices for their ability to be synchronised by dexamethasone after multiple days in culture, so results are not strictly comparable with those in figure 6.3C, part of their initial slice preparation protocol is to synchronise slices with dexamethasone before adding the dishes to the photomultiplier tube system. The BEC-depleted slices were arrhythmic after the dexamethasone treatment during tissue preparation, indicating that lung slices from naphthalene-treated animals are insensitive to dexamethasone as a synchronising agent. In contrast, the results obtained from the *Ccsp-GR*$^{-/-}$ mice clearly show robust rhythms when placed into

culture and after dexamethasone treatment once initial rhythms had dampened (figure 6.3). These results, and those from *Ccsp-Bmal1*$^{-/-}$ mice (Gibbs et al. 2014) are summarised in table 6.2.

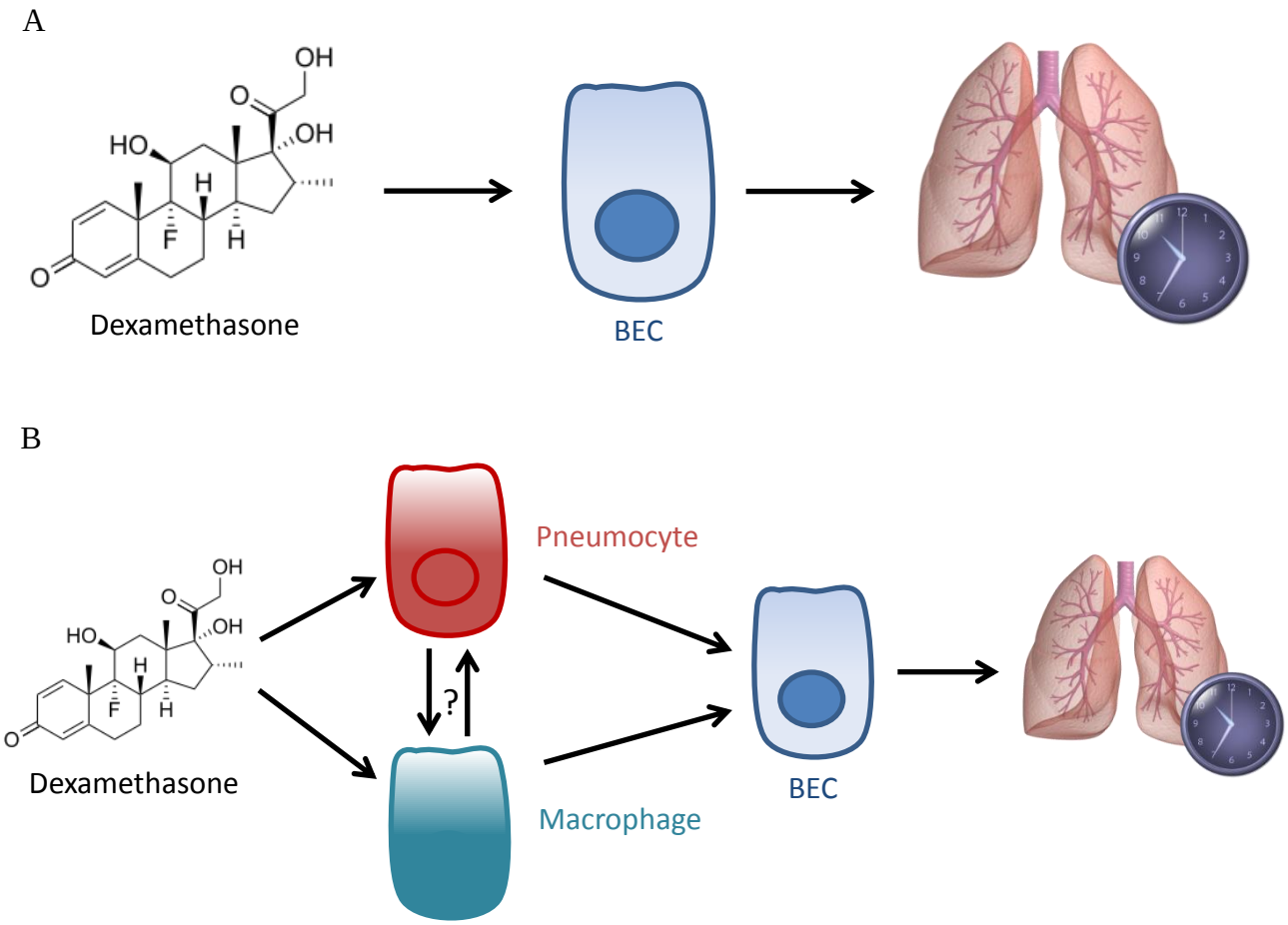

Figure 6.7: Model hypotheses for synchronising effects of dexamethasone in the lung
A) Bronchiolar epithelial cells (BECs) are gatekeeper cells which convey timing information to the rest of the lung. Dexamethasone exerts its effects through action in these cells, which feedback to the rest of the tissue. This initial hypothesis is compatible with data from BEC-depleted animals, but is inconsistent with data from *Ccsp-GR*$^{-/-}$ animals which retain the ability to be synchronised by dexamethasone despite lacking GR in BECs. B) Modified hypothesis to account for dexamethasone synchronisation in *Ccsp-GR*$^{-/-}$. BECs retain gatekeeper function, but dexamethasone stimulation is interpreted by another cell type upstream.

Condition	Whole lung rhythmicity?	Dexamethasone synchronisation?	Reference
Wild-type/untreated (controls)	✓	✓	Each of the below
Naphthalene (BEC-depleted)	x	x	Gibbs et al. 2009
***Ccsp-Bmal1*$^{-/-}$ (BEC clock disrupted)**	✓	unknown	Gibbs et al. 2014
***Ccsp-GR*$^{-/-}$ (BEC GR disrupted)**	✓	✓	Figure 6.3

Table 6.2: Comparison of lung slice rhythmicity and resetting capacity of dexamethasone treatment in different models

Depletion of bronchial epithelial cells (BECs) results in loss of lung slice rhythmicity which is not rescued with dexamethasone treatment. Neither loss of *Bmal1* or GR in BECs affects whole slice rhythmicity. GR-targeted mice retain the ability to synchronise to dexamethasone, but it is unknown whether *Bmal1*-targeted slices are affected.

This combination of results (Table 6.2) shows that the bronchial epithelial cells (BECs) are required for whole lung rhythmicity and for the lung slice to synchronise in response to dexamethasone treatment (see naphthalene-treated row). However, neither BMAL1 nor GR needs to be present in BECs for the whole lung to retain rhythmic oscillations. This discredits the idea that GR signalling through BECs leads to synchronisation of the rest of the lung, but it remains plausible that another factor may be acting through these cells. Unless dexamethasone is exerting its synchronising effects without interacting with GR in the BECs, additional cell types in the lung must be able to respond to dexamethasone for the *Ccsp-GR*$^{-/-}$ slices to be synchronised. The gatekeeper hypothesis must therefore be modified to include an earlier step, in which other cells can integrate the dexamethasone signal and communicate this to the bronchial epithelium (figure 6.7B). These early responders may be macrophages, which are known to express GR and communicate with the epithelium through gap junctions (Westphalen et al. 2014) or could be the pneumocytes themselves. This raises additional questions regarding cell-cell communication and timing in the lung – if the upstream cells can communicate with the BECs, why can't they

communicate with each other to generate oscillations independently? Why don't BECs require a functional clock themselves to drive oscillations in the rest of the lung? Are they actually just a relay between other cells?

Determination of the sequence and signals involved in relaying timing across the lung could be investigated using multiple knockout models, such as a *LysM-GR*$^{-/-}$ to disrupt macrophage GR, and testing dexamethasone responses; work which is underway in the lab. Disruption of GR expression in other lung cells is risky, as neonatal lethality is likely using other currently-available standard Cre lines which target the lung, but it may be possible to circumvent this outcome by using inducible Cre strains to cause recombination after the lungs have matured (Rawlins & Perl 2012).

It is also possible to target macrophages pharmacologically by using clodronate liposomes to selectively poison phagocytic cells. In this model, clodronate molecules are pre-packaged in liposomes, which are recognised as foreign by macrophages (and other phagocytic cells) and taken up into the cell. The liposome is then degraded, releasing the clodronate which diffuses into the cytosol. The clodronate molecule is processed by Class II aminoacyl-tRNA synthetases to become a toxic ATP analogue – $AppCCl_2p$ (adenosine 5'-(β,γ-dichloromethylene) triphosphate). This new molecule is thought to cross into mitochondria, where it irreversibly binds to the ATP/ADP translocase and inhibits mitochondrial function. The mitochondrial disruption ultimately results in apoptosis of the cell (Frith et al. 2001). Conveniently, this process only occurs in phagocytic cells and specific subsets can be targeted using different delivery methods. For example, intranasal or intratracheal dosing will selectively target airway cells, whereas subcutaneous injection will target draining lymph nodes. It would therefore be possible to deplete airway macrophages *in vivo* and perform rhythmicity assessments on lung slices taken from these animals. If macrophages were the integrator of the dexamethasone synchronising signal, it would be expected that the lung may be rhythmic initially but would not be able to be synchronised by dexamethasone treatment. If, however, it was a lung cell which relayed the dexamethasone signal, synchronisation would still occur.

6.4.3 Pulmonary inflammatory phenotype of *Ccsp-GR*$^{-/-}$ mice

Although an intact clock in the bronchial epithelium is not required for overall lung rhythmicity, it is required for appropriate circadian regulation of the inflammatory response (Gibbs et al. 2014). *Ccsp-Bmal1*$^{-/-}$ mice are pro-inflammatory and lose circadian gating of their neutrophilic response to aerosolised lipopolysaccharide. Loss of the gated neutrophilic response was also observed in adrenalectomised animals despite retention of intact clock gene oscillations in whole lung tissue (chapter 3). Therefore, intact whole lung rhythmicity in the *Ccsp-GR*$^{-/-}$ mice does not preclude further investigation into the possible loss of rhythmic innate inflammation.

The results from timed inflammatory challenges in *Ccsp-GR*$^{-/-}$ mice show no difference in neutrophil influx at CT0, but increased neutrophilia at CT12. This is consistent with a role for GR signalling in the bronchial epithelium reducing inflammation at CT12. At CT0, circulating glucocorticoids (Gcs) are at their nadir (chapter 3) and so loss of the receptor, GR, may not have much of an impact. At CT12, circulating Gcs are high and therefore disruption of GR will abolish the protective effects of the elevated endogenous ligand concentration at this time point. This is exemplified by the ChIP data from Gibbs et al. (2014) which clearly showed greater binding of GR to the *Cxcl5* locus at CT12 compared to CT0, correlating with greater suppression of *Cxcl5* in whole lung and a lower concentration of CXCL5 in lavage fluid.

However, this is a very simplistic explanation for the mechanism of Gc-GR effects upon circadian immunity in the lung. As detailed in chapter 5, replacement of a rhythmic Gc signal with a consistent circulating concentration (hormone clamp model) does not affect the time-of-day variation in the neutrophilic response. Rhythmicity of ligand availability is therefore not critical for the rhythmic inflammatory response to occur, shifting the focus to events further along the Gc-GR signalling pathway. It is hypothesised that access to the *Cxcl5* locus and GR binding may be under circadian control and it is this which dictates the timing of Gc sensitivity, rather than simply ligand availability. This hypothesis

is compatible with data from Gibbs et al. (2014), where there is reduced GR binding to the *Cxcl5* locus in the *Ccsp-Bmal1*$^{-/-}$ mice.

The enhanced inflammation seen at CT12 in *Ccsp-GR*$^{-/-}$ mice can be reduced by intraperitoneal injection of 1mg/kg dexamethasone before LPS challenge (figure 6.4). This retention of immunosuppressive effects of dexamethasone echoes the results of the rhythmicity studies, where *Ccsp-GR*$^{-/-}$ lungs retain the ability to be synchronised by dexamethasone in culture (figure 6.3C). Disruption of bronchial epithelial cell (BEC) GR therefore predisposes an animal towards a heightened inflammatory state when GR binding is an important anti-inflammatory mechanism (CT12) but does not render them insensitive to synthetic glucocorticoid treatment. This is in stark contrast to the published *Ccsp-Bmal1*$^{-/-}$ work, where loss of the BEC clock not only enhanced inflammatory cell influx but abolished the immunosuppressive effects of dexamethasone.

Whilst Gibbs et al. (2014) highlight the CXCL5 chemokine as a Gc-sensitive mediator of rhythmic neutrophilia, the results of this chapter do not fit this hypothesis, as dexamethasone is an effective suppressor of neutrophilia but not CXCL5 at CT12 in the *Ccsp-GR*$^{-/-}$ animals (figure 6.6). In these experiments, dexamethasone had no effect upon neutrophilia in either genotype at CT0, which is likely due to the large variability in data obtained. A genotype effect was observed in CT0 DEX + LPS groups, which may reflect a suppression of CXCL5 in the wild-type (*GR*$^{flox/flox}$) animals at this time point which is not occurring in the *Ccsp-GR*$^{-/-}$ mice. The comparison of DEX + LPS and LPS-only conditions at CT0 in the wild-type animals does not reach statistical significance, however, so it is impossible to draw this conclusion without further evidence. In the case of interleukin-6, dexamethasone treatment significantly reduced chemokine concentration in all time/genotype groups. This combination of results supports the above theory that the *Ccsp-GR*$^{-/-}$ mice may be less sensitive to dexamethasone-mediated suppression of cytokine production at CT0, as although IL-6 concentration is lower than that of the *Ccsp-GR*$^{-/-}$ LPS-only group, it is still significantly higher than dexamethasone-treated wild-type animals.

As with the rhythmicity studies (above), the intact effect of dexamethasone and the cell types mediating this could be investigated further by selective disruption of GR in other candidate cells or depletion of macrophages. Westphalen et al. (2014) have shown intercellular communication between sessile alveolar macrophages and the pulmonary epithelium to have immunosuppressive effects. In this paper, a subset of alveolar macrophages was described which were relatively immobile and strongly expressed *Connexin 43 (Cx43)*, a protein involved in gap junction formation. The authors hypothesised that these cells formed functional gap junctions with the lung epithelium, which were detected using calcium imaging.

To test the functional relevance of macrophage-epithelium gap junctions in immune regulation, intranasal LPS challenge was used to stimulate a pulmonary inflammatory response in *Cd11c-Cx43*$^{-/-}$ animals (which have disrupted *connexin 43* expression in macrophages) and *Cx43*$^{flox/flox}$ controls. Neutrophil influx in response to LPS challenge was exacerbated in *Cd11c-Cx43*$^{-/-}$ animals compared to controls, indicating an immunosuppressive function of macrophage-epithelium Cx43-mediated communication. Increased concentrations of MIP-1α (macrophage inflammatory protein 1α), CXCL1 and CXCL5 were detected in BAL from the *Cd11c-Cx43*$^{-/-}$ animals, consistent with an increase in the activity of nuclear factor-κB (NF-κB). The authors hypothesise that this reflects a mutually suppressive relationship between macrophages and the pulmonary epithelium, as MIP-1α is predominantly of macrophage origin, whereas CXCL1 and CXCL5 are produced by the epithelium (Westphalen et al. 2014). It is interesting to note that both MIP-1α and CXCL5 production after aerosolised LPS challenge were significantly altered in *Ccsp-GR*$^{-/-}$ animals (table 6.1). Whilst CXCL5 was increased in *Ccsp-GR*$^{-/-}$ mice, MIP-1α was decreased, which could indicate an uncoupling of this macrophage-epithelium crosstalk in which the epithelium is less sensitive to the inhibitory signals from the macrophages (increasing CXCL5) but macrophages show a reduced excitability (reflected in decreased MIP-1α). Further investigation of mechanisms involved in macrophage-epithelium communication and a potential role for GR are required to test this hypothesis.

Breeding of *LysM-GR*$^{-/-}$ is underway, and could be used in inflammatory studies to assess the effects of disrupted macrophage GR expression without losing the cells entirely. Pharmacological depletion is a faster approach, and preliminary studies show a reduction in macrophage number after clodronate treatment in both *Ccsp-GR*$^{-/-}$ and *GR*$^{flox/flox}$ littermate controls but no differences between the two genotypes. These results are promising for future work aimed at using the aerosolised LPS challenge model (with and without dexamethasone pre-treatment) after clodronate depletion of macrophages. If the true immunosuppressive effects of dexamethasone are actually exerted through macrophage GR, then clodronate-treated animals should be insensitive to the dexamethasone pre-treatment. It is possible, however, that clodronate treatment itself may affect the inflammatory response and care must be taken to include appropriate controls. The results of these future experiments will certainly be valuable to both immunologists and pulmonary biologists, given that immune-epithelium crosstalk is a growing research area and a more detailed understanding of how glucocorticoid signalling affects the pulmonary immune system will inform drug development and treatment of pulmonary inflammatory disorders.

6.5 Conclusions

This chapter constitutes novel findings regarding the role of GR in CCSP^{+ve} murine bronchial epithelial cells in regulating both circadian rhythms in the lung and time-of-day variation in response to aerosolised lipopolysaccharide challenge. The production of the *Ccsp-GR*$^{-/-}$ mouse line alone is a unique contribution to the field, as no other lab to date has published using this strain. Whilst it does not appear that bronchial epithelial cell (BEC) GR is critical for maintaining oscillations in lung slices or for mediating the resynchronising effects of dexamethasone, loss of BEC GR does increase the inflammatory response to aerosolised LPS at the CT12 time point. Curiously, this enhanced inflammation is responsive to pre-treatment with systemic injection of dexamethasone, which implicates additional cell types in regulating this effect. These data may therefore provide a starting point for future investigations into immune-epithelium crosstalk in the lung and the relative contributions of cellular clocks and GR signalling in each cell type.

Chapter 7: Discussion

7.1 Summary of key findings

Adrenalectomised mice lack time-of-day variation in neutrophil influx to the lung following aerosolised lipopolysaccharide challenge

Disruption of endogenous glucocorticoid production in mice by adrenalectomy (ADX) does not disrupt (wheel-running) behavioural rhythms (figure 3.2) or clock gene oscillations in the lung (figures 3.3, 4.6B and 4.7B), but does abolish the time-of-day variation in neutrophil invasion of the lung in response to aerosolised lipopolysaccharide challenge (figure 3.4C).

Relative phasing of *Bmal1* and *Per2* expression in the lung is altered after timed daily administration of corticosterone at ZT0.5

Daily injections of 10mg/kg corticosterone at ZT0.5 (endogenous nadir) to adrenalectomised animals resulted in a dampened oscillation in *Bmal1* and a flattened *Per2* expression profile, despite control (un-injected) adrenalectomised animals retaining robust rhythms in both genes (figures 4.6 and 4.7).

The lung retains a rhythmic neutrophilic response to aerosolised lipopolysaccharide despite constant circulating corticosterone concentrations

Utilising a subcutaneous constant-release hormone pellet, replacement of an endogenous corticosterone rhythm with a flat daily average (figure 5.2) did not affect rhythmic pulmonary neutrophilia in response to lipopolysaccharide (figure 5.5B).

Genetic targeting of the glucocorticoid receptor in bronchial epithelial cells disrupts the pulmonary inflammatory response but the tissue retains anti-inflammatory sensitivity to dexamethasone

Ccsp-GR$^{-/-}$ mice, a novel strain which lacks the glucocorticoid receptor in the bronchial epithelial cells (figures 6.1 and 6.2), retain rhythmic oscillations of PER2-Luc-driven bioluminescence in the lung, which were capable of being resynchronised by dexamethasone (figure 6.3). The *Ccsp-GR*$^{-/-}$ mice show enhanced neutrophil influx compared to wild-type littermates when challenged with aerosolised LPS at CT12, but this is suppressed by dexamethasone administration (figure 6.6).

7.2 Discussion

The experiments contained within this thesis have been designed and performed with the aim of elucidating the role of a rhythmic glucocorticoid signal in regulating time-of-day variation in pulmonary inflammation. Circadian rhythms are a pervasive feature of life on Earth, and a molecular circadian clock has developed independently in many kingdoms – including plants, animals, bacteria and fungi (Dunlap 1999). Each of these groups exhibits daily oscillations in gene transcription and possession of a clock synchronised with the external environment is thought to confer an evolutionary advantage (Pittendrigh & Minis 1972; Woelfle et al. 2004). In mammals, the circadian clock is known to regulate multiple aspects of physiology and pathology, including hormone secretion, locomotor activity and response to inflammatory stimuli (Keller et al. 2009; Nakamura et al. 2011; Gibbs et al. 2012; Gibbs et al. 2014).

Possession of a pacemaker, such as a circadian oscillator, enables temporal organisation of critical processes (Pittendrigh 1993) – either to synchronise activities to anticipated changes in the external environment (e.g. food availability, UV exposure) or to separate incompatible processes within a cell (e.g. shielding the nitrogenase enzyme crucial for nitrogen fixation from high levels of oxygen produced during photosynthesis in *Synechococcus* (Golden et al. 1997)). It is therefore not surprising that a process as energetically costly (transcription of cytokines and chemokines, cell migration and pathogen neutralisation all require energy) and context-dependent as an immune reaction is under circadian control, in order to time responses appropriately without being detrimental to other cellular processes by diverting energy and transcriptional machinery away unnecessarily. Much has recently been learnt about how the immune system is regulated in a rhythmic manner, including temporal variations in immune responsiveness to challenge, the effects of circadian disruption upon immune activity, interactions between components of the molecular clock and core immune proteins, and a role for circadian rhythms in the endocrine system as a modulator of inflammatory rhythms (discussed in the following sections).

7.2.1 Circadian rhythms in response to immune challenge

The mammalian immune system can be broadly split into two components – innate and adaptive (or acquired) immunity. The innate immune system, comprised of mast cells, macrophages, dendritic cells and granulocytes, provides a generic early response when the body recognises a molecule as 'non-self' (i.e. not part of the host organism). It is triggered when pathogen-associated molecular patterns (PAMPs) on 'non-self' molecules are recognised by pattern recognition receptors such as toll-like receptors (TLRs), which are expressed on immune cells. Multiple TLR subtypes exist, each with specific ligands (e.g. lipopolysaccharide can activate TLR4, whereas bacterial flagellin activates TLR5) but with similar effects upon activation. TLR activation triggers intracellular signalling cascades (summarised in figure 1.3) which ultimately promotes activation of the transcription factor NF-κB, stimulating production of pro-inflammatory cytokines and type 1 interferons (Lu et al. 2008). These factors are then released from the immune cells and act as signalling molecules to influence maturation of other immune cells (colony stimulating factors), cell migration (chemokines), or to trigger release of additional cytokines and thus propagation of the immune response.

By administering TLR ligands at different times of day, it has been possible to investigate potential effects of the circadian pacemaker in regulating the responsiveness of the innate immune system. As early as the 1960s, it was known that susceptibility to lipopolysaccharide in rodents varied significantly across a circadian cycle, with a 3-fold increase in potency if delivered during the light phase compared to the middle of the night (Halberg et al. 1960). This has recently been expanded upon in more targeted experiments using isolated splenic and peritoneal macrophages to identify potential mechanisms for such variation (Keller et al. 2009). Cells were harvested at different time points across a circadian cycle and then challenged with lipopolysaccharide (LPS). Under these stimulated conditions, the macrophages exhibited a significant oscillation in their expression of tumour necrosis factor α (TNFα) and interleukin-6 (IL-6). Upon further investigation of components of the TLR4 signalling pathway in unstimulated cells, the authors found circadian regulation of multiple factors, including regulatory components of NF-κB and members of the mitogen-activated

protein kinase (MAPK) pathways which drive pro-inflammatory signalling (figure 1.3). It therefore appears to be the case that on a cellular level, at least in macrophages, this pathway may be primed to respond more strongly at certain times of the circadian cycle.

Building on the work of Keller et al. (2009), Gibbs et al. (2012) utilised a genetic approach to disrupt the circadian oscillator in macrophages and then tested whether the temporal variation in cytokine production remained. For their initial experiments, Gibbs et al. used intraperitoneal injection of LPS at either CT0 or CT12 to confirm that a subset of cytokines showed a time-of-day variation in the magnitude of response in wild-type animals. Whilst TNFα did not show a significant time-of-day variation, a robust oscillation was found for IL-6, which was used as a biomarker. By breeding mice with a floxed *Bmal1* gene with *LysM*^{cre} mice, the group created the *LysM-Bmal1*$^{-/-}$ strain which lacked functional *Bmal1* in cells of the myeloid lineage – monocytes, macrophages and granulocytes. The *LysM-Bmal1*$^{-/-}$ line lacked circadian oscillations in the core clock genes *Per2*, *Bmal1*, *Cry1*, *Rev-erbα*, *Rev-erbβ* and a clock output gene *Dbp* in isolated peritoneal macrophages, indicating that a functional molecular oscillator had been abolished in this cell type. When the *LysM-Bmal1*$^{-/-}$ animals were subject to the same timed LPS challenges *in vivo*, the temporal variation in IL-6 production was lost.

A significant advance in knowledge was made when Gibbs et al. (2012) proceeded to perform the same experiments in mice which lacked the nuclear hormone receptor REV-ERBα. As the *LysM-Bmal1*$^{-/-}$ animals had a greatly suppressed expression of this receptor (due to lack of rhythmic transcription mediated by the CLOCK:BMAL1 complex, figure 7.1) and reported interactions of REV-ERBα with the TLR signalling pathway and IL-6 production, it was hypothesised that the loss of temporal gating of IL-6 production seen in the *LysM-Bmal1*$^{-/-}$ mice could be due to disrupted REV-ERBα signalling. Their results support this hypothesis, as *Rev-erbα*$^{-/-}$ (global knockout) mice did not show any time-of-day variation in IL-6 production. The effects of REV-ERBα signalling are suppressive (anti-inflammatory) in this case, as loss of the receptor resulted in elevated cytokine production after challenge at CT0 (when the inflammatory

response is at its nadir in wild-type animals). Quite how REV-ERBα exerts this effect remains to be determined, but it appears to be independent of the molecular pacemaker in general as rhythmic transcription of *Bmal1*, *Per2*, *Rev-erbβ* and *Dbp* remained intact in *Rev-erbα*$^{-/-}$ macrophages. Interactions between REV-ERBα and the immune system will be discussed in more detail in section 7.2.2.3.

The influence of the circadian clock is not limited to the innate system, however, as the ability of adaptive immune cells (T cells, specifically) to recognise antigens and proliferate has also been shown to be under circadian control (Fortier et al. 2011). In this case, the protein ZAP70 was proposed as the molecular link between time of day and immune function. ZAP70 is a tyrosine kinase and forms part of the signalling cascade triggered following activation of the T cell receptor upon antigen presentation. Abundance of ZAP70 protein was found to oscillate in lymph nodes of unstimulated mice, and E-box sites were identified in the *Zap70* sequence, although the possibility of transcriptional regulation by the CLOCK:BMAL1 heterodimer (which binds to E-boxes) was not investigated. Again, though, it appears that the immune cell is primed to respond more strongly at particular times of day through regulation of critical signalling molecules and that this may be regulated by the cell's intrinsic molecular oscillator.

7.2.2 Mechanisms linking molecular clock elements to immunity

The mammalian molecular clock is composed of two interlocked transcription-translation feedback loops (figure 7.1). Components of both loops have been shown to interact with key immune signalling molecules, either by modulating their transcription or via protein-protein interactions.

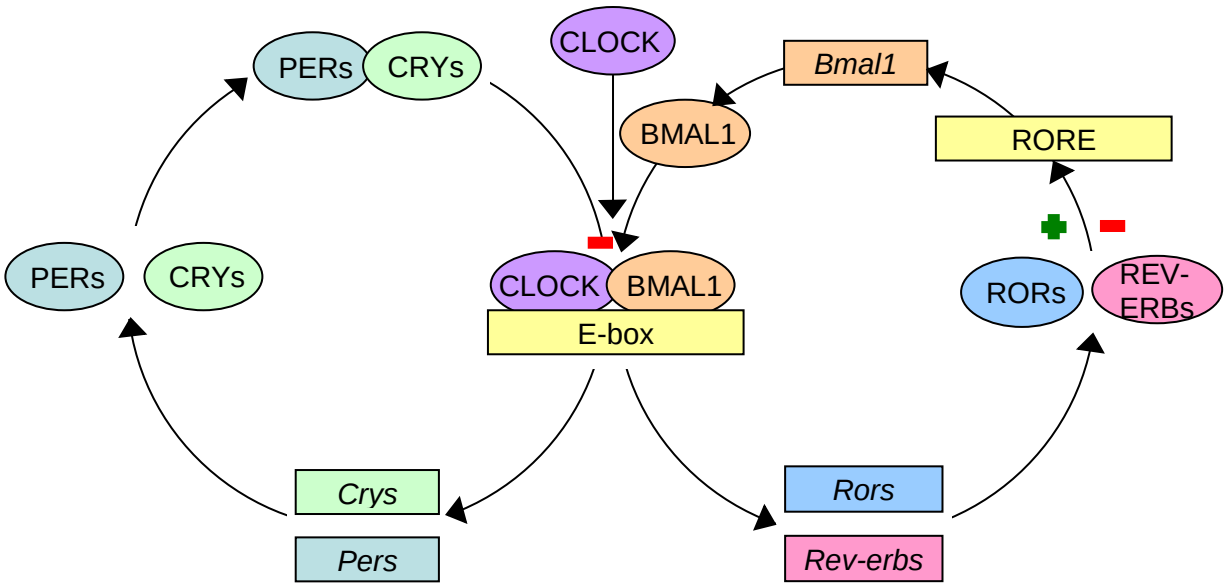

Figure 7.1: The mammalian molecular clock

Interlocked transcription-translation feedback loops, which converge upon the BMAL1-CLOCK dimer, make up the molecular clock in mammalian cells. The BMAL1-CLOCK dimer binds to E-boxes in gene promoters, positively regulating the transcription of genes such as *Crys*, *Pers*, *Rorα* and *Rev-erbα*. PER and CRY proteins heterodimerise and inhibit the activity of BMAL1-CLOCK, forming a negative feedback loop. RORα and REV-ERBα proteins influence transcription through ROR response elements (ROREs) in the promoter regions of genes, including *Bmal1*, to promote or inhibit transcription respectively. Repeat of figure 1.1 for ease of reference.

BMAL1 – brain and muscle arnt-like 1; CLOCK – circadian locomotor output cycles kaput; CRY – cryptochrome; PER – period; ROR – retinoic acid-related orphan nuclear receptor; RORE – ROR response element; + – promotes transcription; - – inhibits transcription.

7.2.2.1 BMAL1/CLOCK

The CLOCK:BMAL1 heterodimer is the critical component linking the two transcription-translation feedback loops. This pairing forms the major positive drive for the molecular oscillator, and binds to E-boxes to promote transcription. Global loss of BMAL1 renders cells arrhythmic, whilst some functional redundancy appears to exist for CLOCK as an analogue, neuronal PAS domain protein 2 (NPAS2), has been shown to compensate for loss of CLOCK in maintaining some aspects of a functional molecular oscillator (DeBruyne et al. 2007).

A direct link between the CLOCK:BMAL1 complex and innate immunity has already been proposed for TLR9-mediated responses, as two putative E-boxes exist in the mouse *Tlr9* promoter and chromatin immunoprecipitation-qPCR

(ChIP-qPCR) measuring CLOCK and BMAL1 binding (individually) in peritoneal macrophages is enriched for the *Tlr9* promoter site (Silver et al. 2012). *Tlr9* is expressed rhythmically in macrophages, B cells, spleen and dendritic cells under constant conditions and confers time-of-day variation in the responsiveness of associated signalling pathways after challenge with a TLR9-specific agonist. It is logical to propose that the CLOCK:BMAL1 complex may regulate other TLRs in a similar manner, which may underlie the oscillations seen in the LPS challenges described above, but *Tlr4* was not found to be rhythmically expressed in the peritoneal macrophages (assessed in Silver et al. 2012, targeted in Gibbs et al. 2012). This implies that regulation of inflammatory receptors by CLOCK:BMAL1 is not a general mechanism for modulation of immune sensitivity and points towards regulation of the intracellular signalling cascades downstream of receptor activation as an additional level of influence.

The Antoch group (Spengler et al. 2012) have reported a novel mechanism of rhythmic inflammatory signalling in which CLOCK, independently of BMAL1, positively regulates NF-κB activity through non-transcriptional means. Using BALB/c mice, they first showed that NF-κB activation via either TLR4 or TLR5 stimulation varied according to time of challenge *in vivo*, with an increase at ZT6 (middle of the light/rest phase) compared to ZT18 (middle of the dark/active phase). By utilising an *IκBα*-luciferase reporter mouse, it was possible to visualise activation of the pathway *in vivo*, as increased bioluminescence indicated increased activity of the NF-κB transcription factor which positively regulates *IκBα* transcription. Following this, *in vitro* experiments were performed using HEK-293T cells transfected with a *κB*-Luc reporter construct to report NF-κB activity. To assess the influence of CLOCK and/or BMAL1 in regulating the NF-κB pathway, the cells were also transfected with combinations of p65- (part of the NF-κB complex), CLOCK- and BMAL1-expressing plasmids. From this, it was discovered that the stimulatory effects of p65 upon luminescence could be increased by co-transfection of CLOCK in a dose-dependent manner. This CLOCK-mediated up-regulation of *κB*-driven bioluminescence (i.e. with CLOCK/p65 co-transfection) was suppressed in the presence of BMAL1 (i.e. with CLOCK/p65/BMAL1 co-transfection), indicating a pro-inflammatory role for CLOCK which could be suppressed by BMAL1. Further investigation *in vivo*

showed impaired NF-κB activity in *Clock*$^{-/-}$animals after TLR5 stimulation, resulting in reduced interleukin-6 production at ZT6 compared to wild-types and further illustrating pro-inflammatory effects of CLOCK. From this evidence, the authors hypothesise that CLOCK, which is expressed in an almost constitutive manner, up-regulates NF-κB activity and this is rhythmically modulated by BMAL1. Thus, the relative phasing of clock genes and protein expression may exert a strong influence upon innate immune signalling and the subsequent inflammation, independently of their transcriptional effects.

7.2.2.2 CRYs

The PERIOD (PER) and CRYPTOCHROME (CRY) proteins form the negative arm of the 'core' feedback loop. There are three known PERs and two CRYs in mammals, each encoded by separate genes (*Per1-3* and *Cry1-2*). In the molecular oscillator, these proteins heterodimerise and suppress the activity of the CLOCK:BMAL1 complex, but the cryptochrome proteins also have independent influences upon inflammatory pathways.

Using bone marrow-derived macrophages from *Cry1*$^{-/-}$*;Cry2*$^{-/-}$ double knockout animals, it was recently shown that CRY proteins have an anti-inflammatory effect upon expression of *Il6*, *Tnfα* and inducible nitric oxide synthase (*iNOS*) under unstimulated conditions (Narasimamurthy et al. 2012). When stimulated with LPS, *Cry1*$^{-/-}$*;Cry2*$^{-/-}$ macrophages showed enhanced production of TNFα and IL-6, suggesting that absence of CRY renders the cells hypersensitive to challenge. The authors hypothesised that again, it is the NF-κB pathway which is the target and used a GFP-tagged non-degradable form of the NF-κB inhibitor IκBα (IκBαM) to test the hypothesis that the NF-κB pathway is constitutively active in *Cry1*$^{-/-}$*;Cry2*$^{-/-}$ fibroblasts. Suppression of NF-κB using the IκBαM significantly reduced the expression of *Il6* in these cells, and it was also found that the *Cry1*$^{-/-}$*;Cry2*$^{-/-}$ fibroblasts have increased abundance of phosphorylated (i.e. targeted for degradation) IκBα compared to wild-type controls. The reduced activity of IκBα in *Cry1*$^{-/-}$*;Cry2*$^{-/-}$ fibroblasts was associated with increased levels of p65 in the nucleus coupled with increased binding activity at NF-κB response elements.

In addition to the increased nuclear localisation of p65, a significant increase in phosphorylated p65 was observed, indicating an increase in its transcriptional activity. The p65 phosphorylation (at serine 276) is modulated by protein kinase A (PKA), and both phospho-p65 and *Il6* production were significantly reduced in *Cry1*$^{-/-}$*;Cry2*$^{-/-}$ fibroblasts upon treatment with a PKA inhibitor. The increase in PKA activity was then linked to an increase in cyclic adenosine monophosphate (cAMP) in the *Cry1*$^{-/-}$*;Cry2*$^{-/-}$ cells under unstimulated conditions. Given this observation, the authors tested the hypothesis that CRY suppresses cAMP production using overexpression of CRY1 and treatment with forskolin, prostaglandin E2 or isoproterenol – all of which increase cAMP in wild-type cells. CRY1 overexpression significantly reduced cAMP production in response to all stimuli tested, suggesting the common mediator adenylyl cyclase was the target of the suppressive effects. These results show an additional level of interaction between the circadian clock and the NF-κB pathway where CRY, a component of the negative arm of the feedback loop, acts as an immuno-suppressor even under unstimulated conditions and that its loss results in enhanced expression of pro-inflammatory cytokines (Narasimamurthy et al. 2012).

7.2.2.3 REV-ERBs/RORs

The *Rev-erb* (α and β) and *Ror* (α, β and γ) genes form the other loop of the molecular clockwork, and their respective proteins compete for ROR response elements (ROREs) where they exert opposite effects upon transcription (REV-ERBs are repressors, RORs are activators). Both REV-ERBs and RORs are nuclear hormone receptors, and whilst the endogenous ligand for REV-ERBs has been identified as heme (Raghuram et al. 2007), the endogenous ligand for the ROR family is proving much more elusive. RORα has been shown to bind cholesterol derivatives (Solt & Burris 2012).

As has been described in section 7.2.1, an association has been found between REV-ERBα and rhythmic expression of a subset of pro-inflammatory cytokines in macrophages (Gibbs et al. 2012). To summarise, wild-type mice exhibited increased production of interleukin-6 in response to systemic LPS challenge at circadian time 0 (CT0) compared to circadian time 12 (CT12). Loss of REV-ERBα in macrophages (either using a *LysM-Bmal1*$^{-/-}$ strain which shows

decreased abundance of *Rev-erbα* or using *Rev-erbα*$^{-/-}$ animals) abolished this temporal gating and resulted in a de-repression of cytokine production at CT0. These results showed an immunosuppressive role for REV-ERBα in macrophages.

This work was expanded upon by Lam et al. (2013), who provided a mechanistic explanation for how REV-ERBs can modulate inflammatory signalling in macrophages. Initial experiments investigating binding of REV-ERBs to DNA (via ChIP) showed significant enrichment at the promoter of *Bmal1*, as anticipated, but also showed enrichment for enhancer sites in the sequences of pro-inflammatory signalling molecules matrix metallopeptidase 9 (*Mmp9*) and chemokine c-x3-c motif receptor 1 (*Cx3cr1*). Enrichment was also found at binding sites of activator protein-1 (AP-1), PU.1 and CCAAT-enhancer-binding proteins (C/EBP); transcription factors which are critical for macrophage differentiation and function (Friedman 2007). The group then analysed *Rev-erbα*$^{-/-}$ *;Rev-erbβ*$^{-/-}$ (double knockout) bone marrow-derived macrophages and found significant increases in expression of *Mmp9* and *Cx3cr1*, corresponding with REV-ERB binding being suppressive at the loci detected previously (Lam et al. 2013).

Further investigation of REV-ERB influences at the *Mmp9* and *Cx3cr1* enhancer sites using global run-on sequencing (GRO-Seq) showed bi-directional transcription of RNA from these enhancer sites (eRNA), and REV-ERB binding may therefore suppress this activity (Lam et al. 2013). This hypothesis was tested by qPCR, and the group found that loss of REV-ERBs (*Rev-erbα*$^{-/-}$*; Rev-erbβ*$^{-/-}$ macrophages) increased the transcription of eRNAs from the *Mmp9* and *Cx3cr1* loci, whereas overexpression of *Rev-erbα* decreased transcription. A reciprocal relationship was found between REV-ERB binding and the histone signature H3K9Ac (histone 3 lysine 9 acetylation, indicative of active transcription), suggesting recruitment of a deactylase complex such as NCoR/HDAC3, which it is known to interact with in mediating the repression of *Bmal1* (Yin & Lazar 2005). The expression of eRNA was strongly correlated with the mRNA expression of the respective genes, and a functional association was tested using knockdown experiments (siRNA, antisense oligonucleotides) to disrupt eRNA

activity, which resulted in a decrease in *Mmp9* and *Cx3cr1* expression both *in vitro* and *in vivo*. These results showed an important role for REV-ERB in modulating macrophage activity through repression of eRNA formation which leads to reduced expression of the target gene (Lam et al. 2013).

RORs are also known to influence immune homeostasis, with RORα involved in lymphocyte development and RORγ identified as a regulator of thymocyte differentiation, proliferation and apoptosis (Jetten 2009). Whilst RORs and REV-ERBs exert opposing effects upon transcription within the circadian oscillator network (i.e. differential regulation *Bmal1* transcription), it appears that both REV-ERBs and RORα have immunosuppressive effects in macrophages (Gibbs et al. 2012; Kopmels et al. 1992). Whilst this initially seems incompatible, evidence from skeletal muscle identifies RORα as a positive regulator of *Rev-erbα* transcription (Delerive et al. 2002), and so loss of RORs may also reduce REV-ERB activity.

In peritoneal macrophages isolated from *staggerer* mice (*Rorα*$^{-/-}$), application of LPS *in vitro* led to enhanced production of interleukin-1β compared to wild-type controls (Kopmels et al. 1992). The hyperexcitability of *Rorα*$^{-/-}$ macrophages was not limited to LPS stimulation, as the authors also tested murabutide and muramyl dipeptide. These compounds do not act through TLR4, and activate an early signalling pathway distinct from LPS resulting in selective phosphorylation and activation of extracellular signal-related kinases (ERKs) - without activation of Jun N-terminal kinase (JNK) or p38 mitogen activated kinase (MAPK) – and a transient activation of NF-κB (Vidal et al. 2001). Both murabutide and muramyl dipeptide also elicited a greater inflammatory response in *Rorα*$^{-/-}$ macrophages compared to wild types (Kopmels et al. 1992).

Conversely, overexpression of RORα in smooth muscle cells using an adenovirus significantly represses IL-6 and IL-8 secretion in both TNFα-stimulated and unstimulated conditions (Delerive et al. 2001). Using an NF-κB-Luciferase reporter construct, Delerive et al. also showed a strong induction of NF-κB activity when the cells were stimulated with LPS, which could be significantly inhibited by co-transfection with a *Rorα*-expressing vector. This suppression of

NF-κB activity was found to be due to reduced nuclear translocation of p65, associated with an increase in NF-κB inhibitor IκBα mRNA. A putative RORE site was identified in the *Iκbα* promoter sequence, mutation of which abolished RORα-mediated transcriptional induction. In addition, Delerive et al. (2001) report that *Iκbα* expression under basal conditions is reduced in the aortas of *staggerer* mice compared to wild-types, providing a potential mechanism for the pro-inflammatory phenotype seen in *staggerer* macrophages (Kopmels et al. 1992) and a further link between RORs and the NF-κB signalling pathway.

7.2.3 Circadian rhythms in immune cell trafficking

Along with intrinsic oscillations within immune cells, such as regulation of *Tlr9* expression and interactions between the molecular clockwork and NF-κB signalling pathway, abundance of the cells themselves has also been shown to vary across a circadian cycle. Whilst this will have little impact upon *in vitro* studies where equal numbers of cells are plated and challenged at different times, it may play a key role in generating circadian rhythms in the response to immune challenge *in vivo*. This phenomenon may have synergistic (i.e. more cells which are more responsive followed by fewer cells which are less responsive – generating a high amplitude rhythm through 'constructive interference') or antagonistic (i.e. more cells which are less responsive followed by fewer cells which are more responsive – generating a lower amplitude rhythm through 'destructive interference') effects with the intrinsic oscillator upon generating rhythms in immune responsiveness.

Circadian rhythms have been found in circulating concentrations of T and B cells (Haus & Smolensky 1999; Born et al. 1997; Pelegrí et al. 2003) and in T cell responses to antigen-presenting cells *in vivo* (Fortier et al. 2011). In this case, the acrophase of circulating lymphocyte concentration occurs during the light phase in mice (Haus & Smolensky 1999; Scheiermann et al. 2012), coinciding with the increased vaccination efficacy seen at ZT6 by Fortier et al, although Fortier and colleagues did not see any oscillation in T cell number in lymph nodes, the main site of T cell stimulation. It has also been shown that neutrophils and monocytes also oscillate in the same phase in mice under basal conditions, and homing to tissues occurs in anti-phase (Scheiermann et al. 2012).

The rhythmic trafficking of immune cells between bone marrow, lymph and target tissues is dependent upon local adrenergic signalling and cell-specific profiles of rhythmic adhesion molecule expression (Scheiermann et al. 2012). In further work utilising timed LPS delivery, Scheiermann and colleagues also showed rhythmic trafficking of immune cells under stimulated conditions which matched the basal profiles observed – neutrophil infiltration to the liver was highest after intraperitoneal injection of LPS administration at night. The diurnal variation seen in wild-type animals was lost when the adhesion molecule *Icam1* was knocked out, reducing nocturnal neutrophil influx to levels consistent with a daytime challenge. The reduced neutrophil influx seen in *Icam1*$^{-/-}$ animals was associated with a protective effect upon overall survival. These data therefore show an additional layer of rhythmic immunity, governed by the receptiveness of target tissues to immune cell invasion and the daily oscillations in immune cell migration.

7.2.4 The role of glucocorticoids and the glucocorticoid receptor in inflammation

Whilst oscillations in leukocyte trafficking are dependent upon neural input from the autonomic nervous system (Scheiermann et al. 2012) humoral factors are also known to play a role in immunomodulation. The glucocorticoid (Gc) hormones – cortisol in humans and corticosterone in rodents – are the most potent anti-inflammatory molecules known, and have been utilised in the clinic for over 60 years (Kirwan et al. 1999). These steroids circulate in the bloodstream with concentrations which vary across the day, peaking during the active phase of the animal (figure 3.2) and so are in anti-phase to the leukocyte invasion rhythm. This may reflect an interaction between the two systems to fine-tune the responsiveness of the organism.

As depicted in figure 1.5, glucocorticoids exert their effects by binding to the glucocorticoid receptor (GR) which can then act as a transcription factor or exert effects through protein-protein interaction and non-genomic signalling cascades. Upon activation by ligand binding, the GR-Gc complex can translocate into the nucleus and influence transcription in multiple ways. GR can recognise positive

glucocorticoid response elements (GREs) or negative glucocorticoid response elements (nGREs) to influence gene expression directly (activation and repression, respectively), which is achieved through recruitment of co-factors and chromatin remodelling complexes such as nuclear co-repressor 1 - NCoR (Chen & Evans 1995). Additionally, GR can exert indirect transcriptional effects through interacting with other transcription factors. The anti-inflammatory effects of GR signalling are thought to mainly be achieved by indirect repression, where GR inhibits NF-κB function by preventing binding of p65 to its response elements on DNA. However, the GR can also activate intracellular signalling cascades such as the MAPK pathways through rapid non-genomic signalling which may have additional anti-inflammatory effects (Ayroldi et al. 2012).

7.2.4.1 The role of glucocorticoids and the glucocorticoid receptor in regulating rhythmic responses to inflammatory challenge

The work contained in this thesis specifically addresses the question of whether glucocorticoid signalling is a regulator of circadian rhythms in innate inflammation. Part of this work (chapter 3) has already been published within a larger project investigating circadian rhythmicity in the pulmonary inflammatory response and the contribution of functional circadian oscillations in the bronchial epithelium (Gibbs et al. 2014). In this paper, we reported significant differences in cell influx to the lung after aerosolised lipopolysaccharide (LPS) challenge at different times of day. Elevated neutrophilia was seen when mice were challenged in the morning compared to the evening, which corresponded with time-of-day variation in the production of CXCL5, a potent neutrophil chemoattractant. This temporal gating of immune cell recruitment to the lung was lost, however, when the core clock gene *Bmal1* was disrupted in $CCSP^{+}$ bronchial epithelial cells (BECs) using *Ccsp-Bmal1*$^{-/-}$ mice. Loss of *Bmal1* in BECs was associated with enhanced neutrophil influx after LPS challenge at both time points, along with increased expression of pro-inflammatory cytokines *Cxcl5*, *Ccl20* and *Ccl8*. The elevated neutrophilia and CXCL5 production in *Ccsp-Bmal1*$^{-/-}$ animals when compared with littermate controls (*Bmal1*$^{flox/flox}$) did not translate into a more effective immune response, however, as neutrophil activity (measured by myeloperoxidase assay) did not show any corresponding increase, and *Ccsp-*

Bmal1$^{-/-}$ mice were equally susceptible to bacterial colony formation in the lung after infection with *Streptococcus pneumoniae*.

In order to assess the contribution of a rhythmic glucocorticoid signal in regulating time-of-day variation in cell influx, timed inflammatory challenges were employed in adrenalectomised animals (chapter 3; Gibbs et al. 2014). Adrenalectomy suppressed the circadian rhythm in circulating corticosterone and time-of-day variation in neutrophilia and CXCL5 production were lost. Curiously, given the significant enhancement of the inflammatory response to systemic challenge after adrenalectomy (chapter 3, Gibbs et al. 2014 supplementary material), the loss of gating was not associated with an overall de-repression of pulmonary inflammation and both neutrophilia and CXCL5 production remained within the range of intact animals. These results clearly implicate adrenal-derived factors (hypothesised to be glucocorticoids) in mediating the time-of-day variation in pulmonary innate inflammation, but suggest that these factors act as more of a fine-tuning timing signal rather than critical suppressors of inflammation as they appear to be in the systemic model.

It was hypothesised that the effects of glucocorticoids would be exerted through the glucocorticoid receptor, which is known to bind to an enhancer element in the *Cxcl5* promoter to suppress transcription. Chromatin immunoprecipitation (ChIP) studies measuring GR occupancy at this element provided further evidence for the involvement of glucocorticoid signalling in regulating the temporal getting of pulmonary neutrophilia as a significant time-of-day variation in GR binding was found in wild type animals (Gibbs et al. 2014). The pattern of GR binding was in anti-phase to that of *Cxcl5* expression, as expected, peaking at CT12 when endogenous glucocorticoid production is most pronounced. When the same assessments were performed for *Ccsp-Bmal1*$^{-/-}$ lungs, the time-of-day variation was lost and GR occupancy was reduced, despite normal circulating glucocorticoid rhythms. *Ccsp-Bmal1*$^{-/-}$ animals also showed increased enrichment for the H3/K27Ac marker at the *Cxcl5* locus, indicating an active chromatin state in these animals (Creyghton et al. 2010) which is consistent with the enhanced CXCL5 production observed. These results indicate a significant effect of clock gene oscillations in the bronchial epithelium, or the presence of BMAL1 in these

cells, in regulating the capacity of GR to rhythmically bind to this site and suppress pro-inflammatory cytokine production.

Loss of *Bmal1* in the bronchial epithelium may also reduce the capacity for dexamethasone-bound GR to bind DNA as *Ccsp-Bmal1*$^{-/-}$ animals were also resistant to the immunosuppressive effects of dexamethasone pre-treatment, although ChIP studies were not performed in these conditions. In wild-type littermate controls (*Bmal1*$^{flox/flox}$), intraperitoneal injection of 1mg/kg dexamethasone 1 hour before aerosolised LPS exposure at CT0 results in a significant reduction of both neutrophilia and CXCL5 production. Both of these effects are lost in *Ccsp-Bmal1*$^{-/-}$ animals. The insensitivity of *Ccsp-Bmal1*$^{-/-}$ mice to dexamethasone appears to be restricted to the bronchial epithelium as the concentration of interleukin-6, a macrophage-derived cytokine, is equally suppressed in both genotypes. Taken together, the data presented in the paper support an interaction between glucocorticoid signalling and an intact circadian pacemaker in the bronchial epithelium driving rhythmic neutrophil influx via rhythmic production of CXCL5.

The data presented in the rest of this thesis (chapters 4-6) build upon a model of glucocorticoid signalling being a critical regulator of time-of-day variation in the pulmonary inflammatory response. In addition to the evidence from adrenalectomised animals (chapter 3), timed daily administration of glucocorticoids (chapter 4), a hormone clamp model (chapter 5) and genetic manipulation (chapter 6) were employed to further examine the interplay between glucocorticoids, the glucocorticoid receptor (GR) and clock gene oscillations in the lung and their influence upon circadian variation in immune responsiveness in the lung (figure 7.2).

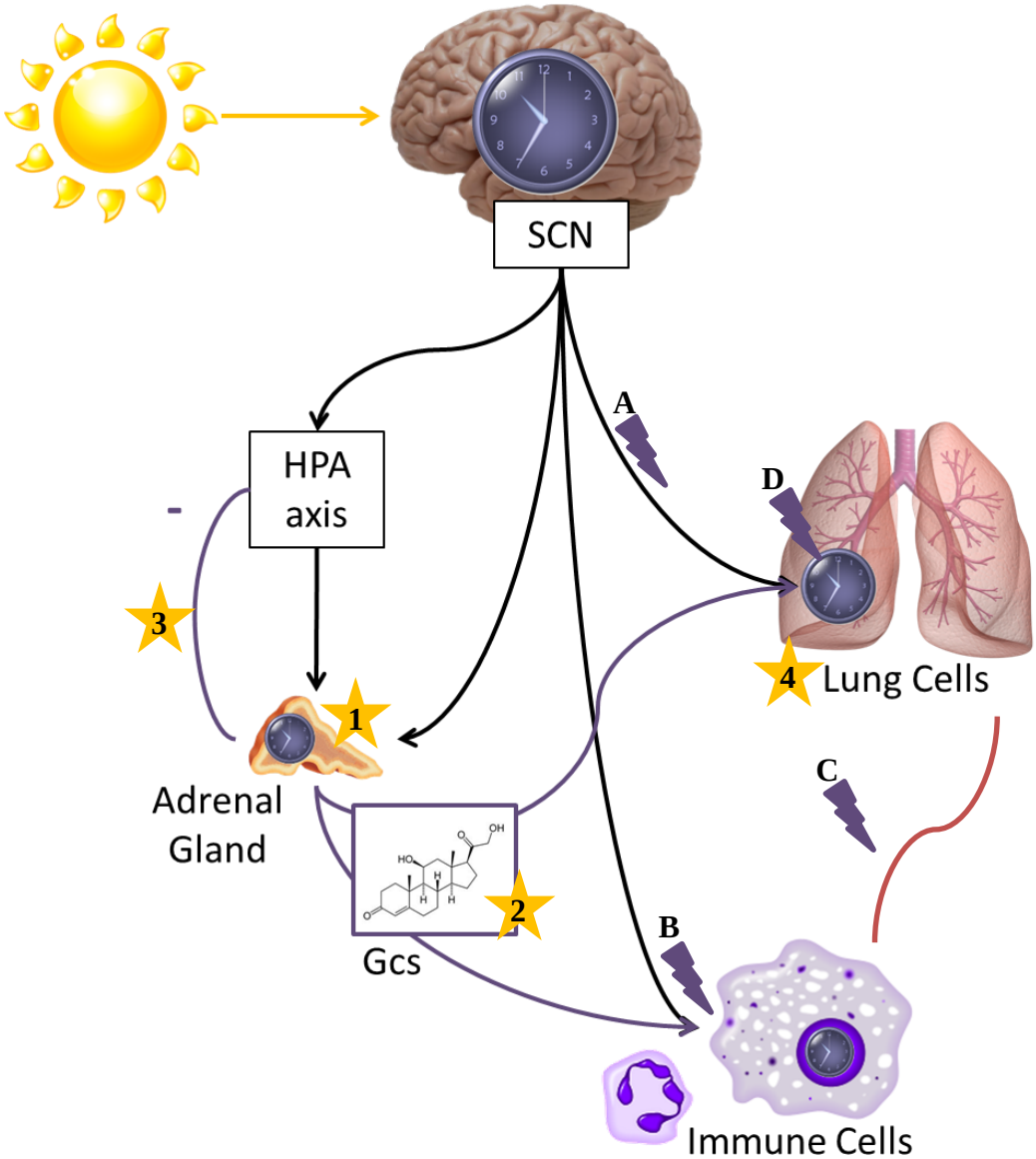

Figure 7.2: Graphical representation of hypotheses tested and additional areas of interest
The circadian clock is arranged in a hierarchical format, with a master pacemaker in the suprachiasmatic nucleus (SCN) of the brain. This clock is entrained by light and communicates to clocks in peripheral tissues to synchronise oscillations across the body via a combination of neural and humoural signals (black arrows). Stars indicate hypotheses tested within this project. Information yielded: 1) Adrenal glands are required to be present for the rhythmic neutrophilic response to pulmonary endotoxin to manifest, 2) Phase-reversal of clock gene expression in the lung via timed administration of glucocorticoids did not occur in our hands, 3) The rhythmic response to pulmonary endotoxin persisted even with constant circulating glucocorticoid concentrations, 4) Disruption of glucocorticoid receptor signalling in bronchiolar epithelial cells alters the rhythmic response to pulmonary endotoxin. Lightning bolts indicate areas not yet covered: A) Contributions of non-Gc signals, B) Importance of glucocorticoid receptor signalling in immune cells, C) Role of immune-epithelium cross-talk, D) Circadian remodelling of chromatin architecture in target tissue.

Building on the evidence obtained from adrenalectomised animals, administration of glucocorticoids in a rhythmic manner could be utilised to link the pattern of neutrophilia more strongly to rhythmic Gc signalling (as opposed to simply 'adrenal-derived factors') – for example, by injecting adrenalectomised mice with corticosterone in the morning or evening and then performing the timed LPS challenges. In this case, if mimicking the endogenous pattern of Gc concentrations led to a rhythmic neutrophilia comparable to intact animals, it would indicate that the rhythmic corticosterone signal was driving the inflammatory rhythm. However, rhythmic neutrophilia has already been tied to functional circadian oscillations in the bronchial epithelium of the lung, over and above the rhythm of circulating Gcs - *Ccsp-Bmal1*$^{-/-}$ animals retain a circadian profile of Gcs but lack rhythmic GR binding and neutrophilia (Gibbs et al. 2014). Therefore, a more valuable experiment was designed, which aimed to manipulate the phase of clock gene oscillations in the lung using Gcs in order to determine whether a phase reversal of circadian gene expression in the lung could reverse the pattern of neutrophilia.

Despite following a similar protocol to published work using daily corticosterone injections in adrenalectomised animals at ZT0.5 (Sujino et al. 2012), the initial experiment did not indicate a successful reversal of clock gene oscillations in the lung with the dose of corticosterone used. As discussed in chapter 4, this may reflect a difference between the species used (mouse vs. rat) or dose effects (10mg/kg vs. 27mg/kg). Some effects of ZT0.5 injections were observed, such as a dampening of the *Per2* rhythm specifically in this group, and it would be interesting to investigate further whether other clock genes or GR-responsive genes show shifted expression profiles before taking this protocol further with timed inflammatory challenges.

The data from the hormone clamp studies corroborate the evidence from Gibbs et al. (2014) which showed that an endogenous pacemaker in target cells was more influential than a circulating hormone rhythm in generating a rhythmic neutrophilic response, as long as sufficient ligand was available to facilitate GR signalling. Whilst results from adrenalectomised mice showed that low circulating Gc concentrations in ADX animals were insufficient to generate rhythmic cell

influx, even with an intact lung pacemaker, the data presented in chapter 5 clearly show an intact time-of-day variation with no circulating Gc rhythm. These two observations are consistent with a threshold concept, whereby once Gcs reach a certain concentration, Gc-GR signalling in the lung is possible and endogenous inflammatory rhythmicity can occur. Hypothetically, ADX animals may not have reached this threshold to activate pulmonary GR and therefore will not show rhythmic neutrophilia, whereas clamped animals have a greater concentration of circulating Gcs and are capable of mounting a rhythmic response. The combination of these results, coupled with evidence of rhythmic GR binding which is lost in *Ccsp-Bmal1*$^{-/-}$ animals (Gibbs et al. 2014), shows that rhythmic Gc ligand availability is secondary to rhythmic GR-mediated transcriptional effects.

As detailed in chapter 5, attention for future investigations is firmly focussed on the rhythmic interactions of transcription factors and chromatin, rather than simply rhythmic availability of the hormones themselves. Whilst GR protein remains stable in the lung across the circadian cycle (Gibbs et al. 2009) occupancy of chromatin sites appears to be determined by time of day (Gibbs et al. 2014). Whether these effects are mediated by the circadian clock itself or through the action of *Bmal1* specifically remains unclear and it would be valuable to assess rhythmicity of binding in additional arrhythmic clock mutants which retain functional BMAL1 protein, such as *Cry1*$^{-/-}$*;Cry2*$^{-/-}$ mice.

There is already evidence of circadian regulation of chromatin accessibility, either through direct actions of clock proteins themselves or through rhythmic activity of remodelling complexes. For example, CLOCK can act as a histone acetyltransferase (HAT), promoting an active chromatin state by acetylating lysine residues within histones (Doi et al. 2006), and binding of the CLOCK:BMAL1 complex can drive incorporation of a variant histone which increases chromatin accessibility (Menet et al. 2014). Rhythmic remodelling of chromatin architecture could allow some sites to become available for binding at certain times of the circadian cycle and not at others, making binding of transcription factors more or less likely depending upon the time of day.

Although not investigated in a circadian context, the influence of pre-existing chromatin state upon GR binding patterns has been explored by John et al. (2008), who determined that 'GR often binds to constitutive hypersensitive transitions' – i.e. the regions of GR binding were already open and accessible. Further work showed that a minority of GR binding events did not require pre-existing accessible chromatin, indicating that GR and associated complexes can act as pioneer factors and overcome a closed state, but in the majority of cases GR bound to sites which were already open. The relative accessibility of binding sites varied between cell lines, which could give rise to different patterns of GR-responsive genes between different tissues and different times of day simply through cell-specific regulation of baseline chromatin architecture across the circadian cycle (John et al. 2011).

In addition to the influence of local chromatin remodelling, individual binding site motifs can also confer dependency on clock components. For example, Cheon et al. (2013) showed that the *Per2* gene contains a non-canonical GRE half site binding motif in the proximal promoter region which overlaps with an E-box. For this gene, mutation of the E-box or *Bmal1*$^{-/-}$ in mouse embryonic fibroblasts disrupts Gc-mediated induction of *Per2* expression (Cheon et al. 2013). The authors reported that this is not a general mechanism of Gc-mediated transcriptional activation as it does not occur for *Per1*, but it should be an avenue of further research to determine whether similar events occur at other loci and in Gc-repressed genes, such as *Cxcl5*. If this is the case, the loss of gating seen in *Ccsp-Bmal1*$^{-/-}$ animals may actually be a reflection of loss of *Bmal1* specifically reducing GR binding, rather than a more general clock disruption effect upon the local chromatin environment.

The results from *Ccsp-GR*$^{-/-}$ mice (chapter 6) have yielded valuable information about the role of cell-specific GR signalling in regulating the rhythmic neutrophil influx in response to aerosolised LPS. Whilst loss of bronchial epithelial cell (BEC) GR increases neutrophil influx at CT12, no corresponding effect was observed upon CXCL5 concentration, which had previously been strongly associated with neutrophil influx. In addition, administration of dexamethasone at CT12 was able to reduce the increased neutrophilia to within the range of wild-

type controls (*GR*$^{flox/flox}$). No significant differences in neutrophil influx were observed at CT0.

These results are consistent with a role for glucocorticoid signalling suppressing inflammation at CT12, when endogenous Gcs are maximal and (repressive) GR binding to the *Cxcl5* locus is high. Loss of GR would theoretically have most impact at this time point. However, the retention of dexamethasone-mediated suppression of neutrophilia presents an interesting twist, which was unexpected in these animals.

Gibbs et al. (2014) showed that in wild-type animals, dexamethasone administration at CT0 generates a strong anti-inflammatory effect, reducing neutrophilia to numbers comparable to a CT12 challenge. At CT12, however, anti-inflammatory effects appear to be maximal already, and no further reduction is observed with dexamethasone. For the proposed rhythmic chromatin accessibility hypothesis to be true, dexamethasone treatment must overcome the rhythmic closing of chromatin at CT0 to facilitate GR binding and repression of *Cxcl5*. Dexamethasone-bound GR may therefore act more as a pioneer factor, forcing chromatin open at that location, or may have an increased ability to bind through the assisted loading model by recruiting alternative cofactors or remodelling complexes (figure 1.6). The lack of suppression at CT12 can be explained by the theory that the chromatin is already as open as it can be and no additional benefits are gained from dexamethasone administration. For loss of BEC *Bmal1* to abolish the effects of dexamethasone administration at all time points, either the chromatin landscape must be shifted into a 'super-closed' state at that location or repressive cofactor availability disrupted (or both), making it even more difficult for dexamethasone-bound GR to bind to the *Cxcl5* locus and exert repressive effects.

Dexamethasone-bound GR has already been shown to down-regulate gene expression in type II pneumocytes by tethering to critical NF-κB binding sites (see figure 1.5 for illustration of mechanism); an effect associated with repressive changes in the chromatin architecture (Islam & Mendelson 2008). Tri-methylation of histone 3 lysine 4 (H3K4me3) and acetylation of histone 3 lysines 4 and 9

(H3K9/14ac) are markers of active chromatin and associated with GR binding at GR up-regulated genes such as *Per1* and *Sgk1*. Treatment of NIH3T3 and N2A cell lines with dexamethasone results in induction of *Per1* and *Sgk1*, along with an increase in H3K4me3 and H3K9/14ac in the respective promoter regions (Xydous et al. 2014). In genes which are repressed by GR, such as surfactant protein A (*SP-A*), dexamethasone treatment results in reduced H3K9/14ac, along with an increase in H3K9me2 (dimethylation) and antagonism of histone 3 serine 10 phosphorylation (H3S10p) at an NF-κB binding site upstream of the *SP-A* gene. Each of these modifications is regarded as a marker of transcription suppression, and the events were also associated with increased expression and recruitment of histone deacetylases (HDACs) and heterochromatin protein 1α (HP1α), promoting a closed chromatin structure (Islam & Mendelson 2008).

These data suggest the presence of a complex interplay between cell types and signalling pathways. The loss of the BEC clock (*Ccsp-Bmal1*$^{-/-}$) appears to shift chromatin to a more closed state; binding of GR to a repressive *Cxcl5* locus is reduced and no longer rhythmic, and dexamethasone administration is ineffective (Gibbs et al. 2014). However, loss of BEC GR should have a similar impact, as with no GR to bind to the *Cxcl5* locus, dexamethasone treatment should be equally futile, regardless of whether the chromatin is accessible or not.

For dexamethasone to retain an ability to suppress the elevated inflammation in *Ccsp-GR*$^{-/-}$ animals, the ligand must either be working through a non-GR mechanism in these cells, acting in a different cell type or some residual GR must remain in the bronchial epithelium. The hypothesis posed by Gibbs et al. (2014) ties a single cell type (BECs), single chemokine (CXCL5) and single nuclear hormone receptor (GR) together, but the full mechanism of circadian regulation of innate pulmonary inflammation is far from clear. The results contained within this thesis have certainly provided novel information regarding GR regulation of rhythmic pulmonary inflammation, but several questions remain.

7.2.4.1.1 Caveats of work presented

Broad effects of adrenalectomy

The results from adrenalectomised animals (chapter 3) in isolation do not strictly tie the oscillation in neutrophil influx to oscillations in glucocorticoids (Gcs), as the impact of adrenalectomy is much greater than just the loss of rhythmic circulating Gcs. In addition to the steroid hormone corticosterone, which is of interest in this project, the rodent adrenal glands produce aldosterone and catecholamines and are a secondary site of sex steroid production. Loss of Gcs via adrenalectomy may also increase circulating concentrations of hormones further up the Hypothalamus-Pituitary-Adrenal axis pathway, such as CRH (corticotropin releasing hormone) and ACTH (adrenocorticotropic hormone), as there is no longer the negative feedback from Gcs to suppress them. In this study, adrenalectomised animals received saline-supplemented drinking water in order to compensate for the loss of aldosterone and maintain salt balance, but no additional measures were made to account for other hormonal disturbances.

Of the hormones disrupted via adrenalectomy, glucocorticoids are the most likely to influence inflammation and circadian rhythms based on previous literature. Synthetic glucocorticoids, such as dexamethasone, are potent anti-inflammatory agents and are capable of altering the phase of clock gene expression in peripheral tissues (Balsalobre et al. 2000). Activation of GR using the endogenous glucocorticoid corticosterone has similar effects upon both inflammation and phase of clock gene oscillations (Beesley 2010). However, in addition to glucocorticoids, adrenergic signalling is also known to regulate rhythmic inflammatory responses (Scheiermann et al. 2012) and both norepinephrine and epinephrine are produced by the adrenal medulla. The relative contribution of glucocorticoids and catecholamines would be an interesting line of further research (section 7.4.1).

Free vs. total corticosterone

Once synthesised by the adrenals, glucocorticoids are secreted into the bloodstream where the majority of the hormone binds to the carrier proteins CBG (corticosteroid-binding globulin, also known as transcortin) and, to a lesser extent,

albumin. Throughout these experiments, a steroid displacement reagent was used in corticosterone assays in order to measure total circulating corticosterone (both bound and unbound hormone). It is therefore important to note the possibility that the relative abundance of free:bound hormone may fluctuate across the day and differ from the profiles of total hormone which are presented. The binding capacity of CBG is known to oscillate in humans with a period of 24hrs and a lag of approximately 3 hours behind the cortisol rhythm (Angeli et al. 1978), and similar observations have been made in rats (Meaney et al. 1992). However, rhythms of free corticosterone in mice closely follow that of total corticosterone (Malisch et al. 2008), suggesting that the distinction between free and total corticosterone in terms of rhythmic signals may not be critical in the experiments presented in this thesis. Malisch et al. do not report the relative amplitudes of oscillations though, and it would be worth performing a more thorough comparison of total:free corticosterone rhythms in mice to rule out any significant differences between the two patterns for future reference.

The mineralocorticoid receptor

In addition to the glucocorticoid receptor (GR), glucocorticoid hormones can also bind the mineralocorticoid receptor (MR), encoded by the *Nr3c2* gene. Corticosterone will bind to the MR with 10x higher affinity than to GR, and so in tissues which express both receptors (e.g. the hippocampus), corticosterone preferentially binds MR. In these tissues, GR becoming engaged only at high concentrations of Gcs such as at the circadian peak or during stress (de Kloet et al. 1998).

As discussed above, adrenalectomy does not merely remove the Gc signal but also affects the production of aldosterone, the mineralocorticoid ligand for MR. The loss of rhythmic neutrophilia in the ADX animals may therefore be a result of loss of aldosterone-MR signalling. The retention of rhythmicity in the corticosterone-clamped animals (chapter 5) also fits with this hypothesis, as aldosterone production should persist in these animals and MR-driven effects would also remain.

The lung expresses MR in the bronchial epithelium, but, through the use of selective antagonists, the phase-shifting effect of glucocorticoid administration upon PER2-Luc oscillations was determined to be largely GR-driven with MR signalling contributing to the amplitude and non-genomic effects of corticosterone administration (Beesley 2010). However, the specific disruption of GR in the *Ccsp-GR*$^{-/-}$ animals and its effects upon the rhythmic inflammatory response, along with the data of GR binding to the *Cxcl5* promoter in Gibbs et al. (2014), suggest it is GR rather than MR which underlies the results observed in this thesis.

7.2.5 Future work

Multiple lines of research directly follow on from the results presented in this thesis (illustrated in figure 7.1 as lightning bolts and letters), and it is anticipated that the investigations proposed below will supplement this research and clarify the role of rhythmic glucocorticoid signalling in generating rhythmic inflammatory responses.

7.2.5.1 Non-glucocorticoid regulation of rhythmic pulmonary neutrophilia

Having established that the circadian clock in the bronchial epithelium is a more dominant signal than rhythmic availability of adrenal hormones (Gibbs et al. 2014 and chapter 5), it would be beneficial to investigate the contribution of other inputs to the pulmonary pacemaker. Peripheral clocks can be entrained by many factors besides glucocorticoids, including sympathetic and parasympathetic innervation.

Parasympathetic acetylcholine signalling via the vagus nerve can manipulate clock gene rhythms in the lung - unilateral vagotomy disrupts PER2 expression patterns in the ipsilateral trachea whilst the contralateral tissue retains circadian oscillations (Bando et al. 2007). The authors report that the rhythmic PER2 expression pattern in the tracheal epithelium was unaffected by sympathectomy (data not shown, however), indicating that parasympathetic signals were a stronger entrainment signal for the lung than the adrenergic signalling of the sympathetic nervous system. No data is provided in this paper regarding the pacemaker in bronchial epithelial cells, which have been shown as critical drivers

of rhythmic pulmonary inflammation, and so it would be of interest to perform similar experiments and focus on these cells to assess the contribution of nervous signalling in the lung to regulation of pulmonary inflammation.

In addition to nervous input to the lung pacemaker, the autonomic nervous system is known to regulate rhythmic trafficking of immune cells throughout the body (Scheiermann et al. 2012). Whilst the rhythmic pulmonary response to lipopolysaccharide appears to be primarily governed by the bronchial epithelium, it is impossible to ignore the fact that oscillations occur in the concentration and responsiveness of circulating immune cells. In the work of Scheiermann et al. (2012), it was shown that the rhythms in circulating leukocytes, including neutrophils, are driven by adrenergic signalling. By surgically damaging the exteriorised cremaster muscle, it was demonstrated that neutrophil and monocyte numbers were increased in response to traumatic injury at night. Tissue-specific expression of adhesion molecules fluctuated across the day, corresponding to increased leukocyte adhesion and extravasation. These oscillations were abolished after sympathectomy. Whilst it is hypothesised that parasympathetic innervation would exert a greater influence on rhythmic protein expression in the lung (Bando et al. 2007), it may be the case that sympathetic signalling is an important regulator of the lung's receptiveness to circulating immune cells, as is the case in muscle (Scheiermann et al. 2012). The relative contribution of each arm of the autonomic nervous system would therefore be an interesting line of research.

Initial experiments would comprise assessment of adhesion molecule expression in the lung across a circadian cycle, in order to determine whether their expression in the lung oscillates in a similar manner to muscle. If intact animals were found to exhibit oscillations, it would then be worth performing similar assessments in mice with disrupted sympathetic signalling to the lung to see whether such a rhythm is disrupted, followed by timed inflammatory challenge to determine effects on neutrophilia. It is of note that the lung exhibits rhythmic inflammation in anti-phase to systemic and muscular inflammatory responses, which peak at night, and so it may be the case that the lung's acute sensitivity to glucocorticoids and the circadian regulation of chemoattractant production renders the contribution of sympathetic regulation of cell influx negligible. If this is the case,

it may be that no differences in neutrophilia are found with sympathectomy, even if alterations are found in adhesion molecule rhythms.

7.2.5.2 Glucocorticoid signalling in additional cell types

In light of the results from *Ccsp-GR*$^{-/-}$ animals indicating that GR in the bronchial epithelium is not required for the synchronising or anti-inflammatory effects of dexamethasone administration, it would be beneficial to disrupt GR signalling in additional cell types in order to establish which cells are contributing to these effects. As detailed in chapter 6, disruption of GR in pneumocytes presents lethality issues, as glucocorticoid signalling is crucial for appropriate lung development, but inducible Cre lines may be useful to circumvent this.

Along with cell-specific driver sequences, the inclusion of a doxycycline responsive element can confer temporal specificity, enabling recombination to occur after the lungs have developed normally. In this case, the reverse tetracycline transactivator (rtTA) is expressed from a tissue-specific promoter, and a tetO sequence placed before a Cre sequence. When doxycycline is administered, rtTA is produced in target cells, which then binds the tetO sequence and causes Cre expression. Importantly, this expression only occurs while doxycycline is in the system, and so recombination can be induced at different stages of development simply by administering doxycycline at different ages (Rawlins & Perl 2012). By utilising different lung-specific Cre lines, individually and in combination, it will be possible to clarify the contributions of GR signalling in each subset to rhythmic innate inflammation in the lung.

It is also possible to target pulmonary immune cells using a genetic approach, as the *LysM*$^{cre/+}$ line is known to cause recombination in macrophages. Producing a *LysM-GR*$^{-/-}$ strain would facilitate exploration of the role of macrophage GR in generating rhythmic immune responses and in mediating the repressive effects of dexamethasone. Resident alveolar macrophages are known to communicate with the bronchial epithelium (Westphalen et al. 2014), and it is possible that dexamethasone activation of these cells may then cause signalling to the epithelium to cause the resynchronising and immunosuppressive effects seen in chapter 6.

7.2.5.3 Macrophage-epithelium cross-talk

Recent work has illustrated a critical role for macrophage-epithelium crosstalk in regulating the inflammatory response to lipopolysaccharide in the lung (Westphalen et al. 2014). In this paper, a subset of macrophages was found to be sessile, residing in the airways but relatively immobile and not disturbed by bronchoalveolar lavage. These cells expressed much higher quantities of the gap junction channel protein connexin 43 than non-sessile counterparts, indicating the presence of at least two groups of macrophages within the lung. Sessile macrophages formed functional gap junction connections with the lung epithelium, which served to generate synchronised calcium waves in response to intranasal lipopolysaccharide challenge. This was associated with reduced neutrophil invasion and immunosuppression. Deletion of connexin 43 increased secretion of CXCL1, CXCL5 and MIP-1α, increasing neutrophilia and illustrating a mutually suppressive effect of this type of macrophage-epithelium communication. Glucocorticoids can exhibit non-genomic effects upon connexin 43 by promoting phosphorylation and inhibiting intercellular communication in neural progenitor cells (Samarasinghe et al. 2011). It would therefore be very interesting to see whether this mechanism is affected in *Ccsp-GR*$^{-/-}$ or *LysM-GR*$^{-/-}$ animals (or indeed a simultaneous knockout in both cell types with a *GR*$^{flox/flox}$*Ccsp*$^{icre/+}$*LysM*$^{cre/+}$ line) and how this would translate to changes in the rhythmic suppression of neutrophilia.

In addition to genetic targeting of macrophages, cellular depletion may also shed light upon their contribution to rhythmic pulmonary inflammation. Depletion of alveolar macrophages can be achieved via intranasal or intratracheal administration of clodronate liposomes, which can selectively poison phagocytic cells and trigger apoptosis. Theoretically, both sessile and patrolling macrophages would be targeted by this method, and repetition of the rhythmicity and inflammatory challenge experiments of chapter 6 in animals lacking macrophages may reveal that it is these cells which are driving the resetting and immunosuppressive effects of dexamethasone.

7.2.5.4 Circadian remodelling of chromatin architecture

This project has largely focussed on *in vivo* manipulations and broad outcomes, but has returned exciting results regarding which components of the Gc-GR signalling pathway are required to oscillate for rhythmic neutrophilia to occur. Following on from the results presented here, mechanistic studies into circadian oscillations in chromatin structure and transcription factor binding, particularly in the bronchial epithelial cells, should progress understanding of how rhythmic neutrophilia arises.

Rhythmic chromatin accessibility could be investigated using FAIRE-seq (formaldehyde-assisted isolation of regulatory elements – sequencing) and focussing on the *Cxcl5* locus as a key target. This method essentially fixes chromatin and, relying on the fact that more 'open' (nucleosome-depleted) regions are fixed more easily, sequences the fixed DNA. This unbiased approach enables analysis of open regions, areas where a transcription factor *could* bind, but does not necessarily tell you whether it *is* bound. It is a powerful tool for assessing general chromatin accessibility, and when used in conjunction with ChIP for particular transcription factors (such as GR) and qPCR, can tie together circadian regulation of chromatin accessibility, transcription factor binding and transcription of target genes (Simon et al. 2012). This would answer the question of whether the *Cxcl5* locus was more accessible at certain times (CT12) than others (CT0) in wild type animals, and, if performed after dexamethasone treatment, may be used to measure whether this pre-treatment effectively forces the chromatin open and into a more CT12-like state.

Similarly, methods such as ATAC-seq (Assay for Transposase-Accessible Chromatin Sequencing; utilises a transposase to amplify regions of open DNA) in sorted cells or DNase-seq (DNase I hypersensitive sites sequencing; open sites are preferentially targeted by DNase digestion) can also highlight areas of open chromatin, and ChIP studies utilising histone markers can tie this to active transcription or repression. A complementary technique such as RNA-seq could also be employed to link changes in chromatin accessibility and histone markers to quantifiable changes in mRNA across a circadian cycle. These experiments would yield data which could be mined for subsequent projects, and could be

compared with equivalent studies in other tissues to generate a tissue-specific circadian epigenetic map. Such high-level analysis of rhythmic transcription and architecture could prove invaluable to tie future observations to epigenetic mechanisms.

7.2.6 Conclusions

In summary, the work presented in this thesis constitutes novel findings regarding glucocorticoid regulation of rhythmic innate immunity in the lung. Utilising surgical, pharmacological and genetic methods to manipulate glucocorticoid signalling, I have demonstrated a role for GR in the bronchial epithelium (using cell-specific disruption of GR expression) and made a clear distinction between the impact of very low constant concentrations of glucocorticoid ligand (after adrenalectomy) and intermediate constant circulating concentrations (after corticosterone clamp). These findings have advanced understanding of the rhythmic factors and interactions underlying time-of-day variation in neutrophilic response to immune challenge in the lung and opened up new avenues of research at both the chromatin and intercellular level.

Appendices

Appendix 1 - Genotyping reactions, primer sequences and gel recipe

GR flox

Primers:

Name	Sequence
GRflox Forward	5'- GGCATGCACATTACTGGCCTTCT -3'
GRflox Reverse - 4	5'- GTGTAGCAGCCAGCTTACAGGA -3'
GRflox Reverse - 8	5'- CCTTCTCATTCCATGTCAGCATGT -3'

PCR master mix:

GR genotyping (25µl total)				
	x1 (µl)	**x10 (µl)**	**x20 (µl)**	**x30 (µl)**
Water	15.7	157	314	471
Buffer	2.5	25	50	75
$MgCl_2$	2.5	25	50	75
dNTP (10mM)	0.5	5	10	15
Primer 1 (10µM)	0.5	5	10	15
Primer 2 (10µM)	0.5	5	10	15
Primer 3 (10µM)	0.5	5	10	15
TAQ	0.3	3	6	9
gDNA	2	2	2	2

PCR cycling conditions:

Heated Lid = 110ºC

Temperature (ºC)	Time
95	5 mins
Start Cycle	
95	30s
63	1 min
72	1 min
End Cycle	
Repeat cycle x 35	
72	10 mins
12	20 mins

2% agarose-TBE gel used to visualise bands, with Easyladder 1 to gauge size.

WT band: 225bp
Floxed band: 275bp
Null band: 390bp

Ccsp^{icre}

Primers:

Name	Sequence
icre Forward	5'-TCTGATGAAGTCAGGAAGAACC-3'
icre Reverse	5'-GAGATGTCCTTCACTCTGATT-3'

PCR master mix:

Ccsp^{icre} genotyping (25µl total)				
	x1 (µl)	**x10 (µl)**	**x20 (µl)**	**x30 (µl)**
Water	14.72	147.2	294.4	441.6
Buffer	5	50	100	150
$MgCl_2$	2	20	40	60
dNTP (2.5mM)	1.959	19.59	39.18	58.77
Primer 1 (100µM)	0.098	0.98	1.96	2.94
Primer 2 (100µM)	0.098	0.98	1.96	2.94
Go TAQ	0.125	1.25	2.5	3.75
gDNA	1	1	1	1

PCR cycling conditions:

Heated Lid = 110ºC

Temperature (ºC)	Time
94	2 mins
Start Cycle	
94	30s
60	1 min
72	1 min
End Cycle	
Repeat cycle x 30	
72	5 mins

2% agarose-TBE gel used to visualise bands, with Hyperladder IV to gauge size.

icre band: 500bp

Per2-Luc

Primers:

Name	Sequence
Common	5'- CTGTGTTTACTGCGAGAGT-3'
WT Reverse	5'- GGGTCCATGTGATTAGAAAC-3'
Mutant Reverse	5'- TAAAACCGGGAGGTAGATGAGA-3'

PCR master mix:

mPer2::Luc genotyping (25µl total)				
	x1 (µl)	**x10 (µl)**	**x20 (µl)**	**x30 (µl)**
Water	9.527	95.27	190.54	285.81
Buffer	5	50	100	150
$MgCl_2$	2	20	40	60
dNTP (2.5mM)	2.208	22.08	44.16	66.24
Primer 1 (20µM)	1.38	13.8	27.6	41.4
Primer 2 (20µM)	1.38	13.8	27.6	41.4
Primer 3 (20µM)	1.38	13.8	27.6	41.4
GoTAQ	0.125	1.25	2.5	3.75
gDNA	2	2	2	2

PCR cycling conditions:

Heated Lid = 110ºC

Temperature (ºC)	Time
94	2 mins
Start Cycle	
94	30s
58	30s
72	1 min
End Cycle	
Repeat cycle x 30	
72	5 mins

2% agarose-TBE gel used to visualise bands, with Hyperladder IV to gauge size.

WT band: 230bp
Mutant band: 650bp

Agarose gels

For 100ml standard run:
2g LE agarose (for 2% gel)
100ml 0.5x TBE
5µl ethidium bromide

Gels were run in electrophoresis tanks with 0.5x TBE as running buffer.

TBE recipe:

5x	0.5x
54g Tris Base	100ml 5x TBE
27.5g Boric Acid	900ml dH_2O
20ml EDTA (0.5M)	
Fill to 1l dH_2O	

Appendix 2 - Recording media recipe

Makes 1l:

Autoclave measuring cylinder containing 300mls water
Autoclave 1l water

1 pot of DMEM powder (1000mg/l glucose – low glucose DMEM)
4g glucose powder (weigh out in bijou)
4.7ml sodium bicarbonate
10ml HEPES
2.5ml Pen/Strep

Make up to 1l with water

Mix, and filter through 0.22µM membrane
Store at $4^{o}C$

Immediately prior to use:

Add 5% FBS (2.5ml in 50)
Add luciferin – 50µl per 50ml (one aliquot of 0.1M – final concentration 0.1mM)

Appendix 3 – *In situ* hybridisation buffer recipes

Hybridisation buffer

To make 30ml hybridisation solution:

6ml 20x SSC pH7.0-----i.e. to give 4x
15ml Deionised formamide
7ml DEPC-treated water
600µl Transfer RNA (10.9mg/ml)
60µl 0.5M EDTA (pH8.0)

Stir to mix then add gently the following compements to avoid bubbles
600µl 50x Denhart's solution
750µl 10% SDS
3g Dextran sulphate

Warm up to 55°C to facilitate the solubilisation of the dextran sulphate and aliquot in 6ml.
Store at -20°C (up to 6 months).

TEN Buffer

20ml Tris-HCl pH8 1M
4ml EDTA 0.5M
200ml NaCl 5M
Make up to 2l with ddH_2O

Appendix 4 - qPCR sequences and conditions

All primers were used at a concentration of 10pmol/µl.

TaqMan primers

β-actin
Probe 5'-TGCCACAGGATTCCATACCCAAGAAGG-3'
Forward 5'-AGGTCATCACTATTGGCAACGA-3'
Reverse 5'-CACTTCATGATGGAATTGAATGTAGTT-3'

Bmal1
Probe 5'-TGACCCTCATGGAAGGTTAGAATATGCAGAA-3'
Forward 5'-CCAAGAAAGTATGGACACAGACAAA-3'
Reverse 5'-GCATTCTTGATCCTTCCTTGGT-3'

Per1
Probe 5'-ATTCCTGGTTAGCCTGAACCTGCTTGACA-3'
Forward 5'-ACCTTGGCCACACTGCAGTA-3'
Reverse 5'-CTCCAGACTCCACTGCTGGTAA-3'

Per2
Probe 5'-ACTGCTCACTACTGCAGCCGCTCGT-3'
Forward 5'-GCCTTCAGACTCATGATGACAGA-3'
Reverse 5'-TTTGTGTGCGTCAGCTTTGG-3'

SYBR primers

18S
Forward 5'-TCCGACCATAAACGATGCCGACT-3'
Reverse 5'-TCCTGGTGGTGCCCTTCCGTCAAT-3'

β-actin
Forward 5'-AGGTCATCACTATTGGCAACGA-3'
Reverse 5'-CACTTCATGATGGAATTGAATGTAGTT-3'

Bmal1
Forward 5'-CCAAGAAAGTATGGACACAGACAAA-3'
Reverse 5'-GCATTCTTGATCCTTCCTTGGT-3'

Per2
Forward 5'-GCCTTCAGACTCATGATGACAGA-3'
Reverse 5'-TTTGTGTGCGTCAGCTTTGG-3'

Cycling conditions

Temperature (ºC)	Time
95	10 minutes
Start cycle	
95	15s
60	1 min
End cycle	
Repeat cycle x 40	

Reaction recipes

TaqMan *β-actin, Bmal1, Per1, Per2*

	x1 (µl)	x26 (µl)
dH_2O	7.8	202.8
mastermix	10	260
F/sense	0.4	10.4
R/antisense	0.4	10.4
Probe	0.4	10.4
cDNA	1	-

Mastermix – Eurogentec Efficiensee FAST + dTTP RT-QP2X-03+WOUNFB

TaqMan *Rev-erbα*

	x1 (µl)	x26 (µl)
dH_2O	8	208
mastermix	10	260
primer mix	1	26
cDNA	1	-

Mastermix – Eurogentec Efficiensee FAST + dTTP RT-QP2X-03+WOUNFB

SYBR (all)

	x1 well (µl)	x106 wells (¼ plate + 10%) (µl)
SYBR Master Mix	2.5	265
Primer 1	0.25	26.5
Primer 2	0.25	26.5
Nuclease-free water	6	636
cDNA	1	-

Mastermix - Applied Biosystems 2x power mix 4368706

Appendix 5 - Sample ELISA standard curves

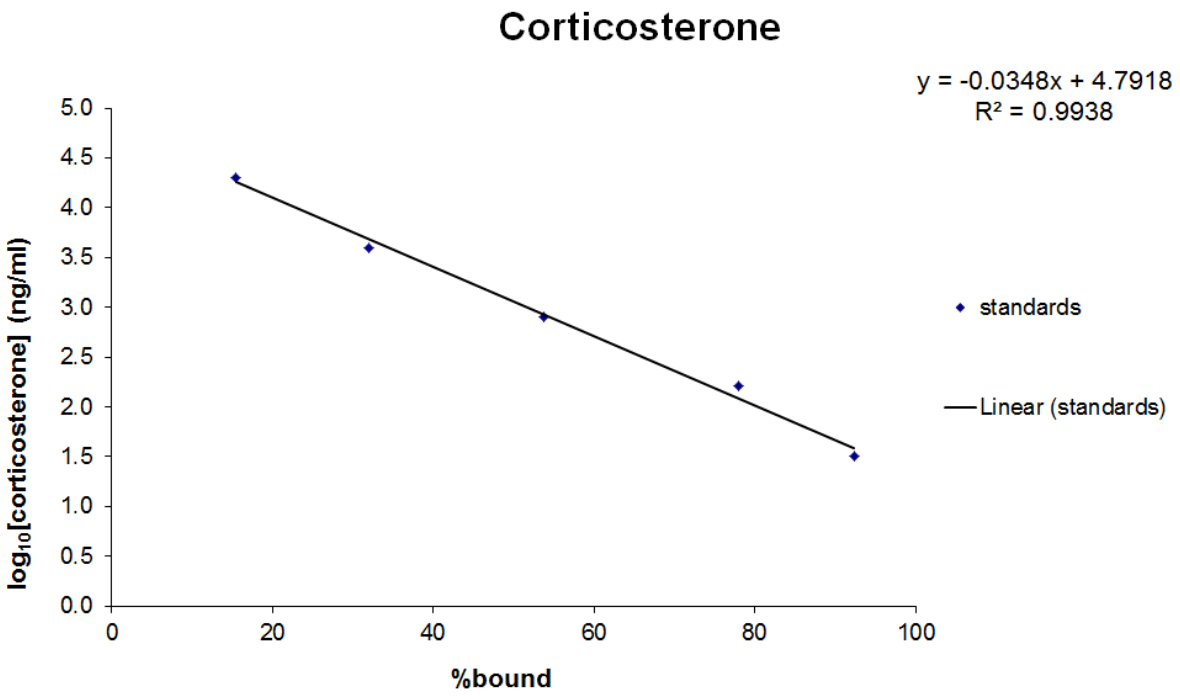

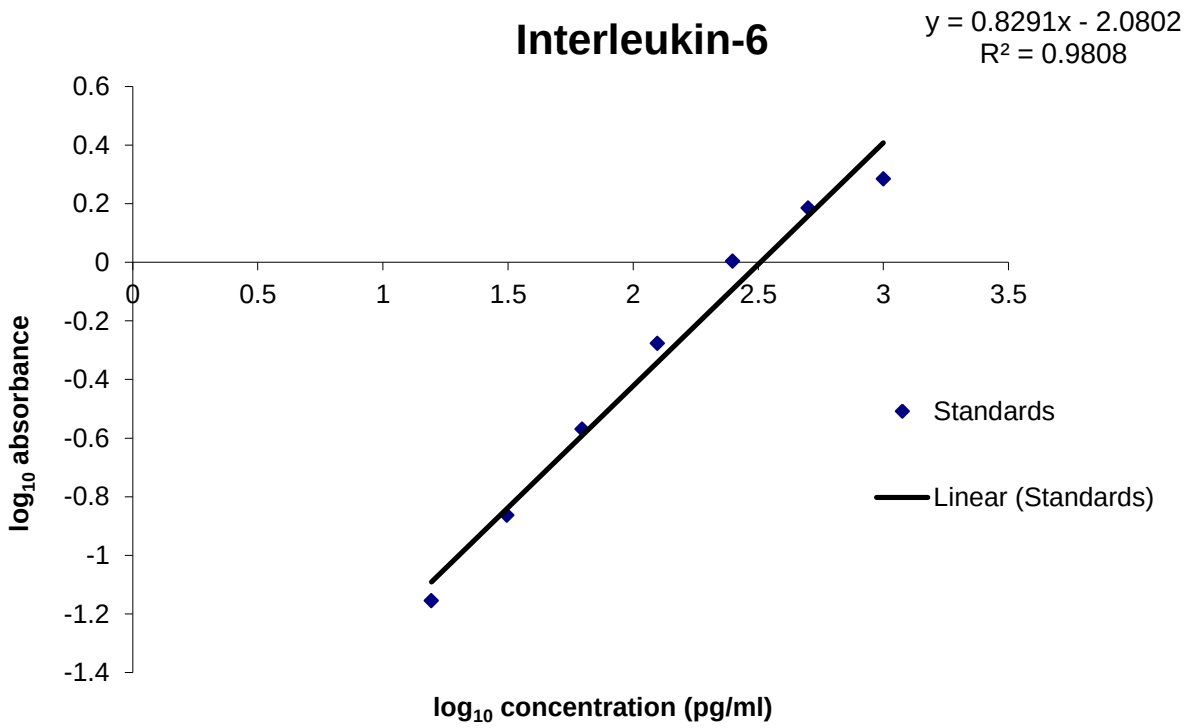

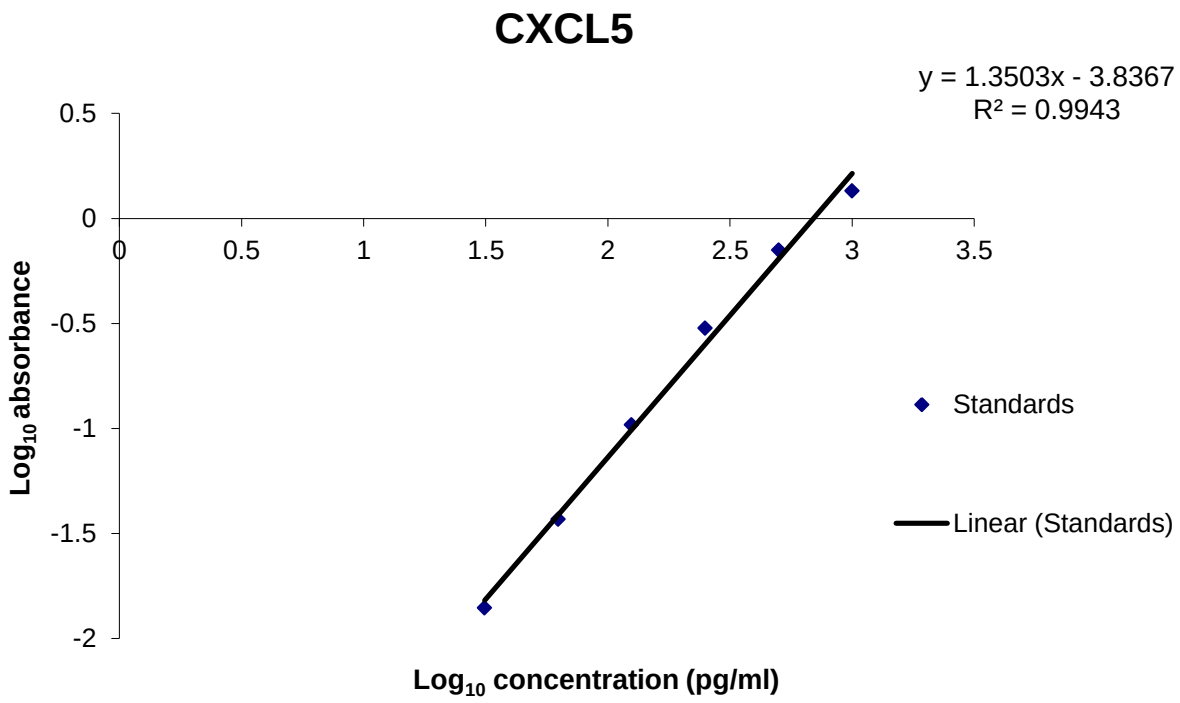
CXCL5
y = 1.3503x - 3.8367
R² = 0.9943
0.5
0
-0.5
-1
-1.5
-2
0
0.5
1
1.5
2
2.5
3
3.5
Log10 absorbance
Log10 concentration (pg/ml)
Standards
Linear (Standards)

Appendix 6 – Corticosterone ELISAs post-adrenalectomy

Chapter 3

Animals underwent a tail bleed at the indicated time point. Blood samples were allowed to clot at room temperature for 2-3 minutes and then spun at 10,000g for 10 minutes at 4ºC. The serum supernatant stored at -80ºC prior to analysis. ELISAs were run using Enzo Life Sciences' corticosterone assay, according to a low volume protocol. All samples were assayed individually at a dilution of 1:40. Animals with a concentration above 25ng/ml were treated with caution for further analyses.

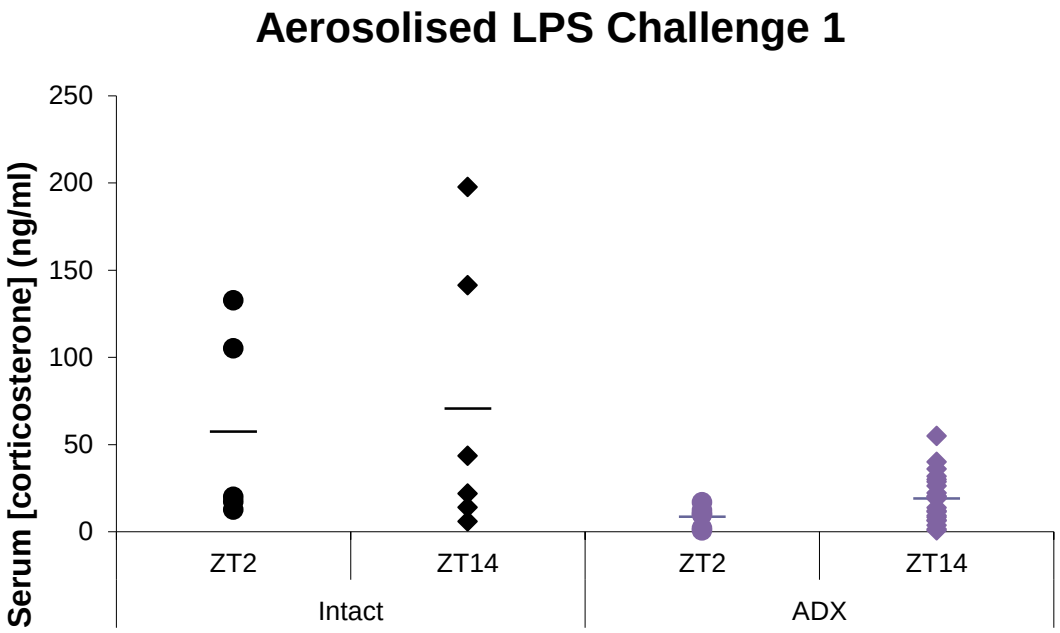

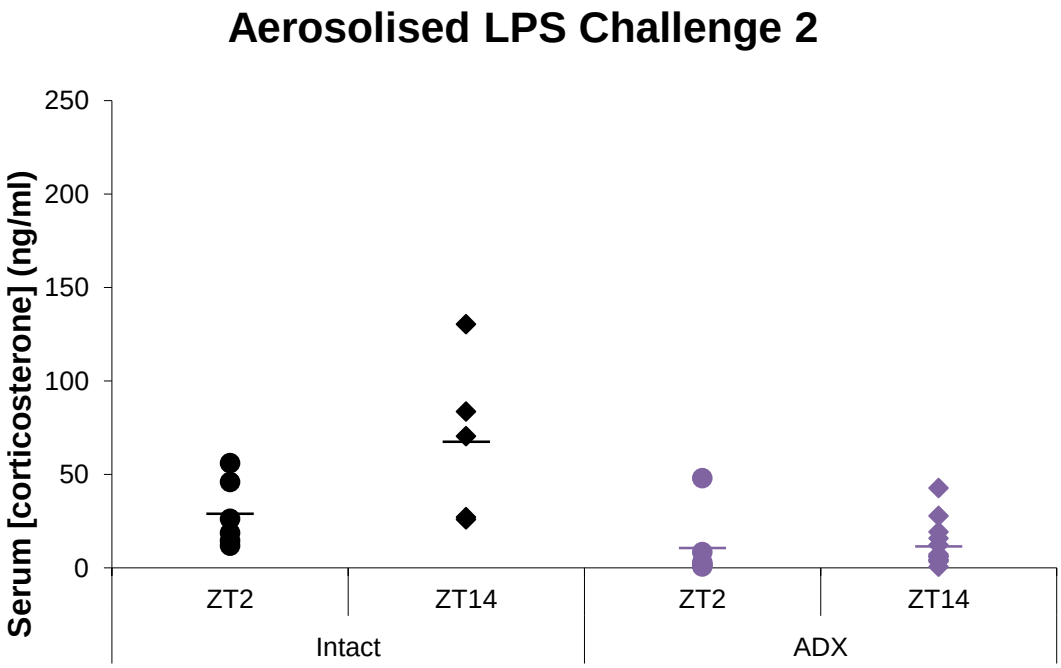

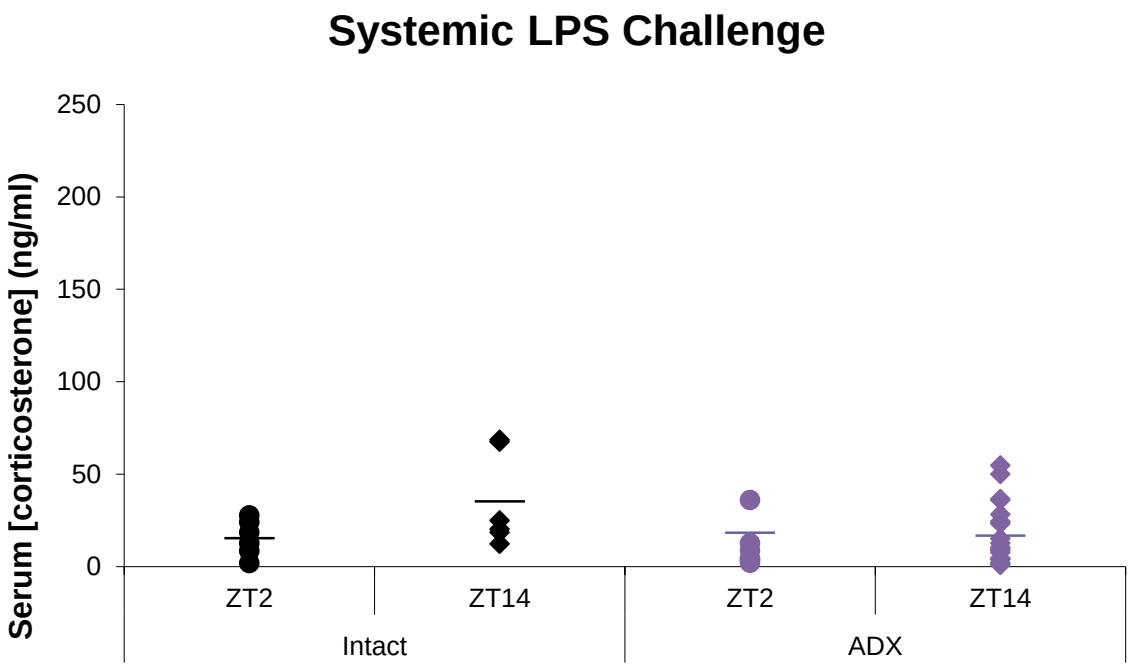

Chapter 4

As above, animals were sampled via tail bleed and assayed using Enzo Life Sciences corticosterone kit. Tail bleeds were performed at ZT14. Animals with a concentration above 25ng/ml were treated with caution for further analyses and those higher than 50ng/ml were excluded.

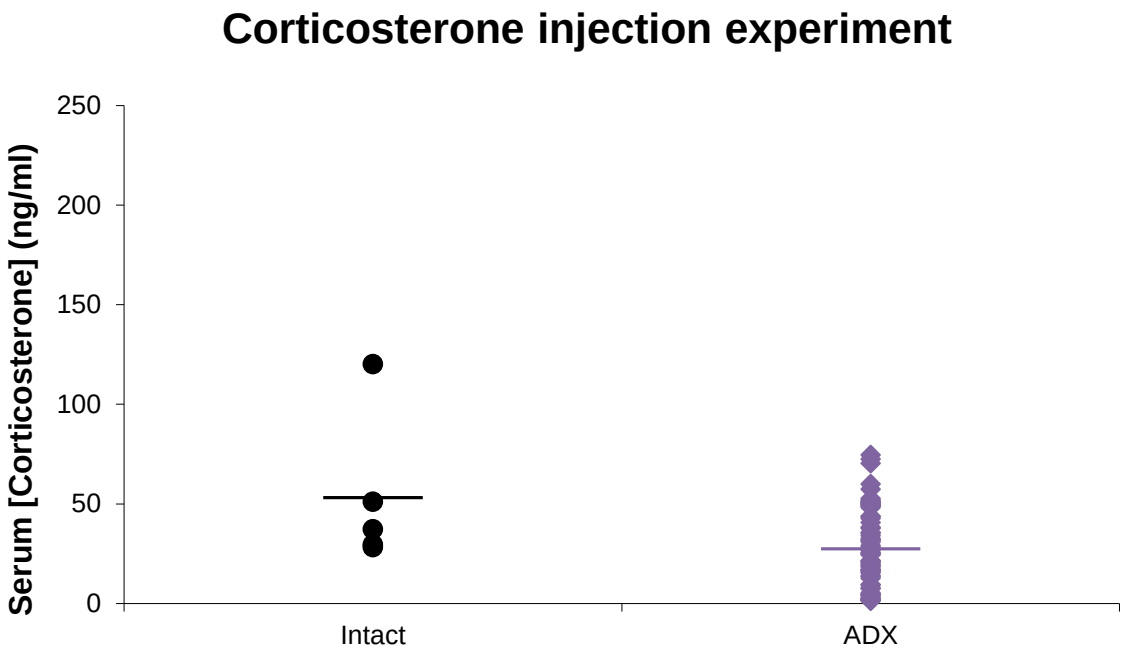

Appendix 7 – Additional corticosterone clamp data

These results are from an experiment performed prior to that shown in figures 5.4 and 5.5. The same experimental design was used, but the lipopolysaccharide challenges took place on day 19-20 of a 21-day lifespan of the hormone implant. It is clear from figure A7.1 that the two groups (clamp and intact) do not differ significantly, but when the trunk blood collected as part of the cull procedure was analysed for corticosterone (A7.2), a time-of-day variation was observed. This made it impossible to conclude whether the results are a true reflection of those obtained with a consistent hormone concentration and so the experiment was performed again and presented in chapter 5.

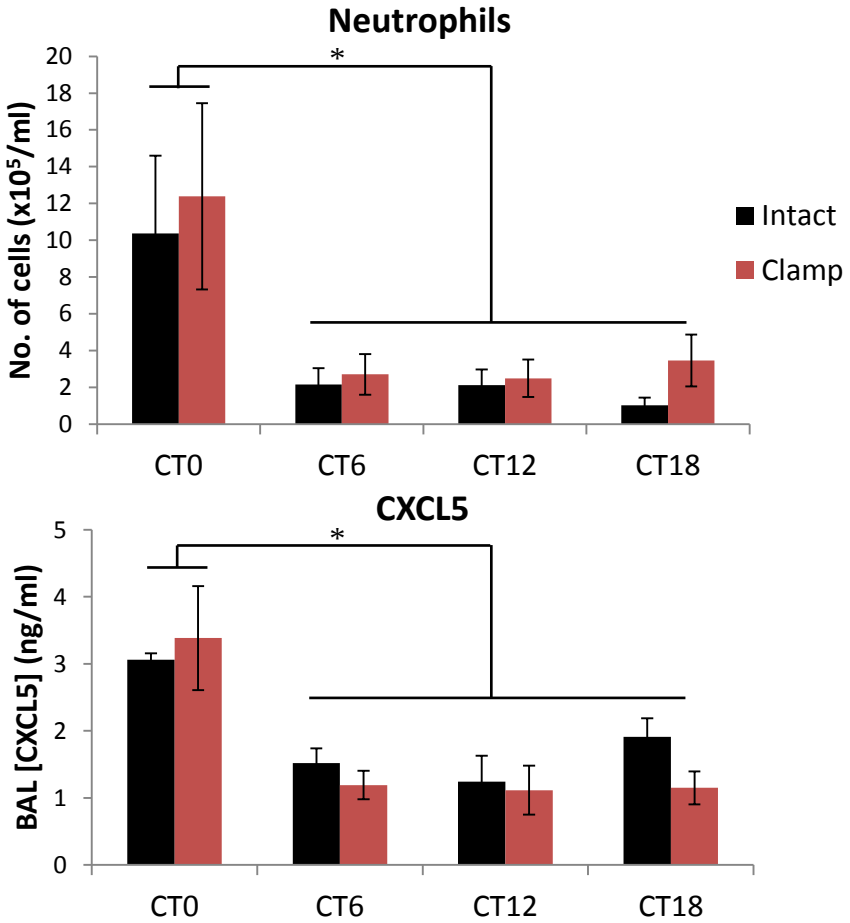

Figure A7.1: Response of intact and corticosterone-clamped mice to aerosolised lipopolysaccharide

Mice were exposed to 2mg/ml lipopolysaccharide (LPS) in saline for 20mins at the indicated time points and culled 5hrs later. Top: Neutrophil counts calculated from cytospin proportions and total cell counts. Bottom: Concentration of the neutrophil chemoattractant CXCL5 in BAL fluid. For all panels, n=6/group.

BAL – bronchoalveolar lavage; CT – circadian time, time of challenge. denotes significant difference at the 0.01 level.*

Two-way ANOVA showed a significant effect of time for both neutrophil count and CXCL5 concentration ($F_{(3,39)}$=14.34, p<0.01 and $F_{(3,31)}$=11.49, p<0.01 respectively) with CT0 concentrations significantly higher than other time points. No significant effect of the hormone clamp was detected (p>0.05).

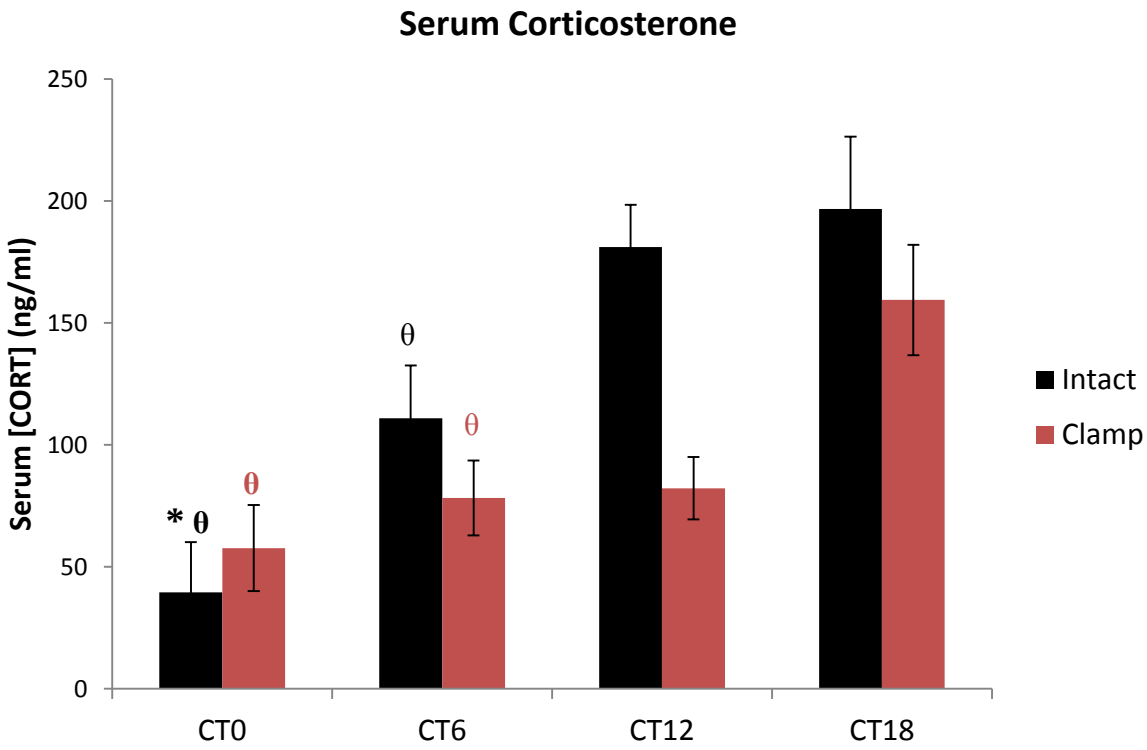

Figure A7.2: Circulating serum corticosterone concentrations after experiment

Corticosterone concentration in serum samples from trunk blood taken 5 hours after lipopolysaccharide challenge at indicated time points. All groups are independent, n=6/condition. * *denotes significantly different from CT12 value (within treatment group), θ denotes significantly different from CT18 value (within treatment group). Standard icons denote p<0.05, bold icons denote p<0.01.*

Analysis of corticosterone concentrations using two-way ANOVA showed a significant effect of time ($F_{(3,40)}$=14.67, p<0.01) and a significant effect of treatment ($F_{(1,40)}$=6.895, p<0.05). Comparison of time points within treatment groups indicated that in intact animals, CT0 concentrations were significantly lower than concentrations at CT12 and CT18 (p<0.01 for each). Concentrations at CT6 were also significantly lower than those at CT18 (p<0.05). In clamped animals, concentrations also varied with time of sampling, with CT0 and CT6 concentrations significantly lower than CT18 (p<0.01 and p<0.05 respectively).

Appendix 8 – *Ccsp*^{icre} Western Blot

Following the results of western blot for GR, β-ACTIN and CCSP in the *Ccsp-GR*$^{-/-}$ and *GR*$^{flox/flox}$ animals, the same process was performed for lungs from the *Ccsp*^{icre} control animals (no floxed genes present). Results are shown below.

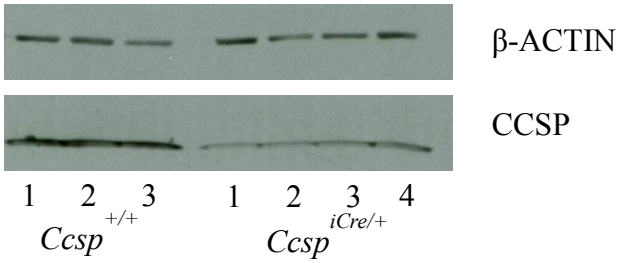

References

Adams, M. et al., 2003. Homodimerization of the glucocorticoid receptor is not essential for response element binding: activation of the phenylethanolamine N-methyltransferase gene by dimerization-defective mutants. *Molecular Endocrinology*, 17(12), pp.2583–92.

Albrecht, U. et al., 1997. A differential response of two putative mammalian circadian regulators, mPer1 and mPer2, to light. *Cell*, 91(7), pp.1055–1064.

Angeli, A. et al., 1978. Differences between temporal patterns of plasma cortisol and corticosteroid-binding globulin binding capacity throughtout the twenty-four hour day and the menstrual cycle. *Journal of Endocrinological Investigation*, 1(1), pp.31–8.

Antoch, M.P., Kondratov, R. V & Takahashi, J.S., 2005. Circadian clock genes as modulators of sensitivity to genotoxic stress. *Cell Cycle*, 4(7), pp.901–7.

Aschoff, J., 1965. Response curves in circadian periodicity. In Aschoff, J., ed. *Circadian Clocks*. Amsterdam: North-Holland, pp. 95–111.

Ayroldi, E. et al., 2012. Mechanisms of the anti-inflammatory effects of glucocorticoids: genomic and nongenomic interference with MAPK signaling pathways. *FASEB Journal*, 26(12), pp.4805–20.

Balsalobre, A. et al., 2000. Resetting of circadian time in peripheral tissues by glucocorticoid signaling. *Science*, 289(5488), pp.2344–2347.

Bamberg, E., Palme, R. & Meingassner, J.G., 2001. Excretion of corticosteroid metabolites in urine and faeces of rats. *Laboratory Animals*, 35(4), pp.307–14.

Bando, H. et al., 2007. Vagal regulation of respiratory clocks in mice. *The Journal of Neuroscience*, 27(16), pp.4359–4365.

Barnes, P.J., 2000. Mechanisms in COPD: differences from asthma. *Chest*, 117(2 Suppl), p.10S–4S.

Barnes, P.J. & Adcock, I.M., 2003. How do corticosteroids work in asthma? *Annals of Internal Medicine*, 139(5 Pt 1), pp.359–70.

Barnes, P.J., Ito, K. & Adcock, I.M., 2004. Corticosteroid resistance in chronic obstructive pulmonary disease: inactivation of histone deacetylase. *The Lancet*, 363(9410), pp.731–3.

Barton, G.M., 2008. A calculated response: control of inflammation by the innate immune system. *The Journal of Clinical Investigation*, 118(2), pp.413–20.

Beam, W.R., Weiner, D.E. & Martin, R.J., 1992. Timing of prednisone and alterations of airways inflammation in nocturnal asthma. *American Review of Respiratory Disease*, 146(6), pp.1524–30.

Bechtold, D.A., Gibbs, J.E. & Loudon, A.S.I., 2010. Circadian dysfunction in disease. *Trends in Pharmacological Sciences*, 31(5), pp.191–198.

Beesley, S., 2010. *Circadian clocks, glucocorticoids and the gated inflammatory response*. University of Manchester.

Berg, T. et al., 2002. Glucocorticoids regulate the CCSP and CYP2B1 promoters via C/EBPβ and δ in lung cells. *Biochemical and Biophysical Research Communications*, 293(3), pp.907–912.

Berson, D.M., Dunn, F. a & Takao, M., 2002. Phototransduction by retinal ganglion cells that set the circadian clock. *Science*, 295(5557), pp.1070–1073.

Bertin, G. et al., 2005. In vivo Cre/loxP mediated recombination in mouse Clara cells. *Transgenic Research*, 14(5), pp.645–654.

Bhaskaran, M. et al., 2007. Trans-differentiation of alveolar epithelial type II cells to type I cells involves autocrine signaling by transforming growth factor beta 1 through the Smad pathway. *The Journal of Biological Chemistry*, 282(6), pp.3968–76.

Blum, I.D., Lamont, E.W. & Abizaid, A., 2012. Competing clocks: Metabolic status moderates signals from the master circadian pacemaker. *Neuroscience and Biobehavioral Reviews*, 36(1), pp.254–270.

Born, J. et al., 1997. Effects of sleep and circadian rhythm on human circulating immune cells. *The Journal of Immunology*, 158(9), pp.4454–64.

Branda, C.S. & Dymecki, S.M., 2004. Talking about a revolution: The impact of site-specific recombinases on genetic analyses in mice. *Developmental Cell*, 6(1), pp.7–28.

Buijs, R.M. et al., 1999. Anatomical and functional demonstration of a multisynaptic suprachiasmatic nucleus adrenal (cortex) pathway. *European Journal of Neuroscience*, 11(5), pp.1535–44.

Buist, A.S., 2003. Similarities and differences between asthma and chronic obstructive pulmonary disease: treatment and early outcomes. *European Respiratory Journal*, 21(39 supplement), p.30s–35s.

Burioka, N. et al., 2010. Asthma: Chronopharmacotherapy and the molecular clock. *Advanced Drug Delivery Reviews*, 62(9-10), pp.946–955.

Busillo, J.M. & Cidlowski, J.A., 2013. The five Rs of glucocorticoid action during inflammation: ready, reinforce, repress, resolve, and restore. *Trends in Endocrinology & Metabolism*, 24(3), pp.109–19.

Bustos, M.L. et al., 2013. Bone marrow cells expressing clara cell secretory protein increase epithelial repair after ablation of pulmonary clara cells. *Molecular Therapy*, 21(6), pp.1251–8.

Buttgereit, F. et al., 2010. Targeting pathophysiological rhythms: prednisone chronotherapy shows sustained efficacy in rheumatoid arthritis. *Annals of the Rheumatic Diseases*, 69(7), pp.1275–80.

Castanon-Cervantes, O. et al., 2010. Dysregulation of inflammatory responses by chronic circadian disruption. *The Journal of Immunology*, 185(10), pp.5796–5805.

Cavigelli, S.A. et al., 2005. Frequent serial fecal corticoid measures from rats reflect circadian and ovarian corticosterone rhythms. *Journal of Endocrinology*, 184(1), pp.153–63.

Chen, J.D. & Evans, R.M., 1995. A transcriptional co-repressor that interacts with nuclear hormone receptors. *Nature*, 377(6548), pp.454–7.

Cheon, S. et al., 2013. Glucocorticoid-mediated Period2 induction delays the phase of circadian rhythm. *Nucleic Acids Research*, 41(12), pp.6161–6174.

Chung, S., Son, G.H. & Kim, K., 2011a. Adrenal peripheral oscillator in generating the circadian glucocorticoid rhythm. *Annals of the New York Academy of Sciences*, 1220(1), pp.71–81.

Chung, S., Son, G.H. & Kim, K., 2011b. Circadian rhythm of adrenal glucocorticoid: Its regulation and clinical implications. *Biochimica et Biophysica Acta - Molecular Basis of Disease*, 1812(5), pp.581–591.

Cima, I. et al., 2004. Intestinal epithelial cells synthesize glucocorticoids and regulate T cell activation. *The Journal of Experimental Medicine*, 200(12), pp.1635–46.

Clausen, B.E. et al., 1999. Conditional gene targeting in macrophages and granulocytes using LysMcre mice. *Transgenic Research*, 8(4), pp.265–277.

Cole, T.J. et al., 1995. Targeted disruption of the glucocorticoid receptor gene blocks adrenergic chromaffin cell development and severely retards lung maturation. *Genes & Development*, 9(13), pp.1608–1621.

Cole, T.J. et al., 2001. GRKO mice express an aberrant dexamethasone-binding glucocorticoid receptor, but are profoundly glucocorticoid resistant. *Molecular and Cellular Endocrinology*, 173(1-2), pp.193–202.

Conway-Campbell, B.L. et al., 2010. Glucocorticoid ultradian rhythmicity directs cyclical gene pulsing of the clock gene period 1 in rat hippocampus. *Journal of Neuroendocrinology*, 22(10), pp.1093–1100.

Creyghton, M.P. et al., 2010. Histone H3K27ac separates active from poised enhancers and predicts developmental state. *Proceedings of the National Academy of Sciences of the United States of America*, 107(50), pp.21931–6.

Cutolo, M. & Masi, A.T., 2005. Circadian rhythms and arthritis. *Rheumatic Disease Clinics of North America*, 31(1), pp.115–29.

Cutolo, M. & Straub, R.H., 2008. Circadian rhythms in arthritis: Hormonal effects on the immune/inflammatory reaction. *Autoimmunity Reviews*, 7(3), pp.223–228.

Dalm, S. et al., 2008. Non-invasive stress-free application of glucocorticoid ligands in mice. *Journal of Neuroscience Methods*, 170(1), pp.77–84.

Damiola, F. et al., 2000. Restricted feeding uncouples circadian oscillators in peripheral tissues from the central pacemaker in the suprachiasmatic nucleus. *Genes & Development*, 14(23), pp.2950–61.

De Kloet, E.R. et al., 1998. Brain corticosteroid receptor balance in health and disease. *Endocrine Reviews*, 19(3), pp.269–301.

DeBruyne, J.P., Weaver, D.R. & Reppert, S.M., 2007. CLOCK and NPAS2 have overlapping roles in the suprachiasmatic circadian clock. *Nature Neuroscience*, 10(5), pp.543–5.

Delerive, P. et al., 2001. The orphan nuclear receptor ROR alpha is a negative regulator of the inflammatory response. *EMBO Reports*, 2(1), pp.42–8.

Delerive, P., Chin, W.W. & Suen, C.S., 2002. Identification of Reverb(alpha) as a novel ROR(alpha) target gene. *The Journal of Biological Chemistry*, 277(38), pp.35013–8.

Dibner, C., Schibler, U. & Albrecht, U., 2010. The mammalian circadian timing system: organization and coordination of central and peripheral clocks. *Annual Review of Physiology*, 72, pp.517–549.

Dickmeis, T., 2009. Glucocorticoids and the circadian clock. *Journal of Endocrinology*, 200(1), pp.3–22.

Doi, M., Hirayama, J. & Sassone-Corsi, P., 2006. Circadian regulator CLOCK is a histone acetyltransferase. *Cell*, 125(3), pp.497–508.

Dubocovich, M.L. et al., 2005. Effect of MT1 melatonin receptor deletion on melatonin-mediated phase shift of circadian rhythms in the C57BL/6 mouse. *Journal of Pineal Research*, 39(2), pp.113–20.

Dunlap, J., 1999. Molecular bases for circadian clocks. *Cell*, 96(2), pp.271–90.

Duong, H.A. & Weitz, C.J., 2014. Temporal orchestration of repressive chromatin modifiers by circadian clock Period complexes. *Nature Structural & Molecular Biology*, 21(2), pp.126–32.

Durrington, H.J. et al., 2014. The circadian clock and asthma. *Thorax*, 69(1), pp.90–2.

Fahrenkrug, J. et al., 2012. Altered rhythm of adrenal clock genes, StAR and serum corticosterone in VIP receptor 2-deficient mice. *Journal of Molecular Neuroscience*, 48(3), pp.584–596.

Fonken, L.K. et al., 2015. Microglia inflammatory responses are controlled by an intrinsic circadian clock. *Brain, Behavior, and Immunity*, 45, pp.171–9.

Fortier, E.E. et al., 2011. Circadian variation of the response of T cells to antigen. *The Journal of Immunology*, 187(12), pp.6291–300.

Friedman, A.D., 2007. Transcriptional control of granulocyte and monocyte development. *Oncogene*, 26(47), pp.6816–28.

Frith, J.C. et al., 2001. The molecular mechanism of action of the antiresorptive and antiinflammatory drug clodronate: evidence for the formation in vivo of a metabolite that inhibits bone resorption and causes osteoclast and macrophage apoptosis. *Arthritis & Rheumatism*, 44(9), pp.2201–10.

Gavériaux-Ruff, C. & Kieffer, B.L., 2007. Conditional gene targeting in the mouse nervous system: Insights into brain function and diseases. *Pharmacology & Therapeutics*, 113(3), pp.619–34.

Gibbs, J.E. et al., 2009. Circadian timing in the lung; A specific role for bronchiolar epithelial cells. *Endocrinology*, 150(1), pp.268–276.

Gibbs, J.E. et al., 2012. The nuclear receptor REV-ERBα mediates circadian regulation of innate immunity through selective regulation of inflammatory cytokines. *Proceedings of the National Academy of Sciences of the United States of America*, 109(2), pp.582–7.

Gibbs, J.E. et al., 2014. An epithelial circadian clock controls pulmonary inflammation and glucocorticoid action. *Nature Medicine*, 20(8), pp.919–26.

Golden, S.S. et al., 1997. Cyanobacterial circadian rhythms. *Annual Review of Plant Physiology and Plant Molecular Biology*, 48, pp.327–354.

Gregor, M.F. & Hotamisligil, G.S., 2011. Inflammatory mechanisms in obesity. *Annual Review of Immunology*, 29, pp.415–45.

Gross, K.L. & Cidlowski, J.A., 2008. Tissue-specific glucocorticoid action: a family affair. *Trends in Endocrinology & Metabolism*, 19(9), pp.331–339.

Guo, H. et al., 2006. Suprachiasmatic regulation of circadian rhythms of gene expression in hamster peripheral organs: effects of transplanting the pacemaker. *The Journal of Neuroscience*, 26(24), pp.6406–6412.

Halberg, F. et al., 1960. Susceptibility rhythm to E. coli endotoxin and bioassay. *Proceedings of the Society for Experimental Biology and Medicine*, 103, pp.142–4.

Hallstrand, T.S. et al., 2014. Airway epithelial regulation of pulmonary immune homeostasis and inflammation. *Clinical Immunology*, 151(1), pp.1–15.

Hattar, S. et al., 2002. Melanopsin-containing retinal ganglion cells: architecture, projections, and intrinsic photosensitivity. *Science*, 295(5557), pp.1065–1070.

Haus, E. & Smolensky, M.H., 1999. Biologic rhythms in the immune system. *Chronobiology International*, 16(5), pp.581–622.

Herrmann, M. et al., 2009. The challenge of continuous exogenous glucocorticoid administration in mice. *Steroids*, 74(2), pp.245–249.

Hirota, T. & Fukada, Y., 2004. Resetting mechanism of central and peripheral circadian clocks in mammals. *Zoological Science*, 21(4), pp.359–368.

Hodes, G.E. et al., 2012. Strain differences in the effects of chronic corticosterone exposure in the hippocampus. *Neuroscience*, 222, pp.269–280.

Hostettler, N. et al., 2012. Local glucocorticoid production in the mouse lung is induced by immune cell stimulation. *Allergy: European Journal of Allergy and Clinical Immunology*, 67(2), pp.227–234.

Hummel, K., 1958. Accessory adrenal cortical nodules in the mouse. *The Anatomical Record*, 132(3), pp.281–295.

Hwang, J.W. et al., 2014. Circadian clock function is disrupted by environmental tobacco/cigarette smoke, leading to lung inflammation and injury via a SIRT1-BMAL1 pathway. *FASEB Journal*, 28(1), pp.176–194.

Islam, K.N. & Mendelson, C.R., 2008. Glucocorticoid/glucocorticoid receptor inhibition of surfactant protein-A (SP-A) gene expression in lung type II cells is mediated by repressive changes in histone modification at the SP-A promoter. *Molecular Endocrinology*, 22(3), pp.585–596.

Iwata, K. et al., 2011. The relationship between treatment time of gemcitabine and development of hematologic toxicity in cancer patients. *Biological and Pharmaceutical Bulletin*, 34(11), pp.1765–8.

Jangani, M. et al., 2014. The methyltransferase WBSCR22/Merm1 enhances glucocorticoid receptor function and is regulated in lung inflammation and cancer. *The Journal of Biological Chemistry*, 289(13), pp.8931–46.

Jetten, A.M., 2009. Retinoid-related orphan receptors (RORs): critical roles in development, immunity, circadian rhythm, and cellular metabolism. *Nuclear Receptor Signaling*, 7(e003).

John, S. et al., 2008. Interaction of the Glucocorticoid Receptor with the Chromatin Landscape. *Molecular Cell*, 29(5), pp.611–624.

John, S. et al., 2011. Chromatin accessibility pre-determines glucocorticoid receptor binding patterns. *Nature Genetics*, 43(3), pp.264–8.

Kadmiel, M. & Cidlowski, J.A., 2013. Glucocorticoid receptor signaling in health and disease. *Trends in Pharmacological Sciences*, 34(9), pp.518–530.

Kalsbeek, A. et al., 2012. Circadian rhythms in the hypothalamo-pituitary-adrenal (HPA) axis. *Molecular and Cellular Endocrinology*, 349(1), pp.20–9.

Kaur, G. et al., 2013. Timing is important in medication administration: a timely review of chronotherapy research. *International Journal of Clinical Pharmacy*, 35(3), pp.344–58.

Keller, M. et al., 2009. A circadian clock in macrophages controls inflammatory immune responses. *Proceedings of the National Academy of Sciences of the United States of America*, 106(50), pp.21407–21412.

Kiessling, S., Eichele, G. & Oster, H., 2010. Adrenal glucocorticoids have a key role in circadian resynchronization in a mouse model of jet lag. *Journal of Clinical Investigation*, 120(7), pp.2600–2609.

Kiessling, S., Sollars, P.J. & Pickard, G.E., 2014. Light stimulates the mouse adrenal through a retinohypothalamic pathway independent of an effect on the clock in the suprachiasmatic nucleus. *PLOS ONE*, 9(3), p.e92959.

Kirwan, J.R., Bálint, G. & Szebenyi, B., 1999. Anniversary: 50 years of glucocorticoid treatment in rheumatoid arthritis. *Rheumatology*, 38(2), pp.100–2.

Ko, C. & Takahashi, J., 2006. Molecular components of the mammalian circadian clock. *Human Molecular Genetics*, 15(Suppl 2), pp.R271–7.

Koike, N. et al., 2012. Transcriptional Architecture and Chromatin Landscape of the Core Circadian Clock in Mammals. *Science*, 338(6105), pp.349–354.

Kopmels, B. et al., 1992. Evidence for a hyperexcitability state of staggerer mutant mice macrophages. *Journal of Neurochemistry*, 58(1), pp.192–9.

Kos, C.H., 2004. Special Article : Methods in Nutrition Cre / loxP System for Generating Tissue-specific Knockout Mouse Models. *Nutrition Reviews*, 62(6), pp.243–246.

Kostadinova, F. et al., 2014. Why does the gut synthesize glucocorticoids? *Annals of Medicine*, 46(7), pp.490–7.

Kuhlman, S.J. et al., 2003. Phase resetting light pulses induce Per1 and persistent spike activity in a subpopulation of biological clock neurons. *The Journal of Neuroscience*, 23(4), pp.1441–1450.

Kwon, I. et al., 2011. Mammalian molecular clocks. *Experimental Neurobiology*, 20(1), pp.18–28.

Lam, M.T.Y. et al., 2013. Rev-Erbs repress macrophage gene expression by inhibiting enhancer-directed transcription. *Nature*, 498(7455), pp.511–5.

Lambert-Langlais, S. et al., 2009. A transgenic mouse line with specific Cre recombinase expression in the adrenal cortex. *Molecular and Cellular Endocrinology*, 300(1-2), pp.197–204.

Lamia, K.A. et al., 2011. Cryptochromes mediate rhythmic repression of the glucocorticoid receptor. *Nature*, 480(7378), pp.552–6.

Le Minh, N. et al., 2002. Glucocorticoid hormones inhibit food-induced phase-shifting of peripheral circadian oscillators. *EMBO Journal*, 20(24), pp.7128–7136.

Lee, C. et al., 2001. Posttranslational Mechanisms Regulate the Mammalian Circadian Clock. *Cell*, 107(7), pp.855–867.

Leliavski, A. et al., 2014. Impaired glucocorticoid production and response to stress in Arntl-deficient male mice. *Endocrinology*, 155(1), pp.133–42.

Leliavski, A. et al., 2015. Adrenal Clocks and the Role of Adrenal Hormones in the Regulation of Circadian Physiology. *Journal of Biological Rhythms*, 30(1), pp.20–34.

Leys, C. et al., 2013. Detecting outliers: Do not use standard deviation around the mean, use absolute deviation around the median. *Journal of Experimental Social Psychology*, 49(4), pp.764–766.

Lightman, S.L. et al., 2008. The significance of glucocorticoid pulsatility. *European Journal of Pharmacology*, 583(2-3), pp.255–262.

Lolait, S.J. et al., 2007. The hypothalamic-pituitary-adrenal axis response to stress in mice lacking functional vasopressin V1b receptors. *Endocrinology*, 148(2), pp.849–56.

Lu, Y.-C., Yeh, W.-C. & Ohashi, P.S., 2008. LPS/TLR4 signal transduction pathway. *Cytokine*, 42(2), pp.145–51.

Mahoney, C.E. et al., 2010. Lateralization of the central circadian pacemaker output: a test of neural control of peripheral oscillator phase. *American Journal of Physiology - Regulatory, Integrative and Comparative Physiology*, 299(3), pp.R751–R761.

Malisch, J.L. et al., 2007. Baseline and stress-induced plasma corticosterone concentrations of mice selectively bred for high voluntary wheel running. *Physiological and Biochemical Zoology*, 80(1), pp.146–56.

Malisch, J.L. et al., 2008. Circadian pattern of total and free corticosterone concentrations, corticosteroid-binding globulin, and physical activity in mice selectively bred for high voluntary wheel-running behavior. *General and Comparative Endocrinology*, 156(2), pp.210–7.

Manwani, N. et al., 2010. Reduced viability of mice with lung epithelial-specific knockout of glucocorticoid receptor. *American Journal of Respiratory Cell and Molecular Biology*, 43(5), pp.599–606.

Marpegán, L. et al., 2005. Circadian responses to endotoxin treatment in mice. *Journal of Neuroimmunology*, 160(1-2), pp.102–9.

Maywood, E.S., Okamura, H. & Hastings, M.H., 2002. Opposing actions of neuropeptide Y and light on the expression of circadian clock genes in the mouse suprachiasmatic nuclei. *European Journal of Neuroscience*, 15(1), pp.216–20.

Maywood, E.S. et al., 2006. Synchronization and maintenance of timekeeping in suprachiasmatic circadian clock cells by neuropeptidergic signaling. *Current Biology*, 16(6), pp.599–605.

McKay, L.I. & Cidlowski, J.A., 2003. Corticosteroids. In Kufe, D. W. et al., eds. *Cancer Medicine 6th Edition*. Hamilton (ON): BC Decker, p. Chapter 62.

Meaney, M.J. et al., 1992. Basal ACTH, corticosterone and corticosterone-binding globulin levels over the diurnal cycle, and age-related changes in hippocampal type I and type II corticosteroid receptor binding capacity in young and aged, handled and nonhandled rats. *Neuroendocrinology*, 55(2), pp.204–13.

Menet, J.S., Pescatore, S. & Rosbash, M., 2014. CLOCK:BMAL1 is a pioneer-like transcription factor. *Genes & Development*, 28(1), pp.8–13.

Meng, Q. et al., 2010. Entrainment of disrupted circadian behavior through inhibition of casein kinase 1 (CK1) enzymes. *Proceedings of the National Academy of Sciences of the United States of America*, 107(34), pp.15240–5.

Mercado, N. et al., 2012. Restoration of corticosteroid sensitivity by p38 mitogen activated protein kinase inhibition in peripheral blood mononuclear cells from severe asthma. *PLOS ONE*, 7(7), p.e41582.

Mestas, J. & Hughes, C.C.W., 2004. Of Mice and Not Men: Differences between Mouse and Human Immunology. *The Journal of Immunology*, 172, pp.2731–2738.

Meyer-Bernstein, E.L. et al., 1999. Effects of suprachiasmatic transplants on circadian rhythms of neuroendocrine function in golden hamsters. *Endocrinology*, 140(1), pp.207–18.

Michailidou, Z. et al., 2008. Glucocorticoid receptor haploinsufficiency causes hypertension and attenuates hypothalamic-pituitary-adrenal axis and blood pressure adaptions to high-fat diet. *FASEB Journal*, 22(11), pp.3896–907.

Miranda, T.B., Morris, S.A. & Hager, G.L., 2013. Complex genomic interactions in the dynamic regulation of transcription by the glucocorticoid receptor. *Molecular and Cellular Endocrinology*, 380(1-2), pp.16–24.

Moberg, G.P. & Clark, C.R., 1976. Effect of adrenalectomy and dexamethasone treatment on circadian running in the rat. *Pharmacology, Biochemistry, and Behavior*, 4(5), pp.617–9.

Moore, R.Y. & Eichler, V.B., 1972. Loss of a circadian adrenal corticosterone rhythm following suprachiasmatic lesions in the rat. *Brain Research*, 42(1), pp.201–6.

Nakamura, Y. et al., 2011. Circadian clock gene Period2 regulates a time-of-day – dependent variation in cutaneous anaphylactic reaction. *Journal of Allergy and Clinical Immunology*, 127(4), pp.1038–1045.e3.

Nakamura, Y. et al., 2014. Circadian regulation of allergic reactions by the mast cell clock in mice. *Journal of Allergy and Clinical Immunology*, 133(2), pp.568–75.

Narasimamurthy, R. et al., 2012. Circadian clock protein cryptochrome regulates the expression of proin fl ammatory cytokines. *Proceedings of the National Academy of Sciences of the United States of America*, 109(31), pp.12662–7.

Panda, S. & Hogenesch, J.B., 2004. It's all in the timing: many clocks, many outputs. *Journal of Biological Rhythms*, 19(5), pp.374–87.

Pekovic-Vaughan, V. et al., 2014. The circadian clock regulates rhythmic activation of the NRF2/glutathione-mediated antioxidant defense pathway to modulate pulmonary fibrosis. *Genes & Development*, 28(6), pp.548–60.

Pelegrí, C. et al., 2003. Circadian rhythms in surface molecules of rat blood lymphocytes. *American Journal of Physiology - Cell Physiology*, 284(1), pp.C67–76.

Piggins, H.D. & Guilding, C., 2011. The neural circadian system of mammals. *Essays in Biochemistry*, 49(1), pp.1–17.

Pittendrigh, C.S. & Minis, D.H., 1972. Circadian Systems: Longevity as a Function of Circadian Resonance in Drosophila melanogaster. *Proceedings of the National Academy of Sciences*, 69(6), pp.1537–1539.

Pittendrigh, C.S., 1993. Temporal Organization: Reflections of a Darwinian Clock-Watcher. *Annual Review of Physiology*, 55, pp.17–54.

Pruett, S.B. & Padgett, E.L., 2004. Thymus-derived glucocorticoids are insufficient for normal thymus homeostasis in the adult mouse. *BMC Immunology*, 5, pp.24–37.

Raghuram, S. et al., 2007. Identification of heme as the ligand for the orphan nuclear receptors REV-ERBα and REV-ERBβ. *Nature Structural & Molecular Biology*, 14(12), pp.1207–13.

Rawlins, E.L. & Perl, A., 2012. Perspective The a“MAZE”ing World of Lung-Specific Transgenic Mice. *American Journal of Respiratory Cell and Molecular Biology*, 46(3), pp.269–282.

Refinetti, R., 1992. Non-parametric procedures for the determination of phase markers of circadian rhythms. *International Journal of Bio-Medical Computing*, 30(1), pp.49–56.

Reppert, S.M. & Weaver, D.R., 2002. Coordination of circadian timing in mammals. *Nature*, 418(6901), pp.935–41.

Richter, C., 1936. Increased salt appetite in adrenalectomized rats. *American Journal of Physiology*, 115, pp.155–161.

Rivers, C. et al., 1999. Insertion of an amino acid in the DNA-binding domain of the glucocorticoid receptor as a result of alternative splicing. *The Journal of Clinical Endocrinology & Metabolism*, 84(11), pp.4283–6.

Roberts, D. & Dalziel, S., 2006. Antenatal corticosteroids for accelerating fetal lung maturation for women at risk of preterm birth. *Cochrane Database of Systematic Reviews*, (3), p.CD004454.

Rooney, S.A., Young, S.L. & Mendelson, C.R., 1994. Molecular and cellular processing of lung surfactant. *FASEB Journal*, 8(12), pp.957–67.

Rosenthal, N. & Brown, S., 2007. The mouse ascending: perspectives for human-disease models. *Nature Cell Biology*, 9(9), pp.993–999.

Rusak, B. & Groos, G., 1982. Suprachiasmatic stimulation phase shifts rodent circadian rhythms. *Science*, 215(4538), pp.1407–9.

Sainio, E.L., Lehtola, T. & Roininen, P., 1988. Radioimmunoassay of total and free corticosterone in rat plasma: measurement of the effect of different doses of corticosterone. *Steroids*, 51(5-6), pp.609–22.

Samarasinghe, R.A. et al., 2011. Nongenomic glucocorticoid receptor action regulates gap junction intercellular communication and neural progenitor cell proliferation. *Proceedings of the National Academy of Sciences of the United States of America*, 108(40), pp.16657–62.

Scheiermann, C. et al., 2012. Adrenergic Nerves Govern Circadian Leukocyte Recruitment to Tissues. *Immunity*, 37(2), pp.290–301.

Schteingart, D.E., 2009. Drugs in the medical treatment of Cushing’s syndrome. *Expert Opinion on Emerging Drugs*, 14(4), pp.661–671.

Shiotsuka, R. & Jovonovich, J., 1974. Circadian and ultradian corticosterone rhythms in adrenal organ cultures. *Chronobiologia*, 1(Suppl 1), pp.109–21.

Sidler, D. et al., 2011. Colon cancer cells produce immunoregulatory glucocorticoids. *Oncogene*, 30(21), pp.2411–9.

Silver, A.C. et al., 2012. The Circadian Clock Controls Toll-like Receptor 9-Mediated Innate and Adaptive Immunity. *Immunity*, 36(2), pp.251–261.

Simon, J.M. et al., 2012. Using formaldehyde-assisted isolation of regulatory elements (FAIRE) to isolate active regulatory DNA. *Nature Protocols*, 7(2), pp.256–67.

Snelgrove, R.J., Godlee, A. & Hussell, T., 2011. Airway immune homeostasis and implications for influenza-induced inflammation. *Trends in Immunology*, 32(7), pp.328–34.

Solt, L.A. & Burris, T.P., 2012. Action of RORs and their ligands in (patho)physiology. *Trends in Endocrinology & Metabolism*, 23(12), pp.619–27.

Son, G.H. et al., 2008. Adrenal peripheral clock controls the autonomous circadian rhythm of glucocorticoid by causing rhythmic steroid production. *Proceedings of the National Academy of Sciences of the United States of America*, 105(52), pp.20970–20975.

Spengler, C.M. & Shea, S.A., 2000. Endogenous circadian rhythm of pulmonary function in healthy humans. *American Journal of Respiratory and Critical Care Medicine*, 162(3 Pt 1), pp.1038–46.

Spengler, M.L. et al., 2012. Core circadian protein CLOCK is a positive regulator of NF-κB – mediated transcription. *Proceedings of the National Academy of Sciences of the United States of America*, 109(37), pp.E2457–65.

Stevens, A., Donn, R. & Ray, D., 2004. Regulation of glucocorticoid receptor gamma (GRgamma) by glucocorticoid receptor haplotype and glucocorticoid. *Clinical Endocrinology*, 61(3), pp.327–31.

Stocco, D.M. & Clark, B.J., 1996. Role of the steroidogenic acute regulatory protein (StAR) in steroidogenesis. *Biochemical Pharmacology*, 51(3), pp.197–205.

Stratmann, M. & Schibler, U., 2006. Properties, entrainment, and physiological functions of mammalian peripheral oscillators. *Journal of Biological Rhythms*, 21(6), pp.494–506.

Sujino, M. et al., 2003. Suprachiasmatic nucleus grafts restore circadian behavioral rhythms of genetically arrhythmic mice. *Current Biology*, 13(8), pp.664–8.

Sujino, M. et al., 2012. Differential entrainment of peripheral clocks in the rat by glucocorticoid and feeding. *Endocrinology*, 153(5), pp.2277–86.

Taniguchi, Y. et al., 2010. Glucocorticoid receptor-beta and receptor-gamma exert dominant negative effect on gene repression but not on gene induction. *Endocrinology*, 151(7), pp.3204–13.

Taves, M.D. et al., 2011. Extra-adrenal glucocorticoids and mineralocorticoids: evidence for local synthesis, regulation, and function. *American Journal of Physiology - Endocrinology and Metabolism*, 301(1), pp.E11–24.

Tomashefski Jr., J. & Farver, C., 2008. Anatomy and histology of the lung. In Tomashefski Jr., J. et al., eds. *Dail and Hammar's Pulmonary Pathology*. New York: Springer, pp. 20–48.

Tronche, F. et al., 1998. Genetic dissection of glucocorticoid receptor function in mice. *Current Opinion in Genetics & Development*, 8(5), pp.532–8.

Tronche, F. et al., 1999. Disruption of the glucocorticoid receptor gene in the nervous system results in reduced anxiety. *Nature Genetics*, 23(September), pp.99–103.

Tsompana, M. & Buck, M.J., 2014. Chromatin accessibility: a window into the genome. *Epigenetics & Chromatin*, 7(1), p.33.

Van Winkle, L.S. et al., 1999. Early events in naphthalene-induced acute Clara cell toxicity: comparison of membrane permeability and ultrastructure. *American Journal of Respiratory Cell and Molecular Biology*, 21(1), pp.44–53.

Vidal, V.F. et al., 2001. Macrophage stimulation with Murabutide, an HIV-suppressive muramyl peptide derivative, selectively activates extracellular signal-regulated kinases 1 and 2, C/EBPbeta and STAT1: role of CD14 and Toll-like receptors 2 and 4. *European Journal of Immunology*, 31(7), pp.1962–71.

Voss, T.C. & Hager, G.L., 2014. Dynamic regulation of transcriptional states by chromatin and transcription factors. *Nature Reviews Genetics*, 15(2), pp.69–81.

Wallace, A.D. & Cidlowski, J.A., 2001. Proteasome-mediated glucocorticoid receptor degradation restricts transcriptional signaling by glucocorticoids. *The Journal of Biological Chemistry*, 276(46), pp.42714–21.

Wang, X. et al., 2012. Novel Method for Isolation of Murine Clara Cell Secretory Protein-Expressing Cells with Traces of Stemness. *PLOS ONE*, 7(8), p.e43008.

Westphalen, K. et al., 2014. Sessile alveolar macrophages communicate with alveolar epithelium to modulate immunity. *Nature*, 506(7489), pp.503–6.

Windle, R.J. et al., 1998. The pulsatile characteristics of hypothalamo-pituitary-adrenal activity in female Lewis and Fischer 344 rats and its relationship to differential stress responses. *Endocrinology*, 139(10), pp.4044–52.

Woelfle, M.A. et al., 2004. The Adaptive Value of Circadian Clocks: An Experimental Assessment in Cyanobacteria. *Current Biology*, 14(16), pp.1481–1486.

Wong, A.P., Keating, A. & Waddell, T.K., 2009. Airway regeneration: the role of the Clara cell secretory protein and the cells that express it. *Cytotherapy*, 11(6), pp.676–87.

Wong, M.H., Chapin, O.C. & Johnson, M.D., 2012. LPS-stimulated cytokine production in type I cells is modulated by the renin-angiotensin system. *American Journal of Respiratory Cell and Molecular Biology*, 46(5), pp.641–50.

Wong, M.H. & Johnson, M.D., 2013. Differential response of primary alveolar type I and type II cells to LPS stimulation. *PLOS ONE*, 8(1), p.e55545.

Wright, J.R., 2004. Host defense functions of pulmonary surfactant. *Biology of the Neonate*, 85(4), pp.326–32.

Xydous, M., Prombona, A. & Sourlingas, T.G., 2014. The role of H3K4me3 and H3K9/14ac in the induction by dexamethasone of Per1 and Sgk1, two glucococorticoid early response genes that mediate the effects of acute stress in mammals. *Biochimica et Biophysica Acta*, 1839(9), pp.866–872.

Yin, L. & Lazar, M.A., 2005. The orphan nuclear receptor Rev-erbalpha recruits the N-CoR/histone deacetylase 3 corepressor to regulate the circadian Bmal1 gene. *Molecular Endocrinology*, 19(6), pp.1452–9.

Yoo, S. et al., 2004. PERIOD2::LUCIFERASE real-time reporting of circadian dynamics reveals persistent circadian oscillations in mouse peripheral tissues. *Proceedings of the National Academy of Sciences of the United States of America*, 101(15), pp.5339–46.

Zheng, B. et al., 1999. The mPer2 gene encodes a functional component of the mammalian circadian clock. *Nature*, 400(6740), pp.169–73.